Assessing dissolution in the tests of planktonic foraminifera using computed tomography (CT): potential for improving paleoceanographic reconstructions

Dissertation zur Erlangung des
Doktorgrades der Naturwissenschaften
im Fachbereich Geowissenschaften der
Universität Bremen

vorgelegt von

Heather Jean Houghton Johnstone

Bremen, 2010

PRÜFUNGSAUSSCHUSS

Gutachter der Dissertation:
• Herr Prof. Dr. Michael Schulz
• Herr Prof. Dr. Gerold Wefer

Tag des öffentlichen Kolloquiums:
15 November 2010

Mitglieder der Kommission:
• Herr Prof. Dr. Michael Schulz
• Herr Prof. Dr. Gerold Wefer
◊ Herr Prof. Dr. Dieter Wolf-Gladrow
• Herr Prof. Dr. Rüdiger Henrich
• Herr Dr. Stefan Mulitza
• Frau Anne Seidenglanz

• MARUM - Center for Marine Environmental Sciences
University of Bremen
D-28334 Bremen, Germany

◊ Alfred Wegener Institute
Am Handelshafen, 12
D-27570 Bremerhaven, Germany

ERKLÄRUNG

Name: Heather Jean Houghton Johnstone

Anschrift: Am Lehester Deich, 70, 28357 Bremen

Hiermit versichere ich, dass ich

1. die Arbeit ohne unerlaubte fremde Hilfe angefertigt habe,

2. keine anderen als die von mir angegebenen Quellen und Hilfsmittel benutzt habe und

3. die den benutzten Werken wörtlich oder inhaltlich entnommenen Stellen als solche kenntlich gemacht habe.

Bremen, August 2010

Heather Johnstone

(Unterschrift)

ACKNOWLEDGEMENTS

ABSTRACT

The tests of planktonic foraminifera are widely used in paleoceanographic research as their chemical composition records the hydrographic conditions in which they grew. Partial solution of tests at the seafloor distorts the primary signal. However, dissolution intensity reflects deep water carbonate chemistry – an important part of the global carbon cycle. This thesis presents a new method of assessing dissolution in the tests of planktonic foraminifera (**Chapter 4**). Cross-sectional images of tests obtained using computed tomography (CT) allowed insight into the progress of dissolution.

Four species of foraminifera (*Globigerinoides ruber* [white variety]; *Globigerinoides sacculifer* [without a sac-like final chamber]; *Neogloboquadrina dutertrei* and *Pulleniatina obliquiloculata*) from core-top samples spanning a range of calcite saturation states ($\Delta[CO_3^{2-}]$) from Pacific, Atlantic and Indian Ocean sites were examined. First signs of dissolution were seen in the inner test calcite well above the calcite saturation horizon, at similar $\Delta[CO_3^{2-}]$ values (of 12-14 μmol/kg) for the four species. At sites close to the calcite saturation horizon dissolution and precipitation of calcite occurs simultaneously within tests. The empty calcite crusts, from which the inner calcite had dissolved, of *N. dutertrei* and *P. obliquiloculata* were relatively resistant to dissolution and were present in samples from sites where $\Delta[CO_3^{2-}] \approx$ -20 μmol/kg. The observed progression of dissolution, which first affects the inner calcite, is compatible with the premise that Mg-rich calcite is preferentially dissolved. Five stages of preservation could be identified, and an empirical dissolution index, XDX, was established based on the appearance of the CT scans. Despite variation in test mass between sites, mass loss in response to dissolution was similar between species and sites at ~0.4 μg per μmol/kg. Calibrations to estimate $\Delta[CO_3^{2-}]$ and initial test mass from XDX were established.

Methods to correct for dissolution effects on Mg/Ca assume that sensitivity to dissolution effects is temporarily and spatially constant. Sensitivity of Mg/Ca to $\Delta[CO_3^{2-}]$ was greatest for *G. ruber*, which lost 0.102 (± 0.036) mmol/mol per μmol/kg, and similar, at less than half this value, for *G. sacculifer*, *N. dutertrei* and *P. obliquiloculata* (**Chapter 5**). *N. dutertrei* from the Caribbean appears to have higher sensitivity than *N. dutertrei* from other sites. Mg/Ca started to decrease from $\Delta[CO_3^{2-}]$ values of 10 – 15 μmol/kg, but these threshold values are likely to be minimum estimates. Calibrations between XDX and ΔMg/Ca provide an independent method of estimating dissolution effects on Mg/Ca.

Comparison of XDX and $\delta^{18}O$ shows that for the small sample sizes typical for analysis, $\delta^{18}O$ values are highly variable and that the variability overwhelms dissolution effects.

First sediment core application of XDX generated a record of $\Delta[CO_3^{2-}]$ for the deep (4,157 m) tropical western Indian Ocean [core WIND28K] consistent with calcite compensation theory (**Chapter 6**). Calcite saturation increased by ~25 μmol/kg over Termination I and ~15 μmol/kg over Termination II while dissolution maxima coincide with transitions to colder stages. The XDX-corrected Mg/Ca-derived temperature record is similar to published records for monsoon dominated sites in the Indian Ocean. Sea surface temperatures were 4 ^{o}C colder during Marine Isotope Stage 3 and 1–1.5 ^{o}C cooler during the last glacial maximum than during the mid-Holocene. Minimum test mass in the XDX-corrected record, during MIS 3, coincides with the lowest temperatures.

Foraminifera tests from a depth transect on the Ontong Java Plateau, representing a range of preservation states, were cleaned using two methods: "Mg-cleaning" and the more rigorous "Cd-cleaning" method, which includes a reductive step and is thought to result in lower Mg/Ca (**Chapter 7**). Scanning electron microscopy showed that reductive cleaning etched tests surfaces, but this minor dissolution did not necessarily decrease Mg/Ca. There was no difference in Mg/Ca between cleaning methods for *G. sacculifer* and *P. obliquiloculata*. Mg/Ca was decreased by reductive cleaning in *G. ruber* (~4%) and *N. dutertrei* (~10%). Offset in Mg/Ca between the two methods was insensitive to preservation state. Reductive cleaning is the more effective method. Tests cleaned using Mg-cleaning retained coccoliths and other sedimentary detritus. There was weak correlation between yield and $\Delta[CO_3^{2-}]$ in core-tops, reaching statistical significance ($p < 0.05$) only in "Cd-cleaned" *N. dutertrei*. Maxima in analytical yield of *G. ruber* and *G. sacculifer* from a deep core from the Indian Ocean (WIND 28K) coincided with episodes of good preservation during deglaciations. It is suggested that monitoring analytical yield may provide a first estimate of dissolution bias of Mg/Ca.

ZUSAMMENFASSUNG

Schalen planktonischer Foraminiferen werden in der Paläozeanographie verbreitet verwendet, da ihre chemische Zusammensetzung die hydrographischen Bedingungen aufzeichnet, unter denen ihr Wachstum erfolgte. Teilweise Lösung der Foraminiferenschalen am Meeresboden jedoch verzerrt das Hauptsignal. Die Lösungsintensität hingegen gibt Aufschluss über die Karbonatchemie des tiefen Ozeans, eine wichtige Komponente des globalen Kohlenstoffkreislaufs. Die vorliegende Arbeit stellt eine neue Methode zur Bestimmung des Lösungsgrades in den Schalen planktonischer Foraminiferen vor (**Kapitel 4**). Mittels Computertomographie generierte Aufnahmen von Gehäusequerschnitten liefern Erkenntnisse zum Fortschreiten der Lösung.

An Oberflächensedimentproben aus dem Pazifik, Atlantik und Indik wurden vier Foraminiferenarten (*Globigerinoides ruber* [weiß]; *Globigerinoides sacculifer*; *Neogloboquadrina dutertrei* und *Pulleniatina obliquiloculata*) untersucht und ein Spektrum an Kalzitsättigungsgraden ($\Delta[CO_3^{2-}]$) abgedeckt. Erste Anzeichen für Lösung wurden am inneren Kalzit des Foraminiferengehäuses deutlich oberhalb des Kalzitsättigungshorizont festgestellt – bei ähnlichen $\Delta[CO_3^{2-}]$-Werten (12-14 µmol/kg) für die vier Arten. An Lokationen, die dicht am Kalzitsättigungshorizont liegen, erfolgen Lösung und Ausfällung von Kalzit innerhalb der Schalen gleichzeitig. Die leeren Kalzitkrusten, deren Inneres gelöst worden war, waren bei *N. dutertrei* und *P. obliquiloculata* relativ robust gegenüber Lösung und wurden in Proben von Lokationen mit $\Delta[CO_3^{2-}]$ ≈ -20 µmol/kg gefunden. Das beobachtete Fortschreiten der Lösung, wovon zunächst der innere Kalzit betroffen ist, passt zur Annahme, dass vorzugsweise Mg-reicher Kalzit gelöst wird. Fünf Erhaltungsgrade konnten identifiziert werden, und ein empirischer Lösungsindex (XDX) wurde basierend auf dem Erscheinungsbild in den CT-Aufnahmen erstellt. Trotz Unterschieden im Schalengewicht zwischen den Lokationen lag die Sensitivität des Schalengewichts gegenüber $\Delta[CO_3^{2-}]$ für die verschiedenen Spezies und Lokationen einheitlich bei ca. ~0,4 µg pro µmol/kg. Kalibrierungen zur Abschätzung von $\Delta[CO_3^{2-}]$ und des ursprünglichen Schalengewichts anhand von XDX wurden ermittelt.

Methoden, die den Einfluss von Lösung auf Mg/Ca korrigieren, gehen davon aus, dass die Sensitivität gegenüber Lösungseffekten zeitlich und räumlich konstant ist. Die Sensitivität von Mg/Ca bezüglich $\Delta[CO_3^{2-}]$ war mit einem Verlust von 0,102 (± 0,036) mmol/mol pro µmol/kg am größten für *G. ruber* und lag für *G. sacculifer*, *N. dutertrei* und *P. obliquiloculata* bei weniger als der Hälfte dieses Wertes (**Kapitel 5**). Karibische *N. dutertrei* scheinen eine höhere Sensitivität aufzuweisen als *N. dutertrei* von anderen Lokationen. Eine erste Abnahme von Mg/Ca wurde bei $\Delta[CO_3^{2-}]$-Werten von 10-15

μmol/kg festgestellt, doch diese Schwellwerte stellen vermutlich Minimalabschätzungen dar. Kalibrierungen zwischen XDX und ΔMg/Ca stellen eine unabhängige Methode dar, den Einfluss von Lösung auf Mg/Ca abzuschätzen. Ein Vergleich von XDX und δ^{18}O ergab, dass bei für die Analyse typischem kleinem Probenumfang δ^{18}O-Werte stark variieren und die Variabilität gegenüber dem Lösungseffekt überwiegt.

Eine erste Anwendung von XDX auf einen Sedimentkern [WIND28K] ergab für den tiefen (4157 m) tropischen westlichen Indischen Ozean einen Verlauf von $\Delta[CO_3^{2-}]$, der konsistent mit der Kalzitkompensationstheorie ist (**Kapitel 6**). Die Kalzitsättigung stieg während der Termination I um ~25 μmol/kg und während der Termination II um ~15 μmol/kg an, während Lösungsmaxima mit Übergängen in kältere Phasen zusammenfallen. Der XDX-korrigierte Verlauf der Mg/Ca-Temperaturen stimmt mit veröffentlichten Daten überein, die aus monsundominierten Regionen des Indischen Ozeans stammen. Meeresoberflächentemperaturen waren im Vergleich zum Holozän im Marinen Isotopenstadium 3 um 4 °C niedriger und während des letzten glazialen Maximums um 1–1,5 °C niedriger. Minima der Schalengewichte im XDX-korrigierten Datensatz fallen während MIS3 mit den niedrigsten Temperaturen zusammen.

Von einem Tiefenschnitt auf dem Ontong Java Plateau (OJP) stammende Foraminiferenproben mit einem Spektrum an Erhaltungsgraden wurden mit zwei verschiedenen Methoden gereinigt: mit der „Mg-Methode" und der gründlicheren „Cd-Methode", die einen Reduktionsschritt beinhaltet und von der man annimmt, dass sie niedrigere Mg/Ca-Werte liefert (**Kapitel 7**). Rasterelektronenmikroskopie ergab, dass die Methode mit Reduktionsschritt die Schalenoberfläche anätzte, aber diese geringe Lösung führte nicht notwendigerweise zu geringeren Mg/Ca-Werten. Kein Unterschied zwischen den Reinigungsmethoden wurde bei Mg/Ca für *G. sacculifer* und *P. obliquiloculata* gefunden. Bei *G. ruber* (~4%) und *N. dutertrei* (~10%) führte der Reduktionsschritt zu geringeren Mg/Ca-Werten. Ein Mg/Ca-Versatz zwischen den beiden Methoden war unabhängig vom Erhaltungsgrad. Die Reinigung mit Reduktionsschritt ist die effektivere Methode. Proben, die mittels Mg-Methode gereinigt wurden, enthielten noch Coccolithen und andere Sedimentpartikel.

Eine schwache Korrelation bestand zwischen Probengewinn und $\Delta[CO_3^{2-}]$-Werten in Oberflächensedimenten; nur für die „Cd-Methode" bei *N. dutertrei* wurde eine signifikante Korrelation gefunden ($p < 0.05$). Maxima im analytischen Gewinn von *G. ruber* und *G. sacculifer* aus einem tiefen Sedimentkern [WIND 28K] fielen während Deglaziationen mit Phasen guter Erhaltung zusammen. Die Ergebnisse legen nahe, dass eine Messung des analytischen Gewinns eine erste Abschätzung für den Lösungsfehler bei Mg/Ca liefern kann.

TABLE OF CONTENTS

5. Calibrating computed tomography based dissolution index (XDX) to dissolution bias of Mg/Ca in planktonic foraminifera......................57

6. Calcite saturation, dissolution-corrected foraminiferal test mass and dissolution-corrected Mg/Ca reconstructed using XDX: a 150 ka record from the western Indian Ocean......................89

1. Introduction

1.1 Motivation

Although carbon makes up only 0.03 % of the mass of the Earth, it lies at the heart of the biological, geological and climatological cycles. Despite its importance, however, many aspects of the carbon cycle remain poorly understood. One example is the association between glacial cycles and atmospheric carbon dioxide (CO_2) levels.

Long before Antarctic drilling revealed that the saw-tooth pattern of ice volume fluctuations through time was similar to records of atmospheric CO_2 [*Petit et al.*, 1999; EPICA Community Members, 2004], the effect of atmospheric composition on glaciation was considered [*Tyndall*, 1861]. Methane (CH_4) and CO_2 act as greenhouse gases [*Arrhenius*, 1896], amplifying solar warming, and initial studies concluded that a rise in atmospheric CO_2 preceded ice melting [*Sowers and Bender*, 1995; *Broecker and Henderson*, 1998]. Recently, improved constraints on timing show that CO_2 does not initiate ice ages [*Stott et al.*, 2007; *Mudelsee*, 2001], leaving the triggers largely unexplained. The relationship between global temperature, CO_2 and the concurrent waxing and waning of the ice sheets, and the mechanisms that link these parameters, are amongst the unsolved mysteries of the Earth system [*Sigman and Boyle*, 2000, *Archer et al.*, 2000].

One key to understanding the links between the carbon and glacial cycles will come from studying patterns of carbonate preservation in deep sea sediments. These sediments contain a large part of the carbon available to react on timescales of thousands of years. Carbonate preservation at the sea-floor is to a large extent controlled by carbonate ion concentration ($[CO_3^{2-}]$) of the deep ocean, a property which is inversely proportional to the concentration of CO_2 in the atmosphere [e.g. *Broecker and Peng* 1982]. The transfer of carbon between deep ocean and atmosphere during a glacial cycle is reflected in the alternating light coloured, high carbonate, and dark, low carbonate, layers in deep sea

sediment cores, whereby low atmospheric CO_2 during a glacial is associated with good preservation of carbonate at the ocean floor [*Arrhenius*, 1952; *Farrell and Prell*, 1989].

An assessment of carbonate preservation is also important in another context. Many of the methods used to reconstruct past climate conditions, rely on chemical analysis of biogenic calcite. Partial dissolution of the carrier destroys the primary signal. Assessment of calcite preservation is therefore an important part of quality control for such proxy data.

This thesis describes the use of computed tomography (CT) to assess dissolution in foraminifera tests. The tests, or shells, of these marine protists make up a large part of the calcite deposited at the sea-floor [e.g. *Langer*, 2008]. Insight to their preservation state sheds light on both the functioning of the carbon cycle and whether proxies based on analysis of test calcite are likely to be biased by dissolution effects.

1.2 The carbon cycle and the glacial cycles

Large changes in the amount of ice, and hence temperature, on Earth is recorded in geological archives around the globe [e.g. *Waelbroeck et al.*, 2002, *EPICA Community Members*, 2004] illustrating a recurring pattern of ice sheet growth and retreat over the past eight hundred thousand years. The world gradually slid into glacial conditions as ice sheets slowly grew, but slow growth was followed by rapid ice retreat, as global temperature suddenly warmed.

The carbon cycle is involved in the transitions from cold to warm phases and back again. Most of the Earth's carbon is locked away in slow reacting reservoirs, such as the rocks of the crust. On glacial-interglacial timescales, it is the terrestrial biosphere, the atmosphere, the sediments of the ocean floor and the dissolved inorganic carbon (DIC) of the ocean which are the important reservoirs. Of these, the ocean is by far the largest, containing more than 90% of the carbon (**Figure 1.1**). This led *Broecker* [1982] to conclude that deep ocean carbonate chemistry must ultimately control the glacial cycles in atmospheric CO_2. For although global ice volume is fundamentally dependant on the variations in solar radiation reaching Earth [*Milankovich*, 1930], CO_2 concentration acts to modify the planet's temperature. The exact mechanisms controlling the feedbacks between CO_2 and warming are not fully established. The roles of the overturning circulation [*Ahn et al.*, 2008], North Atlantic deep water formation and Southern Ocean productivity and ventilation [e.g. *Peacock et al.*, 2006; *Anderson et al.*, 2009; *Skinner et al.*, 2010; *Sigman et al.*, 2010] are thought to play critical roles in explaining the interaction of atmospheric CO_2 and Earth temperature.

In the steady state with input and output fluxes balanced, the carbon system equilibrates between CO_2 in the atmosphere, inorganic carbon dissolved in seawater and calcite sediments at the ocean floor. A perturbation to the carbon system such as addition of CO_2 to the atmosphere, whether by natural or anthropogenic cause, initiates a sequence of events. CO_2 is water soluble and reacts with water to create a weak acid. Although carbonate ion (CO_3^{2-}) acts to buffer against changes in pH this capacity eventually wears out and the pH of the surface ocean (the part in contact with the atmosphere) is reduced.
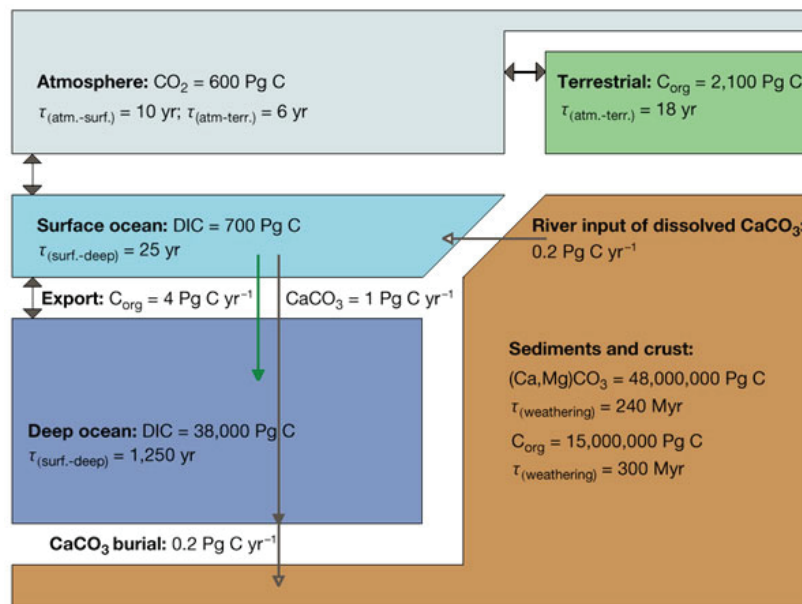
Figure 1.1 Pre-industrial carbon cycle (from *Sigman and Boyle*, 2000) showing the reservoirs and fluxes relevant on glacial/interglacial timescales. These are dissolved inorganic carbon (DIC), calcium carbonate ($CaCO_3$) and organic carbon (C_{org}). Residence time (τ) is reservoir size divided by input or output.

Once the surface ocean mixes down to the deep ocean, which takes about 1000 years [e.g. *Broecker and Peng*, 1982] it is buffered by a secondary system. Calcite contained in seafloor sediments dissolves. This increases the alkalinity (definition in **Section 1.3.1**) of deep ocean water, increasing its capacity to hold CO_2. CO_2 continues to be taken up by the ocean until a new steady state is reached with less carbon in atmosphere and more calcite in the deep ocean. The reorganisation of carbon between its reservoirs is recorded in sediments at the seafloor. The start of an ice age is marked by a reduction in carbonate preservation in the deep ocean, while preservation events mark deglaciations [*Broecker and Peng*, 1987; *Keir*, 1988].

1.3 Reconstructing the carbon and glacial cycles

Proxies exist to quantify many aspects of the carbon cycle and to track transfer of carbon between reservoirs. Gas trapped in ice cores records the amount of CO_2 and CH_4 in the atmosphere [*Petit et al.*, 1999; EPICA Community Members, 2004]. $\delta^{13}C$ analysis, of both ice-core gas and foraminiferal calcite, record the increased transfer of isotopically light ^{12}C from the terrestrial biomass into the ocean and atmosphere during glacial periods [*Shackleton,* 1977; *Shackleton and Vincent*, 1978; *Curry et al.*, 1988; *Broecker and Peng*, 1982; *Ganssen and Sarnthein*, 1983; *Kroon and Ganssen*, 1988; *Mortlock et al.*, 1991].The associated glacial cycle is recorded in the oxygen isotope composition of the ocean. The use of oxygen isotope ratios ($^{18}O/^{16}O$, expressed as $\delta^{18}O$) is the classic paleoceanographic proxy, having been applied and developed over several decades [e.g. *Urey*, 1947; *Shackleton*, 1974; *Bemis et al.*, 1998]. $\delta^{18}O$ represents global ice volume in its relationship with seawater salinity. Precipitation of water with a low $^{18}O/^{16}O$ ratio at the poles, and its segregation in the form of ice, means that $^{18}O/^{16}O$ of the remaining seawater reflects ice volume. Fractionation during calcification is temperature dependent in foraminifera, with low $^{18}O/^{16}O$ being favoured as temperature increases. The two fractionation effects are superimposed. Mg/Ca or alkenone based proxies can be used to estimate temperature and thus isolate salinity [*Mashiotta et al.*, 1999; *Elderfield and Ganssen*, 2000]. The recent development of paired isotope paleothermometry [*Ghosh et al.*, 2006] allows temperature estimates for situations where biogenic carriers are not available and may extend use of the technique.

Test weight of planktonic foraminifera has been suggested as a proxy for $[CO_3^{2-}]$ of ocean surface water [*Barker and Elderfield*, 2002] as, it is speculated, calcification responds to this parameter [*Bijma et al.*, 1999]. However, it is probable that other factors also influence test mass, possible candidates are temperature [*Gonzales-Mora et al.*, 2008], nutrient availability [*de Villiers*, 2004] and salinity [*Bassinot and Johnstone*, in prep.]. Test mass is altered by post-deposition dissolution, which destroys the surface water signal. For future development of test mass as a paleoceanographic proxy an independent measure of dissolution effect on test mass is necessary.

1.3.1 Reconstructing deep sea carbonate chemistry: carbonate ion and calcite saturation proxies

Because the deep ocean contains most of the carbon available to react on glacial-interglacial timescales, a record of the carbon chemistry of deep water is a particularly important part of piecing together the behaviour of the carbon cycle. Proxies used to reconstruct deep sea carbonate chemistry aim to reconstruct any of the various parameters

of the aqueous carbonate system. Proxies exist for pH, carbonate ion concentration ($[CO_3^{2-}]$) and for calcite saturation ($\Delta[CO_3^{2-}]$ or Ω, defined below).

Methods can be grouped into two categories; those based on trace metals incorporated into the tests of marine calcifiers during growth and those that are based on alteration of calcite after deposition on the sea-floor.

Methods based on trace metals incorporated into foraminifera tests

Several promising geochemical proxies are based on the incorporation of trace metals into foraminiferal calcite. The partitioning of trace metals such as Zn and Cd, U and B between seawater and foraminiferal calcite appears strongly dependant on the calcite saturation of the water [*McCorkle et al.*, 1995; *Yu and Elderfield,* 2007; *Marchitto et al.*, 2000; *Russell et al.*, 2004; *Marchitto et al.*, 2005]. Records of deep water saturation have been reconstructed using Zn/Ca [*Marchitto et al.*, 2005]. U/Ca responded to $[CO_3^{2-}]$ in two cultured planktonic species [*Russell et al.*, 2004] and may have application as a $\Delta[CO_3^{2-}]$ proxy in benthic foraminifera [*Raitzsch et al.*, in prep.]. However, there is a temperature effect on U/Ca [*Yu et al.*, 2008] which must be corrected for, as well as diagenetic effects [*H. Kuhnert* pers. com.; Appendix A in **Chapter 6**]. Temperature also influences B/Ca, a $[CO_3^{2-}]$ proxy which has the advantage over Zn/Ca and Cd/Ca that it covers a wider range of saturation states [*Yu and Elderfield,* 2007; *Tripati et al.*, 2009]. pH has been estimated for both deep and surface ocean using $\delta^{11}B$ of benthic [*Sanyal et al.* 1995] and planktonic foraminifera [*Hönisch and Hemming*, 2005]. This method has the advantage that it is not sensitive to $[CO_3^{2-}]$, but responds directly to pH. *Elderfield et al.* [2006] and *Raitzsch et a*l. [2008] demonstrated that Mg/Ca in benthic foraminiferal calcite is sensitive to $[CO_3^{2-}]$, which, while a hindrance to the use of Mg/Ca as a paleo-temperature proxy, could potentially trace $[CO_3^{2-}]$.

Methods based on an assessment of dissolution

The second category of methods to indicate deep water calcite chemistry relies on an evaluation of $CaCO_3$ dissolution at the sea-floor. Such methods include properties of the bulk sediment, such as percentage of $CaCO_3$, as well as assessment of dissolution of specific portions of the sediment [*Farrell and Prell*, 1989; 1991; *Broecker and Clark*, 1999]. A large part of the $CaCO_3$ fraction consists of foraminifera tests [e.g. *Langer*, 2008] and many methods exist to assess their preservation state [*Berger*, 1968, 1970; *Oba*, 1969; *Bé et al.*, 1975; *Thunell*, 1976; *Ku and Oba*, 1978; *Peterson and Prell*, 1985; *Hebbeln et al.*, 1990; *Le and Shackleton*, 1992; *Mekik*, 2006]. Before discussing in detail the effect on dissolution on foraminiferal tests, the next section discusses factors controlling carbonate dissolution at the seafloor.

Factors controlling seafloor dissolution

In contrast to most minerals, where solubility increases with increasing temperature, the dissolution reaction is exothermic in most carbonate minerals and high temperatures favour the solid phase over dissolved ions. Carbonate solubility is also pressure dependent; calcite, for instance, takes up less volume as Ca^{2+} and CO_3^{2-} ions rather than as solid calcite. Although solubility is not as sensitive to pressure as it is to temperature, the great pressure gradient between the shallow and the deep ocean exerts a strong control on solubility. CO_2 is also more soluble at increased pressure which decreases pH. In shallow parts of the ocean (above 3 km water depth), much of the carbonate produced in surface waters is preserved on the sea-floor. In the deep ocean, low temperature and high pressure means that water becomes undersaturated with respect to first aragonite and then, with increasing depth, calcite. Deep sea sediments (deeper than 5 km) contain little carbonate, being mostly composed of pelagic clays.

Further discussion of aspects which can affect calcite solubility requires a consideration of some features of seawater chemistry. References for this section are *Pilson* [1998] and *Zeebe and Wolf-Gladrow* [2001] and references therein. In the long term, the carbonate chemistry of seawater is controlled by the rock weathering cycle. A starting point from which to consider this cycle could be the solution of carbon dioxide (CO_2) in rainwater to produce a weak acid

$$CO_2 \text{ (gas)} + H_2O \rightarrow HCO_3^- + H^+ \rightarrow CO_3^{2-} + 2H^+$$

This acid acts to dissolve carbonate and silicate rocks on land bringing dissolved ions into the ocean. There is a slight excess positive charge from conservative (concentration unaffected by changes in temperature, pressure or pH) cations over the conservative anions which are transported to the ocean. This charge difference, which in typical modern seawater this is only ~0.3 % of the total positive charge, is one way of defining alkalinity.

Several components of seawater can dissociate to accommodate the excess charge. These include borate and phosphate species, but the most important in most natural waters is carbon. Dissolved inorganic carbon in the ocean equilibrates between its four forms: dissolved CO_2, HCO_3^- (bicarbonate ion), CO_3^{2-} (carbonate ion) and H_2CO_3 (carbonic acid). The main component of natural waters is HCO_3^- while CO_3^{2-} is a minor form. The reaction of CO_3^{2-} and H^+ means that $CaCO_3$ dissolves at relatively high pH values compared to silicates. Of the two major polymorphs of $CaCO_3$ aragonite (orthorhombic $CaCO_3$) and calcite (rhombohedral $CaCO_3$) calcite is the most stable and less soluble form. Aragonite is therefore much less abundant at the seafloor than calcite and further discussion refers to calcite.

Predictions about calcite solubility in seawater rely in the first instance on an assessment of calcite saturation of the water. The solubility product of $CaCO_3$, K_{SP} is defined as

$K_{SP} = [Ca^{2+}]$ SATURATION $* [CO_3^{2-}]$ SATURATION

Where [ ] SATURATION denotes concentration at saturation. Saturation state (Ω) of a particular water sample is

$\Omega = ([Ca^{2+}] [CO_3^{2-}])$ SAMPLE $/ K_{SP}$

The rock weathering responsible for delivering dissolved ions to the ocean is so slow that $[Ca^{2+}]$ of the open ocean is essentially constant over glacial-interglacial timescales, although there are minor regional differences due to salinity variations. Therefore $[CO_3^{2-}]$ is the important factor in defining saturation state and the equation above can be reduced to

$\Omega = [CO_3^{2-}]$ SAMPLE $/ [CO_3^{2-}]$ SATURATION

An alternative way to define calcite saturation state at a particular site, which is used in this thesis, is

$\Delta[CO_3^{2-}] = [CO_3^{2-}]$ SAMPLE $- [CO_3^{2-}]$ SATURATION

where $[CO_3^{2-}]$ SAMPLE is the measured value at a particular site and $[CO_3^{2-}]$ SATURATION is the theoretical value of saturation. This is calculated taking into account temperature and pressure (depth) at the site and the main contributors to alkalinity – the carbonate species (predominantly HCO_3^-, followed by CO_3^-) and total DIC with minor contributions from borate ($B(OH)_4^-$) and phosphate (HPO_4^{2-} and PO_4^{3-}) species.

Waters where $\Omega > 1$ ($\Delta[CO_3^{2-}] > 0$) are supersaturated with respect to calcite and waters where $\Omega < 1$ ($\Delta[CO_3^{2-}] < 0$) are undersaturated. The depth in the ocean where $\Omega = 1$ ($\Delta[CO_3^{2-}] = 0$) is referred to as the calcite saturation horizon.

Surface seawater is supersaturated with respect to calcite, in terms of Ω, by a factor of between 3 and 5. Yet it is unusual for calcite to freely precipitate in seawater, even when nuclei are present [*Morse and He*, 1993]. The reasons for this are still unclear although the presence of Mg^{2+} (at 53 mmol/kg Mg^{2+} is the 2nd most abundant cation in seawater after Na^+) may act as an inhibitor of crystal growth. Early calculations of calcite saturation were vastly improved with the discovery of the importance of ion pairing [*Garrels et al.*, 1961]. Ion pairing between Mg^{2+} and CO_3^{2-} reduces the CO_3^{2-} available to react with Ca^{2+} by more than 90%. Production of calcite in the surface ocean therefore generally relies on organically mediated precipitation, apart from some minor and occasional events such as the "whitings" in the shallow seas off the Bahamas.

Just as calcite does not precipitate from a supersaturated solution, calcite does not necessarily start to dissolve in waters undersaturated with respect to calcite. *Morse and Berner* [1972] established that dissolution rate D is a function of undersaturation (Ω) so that

D [% per day] $= k (1- \Omega)^n$

where k is the rate constant and n is the reaction order.

Establishing values for k and n was the subject of much work during the 1980s and 1990s, with no clear consensus on what the values might be. Early experiments with reagent grade calcite in artificial seawater [*Keir*, 1980] gave a very high value of n, of 4.5. In these experiments k was somewhat related to grain size, larger grain size generally having smaller k values. Later analysis, and recalculation of *Keir*'s [1980] results, gave a much lower reaction order of between 1 and 2 [*Hales and Emerson*, 1997]. This revised estimate was still not low enough to explain the difference in rate constants between field observations and laboratory experiments. Compared to reagent grade calcite in artificial seawater, biogenic carbonates at the seafloor dissolve much more slowly than expected. It seems that there are processes at the seafloor which inhibit dissolution of carbonates. One factor is that hydrophobic organic compounds are attracted to mineral surfaces and form a protective coating. Microbial activity has also been observed to physically inhibit calcite dissolution, as bacteria can inhabit dissolution pits and protect the surface from further dissolution. [e.g. *Lüttge and Conrad*, 2004].

Still other reactions at the seafloor enhance dissolution and cause calcite to dissolve even where waters are theoretically supersaturated with respect to calcite. Saturation state is estimated for a large area of water, whereas the sediment surface, sub-surface, and the inside of aggregates, are dynamic sites. In such micro-environments chemistry can deviate far from the saturation state calculated for overlying deep water.

A great deal of carbonate is dissolved at shallow depths, where waters are supersaturated with respect to calcite and the lysocline (the depth of intense dissolution for a particular species or mineral (e.g. foraminiferal lysocline, aragonite lysocline) is located at shallower depths than the calcite saturation horizon. One major offset between deep water and sediment pore waters is due to acidity produced by the oxidative decay of organic matter [*Parker and Berger*, 1971; *Berner*, 1977; *Emerson and Bender*, 1981; *Martin and Sayles* 1996]. Other factors include dissolution within the guts of epipelagic grazers [*Milliman et al.*, 1999] and microbial activity which consumes O_2 and produces CO_2. *Troy et al.* [1997] describes bacteria colonizing the surface of carbonate grains, in this instance causing local dissolution.

Within the sediment, dissolution is most intense at the base of the gas diffusion zone, usually some mm from the surface, where CO_2 can build up in porewaters. Physical factors such as flux and type of sediment control the depth of this zone. Fast burial or clay rich sedimentation can create a protective environment where carbonate particles are preserved [e.g. *Pearson et al.*, 2001]. Some anoxic reactions involving organic carbon degradation can also produce acidity. The electron acceptors of anaerobic degradation are reduced to forms (e.g. Mn^{2+}) which can later react with O_2 and produce protons.

Surface productivity therefore also plays a role in the carbonate content of sediments. Sediments underlying oligotrophic regions of the ocean contain mainly carbonate whereas high productivity areas such as upwelling zones or cold regions such as the Southern Ocean produce sediments low in carbonate. The ratio between organic and inorganic carbon exported to the seafloor may determine the fate of how much of the exported carbonate dissolves. It was even suggested that variation in rain ratio could account for glacial lowering of CO_2 [*Archer and Maier-Raymer*, 1994], but later work established that the calcite saturation horizon and the lysocline did not decouple [*Sigman et al.*, 1998; *Archer*, 1996]. One mechanism which may act as a buffer against productivity induced changes in sediment composition is that ballasting by biogenic calcite is necessary to transport organic material to the sea-floor [*Armstrong*, 2002]. If this were the case, a slight shift in productivity toward silicates would not significantly alter the rain ratio at the sea-floor but would merely alter the amount of organic matter recycled in the water column [*Barker et al.*, 2003a].

Effect of dissolution on foraminiferal tests and their use as a dissolution indicator

The selective nature of carbonate dissolution [*Murray*, 1897; *Schott*, 1935] can be exploited as a preservation indicator for biogenic carbonates such as foraminifera. Much work on the way that living foraminiferal assemblages are modified by dissolution was carried out in the 1960s and 1970s [*Ruddiman and Heezen*, 1967], a great deal of which being done by *Berger* [1968, 1970, 1971]. He assigned the sequence of dissolution susceptibility of tests based on experiments in the open ocean [*Berger*, 1970] and core-tops [*Berger*, 1968] and noted that thin tests of spinose surface dwelling forms, such as *G. ruber* and *G. sacculifer* disappeared first from assemblages while deep dwelling forms *N. dutertrei* and *P. obliquiloculata* were more resistant.

As well as altering species assemblages, dissolution alters the intraspecies population range. Thin chamber walls, such as that of the final chamber, are particularly susceptible to dissolution meaning that poorly preserved samples contain thicker forms for the same size fraction [*Berger*, 1970]. With increasing dissolution, tests develop holes and then break up into fragments. Many indices of dissolution are based on such assessments of

test damage, for instance the *G. menardii* fragmentation index [*Ku and Oba*, 1978]. Similar indices which compare test fragments for a given species to number of whole shells exist for other species [*Peterson and Prell*, 1985; *Le and Shackleton*, 1992].

Berger [1970] commented that transparent tests are found only in well-preserved assemblages, and suggested that tests become opaque due to surface etching. Damage and corrosion of test surfaces due to dissolution was more fully investigated by *Berner and Morse* [1974]. In a detailed study of samples from a depth transect on the Ontong Java Plateau *Bonneau* [1980] observed that the first signs of dissolution, such as etching, occurred in supersaturated waters. Below the calcite saturation horizon, dissolution was more pronounced, with the test pores being particularly vulnerable. *Bé* [1975] suggested using such markers to estimate release of $CaCO_3$ at the ocean floor and catalogued the breakdown of the outer layers of calcite. Such descriptive categories continue to be developed as dissolution indices [*Henrich et al.*, 1989; *Baumann and Meggers*, 1996; *Dittert and Henrich*, 2000].

Although *Bé* et al. [1975] found that in laboratory based dissolution experiments with *G. truncatulinoides* that the outer surface was first affected; they noted that for natural samples that the inner calcite appeared most vulnerable to dissolution. This was confirmed by *Brown and Elderfield* [1996] for *G. tumida,* another species with a thick outer crust which remained after the destruction of the inner calcite. The differing dissolution susceptibility of the inner and outer calcite lead *Lohmann* [1995] to suggest that test mass of a particular size fraction could be used to indicate dissolution, as size remained relatively constant while mass declined due to the destruction of the inner calcite. This index was further developed by *Broecker and Clark* [2001]. They estimated mass loss at 0.30 ±0.05 µg per µmol/kg change in $[CO_3^{2-}]$ for *G. sacculifer*, *N. dutertrei* and *P. obliquiloculata* from the 355-415 µm size fraction. This value was confirmed by *Rosenthal and Lohman* [2002] where mass loss for *G. sacculifer* in the 355-425 µm was 0.31 µg per µmol/kg. In the latter study, *G. ruber* from a smaller size fraction (212-300 µm) lost only 0.06 µg per µmol/kg. This has implications for choice of species as dissolution indicator. Fragile tests may not withstand much dissolution and forms that are more robust may record dissolution more effectively.

A major problem with dissolution based proxies is that dissolution happens mainly in the top few mm of the pore-waters and thus may not truly represent deep water chemistry (as described above). However, although proxies based on trace element analysis appear more sophisticated than those based on dissolution, they also have confounding factors associated with them. Species which live in the pore-water such as *Uvigerina* represent pore-water rather than deep water chemistry. Epifaunal species such as *C. wuellerstorfi*

may better represent deep water conditions [*Elderfield et al.*, 2006]. The major complication affecting trace metal incorporation into foraminiferal calcite is probably growth rate. *Russell et al.* [2004] attributes a growth rate effect to U/Ca of planktonic foraminifera in culture. Another source of uncertainty comes from the estimate of the element/Ca (Zn/Ca, B/Ca or U/Ca) ratio in seawater.

Mg^{2+} as control on dissolution

Impurities in the calcite lattice increase dissolution susceptibility. Mg^{2+} is the main trace element in marine carbonates and *Lorens and Willia* [1977] found that calcite with high Mg/Ca dissolved preferentially. Other studies confirm that Mg content of tests decreases in waters undersaturated with respect to calcite [*Hecht et al.*, 1975; *Lorens and Willia*,1977; *Puechmaille*, 1985; *Rosenthal and Boyle*, 1993; *Nürnberg et al.*, 1996; *Brown and Elderfield*, 1996; *Hastings et al.*, 1998; *Dekens et al.*, 2002; *Regenberget al.*, 2006]. *Brown and Elderfield* [1996] attributed dissolution above the calcite lysocline, i.e. in apparently supersaturated waters, to the greater susceptibility of Mg-rich calcite.

Such alteration of Mg/Ca at the seafloor can be a useful indicator of dissolution [*Rosenthal et al.*, 2000; *Fehrenbacher et al.*, 2006]. However, it is a major problem for the Mg/Ca paleotemperature proxy, leading to underestimation of Mg/Ca based temperatures. For this reason, several methods exist to assess the dissolution effect on Mg/Ca specifically (further detail in **Chapter 5**).
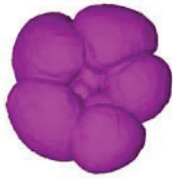
2. Specific objectives and outline of manuscripts

2.1 Specific Objectives

The objectives of this thesis are as follows:

(1) To develop a $\Delta[CO_3^{2-}]$ proxy based on appearance of foraminiferal dissolution in computed tomography (CT) scans

The preservation of carbonate at the sea-floor is, at least partially, controlled by calcite saturation of deep water, an important component of past carbon cycle reconstructions. The tests of planktonic foraminifera make up a significant proportion of sea-floor carbonate sediments [e.g. *Langer*, 2008] and their preservation state provides an estimate of carbonate preservation generally. The inner test is the area most susceptible to dissolution in planktonic foraminifera [*Lohmann*, 1995; *Brown and Elderfield*, 1996]. The imaging technique of CT allows an insight to the inner test structure, and thus, potentially, preservation state.

(2) To develop a method of correcting for the effects of dissolution on test mass

Test mass decreases as the test dissolves and therefore mass can offer a useful measure of preservation state [*Lohmann*, 1995; *Broecker and Clark*, 2001; *Rosenthal and Lohmann*, 2002]. However, environmental conditions influence the initial mass of the test [*Barker and Elderfield*, 2002; *de Villiers*, 2004; *Gonzales-Mora et al.*, 2008]. It is therefore important to be able to separate initial mass from secondary dissolution effects.

(3) To explore whether sensitivity of Mg/Ca to dissolution is similar between ocean basins

Mg/Ca in the tests of planktonic foraminifera is decreased by partial solution of tests at the sea-floor [*Hecht et al.*, 1975; *Lorens and Willia*,1977; *Puechmaille*, 1985; *Rosenthal*

and Boyle, 1993; *Nürnberg et al.*, 1996; *Brown and Elderfield*, 1996; *Hastings et al.*, 1998; *Dekens et al.*, 2002; *Regenberget al.*, 2006]. Use of dissolution proxies to correct for dissolution bias in Mg/Ca relies on a consistent response of Mg/Ca to dissolution.

(4) To develop a method of correcting for the effect of dissolution on Mg/Ca

As the paleotemperature proxy based on Mg/Ca of foraminiferal calcite becomes increasingly routinely used, methods are required to estimate dissolution effects on this paleoceanographic proxy.

(5) To create a record of $\Delta[CO_3^{2-}]$, dissolution-corrected test mass and dissolution-corrected Mg/Ca-derived temperatures for a sediment core spanning a full glacial cycle

Application of the above methods to a down-core record should demonstrate their utility.

(6) To discover if the offset in Mg/Ca between samples prepared for analysis using the Cd-cleaning and Mg-cleaning methods is sensitive to sample preservation state

Of the two preparation methods for Mg/Ca analysis, it is generally accepted that Cd-cleaning (which includes a reductive cleaning step) [*Boyle*, 1981; Martin et al, 2002] is more aggressive than Mg-cleaning [*Barker et al.*, 2003b] and results in lower Mg/Ca values. This is usually attributed to dissolution caused by the reductive cleaning reagent [*Barker et al.*, 2003b; *Rosenthal et al.*, 2004; *Yu et al.*, 2007]. The question has been raised of whether the offset in Mg/Ca between the two cleaning methods decreases for poorly preserved samples where Mg/Ca has already been decreased due to seafloor dissolution [*Barker et al.*, 2003b].

(7) To investigate whether analytical yield relates to preservation state of foraminiferal samples

Sample preparation before Mg/Ca analysis has a high attrition rate where, typically, a significant minority of the sample is lost during cleaning. There is anecdotal evidence that fragile, poorly preserved samples are more difficult to retain during cleaning [*M. Greaves*, pers. com.]. If a correlation between preservation state and yield exists, then monitoring yield could be developed as a measure of quality control for this procedure.

2.2 Strategy, samples and outline of studies

In order to meet these objectives, the following studies were carried out:

Objectives 1 and 2

Chapter 4: **Inside story: An X-ray microtomography method for assessing dissolution in the tests of planktonic foraminifera**

[*H.J.H Johnstone, M. Schulz, S. Barker and H. Elderfield*]

(Accepted for publication in *Marine Micropaleontology*)

This study describes the use of CT to investigate dissolution in the tests of foraminifera. It is known that dissolution first affects the inside of the tests of planktonic foraminiferal [*Lohmann* 1995; *Brown and Elderfield,* 1996]. The technique offers an insight to the inner test structure and the preservation state of tests. Surface samples (core-tops) from sites in the Pacific, Atlantic and Indian Oceans were used to try to eradicate local offsets between $\Delta[CO_3^{2-}]$ of pore waters and that of overlying deep water. Four species of foraminifera (*G. ruber, G. sacculifer, N. dutertrei* and *P. obliquiloculata*) were used to represent a range of morphotypes, initial test mass and initial Mg/Ca, the latter because Mg^{2+} content may control on dissolution susceptibility [*Brown and Elderfield,* 1996].

Calcite saturation ($\Delta[CO_3^{2-}]$) of the 33 sites ranged from 55 μmol/kg to -23 μmol/kg to allow examination of the full range of test preservation. CT scans were compared to $\Delta[CO_3^{2-}]$ in order to establish a dissolution index based on the appearance of dissolution stages in the scanned images.

CT scanning offers the advantage that it is non-destructive. Scanned samples, for which dissolution has been assessed, can be later used for chemical analysis. The same set of samples were used in the follow up study:

Chapter 5: **Calibrating computed tomography based dissolution index XDX to dissolution bias of Mg/Ca in planktonic foraminifera**

[*H.J.H. Johnstone, M. Schulz, J. Yu and H. Elderfield*]

(Revised for *Paleoceanography*)

Samples from the Pacific, Atlantic and Indian Oceans allowed comparison of sensitivity of Mg/Ca to $\Delta[CO_3^{2-}]$ at different sites. The next step was to compare Mg/Ca to the stages of dissolution identifiable in CT images in order to create an independent measure of dissolution bias in Mg/Ca based temperatures.

Chapter 6: **Calcite saturation, dissolution-corrected foraminiferal test mass and Mg/Ca reconstructed using XDX - a 150 ka record from the western Indian Ocean**

[*H.J.H. Johnstone, M. Schulz, T. Kiefer and H. Elderfield*]

(To be resubmitted to *Geochemistry, Geophysics, Geosystems* after the comments of the reviewers have been taken into account)

Methods developed in **Chapters 5** and **6** require testing by application to a sediment core record. Core WIND28K was selected for several reasons. It represents a deep site, 4150 m, in the western Indian Ocean which should be well placed to record transfer of carbon between ocean and atmosphere on glacial-interglacial timescales. The core represents 150 ka and covers a full glacial cycle, including two deglaciations. Additionally, a Mg/Ca-based temperature record had been published for part of the core [*Kiefer et al.*, 2006], in which it was recognized that, due to the situation of the core in waters undersaturated with respect to calcite, it was likely that calculated temperatures were biased by dissolution effects.

Chapter 7: **Effect of preservation state of planktonic foraminifera tests on the decrease in Mg/Ca due to reductive cleaning and on analytical yield**

[*H.J.H. Johnstone, W. Lee, T. Kiefer, M. Schulz and H. Elderfield*]

(To be resubmitted to *Paleoceanography* after the comments of the reviewers have been taken into account)

In order to test the effect that preservation state makes to the offset in Mg/Ca due to reductive cleaning samples from a depth transect on the Ontong Java Plateau were cleaned using both methods.

Core-top samples from the Ontong Java Plateau also allowed comparison of $\Delta[CO_3^{2-}]$ to analytical yield in order to test whether yield has any potential as an indicator of calcite preservation. To explore the relationship between yield and preservation in a sediment core, analytical yield of core WIND28K was examined.
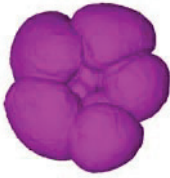
3. Methods

3.1 Computed Tomography (CT)

Computed tomography (named from tomos; slice, graph: write) is a non-destructive method of mapping slices through solid objects. There are two steps to the creation of tomographic slices (**Figure 3.1**).
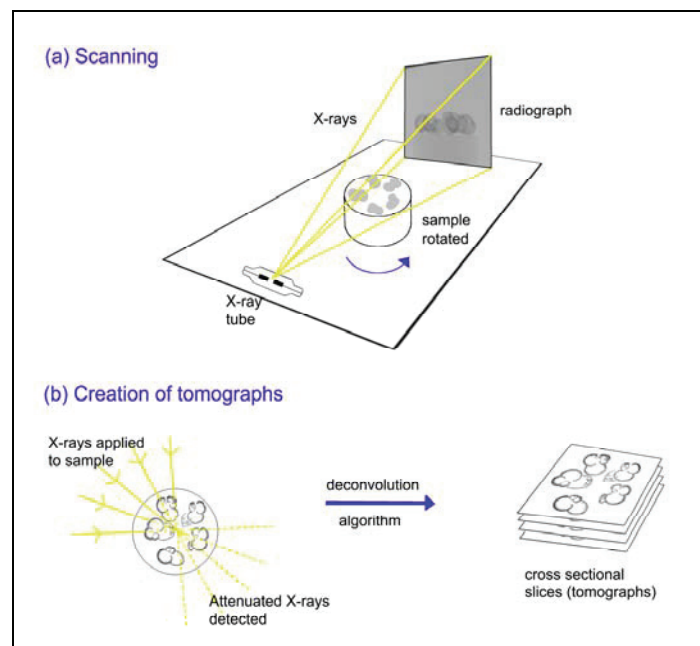
Figure 3.1 Computed tomography (CT) system.

(a) X-rays pass through a sample placed on a rotating stage to produce radiographs from a succession of angles (b) Cross sectional slices are created mathematically from the radiographs using filtered back projection to deconvolve the X-ray attenuation data for each point. Tomographs are maps of X-ray density.

Firstly a series of X-ray images are taken of a sample as it is rotated. The attenuation of X-rays by a sample depends on its density as well as thickness and the arrangement of the material. The mathematics for deconvolving, or back projecting, such a series of X-ray density values was developed well before any practical application was possible [*Radon*, 1917 cited in *Webb*, 1988]. Most modern systems use filtered back projection to increase image sharpness and are based on algorithms developed by *Cormack* [1963, 1964, 1974]. **Figure 3.2** shows reconstructed slices of a sacculifer test.

The technique was originally conceived for use in medicine and the first clinical demonstrations were carried out in the early 1970s [*Ambrose and Hounsfield*; 1972, 1973; *Hounsfield*, 1973]. The utility of the method was quickly apparent and Godfrey Hounsfield and Allan Cormack shared the 1979 Nobel Prize in medicine. Since then CT (computed tomography) (also known as CAT [computed axial tomography]) scans have come into increasingly routine use.
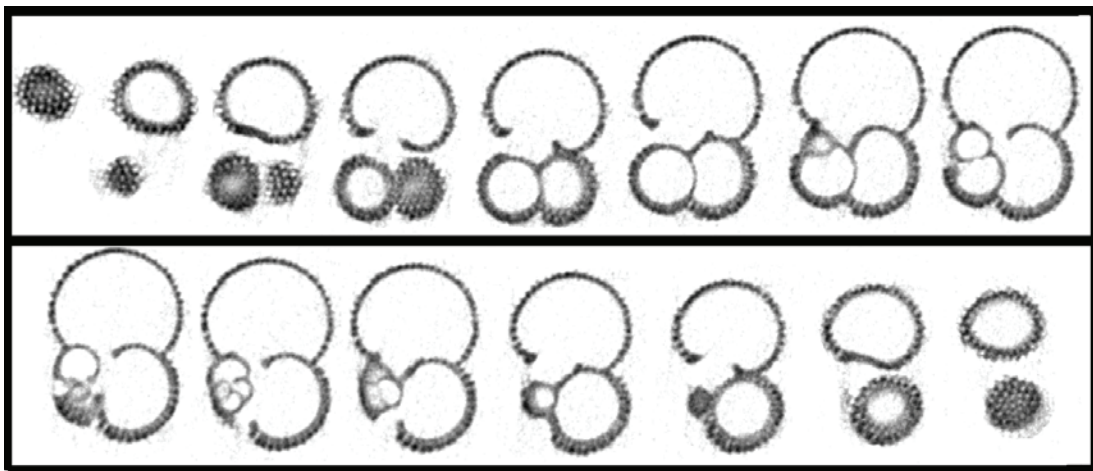
Figure 3.2: A series of progressive CT 'slices' (top left to bottom right) of a well-preserved test of *G. sacculifer*. The test is approximately 0.5 mm long.

Resolution improved continuously in the following decades and the method starts to revolutionise other fields, specifically where, as in medicine, it is required that samples should not be damaged by the imaging process. CT contributes to materials testing, archeology and in particular paleontology – where, for example, scanning offers digital recording of collections (e.g. the Digimorph project [www.digimorph.org]) or study of foraminifera morphology [*Speijer* et al., 2008].

The next advance in the method is the use of a synchrotron source. Due to the much narrower X-ray beam, synchrotron tomography now has sub-micron resolution. This

promises further insights to the natural world and first results from studies of fossil embryos were published in *Nature* [*Donoghue et al.*, 2006].

The tomography system used in this thesis is a Skyscan 1072 desktop system [*Van Dyck and Sasov*, 1998; *Sasov and Van Dyck*, 1998]. It uses a point source to create X-rays which fan out to act on a linear array of detectors. The resolution of ~8 μm is enough to image the inner chamber walls of planktonic foraminifera. CT images of the foraminiferal species used in the studies presented here are online at www.marum.de/en/Foraminifera_imaging_using_micro-CT. Further details of scanning method are given in **Chapter 4**.

3.2 Mg/Ca paleothermometry

The use of Mg/Ca (the ratio of millimoles of Mg to moles of Ca) in foraminiferal calcite to estimate the temperature of past oceans is an increasingly important method in paleoceanography. An advantage of the method is that $\delta^{18}O$ and temperature can be established for the same biotic carrier, allowing calculation of salinity by removal of the temperature effect on $\delta^{18}O$ [e.g. *Mashiotta et al.*, 1999; *Elderfield and Ganssen*, 2000].

Mg/Ca paleothermometry is based on the temperature dependant substitution of Mg for Ca in foraminiferal calcite. The partition coefficient of Mg into foraminferal calcite is an order of magnitude less than for inorganic precipitates, but the sensitivity is greater, at ~10% per $^{\circ}C$ for foraminifera compared to ~3% per $^{\circ}C$ for inorganic calcite [*Katz*, 1973; *Mucci*, 1987; *Lea et al.*, 1999]. Foraminifera apparently modify the seawater from which they calcify in an internal reservoir [*Elderfield et al.*, 1996; *Bentov and Erez*, 2005, 2006]. Some ions, such as Ca^{2+}, are concentrated while Mg^{2+} is removed, altering the typical molar ratio of Mg/Ca of ~5 in modern seawater to values between 1 and 5 mmol/mol in foraminiferal calcite.

The correspondence between Mg content of foraminiferal tests and temperature has been known for some time. [*Chave*, 1954] described that Mg content decreased with latitude. The greater Mg content of subtropical compared to polar species, and lower Mg of deep-dwelling compared to surface-dwelling forms [*Savin and Douglas*, 1973; *Bender et al.*, 1975] was also recognized. Other work suggested that environmental parameters besides temperature, for instance light, nutrient availability and growth rate, also control Mg/Ca content of tests [*Krinsley*, 1960; *Duckworth*, 1977; *Cronblad and Malmgren*, 1981; *Delaney et al.*, 1985; *Izuka*, 1988]. However, later studies of cultured foraminifera [*Nürnberg et al.*, 1996; *Lea et al.*, 1999; *Mashiotta et al.*, 1999], samples from core tops [*Nürnberg*, 1995; *Rosenthal et al.*, 1997; *Hastings et al.*, 1998; *Lea et al.*, 1999] and

sediment traps [*Anand et al.*, 2003] established that temperature acts as a primary control on Mg/Ca. Ambient salinity [*Nürnberg et al*., 1996] and carbonate ion concentration [*Elderfield et al*., 2006; *Raitzsch et al*., 2008] are amongst the secondary controls. The effect of post-depositional dissolution on Mg/Ca is a major problem for application of this proxy [*Hecht et al*., 1975; *Lorens and Willia*,1977; *Puechmaille*, 1985; *Rosenthal and Boyle*, 1993; *Nürnberg et al*., 1996; *Brown and Elderfield*, 1996; *Hastings et al*., 1998; *Dekens et al*., 2002; *Regenberget al*., 2006] (further described in **Chapter 5.1**).

There are two methods of cleaning samples before analysis in common use; both derive from *Boyle* [1981]. In this thesis these are referred to as Mg-cleaning (also known as "oxidative cleaning"), described in *Barker et al*. [2003b] and Cd-cleaning (also known as "reductive cleaning"), based on *Martin et al*. [2002]. **Chapter 7** explores the offset in Mg/Ca between the two cleaning methods for poorly preserved samples. In the other studies involving Mg/Ca in this thesis (**Chapter 5, Chapter 6**) Mg-cleaning [*Barker et al*., 2003b] was used. After cleaning tests are dissolved and analyzed. Mg/Ca values presented in **Chapters 5** and **6** were obtained using OES (Optical Emission Spectrophotometry) at the University of Bremen and ICP-MS (Inductively Coupled Plasma - Mass Spectrometry) at the Godwin Laboratory, University of Cambridge [*Yu et al*., 2005].
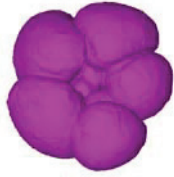
4. Inside story: an X-ray micro-tomography method for assessing dissolution in the tests of planktonic foraminifera

H.J.H Johnstone[1], **M. Schulz**[1], **S. Barker**[2] **and H. Elderfield**[3]

1 MARUM – Center for Marine Environmental Sciences, University of Bremen, Leobener Straße, 28359 Bremen, Germany

2 School of Earth and Ocean Sciences, Cardiff University, Cardiff CF10 3YE, UK

3 Godwin Laboratory for Palaeoclimate Research, Department of Earth Sciences, University of Cambridge, Cambridge CB2 3EQ, UK

_____

_____

Abstract

X-ray computed tomography (CT) provides an insight into the progression of dissolution in the tests of planktonic foraminifera. Four species of foraminifera (*G. ruber* [white], *G. sacculifer*, *N. dutertrei* and *P. obliquiloculata*) from Pacific, Atlantic and Indian Ocean core-top samples were examined by CT and SEM. Inner chamber walls began to dissolve at $\Delta[CO_3^{2-}]$ values of 12-14 µmol/kg. Close to the calcite saturation horizon, dissolution and precipitation of calcite may occur simultaneously. Inner calcite of *G. sacculifer*, *N. dutertrei* and *P. obliquiloculata* from such sites appeared altered or replaced, whereas outer crust calcite was dense with no pores. Unlike the other species, there was no distinction between inner and outer calcite in CT scans of *G. ruber*. Empty calcite crusts of *N. dutertrei* and *P. obliquiloculata* were most resistant to dissolution and were present in samples where $\Delta[CO_3^{2-}] \approx$ -20 µmol/kg. Five stages of preservation were identified in CT scans, and an empirical dissolution index, XDX, was established. XDX appears to be insensitive to initial test mass. Mass loss in response to dissolution was similar between species and sites at ~0.4 µg per µmol/kg. We provide calibrations to estimate $\Delta[CO_3^{2-}]$ and initial test mass from XDX.

4.1 Introduction

Variations in atmospheric CO_2 content on glacial-interglacial timescales are ultimately driven by the carbonate ion ($[CO_3^{2-}]$) content of the deep ocean [*Broecker and Peng*, 1982, 1987; *Sundquist and Broecker*, 1985*; Broecker and Maier-Reimer*, 1992]. Because so many processes may play a role in controlling deep ocean $[CO_3^{2-}]$ [review by *Archer et al.*, 2000], many attempts to reconstruct deep water chemistry focus on an assessment of carbonate dissolution in sediments.

Fluctuations in carbonate preservation have been reconstructed from direct measurements of carbonate content of sediment cores [*Farrell and Prell*, 1989; 1991]. Other properties of bulk sediment such as colour, or proportion of coarse to fine fraction carbonate [*Broecker and Clark*, 1999], can also indicate preservation state. However, properties of carbonates preserved in sediments reflect processes at the sea surface as well as those at the seafloor. Many processes in the surface ocean influence the quantity and character of carbonate in sediments. A change in productivity, or a shift in ecosystem toward or away from carbonate producing species, not only alters the amount of carbonate produced, but also the efficiency with which the various biological phases are transported to the deep

ocean [*Passow and de la Rocha*, 2007]. Dilution of carbonates by silicates and terrigenous materials attenuates the carbonate signal.

In addition to direct controls on carbonate export, conditions in the surface ocean also indirectly affect the nature of carbonates found in sediments. Properties of the sediment flux control susceptibility of carbonates to dissolution, thus modifying the relationship between deep water calcite saturation ($\Delta[CO_3^{2-}]$) and carbonate dissolution. Particle size has a strong effect on carbonate solubility [*Keir*, 1980]. Bioturbation and rain rate control the exposure time of carbonates to deep water sufficiently that accumulation rates can increase despite decreased deep water calcite saturation [*Archer*, 1991]. Above the calcite saturation horizon, acidity produced by the oxidation of organic material within sediments is the most significant cause of carbonate dissolution [*Parker and Berger*, 1971; *Berner*, 1977; *Martin and Sayles* 1996; *Emerson and Bender*, 1981]. A change in the ratio of organic to inorganic carbon arriving at the seafloor alters dissolution intensity [*Archer and Maier-Raimer*, 1994].

The tests of planktic foraminifera make up a significant part of the inorganic carbon exported from the surface ocean and deposited on the seafloor [*Langer*, 2008]. The preservation state of the calcite tests can be used to monitor carbonate dissolution. Many semi-quantitative ways of assessing the preservation state of tests have been developed since *Arrhenius* [1952] compared the ratio of complete tests to fragments. Similar fragmentation indices have been developed for various species [*Berger,* 1968; *Oba*, 1969; *Bé et al*., 1975; *Ku and Oba*, 1978; *Thunell*, 1976; *Hebbeln et al*., 1990; *Mekik*, 2006]. Other indices include the relative abundance of dissolution resistant and dissolution susceptible species [*Berger*, 1970]; the ratio of benthic to planktic tests [*Metzler et al*., 1982] and the abundance of organic linings of certain types of benthic foraminifera, preserved after the calcite test has dissolved [*Le and Shackleton*, 1992; *de Vernal et al*., 1992]. There are also scanning-electron microscopy methods which relate corrosiveness of deep water to breakdown of the test surface [*Henrich et al*., 1989, *Dittert and Henrich*, 2000]. However, because dissolution is initiated on the inside of the test [*Brown and Elderfield*, 1996] the outer appearance may not be sensitive to the first signs of alteration.

The susceptibility of inner calcite to dissolution means that tests become lighter while test size remains fairly constant [*Lohmann*, 1995]. The simplest way to quantify dissolution is to weigh the tests and test mass has been used to reconstruct changes in deep ocean $[CO_3^{2-}]$ [*Broecker and Clark* 2001, 2002]. This approach works well over constrained areas but it is complicated by the fact that environmental conditions such as nutrient availability [*de Villiers*, 2004] or temperature influence the thickness of the test walls and therefore the initial mass of the test.

Another consideration, receiving increased attention at the moment in light of increasing atmospheric CO_2 and consequent acidification of the surface ocean, is that the $[CO_3^{2-}]$ of the waters where foraminifera form may control how much they calcify, as first reported by *Herron-Allen* [1915]. The association between $[CO_3^{2-}]$ and test mass has been corroborated by more recent evidence. *Spero et al.* [1997] and *Bjima et al.* [1999] found that *Orbulina universa* in culture experiments responded to increased $[CO_3^{2-}]$ by increased calcification. *Barker and Elderfield* [2002] found test mass increased in parallel with $[CO_3^{2-}]$ for *G. bulloides* in the Atlantic and there are now several records which show changes in shell mass reflecting glacial-interglacial cycles [e.g. *Barker et al.*, 2004]. The potential use of test mass as a proxy for surface water $[CO_3^{2-}]$ requires development of a method which reliably indicates the extent to which foraminiferal mass is biased by dissolution, in order to distinguish the effect of surface water $[CO_3^{2-}]$ on initial test mass from the effect of deep water $\Delta[CO_3^{2-}]$ post-mortem.

In this study we use the imaging technique of X-ray computed tomography (CT) to examine foraminifera tests from core-top samples from sites with a range of $\Delta[CO_3^{2-}]$. The method allows observation of the test interior and so provides a new insight into the progression of dissolution.

4.2 Samples and methods

4.2.1 Foraminifera species

Four species of planktonic foraminifer were examined: *Globigerinoides ruber* [*d'Orbigny*, 1839] (white variety); *Globigerinoides sacculifer* [*Brady*, 1877] (without a sac-like final chamber); *Neogloboquadrina dutertrei* [*d'Orbigny*, 1839] and *Pulleniatina obliquiloculata* [*Parker and Jones*, 1865]. Their resistance to dissolution, according to the categorisation of *Berger* [1970], increases along with their depth habitat. The surface dweller *G. ruber* was rated 'very susceptible' to dissolution, ranking first out of the 22 species rated by *Berger* [1970]. Like *G. ruber*, *G. sacculifer* also lives in the mixed layer; it was described as 'susceptible' by *Berger* [1970] (5 out of 22). The thermocline dwellers *N. dutertrei* (16 out of 22) and *P. obliquiloculata* (18 out of 22) are considered 'resistant' to dissolution.

4.2.2 Calcite saturation

CT scans of foraminifera tests were compared to calcite saturation ($\Delta[CO_3^{2-}]$) of the water overlying the core-tops. $\Delta[CO_3^{2-}]$ is defined as:

$$\Delta[CO_3^{2-}] = [CO_3^{2-}]_{\text{IN SITU}} - [CO_3^{2-}]_{\text{SATURATION}}$$

i.e. the difference between the measured carbonate concentration ($[CO_3^{2-}]_{\text{IN SITU}}$) and the calculated theoretical value of calcite saturation ($[CO_3^{2-}]_{\text{SATURATION}}$) [e.g. *Berger et al.*, 1982].

$\Delta[CO_3^{2-}]$ was calculated by the CO2SYS program [*Pelletier et al.,* 2005] using GLODAP [*Key et al*., 2004] and World Ocean Atlas (WOA) [*Locarnini et al*., 2006] data according to the method in *Yu and Elderfield*, [2007]. The depth where $\Delta[CO_3^{2-}]$ is zero is defined as the calcite saturation horizon. This often coincides with the foraminiferal lysocline, the depth where dissolution becomes apparent in foraminifera.

4.2.3 Details of core-tops

The main sample set used in this study was collected from the Ontong Java Plateau (OJP) in the Pacific. This has become a classic area for studying the effects of dissolution [e.g. *Berger*, 1970; *Bonneau et al*., 1980; *Hebbeln et al*., 1990; *McCorkle et al.,* 1995; *Dekens et al*., 2002] due to there being little seasonal temperature variation and small geographical range over a depth transect spanning the calcite saturation horizon. In order to study foraminifers exposed to water with a wide range of calcite saturation states we also used core tops from the Mid-Atlantic Ridge, the Caribbean and the Ceara Rise in the Atlantic. From the Indian Ocean box cores from the Ninety-East Ridge and from part of the WIND cruise transect [*McCave*, 2001] along the East of Madagascar were used. The core-tops, where dated, are Holocene in age. Due to low sedimentation rates some samples from the Indian Ocean date from the early Holocene. **Table 4.1** summarizes details of the cores.

4.2.4 Sample preparation

Samples prepared from fresh sediment (Caribbean, Mid-Atlantic Ridge and Ceara Rise core-tops) were placed in jars with deionised water. Jars were shaken overnight. Samples were then sieved and thoroughly rinsed in deionised water. Foraminifera were picked from the 300 - 355 µm size fraction. A large sample (ideally 70 - 100 tests) was weighed on a microbalance to obtain average test mass.

4.2.5 X-ray computed tomography (CT) scanning

Computed tomography uses X-rays to produce images of an object from many different angles. The X-ray attenuation calculated from these 'shadow images' is used to create virtual cross-sectional slices through the object showing details of the inner structure. The greyscale values of the images are maps of the X-ray density, a property which depends both on the mineral density (atomic number) and the arrangement of the material (thickness and microporosity).

Core	Water depth	lat [°N]	long [°W]	Core type	Depth in core [cm]	Δ[CO₃²⁻] [μmol/kg]	Age [year]
OJP							a
1BC3	1616	-2.2	-157.0	box core	0-5	13.8	
1.5BC33	2015	-1.0	-157.9	box core	0-5	9.3	
2BC13	2301	0.0	-158.9	box core	0-5	4.9	
2.5BC37	2445	0.0	-159.5	box core	0-5	4.3	
3BC16	2959	0.0	-160.5	box core	0-5	-2.2	
3BC24	2965	0.0	-160.4	box core	0-5	-2.3	
4BC51	3411	0.0	-161.0	box core	0-5	-5.8	
4.5BC53	3711	0.0	-161.4	box core	0-5	-11.8	
5BC54	4025	0.0	-161.8	box core	0-5	-14.7	
5.5BC58	4341	0.0	-162.2	box core	0-5	-22.4	
6BC74	4438	0.0	-162.7	box core	0-5	-22.9	
BC66	4400	0.0	-162.7	box core	0-5	-23.0	
Caribbean Sea							
M35014	1604	17.8	63.7	multi-core	0-2	54.8	
M35010	2696	18.9	64.1	multi-core	0-2	40.9	
M35026	3815	17.5	67.0	multi-core	0-2	12.1	1,175 b
M35024	4710	17.0	66.0	multi-core	0-2	3.6	
Ceara Rise							
GeoB1503	2298	2.3	30.7	multi-core	0-2	43.6	
GeoB4415	3584	5.9	45.0	multi-core	0-2	22.2	
GeoB4416	3903	5.7	45.1	multi-core	0-2	18.6	
GeoB4406	3709	5.1	43.8	multi-core	0-2	16.2	
GeoB4413	4291	6.1	44.2	multi-core	0-2	5.1	
GeoB4403	4503	6.1	43.4	multi-core	0-2	-2.5	
Mid-Atlantic Ridge							
GeoB4420	2763	16.5	46.5	multi-core	0-2	35.5	
GeoB4421	3176	17.0	46.0	multi-core	0-2	27.8	
GeoB4424	4779	18.2	44.0	multi-core	0-2	-8.9	
Western Indian Ocean							c
WIND 11B	2382	-28.5	-48.2	box core	0-2	16.5	
WIND 20B	2274	-20.1	-49.2	box core	0-2	14.7	
WIND 10B	2871	-29.1	-47.5	box core	0-2	11.3	
WIND 33B	3520	-11.2	-58.8	box core	0-2	-3.6	
WIND 5B	3684	-31.6	-47.6	box core	0-2	-2.0	
WIND 25B	3935	-11.8	-50.6	box core	0-2	-10.2	
WIND 23B	4004	-13.1	-51.0	box core	0-2	-12.4	
WIND 13B	4065	-23.9	-49.0	box core	0-2	-13.0	
WIND 28B	4147	-10.2	-51.8	box core	0-2	-11.6	
WIND 6B	4150	-31.3	-47.6	box core	0-2	-13.5	
WIND 12B	4196	-25.8	-47.9	box core	0-2	-17.6	
Ninety-East Ridge, Indian Ocean							
V29-9	2900	-2.9	-89.1	box core	5	7.6	
RC14-33	3810	-2.4	-90.0	box core	3	-5.1	
RC14-31	3860	-9.0	-88.6	box core	3	-7.0	

a Core tops from the OJP covering a similar geographic and depth range as the ones used here, have been dated to between 3 and 6 ka [*Barker et al.,* 2007; *Dekens et al.,* 2002]

b *Schmuker* [2000] cited in *Regenberg* [2006]

c WIND coretops range in age from between 5,500 and 11,900 years T. Kiefer and I.N. McCave, pers. com.

Table 4.1 Details of the core-tops used in this study

Foraminifera were scanned using a Skyscan 1072 micro-CT desktop scanner [*Van Dyck and Sasov*, 1998; *Sasov and Van Dyck*, 1998]. This system uses an air-cooled point X-ray source and gives a resolution of ~7 μm in the scanned cross-section. Scans are sufficiently high resolution to show all but the very smallest inner chambers of foraminifera tests and while not resolving the pores completely, their presence or absence can be detected.

CT scanning was carried out at the Department of Earth Sciences, University of Cambridge. Tests were glued to the sample holder using water soluble glue so that they could be afterwards recovered. Tests were scanned in small batches of 8 to10 tests. They were carefully arranged so that, as far as possible, they did not touch each other and the apertures faced in the same direction. All samples were scanned under the same conditions: anode voltage was set at 80kV and the rotation step was 0.9^{o}. A 0.5 mm Al filter was used to cut out the softest X-rays and therefore reduce beam hardening effects. Exposure time was 4.5 seconds which gave a total scan time of around 50 minutes.

Cross-sections were reconstructed by Skyscan's own software which uses the Feldkamp cone-beam algorithm [*Feldkamp et al*., 1984]. A 10 % beam hardening correction was applied to reduce this artefact. The threshold values for the greyscale of the reconstructed slices were kept constant (scan value 0.010 was set to colour 255 [white]; value 0.150 set to colour 0 [black]) so that samples could be compared to one another. For image analysis the free software ImageJ [*Rasaband*, 1997] was used as well as the Skyscan Company's own analysis software, CTan. After CT scanning, some samples were further examined by SEM (scanning electron microscopy) at University of Bremen.

4.3 Progression of dissolution in the tests of planktonic foraminifera

4.3.1 Observations from CT and SEM

Most of the tests examined here had already undergone at least minor diagenesis. They had been altered from 'glassy' transparent tests to 'frosty' white ones. Glassy tests were abundant in samples from shallow sites on the Ceara Rise and in the Caribbean where $\Delta[CO_3^{2-}]$ values were greater than 40 μmol/kg. Although glassy tests often had thin walls, particularly *G. ruber*, they appeared well preserved. Many tests of *G. ruber* retained their spines. Another indication of the excellent preservation of these samples was the presence of aragonitic pteropods. Tests from these highly oversaturated sites were firm and resistant to being crushed. CT scans gave a very dark, sharp image where the inner chambers walls were clearly delineated and the pores of the outer wall apparent.
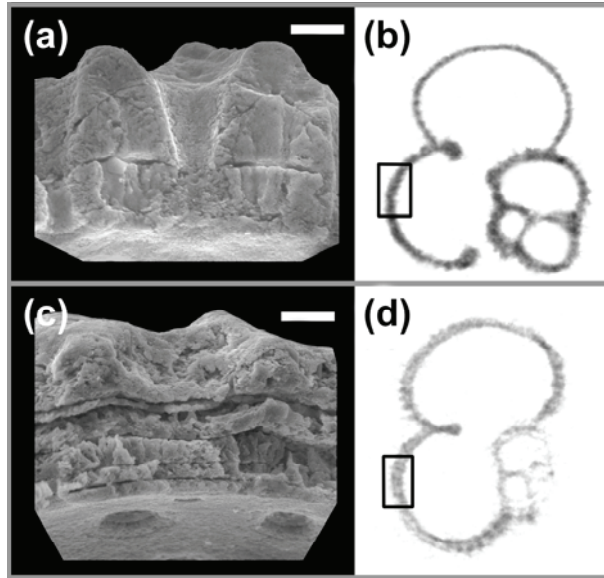
Figure 4.1 Effect of dissolution on the tests of *G. ruber* and its appearance in scanning electron microscope (SEM), on left hand side (LHS), and computed tomography (CT), on right hand side (RHS), images. Scale bar for SEM is 5 μm. Column width for CT image is ~400 μm. Black rectangles show the approximate position of the SEM image in the CT scan. Samples are from the OJP, 300-355 μm size fraction. Water depth (and $\Delta[CO_3^{2-}]$) are as follows: (a, b) 1616m (13.8 μmol/kg); (c, d) 2301m (4.9 μmol/kg).

Tests from sites where $\Delta[CO_3^{2-}]$ was between 20 and 10 μmol/kg were usually white and opaque, but appeared reasonably well-preserved. Pore structures were clear in SEM (**Figures 4.1a, 4.2a, 4.3a, 4.4a**) and could often be distinguished in CT (**Figures 4.2b 4.4b**). Dissolution became apparent in CT scans by the affected areas losing edge definition and becoming paler in colour. The change in colour is due to the development of microporosity, i.e. porosity below the resolution of the scanner, in the test calcite. SEM shows that even in well preserved tests slight separations exist between layers of calcite (**Figures 4.1a, 4.2a, 4.3a, 4.4a**). As dissolution proceeds these gaps widen (**Figures 4.1c, 4.2e, 4.3c, 4.4c**), resulting in a lighter grey colour in the scanned image (**Figures 4.1d, 4.2f, 4.3d, 4.4d**).
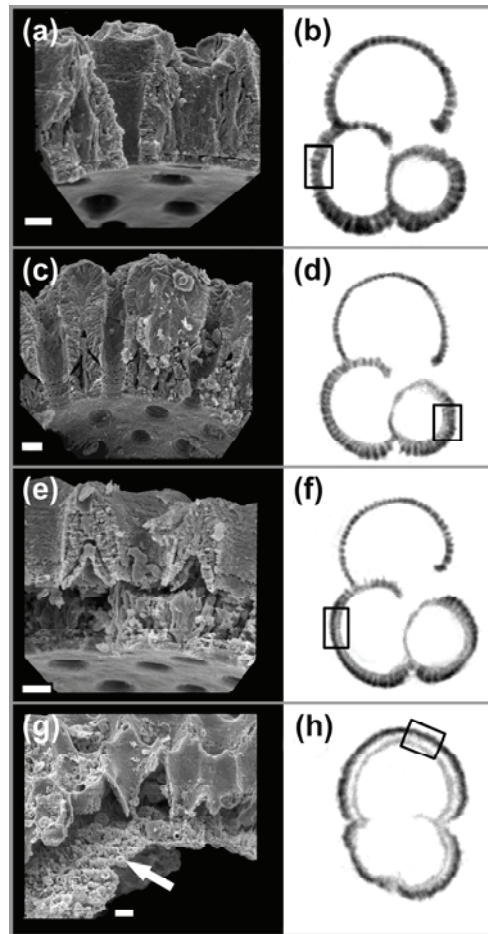
Figure 4.2 Effect of progressive dissolution on tests of *G. sacculifer* and its appearance in SEM (LHS; scale bar 5 µm) and CT (RHS; column width ~400 µm), images. Black rectangles show the approximate position of the SEM image. Samples are from the OJP, 300-355 µm size fraction. Water depth (and $\Delta[CO_3^{2-}]$ in µmol/kg) are as follows: (a, b) 1616 m (13.8); (c, d) 2445 m (4.3); (e, f) 2965m (-2.3); (g, h) 3711m (-11.8).

The first signs of dissolution were first evident in the smallest inner chambers of all four species. The thin walls of the small chambers became blurred and indistinct compared to the clear images obtained from tests from sites with higher $\Delta[CO_3^{2-}]$. CT scans of tests from progressively lower calcite saturations showed that dissolution advanced from the smallest inner chambers to the larger chambers. Chamber walls became increasingly pale and finally absent. **Figure 4.1d** shows a CT scan of *G. ruber* where the smallest chambers have dissolved.

Dissolution progressed from the walls of the small chambers to the intermediate chambers until all of the inner calcite was affected. We use the definition of *Brown and*

Elderfield [1996] where 'inner calcite' defines all the chambers inside the test as well as the calcite of the inner part of the outer wall. 'Outer calcite' refers to the outer part of the outer wall of the test, also called crust calcite. CT images of slightly dissolved *G. sacculifer, N. dutertrei* and *P. obliquiloculata* show a distinction between pale, porous inner calcite and darker outer calcite (**Figures 4.2d, 4.3d, 4.4d**). In *G. ruber*, which lacks an outer crust, scans show that the whole of the test wall became lighter in colour (**Figure 4.1d**). The outer calcite of *G. sacculifer, N. dutertrei* and *P. obliquiloculata* was also altered in partly dissolved tests. In these samples pore structures were less clearly defined (**Figures 4.2f, 4.3d, 4.4d**) than in scans of tests from shallower sites.
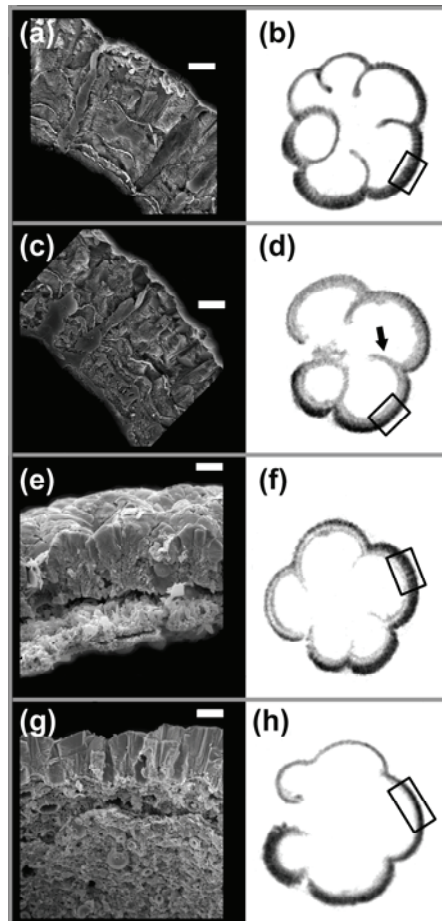
Figure 4.3 Effect of progressive dissolution on the wall structure of *N. dutertrei* shown in SEM (LHS; scale bar 10 µm) and CT (RHS; column width ~400 µm) images. (a) and (b) are polished sections. Black rectangles show the approximate position of the SEM image. Samples are from the OJP, 300-355 µm size fraction. Water depth (and $\Delta[CO_3^{2-}]$ in µmol/kg) are as follows: (a, b)1616 m (13.8); (c,d) 2965 m (-2.3); (e, f) 3711 m (-11.8); (g, h) 4341 m (-22.4).

The distinction between light inner calcite and dark outer calcite was more conspicuous in samples from around the calcite saturation horizon. Tests from such sites appeared partially dissolved under the binocular microscope. The outer test surface was dull and powdery and tests were easy to crush, forming small particles. CT showed that by this stage the smallest chamber walls of all four species were usually missing. Tests of *G. ruber* were scarce at these sample depths. CT scans of this species gave a pale image with no obvious pores in the test wall. Scans of *G. sacculifer*, *N. dutertrei* and *P. obliquiloculata* showed a clear division into a dark outer calcite and pale inner calcite (**Figures 4.2f, 4.3f, 4.4f**). As with *G. ruber*, pore structures of these three species were no longer apparent in CT (e.g. **Figure 4.4d**). SEM confirmed that pores no longer ran through the whole test wall (**Figure 4.4c**). Although the form of the larger inner chamber walls was usually present, the walls themselves often appeared thickened and distorted, often with irregular edges (**Figures 4.3d, 4.4f**). Even though tests appeared altered and partially dissolved, the width of the outer test wall, taking into account both the dark outer layer and the pale inner layer, was frequently as thick as that of well preserved tests. The material lining the inside of the outer wall may be partially composed of remnants of inner calcite. SEM showed that it also contained abundant coccolith plates suggesting that sediment particles had been incorporated to the test (**Figures 4.2g, 4.3e**).

Below the calcite saturation horizon the pale, porous material of the inner test gradually dissolved (**Figure 4.4g, 4.4h**) until, for *N. dutertrei* and *P. obliquiloculata*, eventually only the outer crust remained (**Figure 4.3g, 4.3h**). Extremely dissolved *G. sacculifer* did not quite reach this stage and a small amount of the inner part of the penultimate chamber was always present even in the most dissolved samples. Between -15 to -20 µmol/kg $\Delta[CO_3^{2-}]$ core-top samples consist mainly of the outer crust calcite of deep dwelling species.

The exterior surface of the outer test wall was also etched and dissolved by the undersaturated waters below the calcite saturation horizon. The outer surface of tests from deep sites (undersaturated with respect to calcite) showed structural breakdown and loss of material from the outer wall, as previously documented by *Bonneau* [1978].
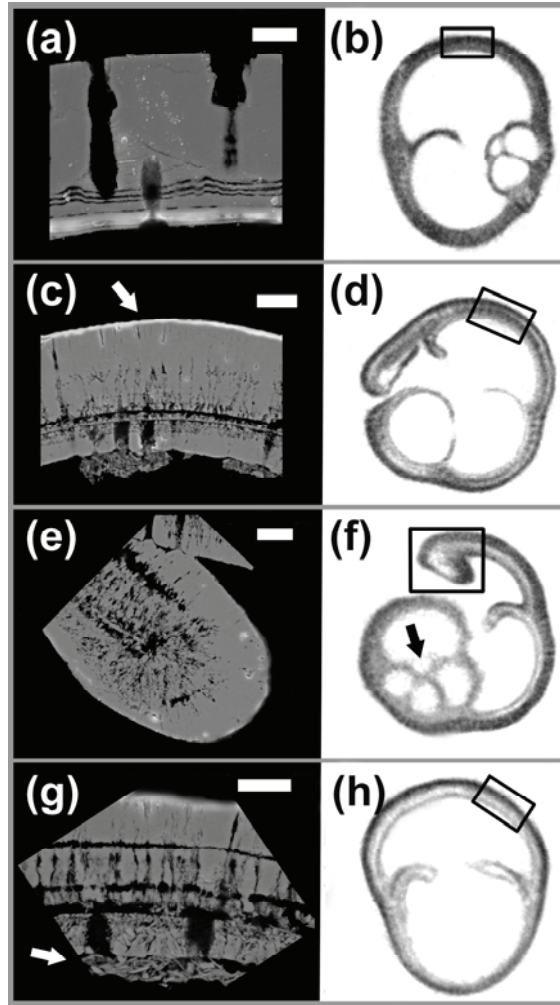
Figure 4.4 Effect of progressive dissolution on tests of *P. obliquiloculata* shown in SEM images of polished sections (LHS; scale bar 10 μm) and CT (RHS; column width ~400 μm). Black rectangles show the approximate position of the SEM image. Samples are from the OJP, 300-355 μm size fraction. Water depth (and $\Delta[CO_3^{2-}]$ in μmol/kg) are as follows: (a, b)1616 m (13.8); (c, d) 2301 m (4.9); (e, f) 3711 m (-11.8); (g, h) 4025 m (-14.7).

Figure 4.5 shows the sequence of dissolution in *N. dutertrei* using observations from CT. A sample of seven tests was taken from various different depths on the OJP. Each individual chamber wall was assessed for dissolution and assigned to one of 6 categories of preservation. As water depth increased, inner chamber walls were progressively dissolved. Below the calcite saturation horizon all of the inner calcite was severely affected by dissolution. The advance of dissolution through the test by alteration and then removal of inner calcite until, finally, only an outer crust was left, is exactly as described by *Brown and Elderfield* [1996] for *G. tumida*.
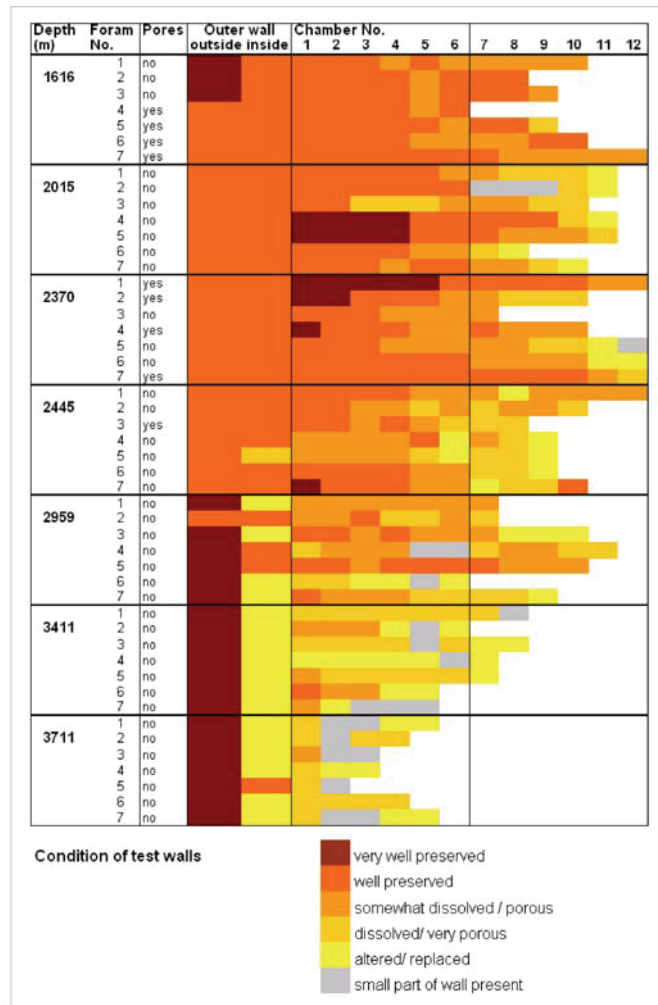
Figure 4.5 The progress of dissolution in *N. dutertrei*. Samples come from the Ontong Java Plateau. Depth (in m) is given in left hand column, along with sample number. Each chamber wall, and also the outer and inner calcite of the outer wall, was assigned to one of six categories according to its preservation state. Dissolution first affects the very smallest chambers and works inwards. Below the calcite saturation horizon (~3000 m) dissolution becomes much more severe, small chamber walls disappear while outer calcite becomes denser and the pores no longer penetrate the test wall.

In contrast to the inner calcite, CT scans showed the outer layer of the outer wall of moderately dissolved tests to be solid with no trace of pores (e.g. **Figure 4.3f**). SEM shows that tests from sites around the calcite saturation horizon often blocked with coccoliths and other detritus (White arrows in **Figure 4.6 (b** and **c)**).

33
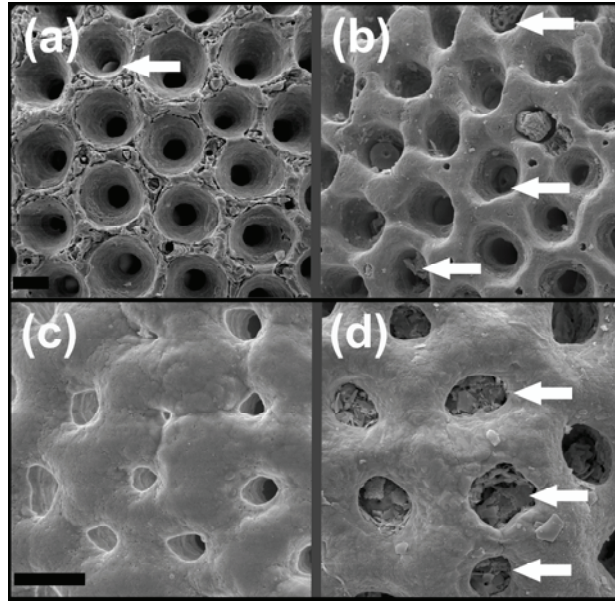
Figure 4.6 Outer surface of *G. sacculifer* [(a) and (b)] and *N. dutertrei* [(c) and (d)] tests from sites above, (a) and (c), and below, (b) and (d), the calcite saturation horizon. Samples are from the OJP, 300-355 µm size fraction. Scale bars (black) 10 µm. Water depth (and $\Delta[CO_3^{2-}]$ in µmol/kg) are as follows: (a, c) 2015 m (9.3); (b, d) 2965 m (-2.3).

4.3.2 Variation in initial wall thickness

One immediate insight from CT is that the initial thickness of the test wall can vary widely, both within and between sample sets. The more heavily calcified, deeper dwelling foraminifera species had the widest range of wall thickness as well as the thickest walls. For example *P. obliquiloculata* from shallow samples on the OJP and WIND transects contain tests with a range of wall thicknesses (from ~25 µm to ~45 µm). **Figure 4.7** shows two *P. obliquiloculata* from the same core-top sample (WIND 20B, 2274 m water depth). These two tests, one of which is approximately double the mass of the other, both have only very slight signs of dissolution; the difference in the thickness of the wall is primary. Under the binocular microscope, the thick-walled type appeared more heavily calcified, with a shiny outer layer. Despite the clear difference between end members individual test mass from the 1616 m sample (in this case a larger size fraction of 355 - 425 µm was used) on the OJP had a normal distribution.
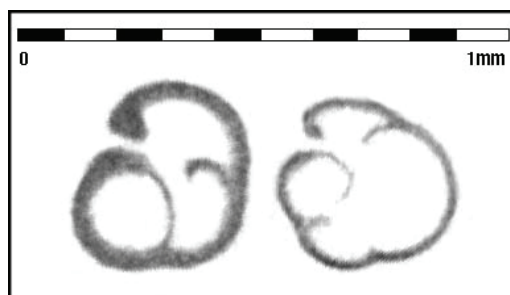
Figure 4.7. CT slices of two *P. obliquiloculata* tests illustrate the range in test wall thickness within one sample. Tests are from Western Indian Ocean (WIND20B, 2274 m water depth). Scale bar is 1mm. Both tests show some initial signs of dissolution but the difference in wall thickness is primary. The thick test is approximately double the weight (~40 μg) of the thin one (~20 μg).

The sample set from along the coast of Madagascar in the Indian Ocean (WIND core-tops) had the widest range of wall thickness between samples, presumably because of the wide geographical and age range of these samples. *N. dutertrei* from the OJP also showed fluctuations in average test thickness between different samples; and the variation in test mass in this species reflects variation of the initial wall thickness. Samples from 2445 m (2.5BC37) and 2959 m (3BC16) have thinner walls (~35 μm) than those of the three shallower samples (where wall thickness was ~40 μm).

4.3.3 Effect of dissolution on test mass and test volume

Variation in wall thickness means that test mass for each species is not geographically constant (**Figure 4.8**). *G. ruber*, *G. sacculifer* and *N. dutertrei* tests from the Atlantic/ Caribbean (where surface water $[CO_3^{2-}]$ is ~105 μmol/kg) are 20-25% heavier than those from the OJP in the Pacific (where surface water $[CO_3^{2-}]$ is ~75 μmol/kg).

Test mass decreased linearly with decreasing $\Delta[CO_3^{2-}]$, from $\Delta[CO_3^{2-}]$ values well above saturation (**Figure 4.8, Table 4.2**). Assuming that the average mass for tests in a sample was initially that of those from the shallowest site from each transect, tests can sustain a large loss of mass before tests disintegrate. Extremely dissolved *P. obliquiloculata* have lost ~50% of their initial mass. *G. sacculifer* and *N. dutertrei* can lose ~40%, and even the thin-walled and fragile *G. ruber* can lose ~30%, of initial mass. As previously observed, significant dissolution of foraminifera tests occurs where deep water is oversaturated with respect to calcite [*Brown and Elderfield*, 1996]. In this study more than half of the mass loss occurred above the calcite saturation horizon (**Figure 4.8**).

Linear regressions (**Table 4.3**) were estimated for OJP and Ceara Rise samples from sites where $\Delta[CO_3^{2-}] < 20$ μmol/kg. CT scans show negligible dissolution above this value of

calcite saturation. Despite the difference in initial mass, the response of mass to dissolution was similar for all four species from both sites, decreasing by 0.20 (±0.11) to 0.51 (±0.38) µg per 1 µmol/kg decrease in $\Delta[CO_3^{2-}]$ (**Table 4.3**).
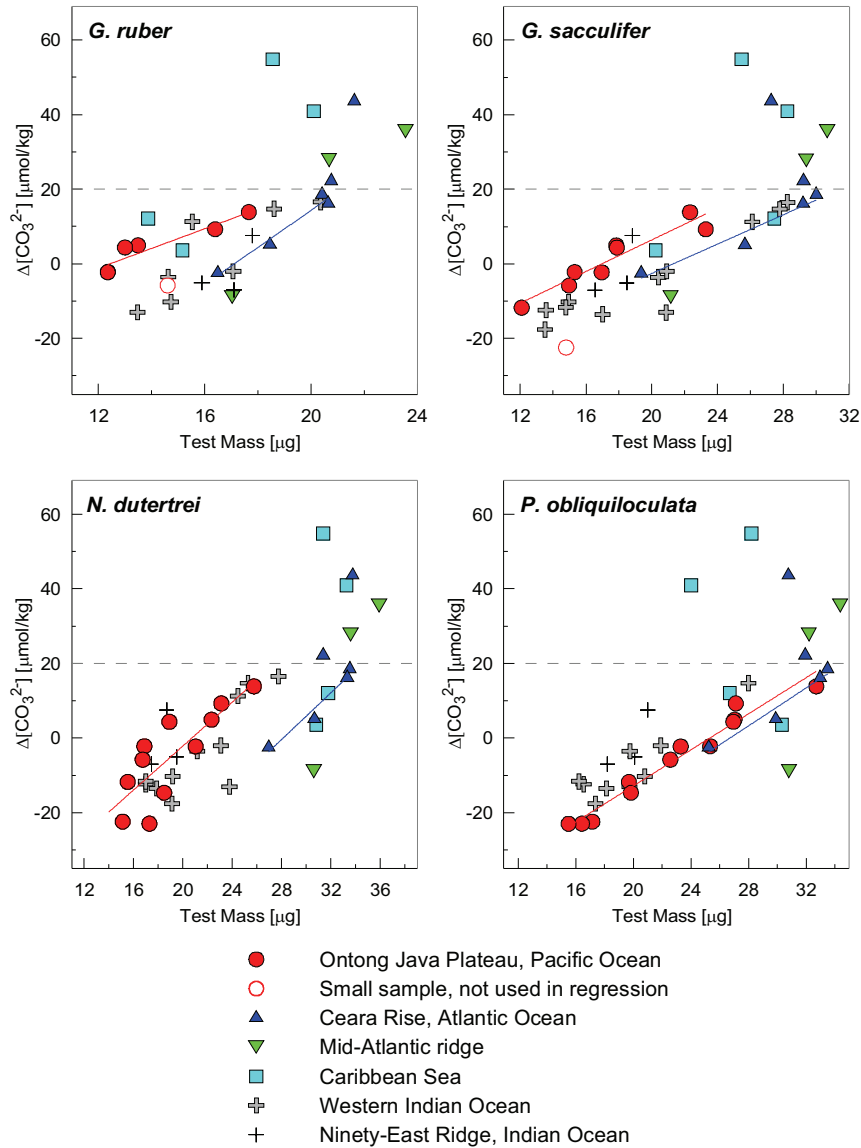
Figure 4.8 Test mass versus $\Delta[CO_3^{2-}]$ for four species of planktonic foraminifera. Samples from the deepest sites on the Ontong Java Plateau (open circles) were not included in regressions as samples contained few tests. Parameters for regressions are given in **Table 4.3**. The loss of test mass in response to calcite undersaturation is similar between species and for both OJP and Ceara Rise sites at ~0.4 µg per µmol/kg.

Core	G. ruber				G. sacculifer				N. dutertrei				P. obliquiloculata			
	Ave. mass [µg]	No. scanned	XDX	Half 95% CI	Ave. mass [µg]	No. scanned	XDX	Half 95% CI	Ave. mass [µg]	No. scanned	XDX	Half 95% CI	Ave. mass [µg]	No. scanned	XDX	Half 95% CI
Ontong Java Plateau																
1BC3	17.7	45	0.4	0.1	22.9	40	0.1	0.1	25.8	37	0.3	0.1	32.7	41	0.3	0.1
1.5BC33	16.4	54	0.3	0.1	23.3	63	0.6	0.1	23.1	67	0.6	0.1	27.1	49	0.6	0.2
2BC13	13.5	43	0.8	0.2	17.8	42	1.1	0.3	22.3	36	1.0	0.3	27.0	36	1.4	0.4
2.5BC37	13.0	56	0.7	0.1	17.9	56	1.8	0.3	18.9	70	1.0	0.2	26.9	37	1.3	0.3
3BC16	12.4	42	1.3	0.2	15.3	52	2.5	0.2	16.9	65	1.8	0.2	25.3	31	1.9	0.4
3BC24	12.4	40	1.4	0.2	17.0	41	2.2	0.3	21.0	39	1.4	0.3	23.3	56	2.2	0.3
4BC51	s 14.6	5	1.8	0.6	15.0	59	3.1	0.2	16.7	70	3.0	0.1	22.6	49	3.2	0.2
4.5BC53					12.1	23	3.2	0.3	15.5	71	3.8	0.1	19.7	36	3.6	0.2
5BC54									18.5	22	3.7	0.2	19.8	30	3.7	0.2
5.5BC58					s 14.8	14	3.0	0.7	15.1	43	3.9	0.1	17.1	35	3.9	0.1
6BC74									s 17.3	8	4.0	0.0	16.4	29	3.9	0.1
BC66													s 15.5	7	4.0	0.0
Caribbean Sea																
M35014	18.6	29	0.2	0.1	25.5	35	0.2	0.1	31.4	39	0.3	0.1	s 28.2	5	0.1	0.3
M35010	20.1	20	0.1	0.1	28.2	21	0.1	0.1	s 33.3	8	0.2	0.1	24.0	17	0.1	0.2
M35026	13.9	29	0.1	0.1	27.4	32	0.0	0.0	31.8	41	0.3	0.1	s 26.7	10	0.2	0.2
M35024	15.2	27	0.7	0.2	20.2	33	1.5	0.3	30.8	43	0.9	0.2	30.3	24	1.2	0.5
Ceara Rise																
GeoB1503	21.6	31	0.3	0.1	27.2	29	0.0	0.0	33.7	27	0.2	0.2	30.8	29	0.2	0.2
GeoB4415	20.8	37	0.4	0.2	29.2	45	0.1	0.1	31.4	51	0.3	0.2	31.9	35	0.1	0.1
GeoB4416	20.4	32	0.3	0.2	30.0	43	0.1	0.1	33.5	47	0.2	0.1	33.5	39	0.3	0.1
GeoB4406	20.6	31	0.1	0.1	29.2	44	0.1	0.0	33.3	48	0.1	0.1	33.0	35	0.1	0.1
GeoB4413	18.5	39	0.6	0.2	25.7	46	0.4	0.2	30.6	48	0.3	0.1	29.9	40	0.2	0.1
GeoB4403	16.5	39	1.8	0.3	19.4	44	2.6	0.3	26.9	55	2.0	0.3	25.2	39	2.3	0.2
Mid-Atlantic Ridge																
GeoB4420	23.6	30	0.2	0.1	30.6	40	0.1	0.1	35.9	42	0.2	0.1	34.4	22	0.1	0.1
GeoB4421	20.7	30	0.6	0.2	29.4	35	0.7	0.4	33.6	44	0.3	0.1	32.2	27	0.2	0.2
GeoB4424	17.0	28	1.0	0.3	21.1	34	2.2	0.2	30.6	51	1.2	0.2	30.8	21	0.5	0.2
Western Indian Ocean																
WIND 11B	20.4	33	0.4	0.1	28.2	30	0.1	0.1	27.7	29	0.3	0.2				
WIND 20B	18.6	34	0.2	0.1	27.8	30	0.1	0.1	25.3	27	0.2	0.1	28.0	35	0.5	0.3

Sample	Mass	n	CI		Mass	n	CI		Mass	n	CI		Mass	n	CI	
WIND 10B	15.5	28	0.4	0.1	26.1	28	0.1	0.1	24.4	29	0.4	0.2				
WIND 33B	14.6	30	0.8	0.3	20.4	31	1.4	0.6	21.2	28	1.2	0.2	19.8	30	0.9	0.2
WIND 5B	17.1	30	0.8	0.2	20.9	62	2.5	0.2	23.1	30	2.6	0.3	21.9	27	2.3	0.4
WIND 25B	14.7	36	0.6	0.2	14.9	30	1.3	0.4	19.2	26	1.9	0.4	20.8	29	1.5	0.3
WIND 23B					13.6	28	3.5	0.3	17.0	28	3.4	0.3	16.5	31	3.6	0.2
WIND 13B	13.5	35	1.7	0.3	20.9	61	2.7	0.2	23.8	30	2.2	0.4	19.7	30	3.0	0.3
WIND 28B					s 14.8	13	2.8	0.6	17.0	30	3.1	0.4	16.2	28	3.4	0.3
WIND 6B					17.0	38	2.8	0.3	17.9	30	3.6	0.2	s 18.1	10	3.7	0.3
WIND 12B					s 13.5	15	3.6	0.3	19.1	15	3.5	0.3	s 17.4	14	3.6	0.3
Ninety-East Ridge, Indian Ocean																
V29-9	17.8	18	0.9	0.4	18.8	9	0.8	0.6	18.7	10	1.1	0.5	21.0	20	1.1	0.3
RC14-33	15.9	20	1.2	0.5	18.5	9	3.2	0.3	19.5	9	1.4	0.4	20.1	20	1.8	0.6
RC14-31	17.1	20	1.3	0.7	16.5	9	3.0	0.9	17.4	10	2.5	0.5	18.2	19	3	0.6

s indicates small sample where average test mass was calculated from less than 15 tests

CI is confidence interval

Table 4.2 XDX and average test mass for four species of planktonic foraminifera.

	Ontong Java Plateau (OJP)				Ceara Rise			
Species	m	c	1/m [μg per μmol/kg]	r^2	m	c	1/m [μg per μmol/kg]	r^2
G. ruber	2.64 (±1.33)	-33 (±19)	0.38 (±0.19)	0.88	5.04 (±2.84)	-86 (±54)	0.20 (±0.11)	0.97
G. sacculifer	2.12 (±0.73)	-36 (±13)	0.47 (±0.16)	0.90	1.98 (±1.48)	-81 (±39)	0.51 (±0.38)	0.94
N. dutertrei	2.93 (±1.57)	-61 (±30)	0.34 (±0.18)	0.67	3.12 (±1.95)	-88 (±61)	0.32 (±0.20)	0.96
P. obliquiloculata	2.42 (±0.33)	-61 (±8)	0.41 (±0.06)	0.96	2.52 (±1.62)	-67 (±50)	0.40 (±0.26)	0.96

m is slope of the regression

c is the intercept on the y-axis

1/m is the mass lost (in μg) per 1 unit decrease in μmol/kg $\Delta[CO_3^{2-}]$

± is half of 95 % confidence interval

Table 4.3 Parameters for the regressions plotted in **Figure 4.8**.

Regressions are fitted to Ontong Java Plateau (red line) and Ceara Rise (blue line) data below $\Delta[CO_3^{2-}]$ values of 20 µmol/kg (dashed line) as dissolution appears insignificant above this value. The deepest sample of *G. ruber* and *G.* These values are consistent with that of *Broecker and Clark* [2001a], who used a larger size class (355 – 415 µm) of *G. sacculifer*, *N. dutertrei* and *P. obliquiloculata* from the OJP, Ceara Rise and Ninety-East Ridge but found a similar gradient (0.30 ±0.05 µg per µmol/kg) between test mass and $\Delta[CO_3^{2-}]$. *Rosenthal and Lohmann* [2002] also found a response in the same range, 0.31 µg per µmol/kg, for *G. sacculifer* (300-400 µm size fraction) from the Sierra Leone Rise.

$\Delta[CO_3^{2-}]$ therefore correlates with mass lost to dissolution, ΔM, where,

$$\Delta M = \text{mass}_{INITIAL} - \text{mass}_{MEASURED} \tag{1}$$

Mass $_{INITIAL}$ is the original mass before any dissolution effect, and mass $_{MEASURED}$ is the actual measured mass. Values used for mass $_{INITIAL}$ are averaged from samples above 20 µmol/kg, for sites where there are samples available from these depths. For the OJP sample set, mass $_{INITIAL}$ was that of the shallowest sample in the transect. **Figure 4.9** shows $\Delta[CO_3^{2-}]$ versus ΔM with one regression plotted for all samples of one species.

Species	All sites			
	a	$\Delta[CO_3^{2}]$ CRITICAL(mass)	1/*a*	r^2
		[µmol/kg]	[µg per mol/kg]	
G. ruber	-3.07 (±1.70)	16 (±7)	-0.33 (±0.18)	0.59
G. sacculifer	-2.11 (±0.43)	12 (±2)	-0.47 (±0.10)	0.90
N. dutertrei	-2.82 (±0.82)	13 (±5)	-0.35 (±0.10)	0.77
P. obliquiloculata	-1.83 (±0.48)	10 (±4)	-0.55 (±0.14)	0.80

± is half of 95 % confidence interval

a is slope on regression

$\Delta[CO_3^{2-}]_{CRITICAL(mass)}$ is intercept on y axis where no mass has been lost to dissolution, ie Δmass = 0

1/a is average mass lost (in µg) per 1 unit decrease in µmol/kg

Table 4.4 Parameters for regressions in **Figure 4.9**.
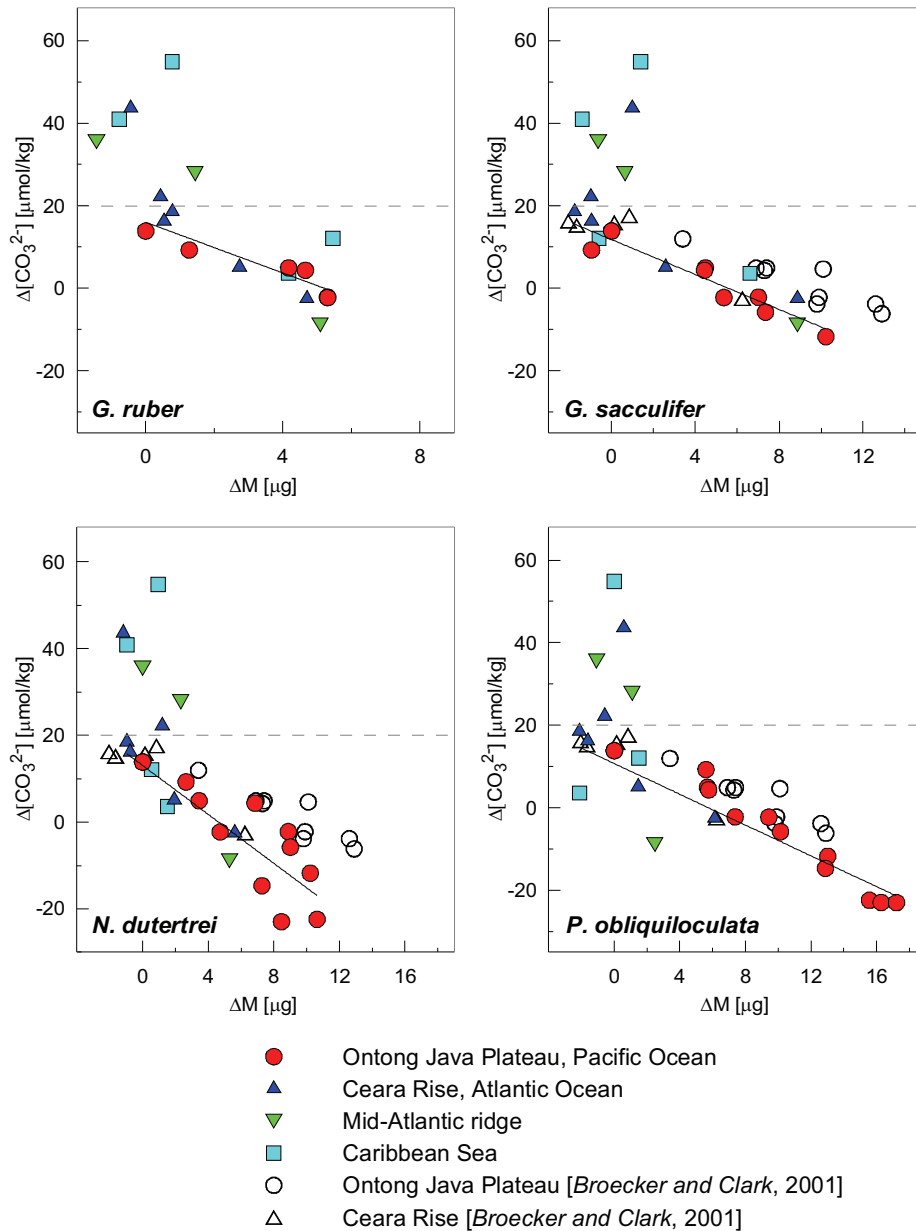
Figure 4.9 Mass lost to dissolution (ΔM) versus Δ[CO$_3^{2-}$] for four species of planktonic foraminifera. Regressions are fitted to all data of this study below Δ[CO$_3^{2-}$] values of 20 μmol/kg (dashed line) as dissolution appears insignificant above this value. Parameters for regressions are given in **Table 4.4**. Despite variation in initial mass, correlation between Δ[CO$_3^{2-}$] and Δmass is similar between sample sites and between species. Test mass data of Broecker and Clark (2001) (355 – 415 μm size fraction) also gives similar regressions.

As well as similar sensitivity to $\Delta[CO_3^{2-}]$ (**Figure 4.9, Table 4.4**), tests reached a similar minimum mass (**Figure 4.8**). *G. ruber* and *G. sacculifer* from the OJP reached a minimum mass of around 12 µg in the core-tops where they were still found in sufficient quantity to take a sample. Tests of *N. dutertrei* and *P. obliquiloculata* reached a minimum mass of ~15 µg. These species were still very abundant in the deepest samples used in this study. Tests of *N. dutertrei* and *P. obliquiloculata* with mass of ~15 µg appeared as if they could still thin further. The linear correlation between $\Delta[CO_3^{2-}]$ and ΔM suggests that 'dissolution resistance' is sensitive to initial test mass. *G. ruber* and *G. sacculifer* are lost first from assemblages only because they are lighter initially and *N. dutertrei* and *P. obliquiloculata* are preserved to lower $\Delta[CO_3^{2-}]$ values because they are more massive.

As described in 3.1, the early stages of dissolution did not have a measurable effect on the thickness of the test walls. The term 'wall thickness' here refers to the whole distance across the test wall, i.e. the width from the outer to the inner edge, irrespective of whether the intervening material has become more porous. The walls of partially dissolved tests from around the calcite saturation horizon were often as wide as those of well preserved samples. Like test mass, test volume decreased linearly with decreasing $\Delta[CO_3^{2-}]$ (**Figure 4.10a**). Due to the porous nature of the inner material of the test around the calcite saturation horizon, density is lowest for samples from these depths (**Figure 4.10b**). Below the calcite saturation horizon density increased as the porous inner material dissolved.
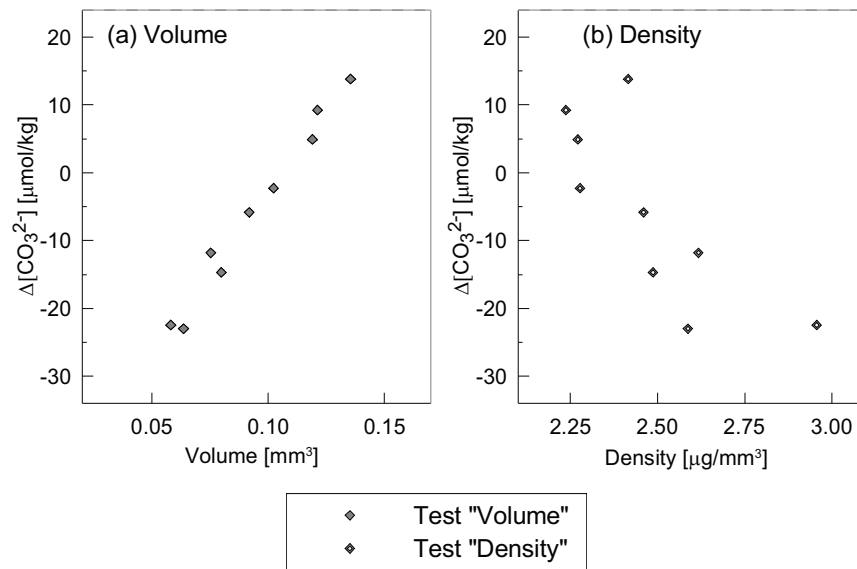
Figure 4.10 (a) $\Delta[CO_3^{2-}]$ versus volume (b) $\Delta[CO_3^{2-}]$ versus density of *P. obliquiloculata* from the OJP. Volume is test plus any material contained within it. Although volume decreases steadily down the depth transect the material of the test becomes more porous. Lowest densities occur around the calcite saturation horizon.

4.3.4 Greyscale as dissolution indicator

The development of microporosity as spaces and gaps developed within the test wall (**Figure 4.2e, 4.2f**), and the addition of disseminated material to the inner walls of the test (**Figure 4.2g, 4.2h**), meant that during the initial stages of dissolution the colour of the scanned images generally became lighter (**Figure 4.11**). Within a certain range, greyscale indicates dissolution. For example greyscale correlates with $\Delta[CO_3^{2-}]$ for sacculifer from between 20 and -10 µmol/kg on the OJP ($r^2 = 0.72$) and *P. obliquiloculata* below 20 µmol/kg on the OJP ($r^2 = 0.79$). As dissolution progressed, the dark colour values of the outer crust dominated, and the correlation between greyscale and $\Delta[CO_3^{2-}]$ broke down.

The initial width of the test wall exerts some control on the colour values of the scans. Tests of *G. ruber*, *G. sacculifer* and *N. dutertrei* from the Atlantic gave lower greyscale values than Indo-Pacific samples due to their greater initial mass (**Figure 4.7**, **Figure 4.11**). Taking the ratio of light (greyscale values 171 to 210) to dark (greyscale values 0 to 170) pixels in the scanned image circumvents this problem to some extent and allows one regression to be fitted for all sample sets for one species. This greyscale ratio correlates well with $\Delta[CO_3^{2-}]$ for *G. ruber* ($r^2 = 0.52$); *G. sacculifer* ($r^2 = 0.55$) and *P. obliquiloculata* ($r^2 = 0.53$) but less well for *N. dutertrei* ($r^2 = 0.24$).

In principle this should provide a measure of dissolution, with one caution. Greyscale values are skewed by sediment trapped inside the test and this must be cleaned from the images. As tests dissolve and interact with the sediment, what is selected as part of the test becomes increasingly subjective.
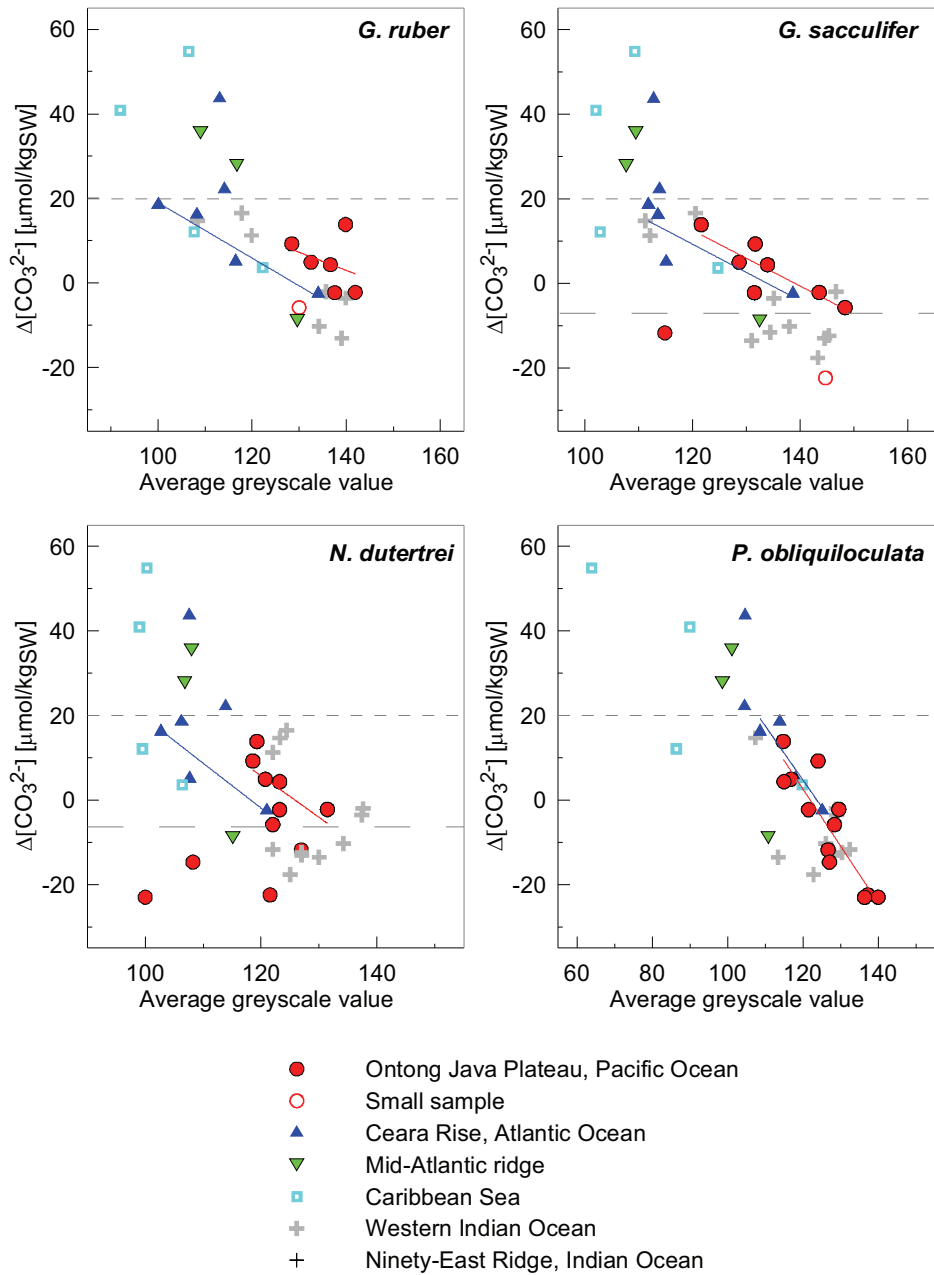
Figure 4.11 $\Delta[CO_3^{2-}]$ versus average greyscale value for four species of foraminifera. Average greyscale values were obtained from one central CT slice for each test in a sample. Upper dashed line indicates calcite saturation of 20 μmol/kg, above which dissolution appears insignificant. Lower dashed line is the limit where greyscale values stop increasing (becoming lighter in colour). Below this value outer crust calcite dominates and greyscale decreases towards darker values. Regressions are plotted for OJP (red line) and Ceara Rise (blue line) samples within the dashed grey lines for *G. sacculifer* and *N. dutertrei*.

4.4 Towards an independent measure of dissolution in foraminifera tests: establishing dissolution index XDX

Due to the complex way in which dissolution proceeds there is no simple, measurable quantity that identifies its progression. Greyscale values of CT scans can indicate preservation state of foraminifera tests, and may provide a useful marker of dissolution in some circumstances. However, greyscale can be distorted by clay or sediment inside the test. The approach we have taken, therefore, is to develop an empirical dissolution index, XDX, based on the appearance of the CT scans. The index is based on the premise that dissolution proceeds in a sequence of stages and that the appearance of dissolution features in the CT scans can be recognised by eye. This avoids the need to manipulate the images. The index contains 5 categories from perfectly preserved to extremely dissolved tests (**Figure 4.12**).

The categories are defined as follows:

Dissolution stage **XDX 0**: Perfect tests. CT scans show no signs of dissolution. Test walls are imaged as clear dark lines. Pores in the outer wall often visible. Test walls of *G. ruber* are often very thin, particularly the final chamber.

Dissolution stage **XDX 1:** Well-preserved tests. The first stages of dissolution are evident. Although scans show the test wall as dark and solid, the edges may appear indistinct. The smallest inner chambers are missing. Pores may be detectable.

Dissolution stage **XDX 2:** Poorly preserved tests. CT scans show a difference in colour between pale inner calcite and a dark dense outer layer. The walls of all but the largest chambers missing. Pores generally absent.

Dissolution stage **XDX 3:** Poorly-preserved, partially replaced tests. Around the calcite saturation inner calcite is porous and appears pale in the scanned image. Thick inner chambers and rough edges of the inner suggest replacement of calcite and addition of material. Smallest chambers missing. In species with a gametogenic crust the outer layer of the test is dark with no pores.

Dissolution stage **XDX 4:** Severely dissolved tests. No inner calcite present; only the outer crust is left. *G. sacculifer* does not often show stage 4, usually part of the inner calcite of penultimate chamber is present in even severely dissolved tests. This stage is not seen in *G. ruber*.
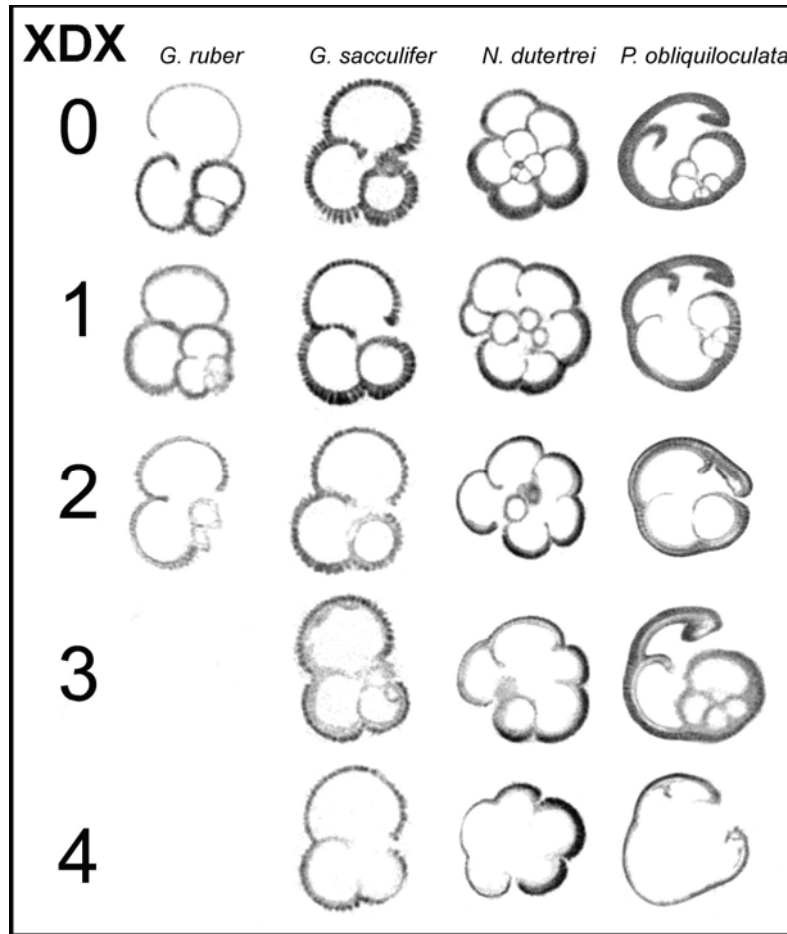
Figure 4.12 Typical CT slices for each stage of dissolution index, XDX. Not all the information used to decide the stage of dissolution can be shown in a single slice but a central CT slice through typical examples of *G. ruber*, *G. sacculifer*, *N. dutertrei* and *P. obliquiloculata* gives an impression of the different categories. XDX 3 is typical of tests just below the calcite saturation horizon.

It is not possible to show in one CT slice all the factors that decide into which category of dissolution a test should be placed. This necessitates looking at all the slices to ascertain the condition of the small chambers. **Figure 4.12** shows a typical example of a central section through a test at each XDX stage for *G. ruber*, *G. sacculifer*, *N. dutertrei* and *P. obliquiloculata*.

In order to test whether this dissolution index was reproducible an experiment was carried out where ten volunteers graded images of 40 tests according to a checklist. The average of the correlation of their results ($r^2 = 0.85$) with HJ's values suggests that the XDX, while essentially subjective, is reproducible.

4.4.1 Estimation of $\Delta[CO_3^{2-}]$ from XDX

Because dissolution index XDX is a based on the processes of dissolution, it is insensitive to fluctuations in test mass and one regression can be plotted for each species from all sample sites (**Figure 4.13**, **Table 5**). Although XDX is based on arbitrary categories according to features that can be identified in CT scans, the relationship between $\Delta[CO_3^{2-}]$ and XDX is approximately linear. Linear regressions were estimated for all data below 20 µmol/kg $\Delta[CO_3^{2-}]$ as dissolution appeared to be negligible above this value.

The relationship between XDX and $\Delta[CO_3^{2-}]$ provides a means to estimate $\Delta[CO_3^{2-}]$ from XDX for other open ocean sites with low organic carbon content.

$$\Delta[CO_3^{2-}] = d * XDX + \Delta[CO_3^{2-}]_{CRITICAL(XDX)} \tag{2}$$

Where d is the slope of the regression and $\Delta[CO_3^{2-}]_{CRITICAL(XDX)}$ is the value where XDX is zero. Values are given in **Figure 4.13**.

The linear relationship between $\Delta[CO_3^{2-}]$ and XDX is weakest around the calcite saturation horizon where XDX stages 2 and 3 are both present at similar $\Delta[CO_3^{2-}]$ values. This reflects the complex processes occurring at these water depths.

All four species show a similar $\Delta[CO_3^{2-}]_{CRITICAL(XDX)}$ value of between 12-14 µmol/kg $\Delta[CO_3^{2-}]$ (**Figure 4.13**) where dissolution becomes noticeable in foraminifera tests. Despite the difference in 'dissolution resistance' of the outer calcite of the test, the sensitivity of the inner calcite to dissolution is similar between species.

4.4.2 Use of XDX to correct dissolution bias in test mass

The relationship between XDX and ΔM (loss of test mass due to dissolution) is approximately linear (**Figure 4.14**). XDX can be used to approximate ΔM according to,

$$\Delta M = e * XDX \tag{3}$$

where e is slope of the regression. Values are given in **Figure 4.14**.

An estimate can be made of initial test mass, according to a rearrangement of equation (1) to,

$$Mass_{INITIAL} = Mass_{MEASURED} + \Delta M$$

Values of $\Delta[CO_3^{2-}]_{CRITICAL(mass)}$ are similar between species at 10-16 µmol/kg, and are also similar to the critical $\Delta[CO_3^{2-}]$ values where XDX starts to record dissolution.
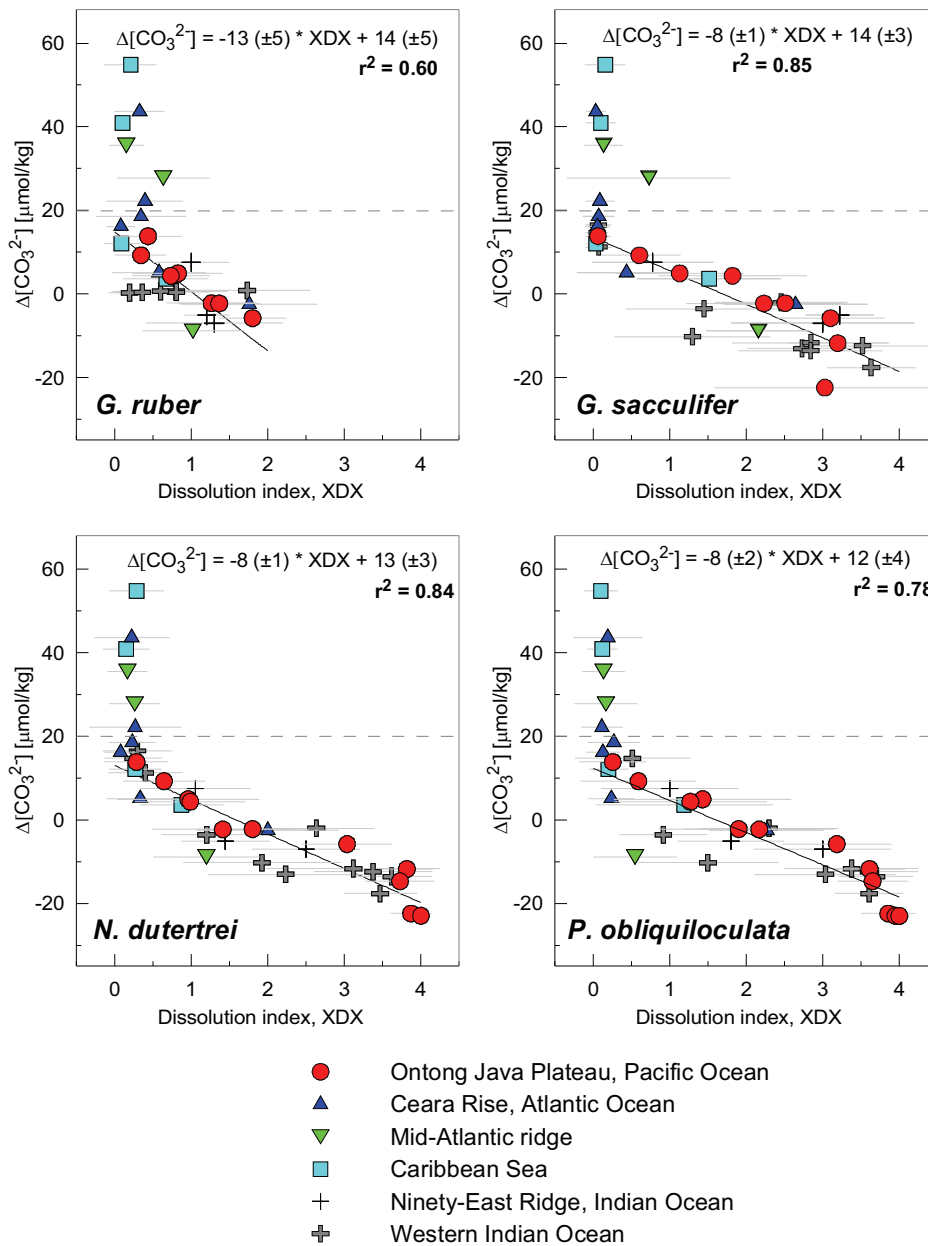
Figure 4.13 Dissolution index, XDX, versus $\Delta[CO_3^{2-}]$ for four species of planktonic foraminifera. Regressions are plotted for all data below 20 µmol/kg $\Delta[CO_3^{2-}]$ (dotted line) as dissolution appears to be insignificant above this value. Individual values of XDX were not taken into account in estimating regression coefficients. Parameters for the regressions, equation (2), are shown, ± is half of 95 % confidence interval. Grey bars are 1σ.
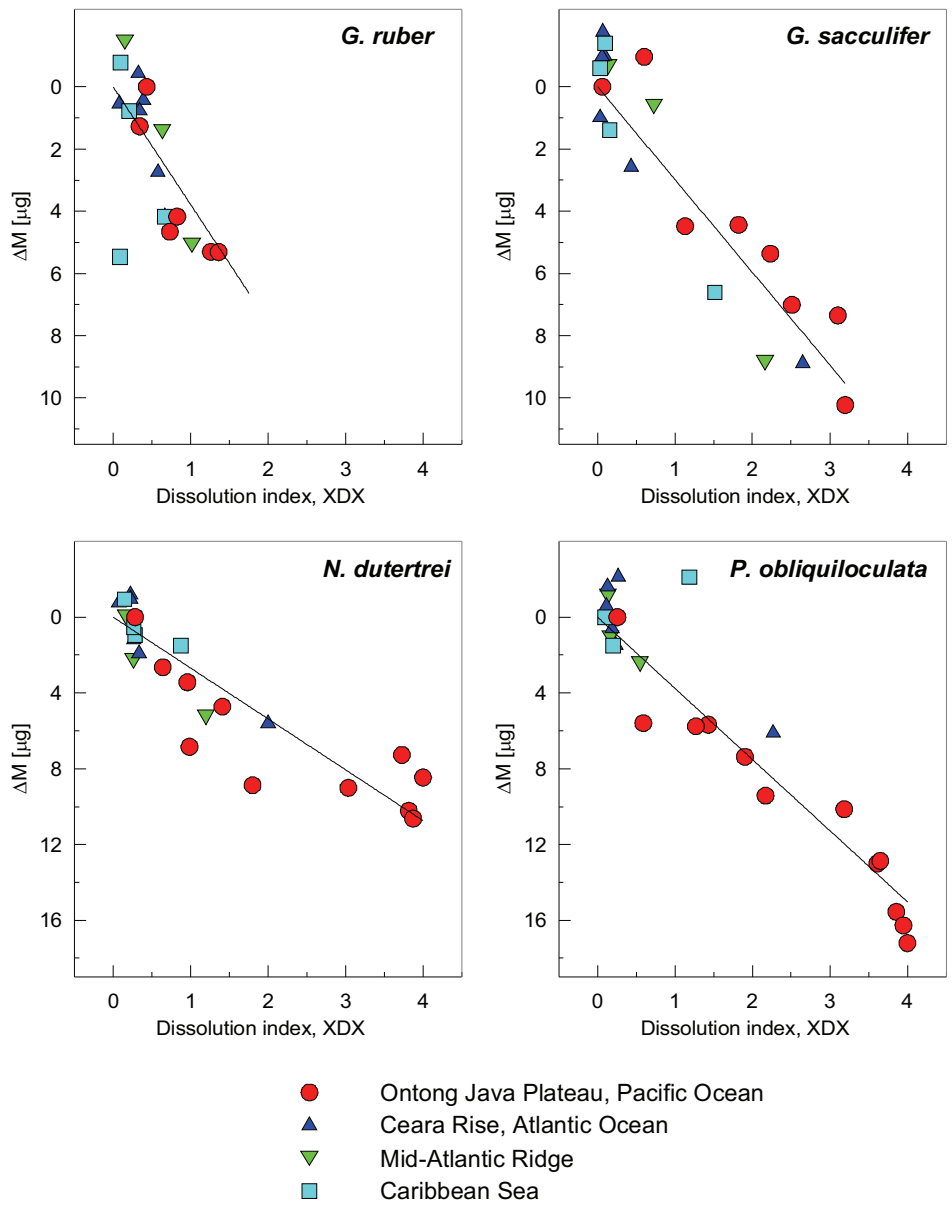
Figure 4.14 XDX versus ΔM (mass lost to dissolution) for each species. Parameters for regressions, equation (3), are shown, ± is half of 95 % confidence interval.

4.4.3 Most useful species as dissolution indicators

Correlation between both XDX and $\Delta[CO_3^{2-}]$ (**Figure 4.13**) and XDX and ΔM (**Figure 4.14**) is weakest for *G. ruber*. One reason for this may be that, as *G. ruber* does not show the more advanced stages of dissolution, the allocation of XDX values may be less accurate for this species. Its lack of an outer crust, and thus the more advanced stages of dissolution, limits the use of this species as a dissolution indicator. The correlation between $\Delta[CO_3^{2-}]$ and ΔM is also lowest for this species (**Table 4.4**). This may be due to variation in initial mass, but could also suggest that that the association between deep-water $\Delta[CO_3^{2-}]$ and preservation-state of *G. ruber* is not as clear for this species as for the other species tested here. This appears to be the case for *G. ruber* from the OJP in particular, where the indications of dissolution – greyscale value, the greyscale ratio of light to dark and XDX – all suggest that the shallowest sample of *G. ruber,* from 1616 m on the OJP, is more dissolved than the sample from 2015 m. Taking the test mass of the 1616 m sample as mass $_{INITIAL}$, as we have done here, will lead to an underestimate of mass lost in response to dissolution. Tests of *G. ruber* from the OJP are older than other species from the same sample, and have been mixed upward from deeper in the sediment [*Barker et al.* 2007]. More generally, the high sensitivity to dissolution of shallow-dwelling foraminifera may mean that atypically well-preserved tests are over represented in samples from dissolved sections. The few tests of *G. sacculifer* from the deepest site on the OJP appeared less dissolved than those from shallower sites.

The stages of dissolution were shown most clearly in thermocline-dwelling species, *N. dutertrei* and *P. obliquiloculata,* which have a distinct outer crust. A similar pattern of dissolution as observed in these latter two species was seen in other thermocline-dwelling species with a relatively closed form and a thick outer crust: *Globorotalia tumida, Globorotalia menardi, Globorotalia hirsuta, Neogloboquadrina pachyderma* and *Globorotalia inflata* (not further discussed here).

4.5. Dissolution of foraminiferal tests at the seafloor

4.5.1 Causes of calcite dissolution above the calcite saturation horizon

In this study foraminifera tests from sites highly oversaturated with respect to calcite ($\Delta[CO_3^{2-}] > 20$ μmol/kg) showed no detectable signs of dissolution. Foraminiferal test mass started to decrease where $\Delta[CO_3^{2-}]$ was ~15 μmol/kg. The first slight signs of dissolution were apparent in CT scans at comparable $\Delta[CO_3^{2-}]$ values. Two factors may contribute to the dissolution of foraminifera tests above the calcite saturation horizon. One is that impurities in the test calcite may enhance the solubility of foraminiferal

calcite. The other issue is that acidity produced by the degradation of organic matter promotes dissolution in sediment pore waters.

No evidence of respiration driven dissolution

Although dissolution indices based on foraminifera aim to reconstruct deep water $\Delta[CO_3^{2-}]$, considerable calcite dissolution takes place at sites above the calcite saturation horizon due to acidity produced within sediment pore waters by organic matter degradation [*Parker and Berger*, 1971; *Berner*, 1977; *Martin and Sayles* 1996; *Emerson and Bender*, 1981].

Previous studies have recorded respiration-driven dissolution above the calcite saturation horizon at locations close to sites used here. Benthic flux chambers at 3272 m water depth ($\Delta[CO_3^{2-}] \approx 25$ μmol/kg) on the Ceara Rise (Site CR2 of *Jahnke and Jahnke* [2004]) recorded the consumption of oxygen due to the degradation of organic matter. However, CT scans of foraminifera from sites where $\Delta[CO_3^{2-}]$ is ~20 μmol/kg on the Ceara Rise support the observations of *Broecker and Clark* [2003] that tests are well preserved. The calcite dissolution taking place must be due to dissolution of something other than foraminifera tests.

Further evidence for lack of test dissolution in response to pore water acidity is the similarity of preservation state of tests within one sample. Dissolution rate decreases towards the sediment water interface due to buffering by supersaturated deepwater, *Martin and Sayles* [1996] record pore water NO_3^- and Ca^{2+} increasing steadily in the top 10 cm of the sediment at 3279 m (site B of *Martin and Sayles* [1996], $\Delta[CO_3^{2-}] \approx 25$ μmol/ kg) on the Ceara Rise as organic matter is oxidised and $CaCO_3$ is dissolved. They model the maximum rate of $CaCO_3$ dissolution at 3 cm at this site. Core-tops used in our study represent sediment depths of 0-2 to 0-5 cm. Thus samples intersect with the zone of organic matter driven dissolution. Given the gradient in dissolution intensity in the top few cm of the sediment, as long as the mixing rate of tests within the sediment was slower than establishment of the chemical gradient, we should find a range of dissolution states within samples from above the calcite saturation horizon. However, although one sample (GeoB4420), from the shallowest site on the Mid-Atlantic Ridge, contained tests (of *G. ruber* and *G. sacculifer*) with a range of preservation states this was generally not the case (**Figure 4.13**). The standard deviation of XDX for samples from above the calcite saturation horizon was not greater than for samples from deeper sites. Samples from these shallow sites typically contained tests with only slight signs of dissolution and did not contain any poorly preserved tests.

Mg dependent dissolution

Brown and Elderfield [1996] attribute the observation that tests start to dissolve in over saturated waters to the fact that tests contain Mg, Mg-rich being more soluble than pure calcite. Mg incorporation to tests is temperature dependent [*Nürnberg et al.,* 1996] and the ratio of Mg to Ca (in mmol/mol) increases by ~9% for every 1° C increase in temperature [*Anand et al.,* 2003]. The four studied species live at different depths in the water column and so their Mg/Ca values should decrease in the order *G. ruber > G. sacculifer > N. dutertrei / P. obliquiloculata* and indeed this order is similar to the dissolution susceptibility ranking of *Berger* [1970]. However, despite their different Mg contents, all four species show a similar loss of mass in response to calcite undersaturation (**Figure 4.8**, **Table 4.4**). *G. ruber* and *G. sacculifer,* the Mg/Ca of which should reflect warm mixed layer conditions, did not lose more mass per µmol/kg $\Delta[CO_3^{2-}]$ than the deeper dwelling, low Mg/Ca species, *N. dutertrei* and *P. obliquiloculata.*

The trace amount of Mg^{2+} in foraminiferal calcite is not distributed evenly through the test. Chemical mapping techniques of *G. ruber*, *G. sacculifer*, *N. dutertrei* [*Sadekov et al.*, 2005] and *P. obliquiloculata* show bands of Mg rich calcite associated with organic layers in the test [*Kunioka et al.*, 2006]. *Erez* [2003] describes two kinds of biomineralized calcite in foraminifera; 5% high Mg primary calcite and 95% secondary low Mg calcite. The former is precipitated in granules along the organic layers that provide the substrate for calcification. This granular calcite may be particularly susceptible to dissolution, as solubility is sensitive to crystal size. X-ray diffraction studies have shown that crystallinity increases with dissolution, as small crystals are preferentially dissolved [*Bassinot et al.*, 2004]. In foraminifera calcite crystal size and Mg content may anyway be closely related as Mg^{2+} incorporation can be used to control crystal size in $CaCO_3$ [*Kwak et al.*, 2005]. The increase in crystallinity due to dissolution has been calibrated directly to decrease in Mg/Ca [*Nouet and Bassinot*, 2007].

Despite the variation in bulk Mg/Ca between species, maximum Mg/Ca values appear to be similar. In the samples examined by *Sadekov et al.* [2005] the highest Mg/Ca values were between 6 and 8 mmol/mol for *G. ruber* and *G. sacculifer*. This is comparable to the highest Mg/Ca values, of ~7 mmol/mol, measured in *P. obliquiloculata* [*Kunioka et al.*, 2006]. Maximum Mg/Ca mapped *N. dutertrei* was only slightly lower, at 5 - 6 mmol/mol [*Sadekov et al.,* 2005]. The similarity of maximum Mg/Ca values could explain why dissolution starts at similar $\Delta[CO_3^{2-}]$ values for all the species examined here despite characteristically different bulk Mg/Ca.

SEM of tests from sites above the calcite saturation horizon show that in the early stages of dissolution, spaces develop between layers of calcite (**Figures 4.1b, 4.2b, 4.4b**). This

could be where layers of Mg-rich, low crystallinity calcite have been dissolved out. Other evidence of preferential dissolution of Mg-rich calcite was that crust calcite, low in Mg, was less sensitive to dissolution than inner calcite. The outer crust calcite of partially dissolved tests of *G. sacculifer*, *N. dutertrei* and *P. obliquiloculata* produce a distinct dark layer in CT scans, indicating better preservation of this part of the test. Scans of *G. ruber*, which lacks a low Mg outer layer, showed no such division of the test calcite.

It has been observed previously that properties intrinsic to tests make them more susceptible to dissolution than pure calcite. *Berger* [1970] detected an increase in solubility of foraminifera tests at water depths of 2000 – 2500 m ($\Delta[CO_3^{2-}]$ approximately 4 to 10 µmol/kg) in the central Pacific. These samples were in tubes suspended from wires and were not in contact with the seafloor. Water could pass through the gauze bounding the ends of the tubes and so the tests would be exposed to ambient water. In a parallel experiment with spheres formed from single calcite crystals, the spheres were more resistant to dissolution than foraminiferal calcite. The first increase in solubility for the calcite spheres occurred at 3,600 m [*Peterson*, 1966 cited in *Berger*, 1970].

The pattern of dissolution observed in CT scans is consistent with the premise that Mg-rich parts of foraminifera tests are particularly susceptible to dissolution. CT scans of *N. dutertrei* and *P. obliquiloculata*, showed that Mg-rich inner calcite was affected by dissolution before the low Mg outer crust (**Figures 4.2c, 4.3c**). Several studies show that *G. ruber* has a more homogenous distribution of Mg [*Eggins et al*., 2003; *Gehlen et al*., 2004] and in this species dissolution affected the whole of the test wall (**Figure 4.1b**).

4.5.2 Processes of dissolution at depths close to and below the calcite saturation horizon

Selective preservation of more massive forms

Tests from sites from around the calcite saturation horizon have lost mass (**Figure 4.8**) and appear partially dissolved. However, as described in 3.1, the breadth of the test wall is similar, or can be thicker, in tests from sites where $\Delta[CO_3^{2-}] \approx 0$ compared to those from shallow sites (**Figure 4.3a, 4.3b**). The outer crust calcite, where present, appears dark and solid in CT scans. This surrounds an inner layer composed of porous fine grained material.

One explanation for the thick walls of partially dissolved tests is that in sediments overlain by undersaturated deepwater the most robust thick-walled tests are selectively preserved. Thick walls, both of the outer test and the inner chambers (**Figure 4.4c**) in samples from around the calcite saturation horizon could be a primary feature. In this

study the thinnest tests were found in the shallow samples from the Caribbean and Ceara Rise, the sites with the highest $\Delta[CO_3^{2-}]$. Thin shells can sustain less mass loss before breaking up than thicker ones. A linear relationship between $\Delta[CO_3^{2-}]$ and ΔM (**Figure 4.8**) would mean that, in the same way that fragile thin walled species are lost from assemblages [*Berger,* 1968], thin walled specimens within a species would be first dissolved. The few specimens of *G. ruber* from 3411 m on the OJP, although partially dissolved, appeared to have initially thicker walls (~30 μm compared to ~ 25 μm) than those from shallower sites.

Other studies have also found that tests preserved in sediment become increasingly unrepresentative of surface water forms with increasing depth of deposition. *Bé et al.* [1975] noted that *G. ruber* from a deep site (~5,500 m in the west central North Atlantic) was different from the *G. ruber* found in shallower sites, having smaller pores and also a crystalline outer crust. In this study, *G. ruber* from deep sites (**Figure 4.1b**) tended to have a thicker final chamber than those from shallow sites (**Figure 4.1a**); presumably because they came from a larger size class but have lost their original final chamber [*Berger*, 1970]. These subtle effects of selective preservation mean that analysed parameters down a depth transect represent not only the effects of dissolution but also changes in the analysed population.

Precipitation of calcite within sediments

Another explanation for the fine grained material inside foraminifera tests from sites around the calcite saturation horizon would be that it is, at least partially, formed by the precipitation of calcite at the seafloor.

Jahnke and Jahnke [2004] reviewed benthic flux data from the Ceara Rise, Cape Verde Plateau and the OJP and found that sediments high (>5%) in $CaCO_3$ underlying supersaturated waters produced little flux of alkalinity despite oxidation of organic matter and increased Ca^{2+} and alkalinity in the sediment. To explain this *Jahnke and Jahnke* [2004] proposed that $CaCO_3$ must precipitate in the top few millimetres of the sediment surface. *Broecker and Clark* [2003] suggested a similar mechanism whereby fine layers of calcite (which they called Weyl coatings) precipitate onto the tests of foraminifera at sites where organic matter was degraded in waters oversaturated with respect to calcite.

We saw no evidence of new $CaCO_3$ overgrowths on tests from sites where $\Delta[CO_3^{2-}]$ >10 μmol/kg either by CT or SEM. It is possible that small scale features would not be detected using our methods, or it may be that the perfect biomineralised surface of well-preserved tests at these high saturation values does not offer a good surface for nucleation of new calcite. Calcite precipitation may be occurring elsewhere in the sediment.

However, at depths close to the calcite saturation horizon, there is some evidence that $CaCO_3$ forms inside the tests of foraminifera. CT of samples from 3,000 m on the OJP ($\Delta[CO_3^{2-}] \approx 0$ µmol/kg) once more supports the observations of *Broecker and Clark* [2003], in this case that foraminifera are appreciably dissolved. This is at a similar depth to Station NS (2972 m on the OJP) of *Jahnke et al.* [1994] where, again, no Ca^{2+} or alkalinity flux was detected from the sediment even though electrodes show that the degradation of organic matter is consuming oxygen and that calcite is mobilised in the pore waters. SEM and CT of tests from similar sites show signs of calcite precipitation. The observation that pore structures infill in poorly preserved tests (**Figures 4.2f, 4.2g, 4.2h, 4.3d, 4.3f, 4.4c, 4.4d, and 4.6b, 4.6d**) suggests that calcite may simultaneously precipitate and dissolve within the test. The apparent thickening of the inner chamber walls (**Figure 4.4f**) and the fine grained material coating the inside of the outer test wall (**Figures 4.2g, 4.3e**) could also be partially formed of new $CaCO_3$. The presence of coccoliths suggests that some of this is material from the sediment which has become incorporated into tests (**Figures 4.2g, 4.3e, 4.4g, 4.9**).

One finding of *Nouet and Bassinot* [2007] may provide evidence for precipitation of $CaCO_3$ inside foraminifera tests at sites close to the calcite saturation horizon. Crystallinity generally increases with water depth as less well ordered calcite, high in Mg, is preferentially dissolved. In their sample from just above the calcite saturation horizon from the Sierra Leone Rise (Station D), *Nouet and Bassinot* [2007] find an increase in the high Mg calcite phase which had previously been decreasing down the transect. (Although it should be noted that the data of *Bonneau* [1980] show a similar increase in crystallinity around the calcite saturation horizon in only one [*P. obliquiloculata*] of the five species examined.)

Below the calcite saturation horizon the main process affecting foraminifera tests is dissolution. *Jahnke et al.* [1994] detected a calcite flux from the sediment at 4439 m (their Station US) on the OJP. Scans of foraminifera from similar depths (e.g. **Figure 4.3g, 4.3h**) shows that there is little fine grained material in the inner test and that severe thinning of the test walls has occurred.

4.6 Conclusions

This work proposes a method of assessing dissolution in the tests of planktonic foraminifera. X-ray computed tomography (CT) provides an insight into the way that dissolution proceeds. Foraminifera tests, from the tropical sites with low organic carbon used in this study, showed a consistent relationship between preservation state, illustrated in the CT scans, and calcite saturation.

Foraminiferal calcite started to dissolve well above the calcite saturation horizon. Damage was apparent to the smallest inner chambers of the test at $\Delta[CO_3^{2-}]$ values of ~15 µmol/kg. This value was similar for all four species of foraminifera examined here, despite their apparently different dissolution resistance. Test mass started to decrease at comparable values of calcite saturation.

In the intermediate stages of dissolution, CT scans of *G. sacculifer*, *N. dutertrei* and *P. obliquiloculata* show a clear distinction between the inner and outer calcite of the test. Inner calcite was disproportionately affected by dissolution, becoming pale and porous, while outer calcite remained solid. Colour values in the tomography scans generally became lighter as the test dissolved, due to the development of microporosity in the test calcite. Greyscale correlates with $\Delta[CO_3^{2-}]$ to some extent and could be a useful indicator of dissolution in some circumstances. However, greyscale values are also affected by initial test mass and by sediment trapped in the test.

At depths close to the calcite saturation horizon ($\Delta[CO_3^{2-}]$ between 5 and -5 µmol/kg) material was incorporated into the test, illustrated by the infilling of test pores. SEM images of samples from this depth range characteristically show fine grained porous material on the inside of tests. CT images show this material as a pale phase with irregular edges, which tends to follow the original form of the test. Some of this material may originate from the sediment, as it contains many coccoliths. It may also partly be $CaCO_3$ precipitated within the sediment. This material dissolves in deeper sites (< -10 µmol/kg), finally leaving an empty crust.

The pattern of dissolution of the tests of planktonic foraminifera is consistent with the explanation that Mg content, or crystallinity of inner calcite, makes it more susceptible to dissolution than pure calcite. The low-Mg outer calcite of *N. dutertrei* and *P. obliquiloculata* was the most resistant to dissolution. Calcite crusts of these species were abundant even in samples from the most undersaturated sites (~ -20 µmol/kg) used here. *G. ruber*, which lacks an outer crust, showed only the early stages of dissolution. This limits the use of *G. ruber* as a dissolution indicator.

Test mass varies between locations. Tests of *G. sacculifer* and *N. dutertrei* from the Atlantic were heavier than those from the Pacific. Wall thickness (hence test mass) within a species varied most for the heavily calcified species *N. dutertrei* and *P. obliquiloculata*. Despite variation in initial mass, and the complexity of dissolution processes, loss of test mass (ΔM) was similar between species and sites at ~0.4 µg per µmol/kg.

We established a dissolution index, XDX, based on stages of dissolution identified in the CT scans. Because XDX is based on the process of dissolution it appears to be insensitive to initial test mass. The relationship between XDX and $\Delta[CO_3^{2-}]$ is approximately linear. We provide calibrations between both XDX and $\Delta[CO_3^{2-}]$ and XDX and mass lost to dissolution (ΔM).

---

5. Calibrating computed tomography based dissolution index (XDX) to dissolution bias of Mg/Ca in planktonic foraminifera

H.J.H. Johnstone[1], M. Schulz[1], J. Yu[2] and H. Elderfield[3]

[1] MARUM – Center for Marine Environmental Sciences, University of Bremen, Leobener Straße, 28359 Bremen, Germany

[2] Lamont-Doherty Earth Observatory of Columbia University, 61 Route 9W, PO box 1000, Palisades, NY, 10964-8000, USA

[3] Godwin Laboratory for Palaeoclimate Research, Department of Earth Sciences, University of Cambridge, Cambridge, UK

Abstract

Temperatures derived from Mg/Ca of planktonic foraminifera are distorted when partial dissolution of the test occurs, and methods are required to quantify this source of inaccuracy. Here we compare a dissolution index (XDX), based on X-ray computed tomography scans, to Mg/Ca for four species of foraminifera (*G. ruber* [white], *G. sacculifer* [without sac], *N. dutertrei* and *P. obliquiloculata*) from core-top sediments from the Ontong Java Plateau, the tropical Atlantic and western Indian Ocean. An estimate of ΔMg/Ca (reduction in Mg/Ca due to dissolution) was made for each sample. ΔMg/Ca decreased linearly from deepwater calcite saturation ($\Delta[CO_3^{2-}]$) values of between 10 (±4) (*G. sacculifer*) and 15 (±5) µmol/kg (*N. dutertrei*). These $\Delta[CO_3^{2-}]$ values are minimum estimates of the threshold below which planktonic Mg/Ca is affected by dissolution, as they are limited by assumptions made in calculating ΔMg/Ca. Sensitivity of Mg/Ca to $\Delta[CO_3^{2-}]$ was greatest for *G. ruber*, where it decreased by 0.102 (± 0.036) mmol/mol per µmol/kg, and similar for *G. sacculifer* (0.047 ±0.015 mmol/mol per µmol/kg), *N. dutertrei* (0.037 ±0.010 mmol/mol per µmol/kg) and *P. obliquiloculata* (0.040 ±0.008 mmol/mol per µmol/kg). Sensitivity was similar for all locations for each species, apart from *N. dutertrei* from the Caribbean which appears to be more sensitive than *N. dutertrei* from other sites. Calibrations between XDX and ΔMg/Ca can be used to estimate dissolution bias on Mg/Ca. For the small sample sizes typical for $\delta^{18}O$ analysis, natural variability overwhelms dissolution effects and there was little correlation between XDX and $\delta^{18}O$.

5.1 Introduction

The tests of microscopic plankton, foraminifera, play a vital role in paleoceanography as carriers of surface hydrographic signals. However, their calcite tests are vulnerable to dissolution, and this has been shown to alter geochemical proxies such as $\delta^{18}O$ and Mg/Ca [*Wu and Berger*, 1989, 1991; *Lorens and Willia*, 1977; *Brown & Elderfield*, 1996; *Hastings et al.,* 1998; *Rosenthal et al.,* 2000; *Dekens et al.,* 2002, *Regenburg et al.,* 2006]. Mg/Ca, in particular is very sensitive to dissolution; the principal secondary control of a proxy that has vastly increased the information available to paleoceanographers. This paleotemperature proxy was developed during the 1990s [*Nürnberg,* 1995*; Nürnberg et al.,* 1996; *Rosenthal* 1997; *Hastings et al.,* 1998; *Mashiotta et al.,* 1999; *Lea et al.,* 1999; *Elderfield and Ganssen*, 2000] and has come into

increasingly routine use in the last decade. It is based on recognition that Mg incorporation into foraminifera tests is temperature dependent. Mg/Ca of test calcite therefore offers a means to isolate the temperature component from carbonate $\delta^{18}O$, based on the same biotic carrier [e.g., *Mashiotta et al.,* 1999]. However, Mg incorporation to the test affects test solubility [*Brown and Elderfield*, 1996] with the consequence that partial dissolution of the test after deposition on the seafloor preferentially removes Mg-rich parts of the test, biasing temperatures towards lower, colder values. An assessment of test preservation is therefore vital to estimate the accuracy of temperatures derived using this proxy.

There are several methods that aim to quantify the effect of dissolution on planktonic Mg/Ca. Evaluation of corrosivity of deepwater at a particular location, based on current core depth or calcite saturation [*Dekins et al.,* 2002], offers a useful correction over short time periods. However, calcite chemistry of deepwater varies through a glacial cycle, thus fluctuations in calcite preservation may confound temperature comparisons between interglacial and glacial periods. Change in preservation has been suggested to account for some of the disparity between sea surface temperatures (SST) records based on different proxies during the last deglaciation [*Mix*, 2006]. On timescales greater than several thousand years, therefore, a direct method of assessing the effect of calcite dissolution on Mg/Ca is necessary.

One established method of assessing dissolution in sediment samples is to compare the number of test fragments to intact tests of a particular species of foraminifera [*Berger,* 1968; *Oba*, 1969; *Bé et al*., 1975; *Ku and Oba*, 1978; *Thunell*, 1976]. These dissolution indices exist for many species and have been directly compared to Mg/Ca [*Mekik and Francois*, 2006]. Consistent changes in the crystallinity of test calcite due to dissolution [*Bassinot et al*., 2004] also has potential to correct for dissolution effect on Mg/Ca [*Nouet and Bassinot*, 2007].

An examination of foraminifera tests themselves during the early stages of dissolution, before they fragment, reveals that material is first lost from the inside of the test, while the outer layer remains reasonably intact [*Brown & Elderfield*, 1996; *Johnstone et al.,* in press (**Chapter 4**)]. The effect of preferential loss of inner material is that test weight is reduced while test size remains constant [*Lohmann,* 1995]. Test weight has been directly calibrated to reduction in Mg/Ca [*Rosenthal and Lohmann,* 2002]. This approach requires that initial test weight is constant temporally and spatially. In fact there is evidence that environmental conditions such as nutrient availability [*de Villiers*, 2004] or carbonate ion concentration [*Barker and Elderfield*, 2002] influence the thickness of the test walls and therefore the initial weight of the test.

X-ray computed tomography (CT) can be used to assess dissolution in foraminifera tests [*Johnstone et al.*, in press, (**Chapter 4**)]. Details of inner test structure mapped by this non-destructive imaging technique provide an insight into the preservation state of the planktonic foraminifera (**Figure 5.1**). The index (XDX) is based on the processes of dissolution and appears to be insensitive to initial test mass.

In this study geochemical proxies Mg/Ca and $\delta^{18}O$ are first compared to deepwater calcite saturation ($\Delta[CO_3^{2-}]$) to assess sensitivity to dissolution. The two proxies are then compared directly to XDX to ascertain the potential of XDX to correct for dissolution bias.

.
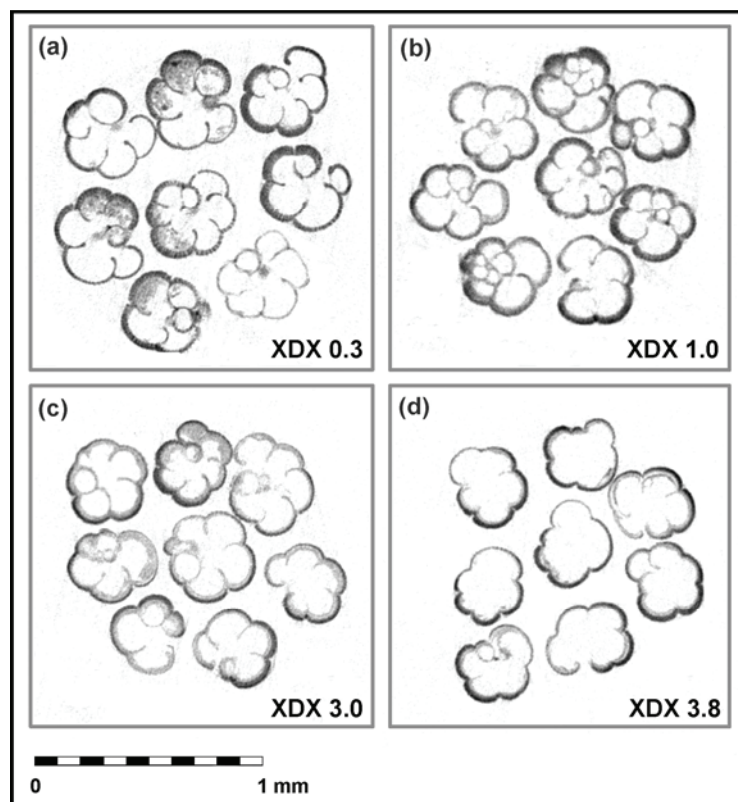
Figure 5.1 X-ray computed tomography 'slices' of *N. dutertrei* tests. Samples are from the Ontong Java Plateau, 300-355 μm size fraction. Dissolution index, XDX, value is shown bottom right of each panel. Index values range from 0: no dissolution to 4: severe dissolution. XDX values assigned for each test are averaged to give XDX value of a sample. (a) 1616 m: tests are well-preserved (although some contain sediment). Test on bottom right has no gametogenic crust. (b) 2445 m: inner calcite shows initial signs of dissolution. (c) 3411 m: inner calcite severely affected by dissolution. (d) 3711 m: little inner calcite remains. The last part of the test to form, the outer crust, is the most resistant to dissolution.

Core	Water depth [m]	Lat. [°N]	Long. [°W]	Δ[CO$_3^{2}$] [μmol/kg]	SST [°C] Ann.	SST [°C] Warm.
Ontong Java Plateau						
1BC3	1616	-2.2	-157.0	14	29.3	29.4
1.5BC33	2015	-1.0	-157.9	9	29.2	29.3
2BC13	2301	0.0	-158.9	5	29.2	29.3
2.5BC37	2445	0.0	-159.5	4	29.2	29.3
3BC16	2959	0.0	-160.5	-2	29.2	29.3
3BC24	2965	0.0	-160.4	-2	29.2	29.3
4BC51	3411	0.0	-161.0	-6	29.2	29.3
4.5BC53	3711	0.0	-161.4	-12	29.2	29.3
5BC54	4025	0.0	-161.8	-15	29.2	29.3
5.5BC58	4341	0.0	-162.2	-22	29.2	29.3
6BC66	4400	0.0	-162.7	-23	29.2	29.3
6BC74	4438	0.0	-162.7	-23	29.2	29.3
Caribbean						
M35014	1604	17.8	63.7	55	26.6	27.6
M35010	2696	18.9	64.1	41	26.4	27.5
M35026	3815	17.5	67.0	12	26.6	27.6
M35024	4710	17.0	66.0	4	26.6	27.6
Ceara Rise						
GeoB4415	3584	5.9	45.0	22	27.9	28.3
GeoB4416	3903	5.7	45.1	19	27.9	28.3
GeoB4406	3709	5.1	43.8	16	27.9	28.3
GeoB4413	4291	6.1	44.2	5	27.9	28.2
GeoB4403	4503	6.1	43.4	-3	27.9	28.2
Mid-Atlantic Ridge						
GeoB4420	2763	16.5	46.5	36	26.9	27.8
GeoB4421	3176	17.0	46.0	28	26.6	27.8
GeoB4424	4779	18.2	44.0	-9	26.6	27.5
West Indian Ocean						
WIND 11B	2382	-28.5	-48.2	17	22.7	24.7
WIND 20B	2274	-20.1	-49.2	15	25.8	27.4
WIND 10B	2871	-29.1	-47.5	11	22.2	24.2
WIND 33B	3520	-11.2	-58.8	-4	27.0	28.3
WIND 5B	3684	-31.6	-47.6	-2	20.9	23.0
WIND 25B	3935	-11.8	-50.6	-11	26.7	27.7
WIND 23B	4004	-13.1	-51.0	-12	26.6	28.1
WIND 13B	4065	-23.9	-49.0	-13	25.1	26.8
WIND 28B	4147	-10.2	-51.8	-12	26.8	28.1
WIND 6B	4150	-31.3	-47.6	-14	20.9	23.0
WIND 12B	4196	-25.8	-47.9	-18	23.9	25.7

Ann. indicates annual average SST, Warm. is warmest season average [*Rayner et al.*, 2003]

Table 5. 1 Details of the core-tops used in this study.

5.2 Samples and Methods

This study progresses from *Johnstone et al.* [in press (**Chapter 4**)]. In that work planktonic foraminifera from core top samples (**Table 5.1**) were scanned using a micro-CT scanner and assigned values on dissolution index XDX (**Table 5.2**). In the present study, these previously scanned samples were analysed for Mg/Ca and $\delta^{18}O$.

5.2.1 Samples

Core-top samples (**Table 5.1**) cover a range of calcite saturation ($\Delta[CO_3^{2-}]$) states. $\Delta[CO_3^{2-}]$ is a measure of calcite saturation of the deepwater overlying the core site:

$$\Delta[CO_3^{2-}] = [CO_3^{2-}]_{\text{IN SITU}} - [CO_3^{2-}]_{\text{SATURATION}}$$

where $[CO_3^{2-}]_{\text{IN SITU}}$ is the bottom-water carbonate concentration and $[CO_3^{2-}]_{\text{SATURATION}}$ is the value for calcite saturation at the pressure and temperature of the core site. $\Delta[CO_3^{2-}]$ values (**Table 5.1**) are from *Johnstone et al.* [in press (**Chapter 4**)] and were calculated with the CO2SYS.xls program [*Pelletier et al.,* 2005], using Global Ocean Data Analysis Project (GLODAP) [*Key et al.*, 2004] and World Ocean Atlas 2005 [*Locarnini et al.,* 2006] data according to the method described in *Yu and Elderfield* [2007].

Sample sites span the calcite saturation horizon (CSH), the depth where $\Delta[CO_3^{2-}]$ is equal to zero. Deepwater $\Delta[CO_3^{2-}]$ values range from 55 to -23 µmol/kg. The main sample set is from the Ontong Java Plateau (OJP) in the Pacific Ocean. In order to test if sensitivity of Mg/Ca to $\Delta[CO_3^{2-}]$ is similar for different ocean basins, Pacific samples were supplemented with core tops from the Ceara Rise, the Caribbean and the Mid-Atlantic Ridge (MAR). From the Indian Ocean, samples from the East coast of Madagascar (WIND cruise transect [*McCave*, 2001]) were used.

The four species of foraminifera analysed calcify at different depths in the water column [*Hemleben et al.,* 1989], and so have different initial Mg/Ca and $\delta^{18}O$ values. Mixed layer dwellers *Globigerinoides ruber* (white) and *Globigerinoides sacculifer* (without a sac-like final chamber) have high Mg/Ca, and low $\delta^{18}O$, compared to the thermocline-dwelling species *Neogloboquadrina dutertrei* and *Pulleniatina obliquiloculata*.

5.2.2 CT scanning and dissolution index, XDX

Samples were scanned using a Skyscan 1072 desktop X-ray micro-CT scanner [*Sasov and Van Dyck*, 1998; *Van Dyck and Sasov*, 1998] at the Godwin laboratory, University of Cambridge. The scanner uses an air-cooled point X-ray source to create a series of radiographs of a sample as it rotates. Tests were glued to the sample holder using water-

soluble glue and scanned in batches of 8 to 10 tests. Anode voltage was set at 80 kV and the rotation step was 0.9 $^{\circ}$. A 0.5 mm Al filter was used cut out the softest X-rays and so reduce beam hardening effects. Exposure time was 4.5 seconds. Cross sectional slices were reconstructed using Skyscan's own software which uses the Feldkamp cone-beam algorithm [*Feldkamp et al*., 1984]. A 10 % beam hardening correction was applied to reduce edge effects.

Reconstructed slices, with a resolution of ~7 μm, reveal the progress of dissolution through the inner chambers of foraminifera tests. Based on visual inspection of the CT scans each test in a samples were assigned to one of five categories of dissolution that make up dissolution XDX. Values are averaged for each sample. The categories can be summarised as follows:

Dissolution stage **XDX 0**: Tests extremely well preserved, no detectable dissolution.

Dissolution stage **XDX 1**: Slight signs of dissolution, smallest inner chambers affected.

Dissolution stage **XDX 2**: severe dissolution of the small inner chambers.

Dissolution stage **XDX 3**: all of the inner calcite - both the inner chambers and the inside of outer wall - is severely altered.

Dissolution stage **XDX 4**: extreme dissolution, only outer crust remains. This stage is not seen in *G. ruber*, which lacks an outer crust.

5.2.3 Mg/Ca analysis

After CT scanning, batches were recombined to provide samples of ~30 tests for Mg/Ca analysis. Tests were gently crushed between two glass plates in order to open the chambers. Cleaning followed the protocol of *Barker et al.* [2003b] ("Mg cleaning"). Samples were rinsed 5 times with distilled deionised water and twice with methanol to remove clays. Between rinses, samples were treated with one minute of ultrasonication. To remove organic matter samples were heated with 250 μl of an oxidising solution (1 % H_2O_2 buffered with NaOH) for 10 minutes. Every 2.5 minutes samples were removed from the water bath and tapped on the bench to dislodge gas bubbles. After 5 minutes they received a few seconds of ultrasonication in addition. This step was repeated after replacement of the oxidising solution. Any remaining solution was rinsed off with distilled deionised water and samples were transferred to clean vials. A weak acid rinse (0.001 M HNO_3) and two subsequent water rinses ended the cleaning process. Samples were dissolved for analysis in 0.075 M HNO_3.

OJP and WIND core tops were analysed by Inductively Coupled Plasma-Mass Spectrometry [*Yu et al.,* 2005] at the Department of Earth Sciences, University of Cambridge. Long term reproducibility for Mg/Ca is better than 1.5%. Additional samples (Ceara Rise, Caribbean and Mid-Atlantic Ridge core tops) were analysed by Inductively Coupled Plasma-Optical Emission Spectroscopy at University of Bremen. Element lines for Mg/Ca were Ca: 315.89 nm; Mg: 279.55 nm. Reproducibility was within 2%. Duplicate *G. sacculifer* and *N. dutertrei* samples from the OJP (**Table 5.2**) showed no systematic offset in Mg/Ca between the two analytical methods. Most importantly for this study, regressions between $\Delta[CO_3^{2-}]$ and Mg/Ca were practically identical for the two analytical methods.

All temperatures derived from Mg/Ca values were calculated using the species specific equations of *Anand et al.* [2003] as follows:

G. ruber $Mg/Ca = 0.102 * \exp(0.340T)$ (1)

G. sacculifer $Mg/Ca = 0.050 * \exp(0.106T)$ (2)

N. dutertrei $Mg/Ca = 0.38 * \exp(0.92T)$ (3)

P. obliquiloculata $Mg/Ca = 0.12 * \exp(0.18T)$ (4)

where Mg/Ca ratios are in mmol/mol and T is in $^{\circ}$C.

5.2.4 Oxygen isotopes

Samples for δ^{18}O analysis were rinsed to remove the glue with which they were fixed for CT scanning. This glue gave no signal on the Mass Spectrometer. δ^{18}O (**Table 5.2**) was analysed at University of Bremen on a Finnigan MAT 251 with an automated carbonate preparation device. Long term analytical standard deviation is ±0.07 ‰.

Core	XDX †	Mg/Ca [mmol/mol] ICP-OES	Mg/Ca [mmol/mol] ICP-MS	ΔMg/Ca (shallow) [mmol/mol]	ΔMg/Ca (SST) [mmol/mol]	XDX ‡	δ18O [‰]	XDX †	Mg/Ca [mmol/mol] ICP-OES	Mg/Ca [mmol/mol] ICP-MS	ΔMg/Ca (shallow) mmol/mol	XDX ‡	δ18O [‰]
			G. ruber							*N. dutertrei*			
Ontong Java Plateau													
1BC3	0.4		4.81	0.00	2.01	0.22	-2.37	0.3	• 2.37	2.28	0.00	0.07	-0.47
1.5BC33	0.3		4.47	0.34	2.30	0.22	-2.57	0.6	• 2.22	2.10	0.18	0.21	-1.31
2BC13	0.8		4.13	0.68	2.63	0.61	-2.25	1.0		1.81	0.47	0.25	-1.35
2.5BC37	0.7		4.24	0.57	2.53	0.50	-2.35	1.0	• 2.10	1.97	0.31	0.83	-1.55
3BC16	1.3		4.17	0.64	2.59			1.8	• 1.62	1.73	0.55		
3BC24	1.4		4.28	0.53	2.48	1.25	-2.41	1.4	• 1.68	1.75	0.53	1.43	-1.42
4BC51								3.0	• 1.56	1.33	0.95	3.17	-1.15
4.5BC53								3.8	• 1.50	1.44	0.84	3.94	-1.37
5BC54								3.7		1.40	0.88		
5.5BC58								3.9		1.08	1.20	3.88	-0.22
6BC74												4.00	-0.37
6BC66													
Caribbean													
M35014	0.2	4.85		0.34	0.85			0.3	3.07		-0.11		
M35010	0.1	5.53		-0.34	0.08			0.2	s 2.86		0.11		
M35026	0.1	5.22		-0.03	0.48			0.3	2.48		0.49		
M35024	0.7	3.70		1.49	2.00			0.9	1.85		1.12		
Ceara Rise													
GeoB4415	0.4	4.79		0.00	1.31	0.06	-2.63	0.3	2.42		0.00	0.07	-1.37
GeoB4416	0.3	4.81		-0.02	1.29	0.33	-2.08	0.2	2.26		0.16	0.08	-1.13
GeoB4406	0.1	4.73		0.06	1.37	0.19	-2.35	0.1	2.37		0.05	0.07	-1.17
GeoB4413	0.6	4.01		0.77	2.03	0.36	-2.40	0.3	2.05		0.37	0.08	-1.17
GeoB4403	1.8	3.40		1.39	2.64	1.56	-2.30	2.0	1.70		0.72	2.75	-1.05

Mid-Atlantic Ridge

		G. sacculifer						P. obliquiloculata					
GeoB4420	0.2	4.41		-0.04	1.39			0.2	2.25		0.11		
GeoB4421	0.6	4.33		0.04	1.46			0.3	2.48		-0.11		
GeoB4424	1.0	3.21		1.16	2.41			1.2	1.55		0.81		

West Indian Ocean

WIND 11B	0.4		4.05		0.17			0.3		2.12	0.00		
WIND 20B	0.2		4.83		0.74			0.2		2.21	-0.09		
WIND 10B	0.4		3.65		0.36			0.4		1.82	0.30		
WIND 33B	0.8		3.52		2.59			1.2		1.47	0.65		
WIND 5B	0.8		2.35		1.19			2.6		1.39	0.72		
WIND 25B	0.6		3.85		1.90			1.9		1.54	0.57		
WIND 23B								3.4		1.50	0.62		
WIND 13B	1.7		2.72		2.49			2.2		1.29	0.82		
WIND 28B								3.1		1.50	0.62		
WIND 6B								3.6		0.95	1.17		
WIND 12B								3.5		s 1.21	0.90		

		G. sacculifer						*P. obliquiloculata*					

Ontong Java Plateau

1BC3	0.1	• 4.11	4.02	0.00	0.33	0.1	-2.20	0.3		2.84	0.00	0.1	-1.62
1.5BC33	0.6	• 4.08	4.24	-0.22	0.09	0.4	-2.10	0.6		2.66	0.19	0.5	-1.27
2BC13	1.1		3.76	0.26	0.57	1.3	-2.07	1.4		2.33	0.52	1.1	-1.85
2.5BC37	1.8	• 3.89	3.85	0.17	0.48	1.8	-2.14					1.0	-1.19
3BC16	2.5	• 3.70	3.41	0.61	0.92			1.9	2.29		0.55		
3BC24	2.2		3.54	0.48	0.79	3.1	-2.09	2.2		2.39	0.45	1.7	-1.24
4BC51	3.1	• 3.40	3.64	0.38	0.69	3.6	-1.99	3.2		1.90	0.94	3.0	-1.23
4.5BC53								3.6		1.65	1.19	3.7	-1.10
5BC54								3.7		1.62	1.23		
5.5BC58	3.2		ss3.78					3.9		1.46	1.39	3.7	-1.18
6BC74												4.0	-1.00
6BC66								4.0		1.40	1.44		

Caribbean

M35014	0.2	4.16		0.06	-0.16			0.1	s 2.88		0.08		
M35010	0.1	4.27		-0.06	-0.31			0.1	3.03		-0.08		
M35026	0.0	4.01		0.21	-0.01			0.2	s 2.63		0.32		

M35024	1.5	3.39		0.82	0.60			1.2	2.18		0.78		
Ceara Rise													
GeoB4415	0.1	4.08		0.00	0.04	0.0	-2.22	0.1	2.84		0.00	0.0	-1.13
GeoB4416	0.1	3.97		0.11	0.15	0.1	-2.18	0.3	2.57		0.27	0.1	-1.03
GeoB4406	0.1	4.00		0.08	0.12	0.0	-2.22	0.1	2.71		0.13	0.1	-1.57
GeoB4413	0.4	3.64		0.44	0.47	0.1	-2.18	0.2	2.53		0.31	0.2	-1.22
GeoB4403	2.6	3.43		0.65	0.68	3.1	-2.16	2.3	1.89		0.95	3.0	-0.97
Mid-Atlantic Ridge													
GeoB4420	0.1	3.80		0.07	0.23			0.1	3.00		-0.09		
GeoB4421	0.7	3.94		-0.07	0.09			0.2	2.82		0.09		
GeoB4424	2.2	3.46		0.41	0.51			0.5	2.37		0.54		
West Indian Ocean													
WIND 11B	0.1		3.37	0.00	0.10								
WIND 20B	0.1		3.87	-0.50	0.08			0.5		2.31	0.00		
WIND 10B	0.1		3.30	0.07	0.08								
WIND 33B	1.5		3.11	0.27	1.02			0.9		1.80	0.51		
WIND 5B	2.5		2.59	0.78	0.60			2.3		1.53	0.78		
WIND 25B	1.3		3.35	0.03	0.66			1.5		1.66	0.65		
WIND 23B	3.5		2.87	0.50	1.21			3.6		1.42	0.89		
WIND 13B	2.7		2.96	0.42	0.87			3.0		1.47	0.84		
WIND 28B	2.8		s 2.64	0.73	1.45			3.4		1.31	1.00		
WIND 6B	2.8		s 2.37	1.00	0.83			3.7		s 0.90	1.41		
WIND 12B	3.6		s 2.85	0.52	0.79			3.6		s 1.36	0.95		

s small sample consisting of fewer than 15 tests

ss very small sample consisting of less than 5 tests, not used in regression

• duplicate sample, value not used in regressions

XDX † is based on the sample used for Mg/Ca analysis

XDX ‡ is based on the sample used for $\delta^{18}O$ analysis

Table 5. 2 Mg/Ca, $\delta^{18}O$ and XDX for four species of planktonic foraminifera.

5.3 Sensitivity of Mg/Ca to $\Delta[CO_3^{2-}]$

A sensitivity study between $\Delta[CO_3^{2-}]$ and Mg/Ca was carried out to determine the effect of dissolution on this paleotemperature proxy. Our findings are in agreement with previous studies which show that $\Delta[CO_3^{2-}]$ exerts a strong control on Mg/Ca [*Lorens and Willia*, 1977; *Brown & Elderfield*, 1996; *Hastings et al.,* 1998; *Rosenthal et al.,* 2000; *Dekens et al.,* 2002, *Regenburg et al.,* 2006]. All four species show a decrease in Mg/Ca with decreasing saturation and the decrease starts above the calcite saturation horizon (**Figure 5.2**).

Regressions fitted for OJP (all four species), Ceara Rise (all four species) and Indian Ocean (*N. dutertrei* and *P. obliquiloculata*) sample sets (**Table 5.3**) showed sensitivity of Mg/Ca to $\Delta[CO_3^{2-}]$ was similar for each species. Mg/Ca of *G. ruber* from the Ceara Rise was more sensitive to dissolution than *G. sacculifer* from the same site (no overlap on 95% confidence interval of slopes). *Regenberg et al.* [2006] carried out a similar sensitivity study using Caribbean core-tops. The response of Mg/Ca to $\Delta[CO_3^{2-}]$ of *G. ruber* and *G. sacculifer* are comparible to our results for these species (regressions shown on **Figure 5.2**). In that study the apparently higher sensitivity of *G. ruber* compared to *G. sacculifer* did not reach statistical significance.

Mg/Ca of *N. dutertrei* from the Caribbean [*Regenberg et al.,* 2006] appears to be more sensitive to $\Delta[CO_3^{2-}]$ than that of *N. dutertrei* from the other core top samples used here suggesting that sensitivity can vary within a species.

The disparity in Mg/Ca values of shallow (*G. ruber* and *G. sacculifer*) and thermocline dwelling (*N. dutertrei* and *P. obliquiloculata*) species indicates that, despite dissolution, Mg/Ca values retain something of the initial temperature signal. The wide scatter of *G. ruber* and *G. sacculifer* values reflects the range of SST at different sites. Annual average SST at the OJP is ~29 ^{o}C, while SSTs of Indian Ocean sites are between 17 and 21 ^{o}C (**Table 5.1**).
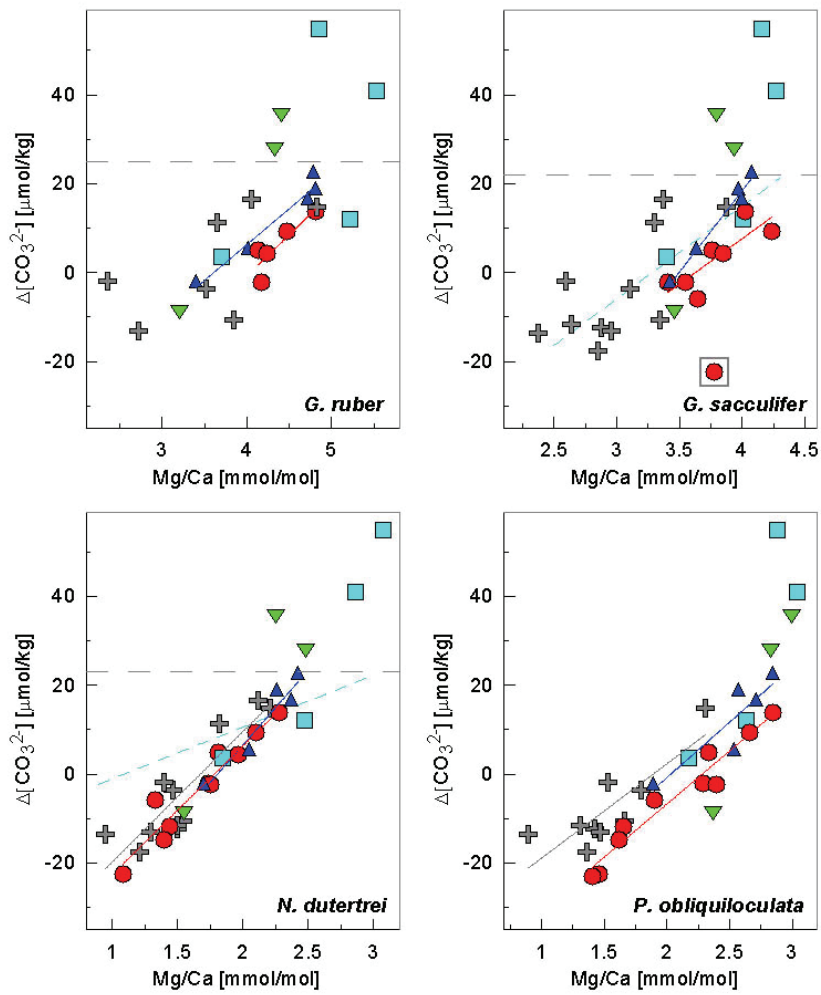
Figure 5.2 Deep water $\Delta[CO_3^{2-}]$ versus Mg/Ca for four species of foraminifera. Samples are from the OJP (red circles), Ceara Rise (blue triangles), Indian Ocean (grey crosses), Caribbean Sea (turquoise squares) and MAR (green triangles pointing down). Grey box round sample point indicate a small sample not used in the regression. Regressions (eq. 5) fitted for *G. ruber* and *G. sacculifer* from OJP (red lines) and Ceara Rise (blue lines) sites and for *N. dutertrei* and *P. obliquiloculata* from OJP, Ceara Rise and Indian Ocean sites (grey lines). Regression coefficients are given in **Table 5.3**. Blue dashed line is regression of *Regenberg et al.* [2006] for Caribbean core tops. Horizontal dashed lines are $\Delta[CO_3^{2-}]$ values where *Regenberg et al.* [2006] detect dissolution effect on Mg/Ca.

	Ceara Rise			Indian Ocean			OJP		
Species	Slope	Intercept	r^2	Slope	intercept	r^2	Slope	intercept	r^2
G. ruber (white)	15 (±3)	-53 (±15)	0.99				20 (±21)	-82 (±90)	0.64
G. sacculifer	35 (±15)	-124 (±58)	0.98				20 (±16)	-74 (±60)	0.69
N. dutertrei	32 (±31)	-57 (±66)	0.91	29 (±11)	-49 (±18)	0.79	29 (±7)	-51 (±12)	0.92
P. obliquiloculata	23 (±43)	-46 (±104)	0.73	21 (±12)	-40 (±19)	0.71	24 (±5)	-54 (±10)	0.95

± is half the 95% confidence interval

Table 5. 3 Coefficients of regressions shown on **Figure 5.2**.

5.3.1 Sensitivity of dissolution induced reduction in Mg/Ca (ΔMg/Ca) to $\Delta[CO_3^{2-}]$

In order that the effect of dissolution on Mg/Ca can be compared for samples with different calcification temperatures, and hence different initial Mg/Ca, we estimate the reduction in Mg/Ca due to dissolution, ΔMg/Ca:

$$\Delta Mg/Ca = Mg/Ca_{INITIAL} - Mg/Ca_{MEASURED} \tag{5}$$

where Mg/Ca $_{INITIAL}$ is Mg/Ca before any dissolution effect and Mg/Ca $_{MEASURED}$ is analysed Mg/Ca (**Table 5.2**). The first stage of calculating ΔMg/Ca is to estimate values of Mg/Ca $_{INITIAL}$.

There are two possible ways to estimate Mg/Ca $_{INITIAL}$. One is to estimate calcification temperature from an appropriate water depth and season for each species and to back calculate Mg/Ca using established calibrations. The other is simply to assume that Mg/Ca values of samples from shallow sites within each sample set are unbiased by dissolution and use these values.

The first approach must be used for shallow dwelling species, *G. ruber* and *G. sacculifer*, from the western Indian Ocean. This sample set covers a wide geographic area spanning a latitudinal range from 10 to 33 ^{o}S and SST is thus dissimilar between sites of shallow and deep samples.

The latter method is appropriate where samples within a set represent similar environmental conditions. Sample sets from the OJP, Ceara Rise, Mid-Atlantic Ridge and the Caribbean each cover a small geographic area. Sites within each set are closely spaced; sea surface temperatures, and the temperature profile of the water column, are

similar. There is less than 1 °C difference in annual average temperatures for sites within each set [*Locarnini et al.,* 2006]. For these sample sets, it is reasonable to assume that Mg/Ca $_{INITIAL}$ values were similar to each other for each sample within the set. Mg/Ca of shallow samples should provide a good estimate of Mg/Ca $_{INITIAL}$ as calcification depth and season is accounted for.

Shallow samples used for Mg/Ca $_{INITIAL}$ were as follows. For the Ceara Rise core top sample GeoB4415, where $\Delta[CO_3^{2-}]$ was 22 μmol/kg was used. Samples from sites where $\Delta[CO_3^{2-}]$ was above 25 μmol/kg were averaged to estimate Mg/Ca $_{INITIAL}$ for each species from the mid-Atlantic Ridge (GeoB4420 and GeoB4421) and Caribbean Sea sample sets (M35014 and M35010). Shallow samples from the western Indian Ocean (WIND20B) and OJP (1BC3) come from sites where $\Delta[CO_3^{2-}]$ is 18 and 14 μmol/kg respectively.

This raises the question of whether samples from the shallowest site within each transect are free from dissolution bias. The shallowest sites for OJP and western Indian Ocean sample sets have $\Delta[CO_3^{2-}]$ values which are below the threshold where *Regenberg et al.,* [2006] identify dissolution effects on Mg/Ca (22-25 μmol/kg). It is possible therefore, that Mg/Ca has been reduced by dissolution (further discussion **Section 5.5.2**). However, an offset in ΔMg/Ca and $\Delta[CO_3^{2-}]$ from pristine values does not alter sensitivity calculated between the two parameters if the relationship is linear, as is assumed.

The equation of the regression between $\Delta[CO_3^{2-}]$ and ΔMg/Ca can be written as:

$$\Delta[CO_3^{2-}] = m * \Delta Mg/Ca + \Delta[CO_3^{2-}]_{CRITICAL} \tag{6}$$

where *m* is the slope of the regression and $\Delta[CO_3^{2-}]$ $_{CRITICAL}$ is the value below which Mg/Ca starts to reduce due to dissolution. Sensitivity to the effect of dissolution on Mg/Ca is given by 1/*m* (mmol/mol reduction in Mg/Ca per 1 μmol/kg decrease in $\Delta[CO_3^{2-}]$).

Parameters for regressions for OJP, Ceara Rise and Indian Ocean sample sets are shown in **Table 5.3**. For *G. ruber* and *G. sacculifer* two methods of calculating Mg/Ca $_{INITIAL}$ were used as described above. For *N. dutertrei* and *P. obliquiloculata* the latter method, using Mg/Ca of shallow samples within each set as Mg/Ca $_{INITIAL}$, was used for the three sample sets.

G. ruber and *G. sacculifer* calcify predominantly in the mixed layer and the photic zone [*Bé*, 1980; *Hemleben et al.*, 1989; *Savin and Douglas*, 1973] and Mg/Ca is thought to represent temperatures close to SST. For these species therefore Mg/Ca $_{INITIAL}$ can be back calculated from SST using the species specific equations of *Anand et al.*, [2003] (Eq. 1 and 2 for *G. ruber* and *G. sacculifer* respectively).

According to the calibration of *Anand et al.* [2003] (eq. 1), Mg/Ca of *G. ruber* from shallow sites ($\Delta[CO_3^{2-}]$ >10 µmol/kg) in the western Indian Ocean represents temperatures close to warm season SST [*Rayner et al.*, 2003] (**Figure 5.3**). Mg/Ca of *G. ruber* from OJP, Ceara Rise, Caribbean Sea and MAR sites, however, underestimates both warm season SST and annual average SST by at least 2 °C (further discussion **Section 5.4.2**). Due to the disparity between SST and Mg/Ca of *G. ruber*, use of SST to estimate Mg/Ca $_{INITIAL}$ for Ceara Rise and OJP *G. ruber* gave $\Delta[CO_3^{2-}]_{CRITICAL}$ values of 55 (±56) µmol/kg for the OJP and 38 (±8) µmol/kg for the Ceara Rise which are much higher than estimates from any other sample set. Mg/Ca values of the shallowest samples within each set appear to offer a better estimate of Mg/Ca $_{INITIAL}$ than SST for most sites for *G. ruber* due to the mismatch of Mg/Ca and SST.
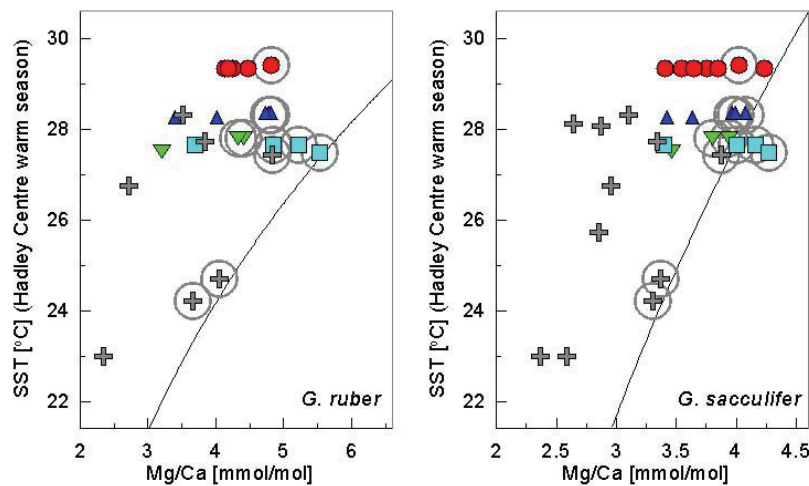
Figure 5.3. Mg/Ca of *G. ruber* and *G. sacculifer* versus SST at sample site. SST is warm season average from HadISST1 1° grid reconstruction for 1870–present [*Rayner et al.*, 2003] extracted using the Climate Explorer application of *Oldenborgh et al.* [2009]. Black curves are Mg/Ca temperature calibrations of *Anand et al.*, [2003]. Samples are from OJP (red circles), Ceara Rise (blue triangles), Indian Ocean (grey crosses), Caribbean Sea (turquoise squares) and MAR (green triangles pointing down). Mg/Ca of *G. ruber* from the western Indian Ocean, and *G. sacculifer* from sites where $\Delta[CO_3^{2-}]$ is above 10 µmol/kg (circled) represent temperatures close to SST.

Mg/Ca of *G. sacculifer* from sites where $\Delta[CO_3^{2-}] > 10$ µmol/kg yield temperatures close to SST (Hadley Centre warm season average) (**Figure 5.3**). There is little difference in regressions whether SST or samples from shallow sites are used as Mg/Ca $_{INITIAL}$ (**Table 5.3**).

N. dutertrei and *P. obliquiloculata* inhabit the thermocline and calcify over a range of depths and hence temperatures [*Ravelo and Fairbanks,* 1992]. Estimates of their depth

habitat vary from place to place [*Shackleton and Vincent*, 1978; *Anand et al.,* 2003] and probably reflect local thermocline structure and chlorophyll maximum rather than a fixed habitat depth.

Thermocline structure east of Madagascar varies with longitude, being deeper at 20 ^{o}S, where the 18 ^{o}C isotherm is at 250 m depth, than at 10 or 30 ^{o}S where the 18 ^{o}C isotherm is at 100 m [*Locarnini et al.,* 2006]. Despite this variation in water column structure $\Delta[CO_3^{2-}]$ and Mg/Ca of *N. dutertrei* from the western Indian Ocean can be fitted with a linear regression ($r^2 > 0.70$) which has similar slope as regressions for OJP and Ceara Rise sites. This suggests a similar Mg/Ca $_{INITIAL}$ for all *N. dutertrei* samples from the Indian Ocean sample set. It may be that calcification is to some extent temperature controlled for this species. *Hemleben et al.* [1989] suggested *N. dutertrei* crust growth is triggered below 15 ^{o}C.

As with *N. dutertrei*, the relationship between $\Delta[CO_3^{2-}]$ and ΔMg/Ca for *P. obliquiloculata* from Indian Ocean sites fits a linear regression ($r^2 > 0.70$), again suggesting Mg/Ca $_{INITIAL}$, and hence calcification temperatures were similar for *P. obliquiloculata* from all our Indian Ocean sites.

The similarity of regressions between $\Delta[CO_3^{2-}]$ and ΔMg/Ca for OJP, Ceara Rise and Indian Ocean sample sets supports use of $\Delta[CO_3^{2-}]$ proxies to correct for dissolution bias of Mg/Ca. **Figure 5.4** shows one regression fitted for all samples for each species. Regression coefficients are given in **Table 5.4**. ΔMg/Ca values are based on Mg/Ca $_{INITIAL}$ estimated from SST for *G. ruber* and *G. sacculifer* from the Indian Ocean and on Mg/Ca of shallowest sites within each transect (as described above) for the other sites as these seem to be the best estimates of ΔMg/Ca.

Much of the variation in ΔMg/Ca of these core top samples can be explained by dissolution. Correlation (r^2) between $\Delta[CO_3^{2-}]$ and ΔMg/Ca is above 0.60 for all four species (**Figure 5.4, Table 5.4**). Sensitivity of ΔMg/Ca to dissolution was similar for *G. sacculifer*, *N. dutertrei* and *P. obliquiloculata*. Sensitivity was higher for *G. ruber* (slopes did not overlap at 95 % confidence interval) than for the other three species.
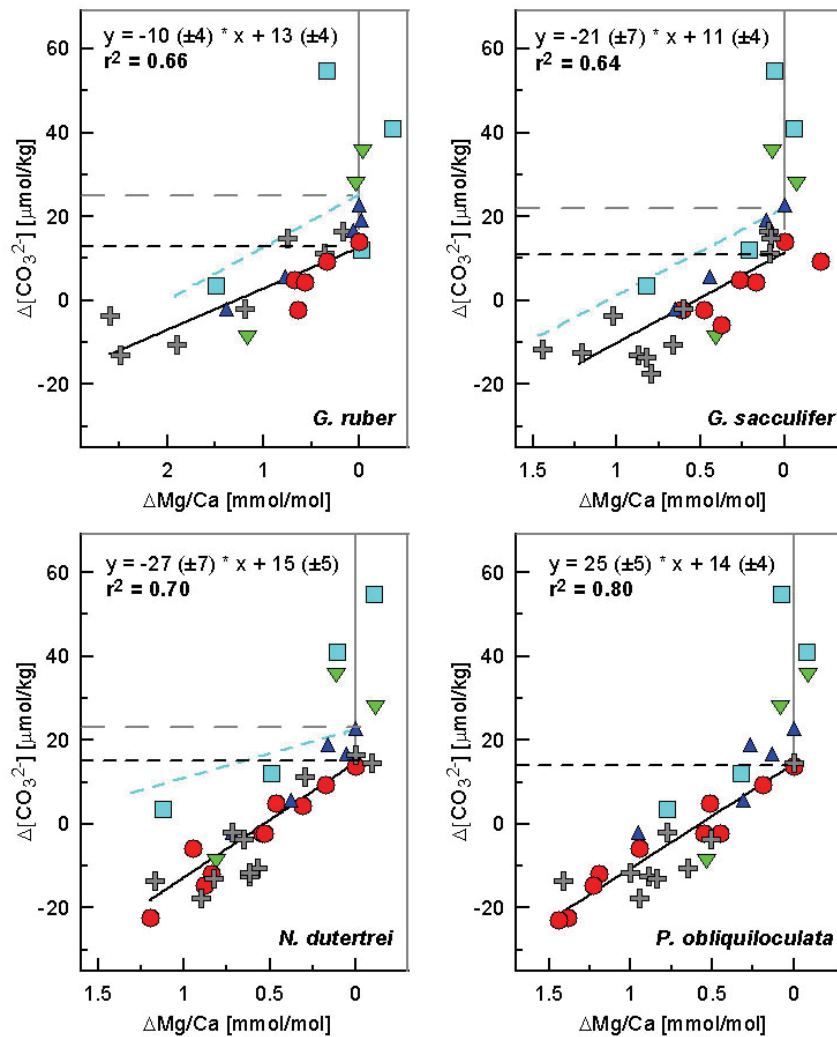
Figure 5.4 Deep water $\Delta[CO_3^{2-}]$ versus ΔMg/Ca for four species of foraminifera. Samples are from OJP (red circles), Ceara Rise (blue triangles), Indian Ocean (grey crosses), Caribbean Sea (turquoise squares) and MAR (green triangles pointing down). ΔMg/Ca is calculated for each sample (described in **Section 5.3**). Parameters for regressions between $\Delta[CO_3^{2-}]$ and ΔMg/Ca for selected sites are in **Table 5.3**. Regressions shown on graphs are averages for all sites, y is $\Delta[CO_3^{2-}]$ and x is ΔMg/Ca. Blue dashed lines are regressions of *Regenberg et al.* [2006]. Here average Mg/Ca from samples above 2000 m water depth ($\Delta[CO_3^{2-}] \approx 50$ µmol/kg) was Mg/Ca INITIAL. Horizontal dashed lines are threshold values of $\Delta[CO_3^{2-}]$ where dissolution affects Mg/Ca found by *Regenberg et al.* [2006] (upper wide dash) and this study (lower, narrow dash).

Species	Indian Ocean				Ontong Java Plateau				Ceara Rise				All samples combined
	slope	$\Delta[CO_3^{2-}]$ CRITICAL	Sensitivity of Mg/Ca to $\Delta[CO_3^{2-}]$ [mmol per µmol/kg]	r^2	slope	$\Delta[CO_3^{2-}]$ CRITICAL	Sensitivity of Mg/Ca to $\Delta[CO_3^{2-}]$ [mmol per µmol/kg]	r^2	slope	$\Delta[CO_3^{2-}]$ CRITICAL	Sensitivity of Mg/Ca to $\Delta[CO_3^{2-}]$ [mmol per µmol/kg]	r^2	Sensitivity of Mg/Ca to $\Delta[CO_3^{2-}]$ mmol per µmol/kg
Mg/Ca of shallow samples used as Mg/Ca INITIAL					Mg/Ca of shallow samples used as Mg/Ca INITIAL				Mg/Ca of shallow samples used as Mg/Ca INITIAL				
G. ruber (white)					-20 (±21)	14 (±11)	-0.050 (±0.052)	0.64	-15 (±4)	17 (±3)	-0.068 (±0.017)	0.99	-0.102 (±0.036)
G. sacculifer					-20 (±16)	8 (±6)	-0.049 (±0.038)	0.69	-35 (±16)	21 (±6)	-0.028 (±0.012)	0.98	-0.047 (±0.015)
N. dutertrei	-29 (±11)	13 (±8)	-0.034 (±0.013)	0.79	-29 (±7)	14 (±5)	-0.035 (±0.008)	0.92	-32 (±31)	20 (±13)	-0.032 (±0.031)	0.90	-0.037 (±0.010)
P. obliquiloculata	-21 (±12)	9 (±10)	-0.047 (±0.027)	0.71	-24 (±5)	13 (±4)	-0.042 (±0.008)	0.94	-23 (±43)	19 (±22)	-0.044 (±0.081)	0.73	-0.040 (±0.008)
SST used to derive Mg/Ca INITIAL					SST used to derive Mg/Ca INITIAL				SST used to derive Mg/Ca INITIAL				
G. ruber (white)	-11 (±6)	17 (±10)	-0.092 (±0.054)	0.79	-22 (±23)	57 (±56)	-0.046 (±0.049)	0.63	-15 (±4)	38 (±8)	-0.065 (±0.018)	0.99	
G. sacculifer	-22 (±11)	12 (±9)	-0.045 (±0.023)	0.69	-20 (±16)	14 (±10)	-0.049 (±0.039)	0.67	-36 (±16)	22 (±7)	-0.028 (±0.012)	0.98	

$\Delta[CO_3^{2-}]$CRITICAL is the intercept on the y-axis, the value of $\Delta[CO_3^{2-}]$ where ΔMg/Ca is zero.

± is half the 95% confidence interval

Table 5.4 Coefficients for regressions between $\Delta[CO_3^{2-}]$ and ΔMg/Ca. Final column gives sensitivity (inverse slope) of ΔMg/Ca to $\Delta[CO_3^{2-}]$ for the regressions shown in **Figure 5.4**.

5.4. Implications of the effect of dissolution on Mg/Ca

5.4.1 Mg/Ca and dissolution susceptibility of foraminiferal calcite

Although it is accepted that Mg/Ca is affected by dissolution in waters oversaturated with respect to calcite [*Brown & Elderfield*, 1996] literature values vary for where dissolution starts to distort Mg/Ca. *Dekens et al*. [2002] suggest that Mg/Ca is affected at all depths below the surface and propose a linear correction based on water depth or $\Delta[CO_3^{2-}]$. *Regenberg et al*. [2006] found threshold $\Delta[CO_3^{2-}]$ values of between 22 and 25 µmol/kg for Caribbean *G. ruber* (white), *G. sacculifer* and *N. dutertrei* and assumed a linear decrease in Mg/Ca below this value.

Our data do not clearly isolate the threshold of dissolution effects on Mg/Ca, there being few samples in the crucial $\Delta[CO_3^{2-}]$ interval between 10 and 30µmol/kg. Regressions between $\Delta[CO_3^{2-}]$ and ΔMg/Ca give $\Delta[CO_3^{2-}]$ CRITICAL values of between 11 (±4) and 15 (±5) µmol/kg. These $\Delta[CO_3^{2-}]$ CRITICAL values are constrained for some sample sets as Mg/Ca INITIAL is defined as the shallowest sample within the set. If there is dissolution above Mg/Ca INITIAL then our $\Delta[CO_3^{2-}]$ CRITICAL values would be too low (**Section 5.5.3**). Our best estimate of $\Delta[CO_3^{2-}]$ CRITICAL probably comes from *G. sacculifer* where SST is used to derive Mg/Ca INITIAL. This gave $\Delta[CO_3^{2-}]$ CRITICAL of 15 (±5) µmol/kg.

These values are lower than those of *Dekens et al*. [2000] and *Regenberg et al.* [2006], but support findings that Mg/Ca of tests is altered by dissolution even in waters oversaturated with respect to calcite. Impurities in the calcite lattice increase dissolution susceptibility. Mg^{2+} is the major impurity in foraminiferal calcite and Mg content has been used to explain enhanced dissolution susceptibility of biogenic calcite [*Walter and Morse*, 1985; *Brown and Elderfield*, 1996; *Yu et al*., 2007].

As described more fully in *Johnstone et al*. [in press (**Chapter 4**)], the pattern of dissolution shown in CT scans is consistent with preferential dissolution of Mg-rich calcite. **Figure 5.1** shows tomography scans of *N. dutertrei* tests in various stages of dissolution. The smallest inner chambers of tests are first affected. Partially dissolved areas of calcite give pale colour values in the scanned image. The progress of dissolution can be seen in the difference between a well-preserved sample (**Figure 5.1a**) and slightly dissolved tests (**Figure 5.1b**). In the latter figure, the colour contrast between inner and outer calcite shows that the chamber walls and the inner layer of the outer wall have been partially dissolved. These are the parts of the test richest in Mg. Around the depth of calcite saturation horizon all of the inner calcite is partially dissolved and porous (**Figure 5.1c**). In severely dissolved samples, only the low Mg outer crust [*Sadekov et al.,* 2005] remains (**Figure 5.1d**).

Although test calcite rich in Mg dissolves preferentially, species with high Mg/Ca do not necessarily lose more Mg/Ca in response to decreasing calcite saturation than species with low initial Mg/Ca. The species highest in Mg, *G. ruber*, may show the greatest reduction in Mg/Ca per 1 μmol/kg change in calcite saturation (**Figure 5.4**, further discussion **Section 5.4.2**), but *G. sacculifer,* with only slightly lower Mg/Ca, shows similar sensitivity as *P. obliquiloculata*, which has much lower Mg/Ca (**Figure 5.2**). Other factors which influence dissolution susceptibility, such as crystallinity, thickness of the test walls or the proportion of crust to inner calcite, could alter correlation between Mg content and dissolution susceptibility between species.

Despite the lack of correlation between the typical Mg/Ca value of a species and the sensitivity of Mg/Ca to dissolution of that species; within one species Mg/Ca may influence dissolution susceptibility. *N. dutertrei* shows differing sensitivity to the effect of dissolution on Mg/Ca at different locations. *N. dutertrei* from the Caribbean shows a greater reduction in Mg/Ca than *N. dutertrei* from other sites [*Regenberg et al.*, 2006]. Caribbean *N. dutertrei* has the highest Mg/Ca of all *N. dutertrei* samples measured here (**Table 5.2**). Mg/Ca of well-preserved Caribbean *N. dutertrei* is 26% greater than those from mid-Atlantic Ridge and 30% more than those from the Ontong Java Plateau. This intraspecies variation in Mg content may affect dissolution susceptibility.

5.4.2 Effect of dissolution on Mg/Ca derived temperatures

Temperatures based on the Mg/Ca of thermocline dwellers are the most disturbed by the effect of dissolution (**Figure 5.6**). Their low Mg/Ca values mean that a small absolute change results in a relatively large change in calculated temperature. In addition, tests of robust, thermocline dwelling species can sustain more loss of material before they disintegrate. *G. sacculifer* shows a similar sensitivity to the effect of $\Delta[CO_3^{2-}]$ on Mg/Ca to that of *N. dutertrei* but the former is typically not preserved in samples at such low values of $\Delta[CO_3^{2-}]$. Therefore the absolute decrease in Mg/Ca is greater for the most dissolution resistant species found in the deepest samples.

Temperatures calculated from *G. ruber* from the OJP show a relatively small change in temperatures between shallow and deep samples. Temperatures are only ~1.5 ^{o}C lower for samples from the deepest site compared to those from the shallowest site. At the OJP decrease in Mg/Ca tails off after a ~0.6 mmol/mol decrease in Mg/Ca (**Table 5.2**, **Figure 5.2**). *Fehrenbacher et al.* [2006] found that *G. ruber* from the Atlantic had a similar sensitivity to the effect of dissolution on Mg/Ca as the *G. ruber* from our OJP sample set. In that study, the response of Mg/Ca of *G. ruber* to calcite undersaturation was similar to that of *G. sacculifer* and lower than that of *N. dutertrei*.

In spite of this evidence of low sensitivity, considering the response of *G. ruber* from the OJP in isolation may be misleading. Temperatures calculated from neither δ¹⁸O

(24.7 ^{o}C using the species specific equation of *Mulitza et al.,* [2003]) nor Mg/Ca (25 ^{o}C) of *G. ruber* from the shallowest (1616 m) sample from the OJP support modern SST of 29 ^{o}C (**Figure 5.3**, **Figure 5.6**). *G. ruber* can continue to calcify below the mixed layer [*Duplessy et al.*, 1981] or favour the winter season [*Wilke et al.*, 2009] which could explain it representing temperatures below SST in some locations. This is presumably not the case for OJP where there is a thick mixed layer and little seasonal temperature change [*Locarnini et al.,* 2006].

The poor representation of SST by Mg/Ca of OJP *G. ruber* for whatever reason (discussion of undetected dissolution effects in **Section 5.5.3**), may cast doubt on sensitivity of Mg/Ca to $\Delta[CO_3^{2-}]$ calculated for this sample set. *G. ruber* from the Ceara Rise, MAR, Caribbean Sea and western Indian Ocean all suggest greater sensitivity of Mg/Ca to $\Delta[CO_3^{2-}]$ than *G. ruber* from the OJP (**Figure 5.3**). Temperatures derived from Mg/Ca of poorly preserved *G. ruber* from the western Indian Ocean (where $\Delta[CO_3^{2-}]$ is -13 μmol/kg) are 4–5 ^{o}C below local SST, indicating water depths of 70–160 m. Atlantic samples are better preserved than those from Indian and Pacific sites. *G. ruber* from the deepest Atlantic sites (where $\Delta[CO_3^{2-}]$ is -2.5 μmol/kg) give temperatures 2–3 ^{o}C less than SST, which corresponds to depths of 80–170 m. These temperatures and depths are colder and deeper than those of the mixed layer and the photic zone.

Unlike the other species analysed here, *G. ruber* has no dissolution-resistant outer crust [*Caron et al.*, 1990]. As dissolution proceeds, microporosity, indicated by light greyscale values in the CT scans, develops in the calcite of the entire test [*Johnstone et al.,* in press (**Chapter 4**)]. If this porosity is due to preferential leaching of Mg-rich calcite, it would explain why bulk Mg/Ca does not represent actual calcification temperatures of poorly preserved *G. ruber*.

Leaching of the inner calcite occurs also in other species. CT scans show that the inner calcite of poorly preserved *G. sacculifer*, *N. dutertrei* and *P. obliquiloculata* is also porous and dissolved. This leached porous calcite presumably contributes little to the Mg/Ca signal of species such as *N. dutertrei* and *P. obliquiloculata,* where the outer crust dominates the signal. *G. sacculifer* does not show the same complete loss of inner calcite as the deeper dwelling species, and even the most dissolved *G. sacculifer* tests contain traces of the inner calcite of the outer wall.

Severely dissolved *G. sacculifer* (XDX > 3) from the OJP represent temperatures 2–3 ^{o}C less than the shallowest samples. Indian Ocean samples give temperatures 4–6 ^{o}C less than local SST. These temperatures represent water depths of ~100 m for OJP and 110–135 m for the Indian Ocean. *Rosenthal et al.*, [2000] suggests that $\delta^{18}O$ and Mg/Ca of progressively dissolved *G. sacculifer* reveals progressive calcification depths. *G. sacculifer* are known to continue to calcify in the thermocline [*Duplessy*,

1981; *Rosenthal et al.*, 2000, *Wilke et al.*, 2008] and these depths and temperatures seem reasonable for the penultimate or final stages of calcification of these species.

Tests of thermocline dwelling foraminifera that have undergone severe dissolution contain no inner calcite and consist only of outer crust (**Figure 5.1d**). Temperatures calculated from these remnants yield temperatures which are reduced compared to shallow samples by ~9 ^{o}C (from 21 ^{o}C to 12 ^{o}C) for *N. dutertrei* and by ~6 ^{o}C (from 23 ^{o}C to 17 ^{o}C) for *P. obliquiloculata* from the OJP according to the calibrations of *Anand et al.*, [2003] (Eq. 3 and 4). If these temperatures indicate accurate calcification temperatures for the outer, gametogenic calcite, these species continue to calcify deep within the thermocline.

P. obliquiloculata, like *N. dutertrei*, inhabits the seasonal thermocline [*Jones* 1967; *Curry et al.*, 1983; *Faul et al.* 2000] and both species are associated with the deep chlorophyll maximum [*Ravelo and Fairbanks*, 1992]. The deep chlorophyll maximum is at ~110 m at on the OJP [*Nathan and Leckie*, 2009]. Temperatures of 12 ^{o}C are found well below this at ~250 m, while 17 ^{o}C represents water depths of ~200 m. Support for calcification at such depths is supported by the depth integrated growth model of *Wilke and Peeters* [2006]. They find calcification continues well below both the chlorophyll and temperature gradient maxima, until depths of 133 m for *N. dutertrei* and 344 m for *P. obliquiloculata*, at their Atlantic sites.

5.4. 3 Systematic bias in Mg/Ca derived temperatures over a glacial cycle

The transfer of CO_2 between ocean and atmosphere within a glacial cycle is associated with peaks in calcite preservation in the deep sea during deglacial transitions [*Berger*, 1977; *Le and Shackleton*, 1992; *Hodell et al.*, 2001]. The shift in $\Delta[CO_3^{2-}]$ has been estimated at 25-30 umol/kg for the deep Pacific during the last deglaciation [*Marchitto et al.*, 2005].

Regressions between $\Delta[CO_3^{2-}]$ and ΔMg/Ca (**Table 5.3**) allow an estimate of dissolution bias of Mg/Ca derived temperatures for such a shift in $\Delta[CO_3^{2-}]$. At sites where $\Delta[CO_3^{2-}]$ changes in the critical range from 15 µmol/kg, where tests are well preserved, to -20 umol/kg, where they are severely dissolved, temperatures of 21 ^{o}C would be measured as 17 ^{o}C by *N. dutertrei*. *P. obliquiloculata* calcification temperatures of 23 ^{o}C would be measured as 20 ^{o}C.

Theoretically, such a shift would lead to an underestimate in typical tropical SST of 28 ^{o}C [*Locarnini et al.*, 2006] by 4 ^{o}C for *G. ruber* and 7 ^{o}C for *G. sacculifer*. Although it may be that neither of these fragile species would represent the entire 25 µmol/kg adjustment; tests of these species are sparse in our samples from sites where $\Delta[CO_3^{2-}]$ is below -15 µmol/kg. A decrease in deepwater calcite saturation from 15 µmol/kg to $\Delta[CO_3^{2-}]$ values of 0 umol/kg would be recorded as an apparent cooling from 28 ^{o}C to 26 ^{o}C by *G. ruber* and from 28 ^{o}C to 24 ^{o}C for *G. sacculifer*. The

absolute reduction in derived temperatures due to dissolution is greater at lower temperatures. SST of 25 °C would be recorded as 21 °C by *G. ruber* and 20 °C by *G. sacculifer* for a similar 15 μmol/kg decrease in $\Delta[CO_3^{2-}]$.

As suggested by *Mix et al.*, [2006] such a preservation artifact in Mg/Ca based SST could explain much of the dissimilarity in records of deglacial warming for the Pacific derived from different biotic carriers. SST derived from Mg/Ca of *G. ruber* for a site at 2830 m water depth the Pacific [*Lea et al.*, 2006] diverges from that calculated from alkenones (which are not affected by calcite saturation state) at a nearby site [*Prahl et al.*, 2006] with the greatest difference between the two proxies, of ~3 °C, occurring during the deglacial transition.

The site of core TR163-22 used by *Lea et al.*, [2006] lies close to the current calcite saturation horizon which is at 2900 m water depth [*Thunell et al.*, 1981]. Mg/Ca of planktonic foraminifera is distorted by dissolution at such values of $\Delta[CO_3^{2-}]$ [*Regenberg et al.*, 2006; **Figure 5.2**]. The deglacial shift in $\Delta[CO_3^{2-}]$ would increase $\Delta[CO_3^{2-}]$ at the site to values >15 μmol/kg, resulting in well-preserved tests.

Mg/Ca of *G. ruber* yields SST of 25 °C during the deglacial transition. Our calibration suggests that SST would be recorded as 21 °C during the preceding episode of poor preservation. The deglacial preservation event could therefore explain the change in offset between foraminifera and alkenone based SSTs.

5.5 Towards an independent correction for dissolution bias of Mg/Ca

5.5.1 Calibration between XDX and ΔMg/Ca

$\Delta[CO_3^{2-}]$ proxy XDX plotted versus ΔMg/Ca (**Figure 5.5**) shows an approximately linear relationship. Correlation between XDX and ΔMg/Ca is strongest for the thermocline dwelling species (*N. dutertrei* and *P. obliquiloculata*). These deep dwelling species have a large amount of outer crust calcite which protects the inner calcite as it dissolves and the progress of dissolution through the test is clearly shown. Correlation between XDX and ΔMg/Ca is least good for *G. ruber* (**Figure 5.5**).

G. ruber does not show the more advanced stages of dissolution as it has no outer crust. This may mean that XDX stages are more difficult to estimate. Another factor may be that *G. ruber*, which is fragile with thin walls, cannot sustain much dissolution. The difference in *G. ruber* populations between samples from shallow and deep sites may be greater for *G. ruber* than is the case for more robust species.
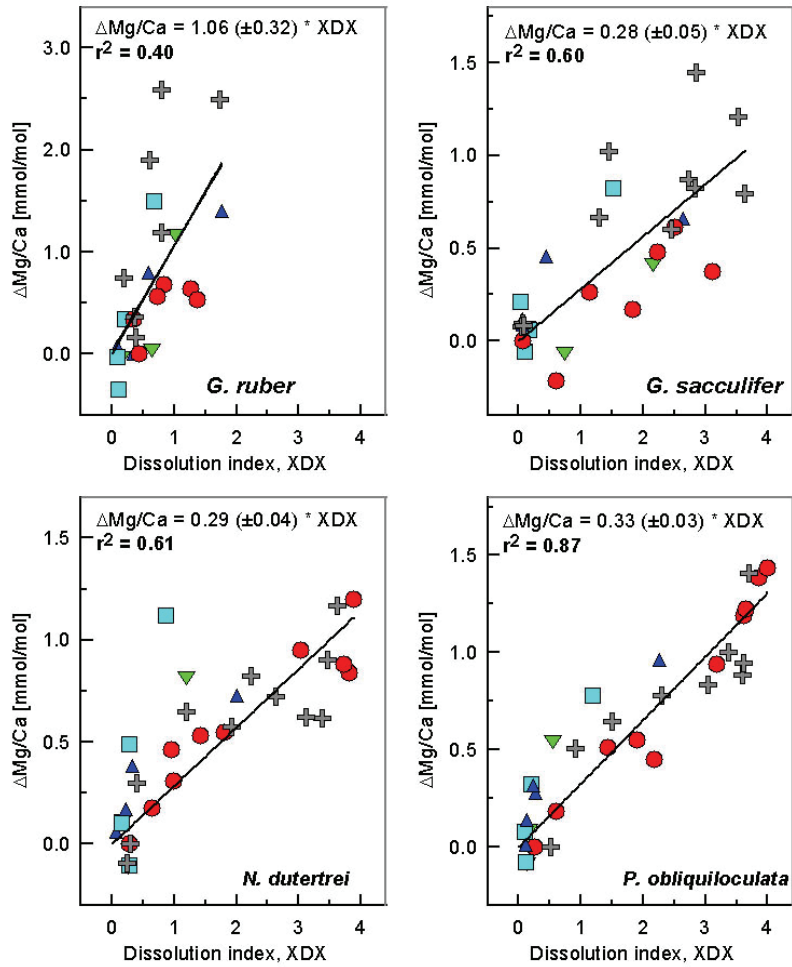
Figure 5.5 XDX versus ΔMg/Ca for four species of planktonic foraminifera. Parameters for the regressions (eq. 7) (forced through the origin) are shown.

Regressions plotted for each species can be used to estimate the reduction of Mg/Ca due to dissolution (ΔMg/Ca) according to:

$$\Delta Mg/Ca = q * XDX \tag{7}$$

where q is species specific gradient of the regression (**Figure 5.5**). ΔMg/Ca can then be combined with analysed Mg/Ca to estimate what dissolution unaffected Mg/Ca would have been, according to a rearrange of equation (1) to:

$$Mg/Ca_{INITIAL} = Mg/Ca_{MEASURED} + \Delta Mg/Ca.$$

5.5.2 Correcting dissolution bias of Mg/Ca using XDX

The effect of applying the corrections is to reduce scatter in derived temperatures (**Figure 5.6**). For all four species corrected temperatures fall into a smaller range than temperatures calculated from analysed Mg/Ca. Final error on temperature is on average ± 1.5 °C for each sample set. This is small compared to the systematic error caused by dissolution, which can be several degrees.

81

Mean temperature [°C]:
Measured: 25.0 (±0.6)   24.9 (±1.5)
Corrected: 26.5 (±0.5)   26.1 (±0.5)

G. ruber

Mean temperature [°C]:
Measured: 26.4 (±1.6)   26.7 (±1.5)
Corrected: 28.5 (±0.8)   27.5 (±0.7)

G. sacculifer

82
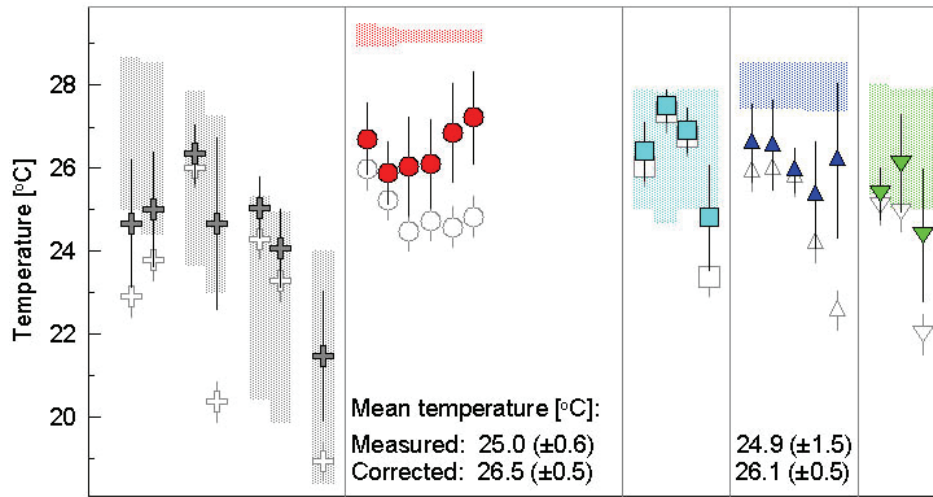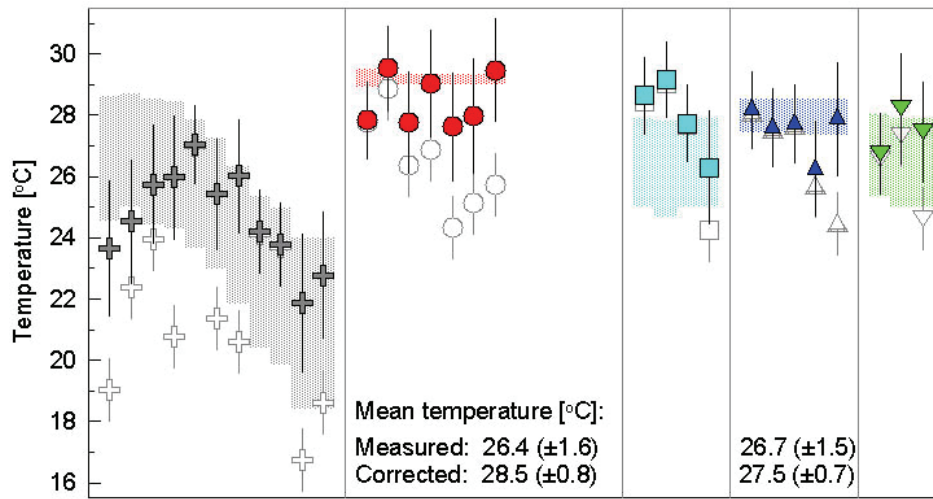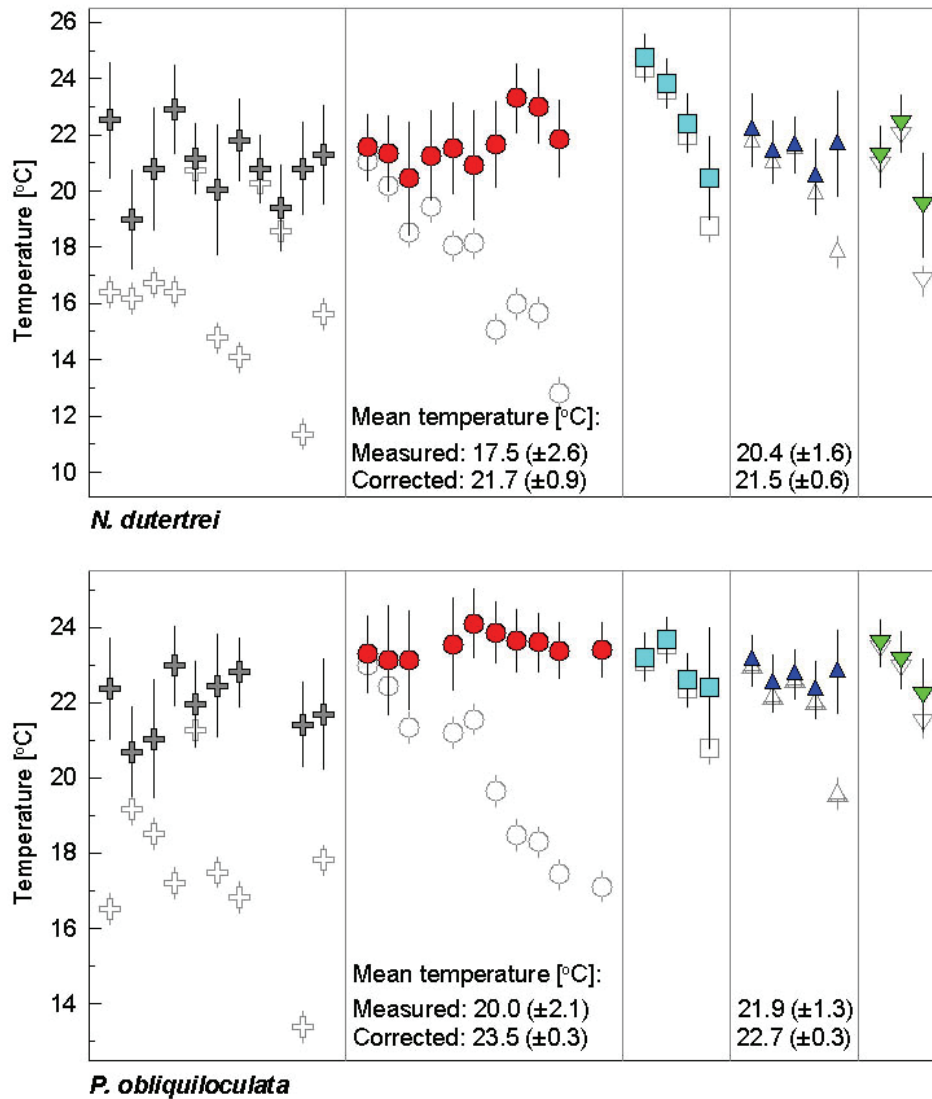
Figure 5.6 (Above and facing page) Effect of using XDX to correct Mg/Ca derived temperatures for four species of foraminifera. Temperatures were corrected using species specific calibrations between XDX and ΔMg/Ca (**Figure 5.5**). Samples are from OJP (red circles), Ceara Rise (blue triangles), Indian Ocean (grey crosses), Caribbean Sea (turquoise squares) and MAR (green triangles pointing down). Uncorrected values are in grey. Vertical grey bars represent uncertainty estimated as follows: a 5% uncertainty was assumed on measured Mg/Ca; for the ΔMg/Ca portion, uncertainty was one standard deviation on the slope of the calibration between XDX and ΔMg/Ca. Errors for each portion were combined when the two values were summed. Dotted areas in *G. ruber* and *G. sacculifer* panels on facing page represent annual range of SST [*Rayner et al.*, 2003] at each site. Mg/Ca of G. ruber from shallow sites on the OJP and Ceara Rise underestimate SST. Dissolution corrected temperatures correct back to the values of shallow sites but not to measured SST. Average temperatures of analysed and corrected samples are shown for OJP and Ceara Rise sample sets, ± is standard deviation.

5.5.3 Is Mg/Ca altered before dissolution is detectable in CT?

Regressions between XDX and ΔMg/Ca are forced through the origin. This is justified as our $\Delta[CO_3^{2-}]$ $_{\text{CRITICAL}}$ values where Mg/Ca is first affected by dissolution (ΔMg/Ca =0) of 11 ($\pm$4) to 15 ($\pm$5) μmol/kg) are similar to $\Delta[CO_3^{2-}]$ values where dissolution is first detectable in CT (XDX = 0) of 12 ($\pm$4) to 14 ($\pm$5) μmol/kg) [*Johnstone et al.*, in press].

These values are lower than $\Delta[CO_3^{2-}]$ values between 25 and 22 μmol/kg where *Regenberg et al.* [2006] identify dissolution effects on Mg/Ca. This suggests that although CT offers a direct assessment of preservation state of tests, scans do not capture early changes in Mg/Ca of a sample which could occur by preferential removal of tests with the highest Mg/Ca, leaving remaining tests intact.

Given the error on the intercepts of the regressions and the error on calculated $\Delta[CO_3^{2-}]$ these differences in threshold values may not be significant. More work on the early effects of dissolution on Mg/Ca is required to identify dissolution thresholds more securely and to ascertain whether such thresholds are globally valid. However, even small differences between in the $\Delta[CO_3^{2-}]$ values where dissolution first affects Mg/Ca and where it is perceived in CT scans would lead to undetectable dissolution effects on Mg/Ca derived temperatures.

In the most severe case, a difference of 10 μmol/kg between threshold of *Regenberg et al.* [2006] at 23 μmol/kg and CT detecting dissolution at 13 μmol/kg for *N. dutertrei* means 21 $^{\circ}$C would be recorded as 19 $^{\circ}$C. A difference of 11 μmol/kg between the $\Delta[CO_3^{2-}]$ of 25 μmol/kg where Mg/Ca is affected [*Regenberg et al.*, 2006] and 14 μmol/kg where dissolution is detectable in CT for *G. ruber* [*Johnstone et al.*, in press (**Chapter 4**)] leads to an underestimate of 3 $^{\circ}$C on SSTs of 25 $^{\circ}$C and 2 $^{\circ}$C in SST of 29 $^{\circ}$C.

Dissolution above the limits of dissolution detection in CT would explain more than half of the offset between temperatures derived from Mg/Ca of *G. ruber* from the shallowest core-top (1BC3) from the OJP of 26 $^{\circ}$C and SST at the site of 29 $^{\circ}$C. Such a mechanism would not explain why Mg/Ca of shallow *G. ruber* from the Indian Ocean does seem to represent SST. The reasons for the offset in Mg/Ca and SST of OJP *G. ruber* remain unclear.

A more significant problem than alteration of Mg/Ca before CT first identifies dissolution is likely to be that, although correcting Mg/Ca for dissolution effects assumes a constant relationship between dissolution and Mg/Ca bias, this may not be the case. XDX offers a poor correction of dissolution bias for *N. dutertrei* from the Caribbean. However, XDX does offer a direct insight to preservation state of tests and, at the least, identifies where Mg/Ca is unreliable.

5.5.4 Comparison of two methods of correcting Mg/Ca: test weight and XDX

Decrease in test weight has been used to correct for the effects of dissolution on Mg/Ca in planktonic foraminifera [*Rosenthal and Lohmann*, 2002]. In order to judge how well using XDX to correct for dissolution bias in Mg/Ca compares to this more established method, we compare correlation (r^2) between (1) ΔMg/Ca and test mass and (2) ΔMg/Ca and XDX for all samples for each species. Test mass for these samples are from *Johnstone et al.* [in press (**Chapter 4**)].

Correlation (r^2) between ΔMg/Ca and XDX is 0.40 for *G. ruber*; 0.60 for *G. sacculifer*; 0.61 for *N. dutertrei* and 0.87 for *P. obliquiloculata*. These are stronger than correlations between ΔMg/Ca and test mass of 0.31, 0.54, 0.37 and 0.64 for the above species. Test mass is controlled by environmental factors and differs between sites, particularly for thermocline dwelling species where the thickness of the outer calcite crust can vary widely. XDX offers an assessment of dissolution which is largely independent of test mass [*Johnstone et al*., in press (**Chapter 4**)]. In the early to mid stages, dissolution does not significantly alter wall thickness but acts to increase porosity of the test calcite. The same stage of dissolution is identifiable in light and heavy tests. This makes XDX more widely applicable as an indicator of dissolution bias than test mass.

5.6 Effect of dissolution on foraminiferal $\delta^{18}O$

Previously published $\delta^{18}O$ for *G. sacculifer* and *P. obliquiloculata* from the OJP has a large amount of scatter. *Wu and Berger* [1989] found 90% of $\delta^{18}O$ data fell in a range of ~0.4 ‰ before any dissolution effects. Our data show a similar range (**Figure 5.7**).
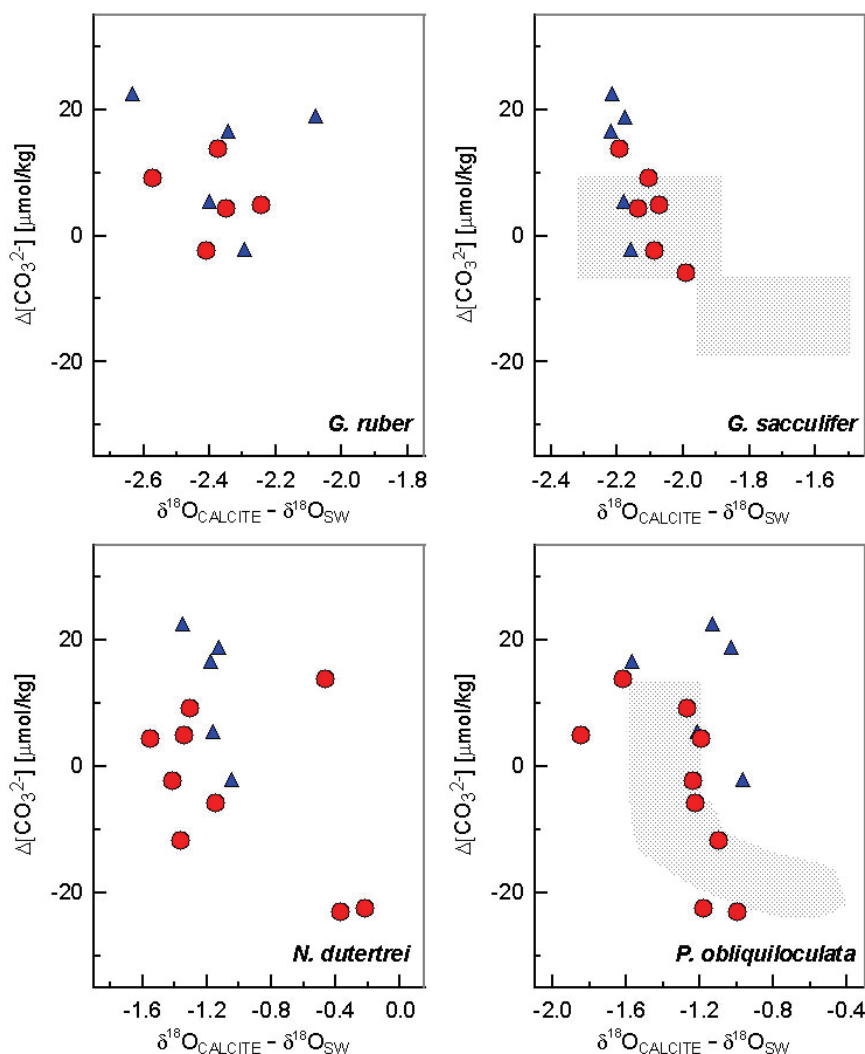
Figure 5.7 Deep water $\Delta[CO_3^{2-}]$ versus $\delta^{18}O_{calcite}$ – $\delta^{18}O_{SW}$ for four species of planktonic foraminifera ($\delta^{18}O_{SW}$ from *LeGrande and Schmidt* [2006]). Samples contain between 6 and 9 tests. Grey dashed areas are values of *Wu and Berger* [1989] for *G. sacculifer* and *P. obliquiloculata* from the OJP.

As discussed earlier, the effect of dissolution is to selectively remove the inner parts of the calcite test. While it might be supposed that this would shift $\delta^{18}O$ towards values of the deeper colder waters where the outer calcite is precipitated, in fact there is little correlation between $\delta^{18}O$ and XDX (**Figure 5.8**). Although highest values of $\delta^{18}O$ generally came from the most dissolved tests (XDX > 3), well-preserved tests

also cover a range of values. For example, well-preserved and poorly preserved *N. dutertrei* from the OJP have similar $\delta^{18}O$ values (**Figure 5.8**). The samples used in this study were small (only 5 to 9 individuals); probably such a small number is insufficient to average out the range of initial values of $\delta^{18}O$. The wide age span of the OJP samples [*Barker et al.*, 2007] and the range of calcification depths, especially for thermocline dwellers, mean that the initial variability could be very high.
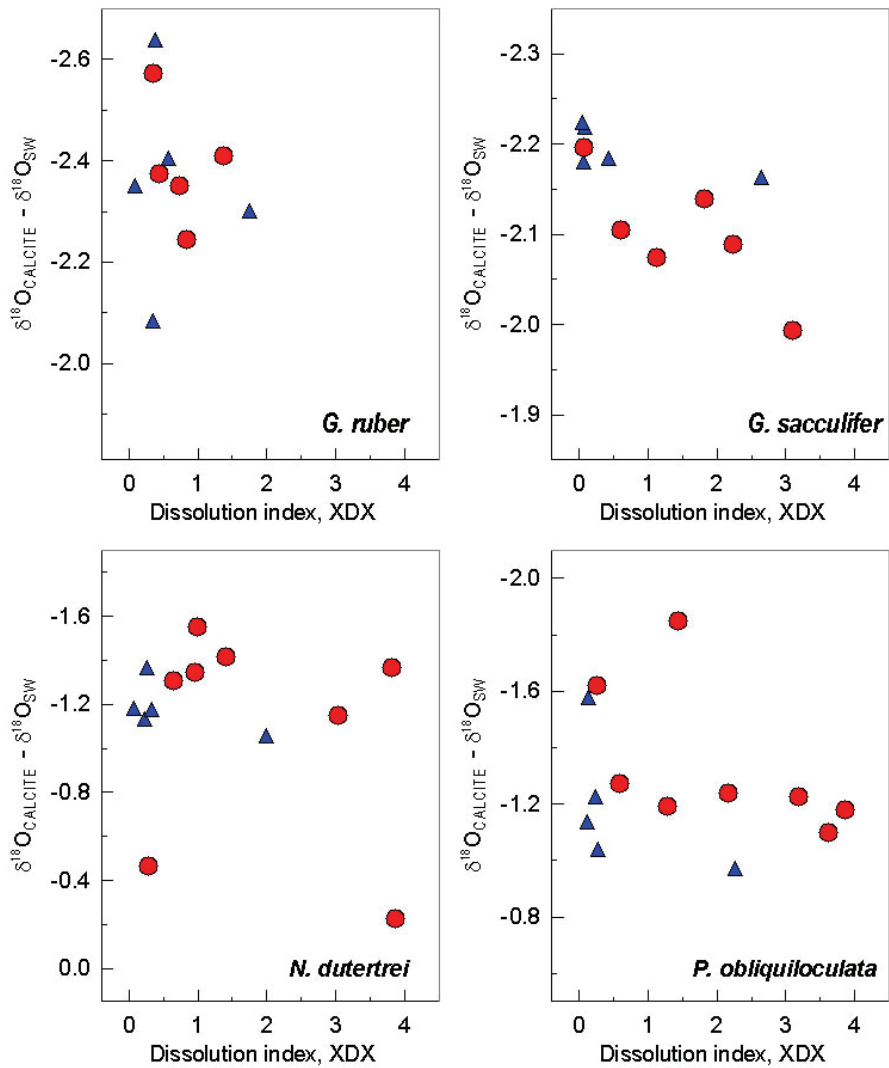
Figure 5.8 XDX versus $\delta^{18}O_{calcite} - \delta^{18}O_{sw}$ ($\delta^{18}O_{sw}$ from *LeGrande and Schmidt* [2006]) for four species of planktonic foraminifera.

5.7 Conclusions

The four species of planktonic foraminifera used in this study show a strong linear decrease in Mg/Ca with decreasing $\Delta[CO_3^{2-}]$. ΔMg/Ca (reduction in Mg/Ca due to dissolution) for each species decreased linearly from $\Delta[CO_3^{2-}]$ values of between 10 ($\pm$4) (*G. sacculifer*) and 15 ($\pm$5) µmol/kg (*N. dutertrei*). These threshold values are minimum estimates as they are limited by the assumptions made in calculating ΔMg/Ca. Sensitivity of Mg/Ca to dissolution was greatest for *G. ruber* and was similar for *G. sacculifer, N. dutertrei* and *P. obliquiloculata*.

Dissolution has large effect on Mg/Ca based temperatures. Mg/Ca of poorly preserved samples underestimate temperatures by up to $4 - 6\ ^{o}C$ for *G. ruber* and *G. sacculifer*; $9\ ^{o}C$ for *N. dutertrei* and $6\ ^{o}C$ for *P. obliquiloculata*.

CT based deepwater $\Delta[CO_3^{2-}]$ proxy XDX correlates positively with ΔMg/Ca. Calibrations provided here provide an independent method of correcting Mg/Ca for dissolution bias. Applying the corrections to the core top samples reduced the scatter of temperature within each set.

Attempts to correct Mg/Ca for dissolution would be confounded if the response of Mg/Ca to partial solution of the test is variable. *N. dutertrei* illustrates this possibility. Mg/Ca of Caribbean *N. dutertrei* apparently shows a greater sensitivity to dissolution than those from other sites. *N. dutertrei* from the Caribbean has the highest Mg/Ca of all the *N. dutertrei* samples measured here and it is suggested that variation in Mg/Ca within one species may control dissolution susceptibility.

Correlation (r^2) was greater between ΔMg/Ca and XDX than it was between ΔMg/Ca and test mass. Unlike test mass which can vary temporarily and spatially XDX offers a direct measure of dissolution.

Analysed values of $\delta^{18}O$ of these core-top samples reflect temperatures within the habitat depth for each species. Because habitat depth range is wide, the small sample size typically used for $\delta^{18}O$ analysis is insufficient to isolate the effect of dissolution.
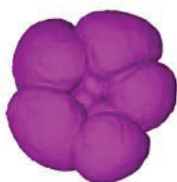
6. Calcite saturation, dissolution-corrected foraminiferal test mass and dissolution-corrected Mg/Ca reconstructed using XDX: a 150 ka record from the western Indian Ocean

H.J.H Johnstone[1]**, T. Kiefer**[2]**, H. Elderfield**[3] **and M. Schulz**[1]

[1] MARUM – Center for Marine Environmental Sciences, University of Bremen, Leobener Straße, 28359 Bremen, Germany

[2] PAGES International Project Office, Zähringerstrasse 25, 3012 Bern, Switzerland

[3] Godwin Laboratory for Palaeoclimate Research, Department of Earth Sciences, University of Cambridge, Cambridge, UK

Abstract

A record of deep sea calcite saturation ($\Delta[CO_3^{2-}]$), derived from X-ray Computed Tomography based foraminiferal dissolution index XDX, was constructed for the past 150 ka for a core from the deep (4,157 m) tropical western Indian Ocean. $\Delta[CO_3^{2-}]$ derived from *Globigerinoides sacculifer* and *Neogloboquadrina dutertrei* record a similar dissolution history. The pattern of preservation is consistent with the theory of calcite compensation. Saturation increased by ~25 μmol/kg over Termination I and ~15 μmol/kg over Termination II. Dissolution maxima coincide with transitions to colder stages. The dissolution-corrected Mg/Ca-derived SST record does not show the post-Termination cooling seen in the original record. Corrected SSTs are similar to records from monsoon dominated sites in the Indian Ocean, with coolest temperatures during MIS 3. Lightest tests coincide with this cool interval, suggesting a temperature control on foraminiferal mass.

To be resubmitted to *Geochemistry, Geophysics, Geosystems* after the comments of the reviewers have been taken into account.

6.1 Introduction

Tropical Indian Ocean surface temperatures influence the Asian Monsoon as well as the climate of Africa and a record of hydrography in this area has great relevance to, at least, regional scale climate [e.g. *Leuschner and Sirocko*, 2000; *Black*, 2005].

However, much of the Indian Ocean seafloor lies beneath the calcite lysocline, meaning that sites of paleoceanographic interest may lie in areas where calcite preservation is compromised. This has implications for temperature records based on analysis of foraminifera tests, as poor preservation reduces Mg/Ca, biasing derived temperatures towards colder values [*Brown and Elderfield*, 1996; *Hastings et al.,* 1998; *Dekens et al*., 2002; *Regenburg et al*., 2006]. Sea floor dissolution also reduces test mass, which has been suggested as a proxy for surface water carbonate ion concentration ($[CO_3^{2-}]$) [*Barker and Elderfield,* 2002].

As well as offering a means to indicate dissolution bias on proxies, tracking calcite dissolution also offers an important insight into the past behaviour of the carbon cycle. The preservation of calcite sediments at the ocean floor records the transfer of carbon to and from the deep ocean over glacial cycles. Palaeoceanographic interest in Indian Ocean cores is thus two-fold. Carbonate preserved in sediments potentially records both surface conditions and deep ocean carbonate chemistry.

A temperature record from southwest Indian Ocean has been published for the last 65 ka [*Kiefer et al.*, 2006] based on Mg/Ca of surface (*Globigerinoides ruber*) and thermocline dwelling (*Neogloboquadrina dutertrei*) foraminifera. One feature of the record is the drop in Mg/Ca values during the glacial termination [*Kiefer et al.,* 2006]. It was noted that foraminfera tests were light in mass during this interval, suggestive of dissolution and consequent bias of Mg/Ca derived temperatures.

The aim of our study was to create a record of dissolution from the same core over the last 150 ka using X-ray computed tomography (CT) based dissolution index, XDX [*Johnstone et al*., in press (**Chapter 4**)]. In this first downcore application of the dissolution index, we aim to create a record of deep-water calcite saturation ($\Delta[CO_3^{2-}]$), initial test mass and to improve Mg/Ca based temperature estimates.

6.2 Material and Methods

6.2.1 Core WIND28K

The core used in this study, WIND28K (10° 09.2' S, 51° 46.2' E), was collected off the north of Madagascar (**Figure 6.1**) close to the Amirante Passage in the south west Indian Ocean during Charles Darwin Cruise 29 [*McCave*, 2001]. The core site lies at 4157 m in the Lower Circumpolar Deepwater (LCDW), around 600m below the modern lysocline [*Elderfield et al.*, 2006].
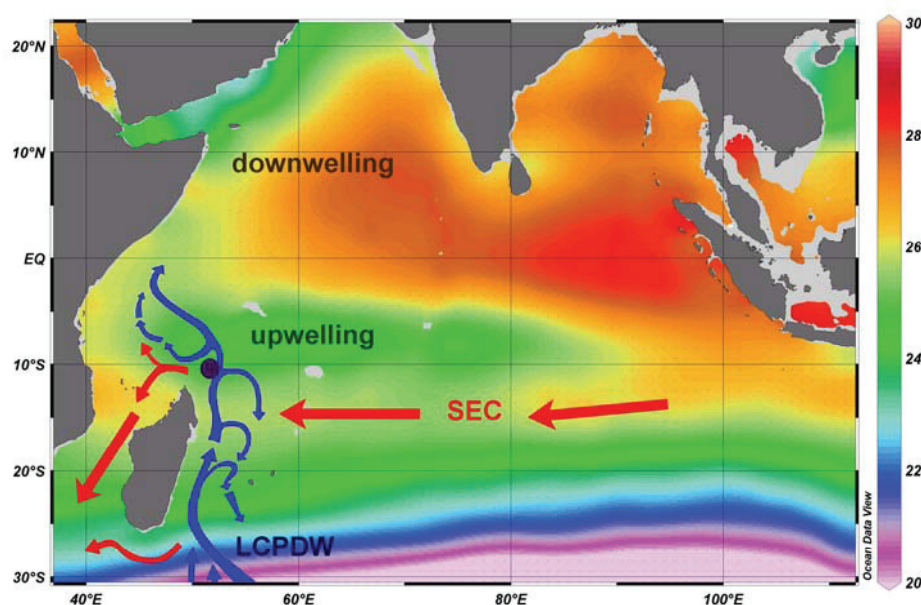
Figure 6. 1 Annual temperatures at 50 m water depth (World Ocean Atlas 2005 [*Locarnini et al.,* 2006] in the Indian Ocean, plotted with Ocean Data View [*Schlitzer*, 2007]). Black spot indicates location of core site WIND 28K (10 ◦ 9.23' S, 51◦ 46.15' E) at 4157m water depth [*McCave et al.,* 2001] North of Madagascar in the Amirante Passage. Blue arrows represent the flow of Lower Circumpolar Deep Water (LCPDW) below 3800 m and red arrows indicate surface currents; SEC: South Equatorial Current, which splits around Madagascar and rejoins, ultimately flowing into the Atlantic. Representation of currents after *McCave et al.* [2005].

Surface water at the site forms from the warm waters of the South Equatorial Current flowing from the East and cool Subantarctic Mode Water which upwells to the north of Madagascar. Upwelling at this location is due to an Ekman divergence associated with the termination of the NE trade winds. Upwelling can occur during both monsoon seasons but is strongest during the SW monsoon (June-September) [*Schott et al.*, 2002, 2009]. Surface temperatures at the site thus have a large seasonable variation ranging from 24^oC (August) to 27.5^oC (March) [Comprehensive ocean-atmosphere database, COADS; *Slutz et al.,* 1985]. Surface water splits around

Madagascar and rejoins, ultimately feeding into the Atlantic via the Agulhas Current [*Gordon,* 2005].

6.2.1 Computed tomography (CT) scanning

G. sacculifer (without a final sac-like chamber) and *N. dutertrei* tests from the 300-355μm size fraction were picked from core WIND28K. The 560 cm of core covering 150 ka was sampled every 10 cm for *G. sacculifer* (54 samples). *N. dutertrei* was sampled at an average spacing of 8 cm over the whole 620 cm of the core (76 samples). Tests were rinsed in deionised water and whirled for a few minutes in a vortex mixer to remove loose sediment from inside the chambers. Samples were then dried in a warm oven and weighed on a microbalance before being scanned. Each sample was scanned in two batches each of 8 to 12 tests using a Skyscan 1072 X-ray micro-CT system. Most samples were scanned at the Alfred Wegener Institute for Polar and Marine Research in Bremerhaven, but around half of the *G. sacculifer* samples were scanned at the Department of Earth Sciences, University of Cambridge. Voltage was 80 kV and exposure time was 4.5 seconds. On examination of the scans, each test was assigned to one of 5 stages of dissolution (from XDX of 0 - no dissolution, to XDX of 4 - extremely dissolved) to give an average value for the sample according to the method of *Johnstone et al.* [in press (**Chapter 4)**].

6.2.2 Use of XDX to estimate $\Delta[CO_3^{2-}]$ and to correct for the effect of dissolution on Mg/Ca and test mass

Previous studies on core tops established calibrations between XDX stages and calcite saturation ($\Delta[CO_3^{2-}]$) [*Johnstone et al.* in press (**Chapter 4**)]. XDX was also calibrated to dissolved mass (ΔM) and the reduction in Mg/Ca due to dissolution ($\Delta Mg/Ca$) [*Johnstone et al.*, subm. (**Chapter 5**)]. Values estimated for the dissolved portion added to the measured value provide an estimate of the initial, pre-dissolution, value. Core tops used in the calibration studies included box cores from the WIND cruise transect [*McCave*, 2001] along the East coast of Madagascar from where core WIND28K was also retrieved.

In this study, XDX was measured for two species of planktonic foraminifera, *G. sacculifer* (without final sac-like chamber) and *N. dutertrei*. For these two species $\Delta[CO_3^{2-}]$, $\Delta Mg/Ca$ and ΔM were calculated from XDX as follows:

$$\Delta[CO_3^{2-}] = a * XDX + b \qquad\qquad (1)$$

$$\Delta Mg/Ca = f * XDX \qquad\qquad (2)$$

$$\Delta M = k * XDX, \qquad\qquad (3)$$

Values of constants *a, b, f* and *k* for *G. sacculifer* and *N. dutertrei* are given in **Table 6.1**.

Species	Δ[CO$_3^{2-}$]		ΔMg/Ca			ΔM		
	a	*b*	*c*	*d*	*f*	*g*	*h*	*k*
G. ruber			-0.102 (±0.036)	14 (±8)		0.33 (±0.18)	13 (±5)	
G. sacculifer	-7.7 (±1.3)	13.7 (±2.8)			0.28 (±0.05)			3.5 (±0.4)
N. dutertrei	-8.3 (±1.3)	13.2 (±2.9)			0.29 (±0.04)			3.0 (±0.4)

± is half of 95% confidence interval

b is the Δ[CO3²⁻] value where XDX is 0, i.e. dissolution is first detected below this value of calcite saturation.

d is the Δ[CO3²⁻] value where Mg/Ca of *G. ruber* is first affected by dissolution.

h is the Δ[CO3²⁻] value where test mass of *G. ruber* is first affected by dissolution.

Table 6.1 Constants for calibrations between XDX and Δ[CO3²⁻] (eq. 1); XDX and ΔMg/Ca (eq. 2, 4) and XDX and ΔM (eq. 3, 5). Values are from *Johnstone et al.* [in press (**Chapter 4**)] and *Johnstone et al.*, [subm. (**Chapter 5**)].

XDX was not measured on *G. ruber* directly. For this species Δ[CO$_3^{2-}$] values calculated from XDX of *G. sacculifer* (designated as Δ[CO$_3^{2-}$]$_{G. sacculifer}$ below) were used to estimate the effect of dissolution on mass and Mg/Ca.

Values obtained from *G. sacculifer* rather than *N. dutertrei* were used as the dissolution susceptibility of *G. ruber* is more similar to that of *G. sacculifer* than to *N. dutertrei* [*Berger*, 1970]. Sensitivity of ΔMg/Ca (reduction in Mg/Ca) and ΔM (reduction in mass) to Δ[CO$_3^{2-}$] for *G. ruber* [*Johnstone et al.* in press (**Chapter 4**); *Johnstone et al.*, subm. (**Chapter 5**)], as follows:

$$\Delta Mg/Ca = c * (\Delta[CO_3^{2-}]_{G. sacculifer} - d) \tag{4}$$

$$\Delta M = g * (\Delta[CO_3^{2-}]_{G. sacculifer} - h) \tag{5}$$

Where *c, d, g* and *h* are constants (given in **Table 6.1**). *d* and *h* are the critical values of Δ[CO$_3^{2-}$] where dissolution starts to affect Mg/Ca and mass of *G. ruber* respectively.

If Δ[CO$_3^{2-}$]$_{G. sacculifer}$ of a particular sample was greater than *d,* or *h*, then samples were above the threshold for dissolution effects on Mg/Ca, or mass, and no correction was made.

6.2.3 Geochemical Analysis

Mg/Ca values for *G. ruber* and *N. dutertrei* and δ¹⁸O for *Cibicidoides wuellerstorfi*, over the past 65 ka have been previously published [*Kiefer et al.*, 2006]. The Mg/Ca record is here extended to 150 ka using previously unpublished data [*T. Kiefer* pers. com.]. This was analyzed at the Department of Earth Sciences, University of Cambridge using a Varian Vista ICP-OES (inductively coupled plasma – optical

emission spectroscopy) and Mg/Ca ratio intensity method [*de Villiers et al.*, 2002]. Additional *G. sacculifer* samples were analysed using a Finnegan Element II ICP-MS at MARUM, University of Bremen. Al, Fe and Mn were measured in addition to Mg and Ca in order to monitor contaminant phases. Uncertainty in temperature estimates based on Mg/Ca is within ± 0.5 °C. Duplicate measurements in both laboratories established that Mg/Ca values from Bremen required addition of 0.26 mmol/mol to match those of Cambridge.

All tests were cleaned before analysis according to the Mg-cleaning ("oxidative cleaning") protocol of *Barker et al.* [2003b]. Mg/Ca was converted to temperature using the species-specific calibrations of *Anand et al.* [2003]. *G. ruber* and *N. dutertrei* were sampled for Mg/Ca every 4 cm where samples allowed. Sample resolution for *G. sacculifer* was 4 cm over the glacial terminations and every 10 cm in the rest of the core. XDX values were linearly interpolated between data points to put Mg/Ca values on the same scale. $\delta^{18}O$ [*Kiefer et al.*, 2006; *T. Kiefer* pers. com.] was analysed at the Godwin Laboratory, University of Cambridge where long term precision is ±0.08 ‰ (1 σ).

6.2.4 Age model

The age model for the core was that of *Kiefer et al.* [2006] (and unpublished data of Kiefer) and is based on ten ^{14}C dates. The top of the core is disturbed. The youngest samples used here are from 20 cm depth in the core and date from almost 7 ka before present. Marine isotope stages (MIS) boundaries referred to are those of *Martinson et al.* [1987].

6.3 Results

6.3.1 Dissolution recorded in core WIND28K

XDX of the two species analysed, *G. sacculifer* and *N. dutertrei* (**Figure 6.2**), showed a similar pattern of dissolution (r^2 = 0.70, p < 0.001). Good preservation (XDX < 1) occurred only during the glacial terminations and early MIS 3. Preservation was poor throughout most of the rest of the core particularly during MIS 2, 4 and 5, especially 5.2 and 5.5.

Foraminiferal test mass is a commonly used measure of dissolution [*Lohman*, 1995; *Broecker and Clark,* 2001; 2002] and test mass records show similarities to dissolution index XDX (**Figure 6.2**). Heaviest tests for all three species occurred during the glacial terminations, where XDX indicates good preservation. Lightest tests were found during MIS 5 which XDX shows generally to be a time of poor preservation.

Stronger correlation between XDX and test mass for *G. sacculifer* ($r^2 = 0.56$) than for *N. dutertrei* ($r^2 = 0.40$) suggests mass of *G. sacculifer* is the better gauge of dissolution in WIND28K. Correlation between dissolution (indicated by XDX of *N. dutertrei*) and mass is lowest in *G. ruber* ($r^2 = 0.23$) implying that mass of this species is less useful as a dissolution indicator.

Although there are similarities between dissolution record XDX and test mass there are also significant differences. None of the test mass records suggest that preservation is better during MIS 3 than during MIS2. XDX records for *G. sacculifer* and *N. dutertrei* are more similar to each other ($r^2 = 0.70$) than the two records of test mass ($r^2 = 0.38$) implying that test mass has varied for reasons other than preservation, as preservation should affect both species equally. There is a large deviation between test mass and XDX at ~42 ka where CT reveals that tests are well preserved but have formed with thin walls (**Figure 6.3**).

The calibration study [*Johnstone et al.*, in press (**Chapter 4**)] suggests that below a critical value of $\Delta[CO_3^{2-}]$ (~15 µmol/kg) *G. ruber*, *G. sacculifer* and *N. dutertrei* tests lose mass linearly as calcite saturation decreases, until they reach a minimum test mass (for the 300 – 355 µm size fraction) of ~12 µg. Mass records of *G. sacculifer* and *N. dutertrei* from WIND28K support this minimum value; few samples weighed less than 12 µg. The minimum value may be a little lower, ~11 µg, for *G. ruber* tests (**Figure 6.2**).

Common features in dissolution, XDX, and Mg/Ca records suggest that preservation state is also reflected in measured Mg/Ca values. Mg/Ca of all three species is highest over the glacial terminations. Lowest values occur during MIS 4 and MIS 5.5. Absence of *G. ruber* and *G. sacculifer*, the species most susceptible to dissolution [*Berger*, 1970], over MIS 4 and 5.5 also testify to the fact that calcite dissolution is severe during these periods.
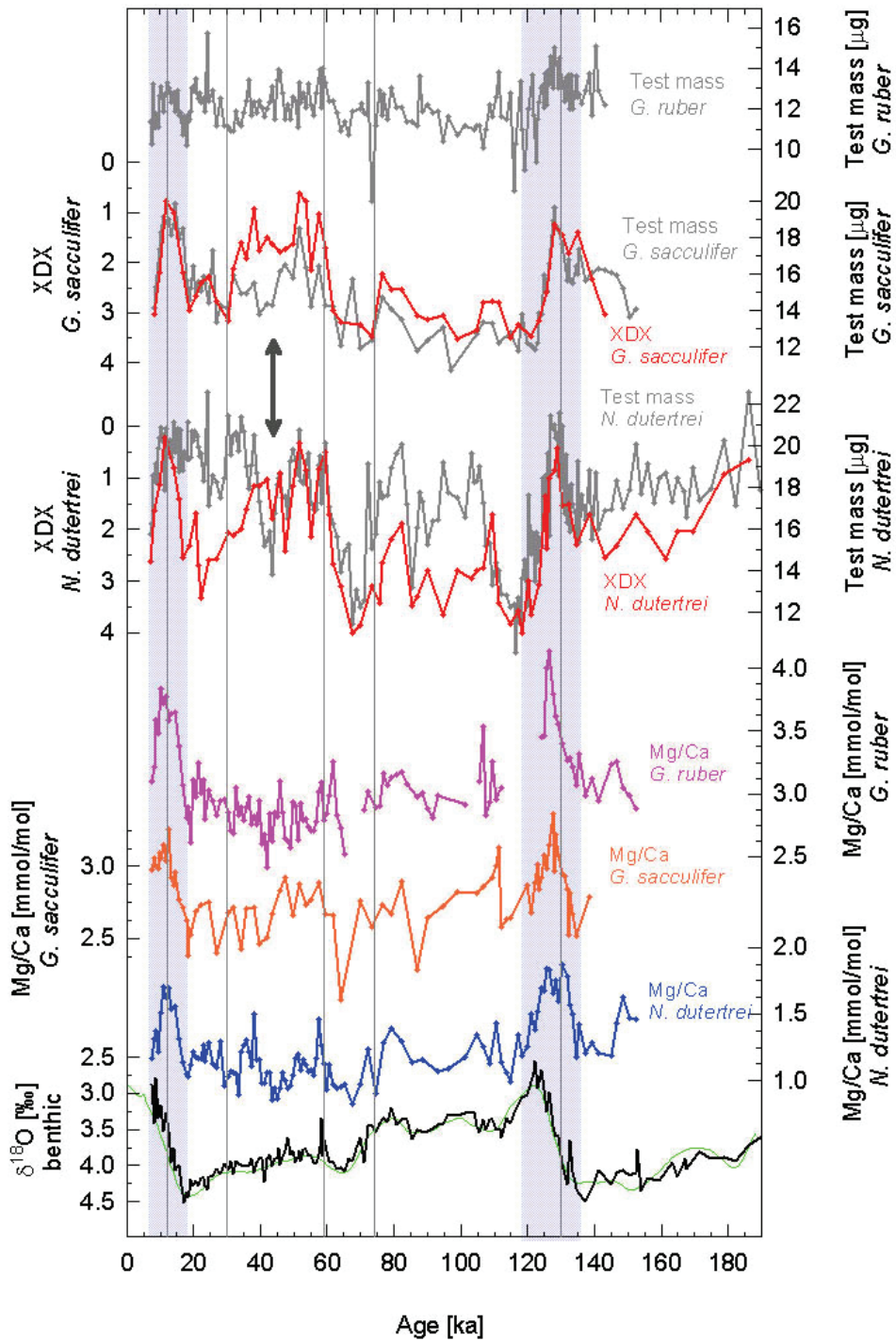
Figure 6.2 Dissolution index, XDX, and Mg/Ca for WIND 28K plotted against age. Red lines are dissolution index XDX for *G. sacculifer* and *N. dutertrei*. Low values indicate good preservation. Test weight record also shown (grey lines) for comparison. Mg/Ca (for *G. ruber* (pink line); *G. sacculifer* (orange) and *N. dutertrei* (blue)) values peak when preservation is good, suggesting dissolution bias. Record of test mass is more similar to XDX for *G. sacculifer* than for *N. dutertrei*. Both *G. sacculifer* and *N. dutertrei* tests are heaviest during the glacial terminations (blue bars). Tests of both these species are light in weight around 42 ka (arrow) even though preservation is good, because tests have thin walls (**Figure 6.3**). Black curve is benthic δ¹⁸O measured on *C. wuellerstorfi* [*Kiefer et al.*, 2006]. Green line is Specmap curve (no scale) [*Imbrie et al.*, 1984]. Dark grey vertical lines mark marine isotope stages (MIS) of *Martinson et al.* [1987].
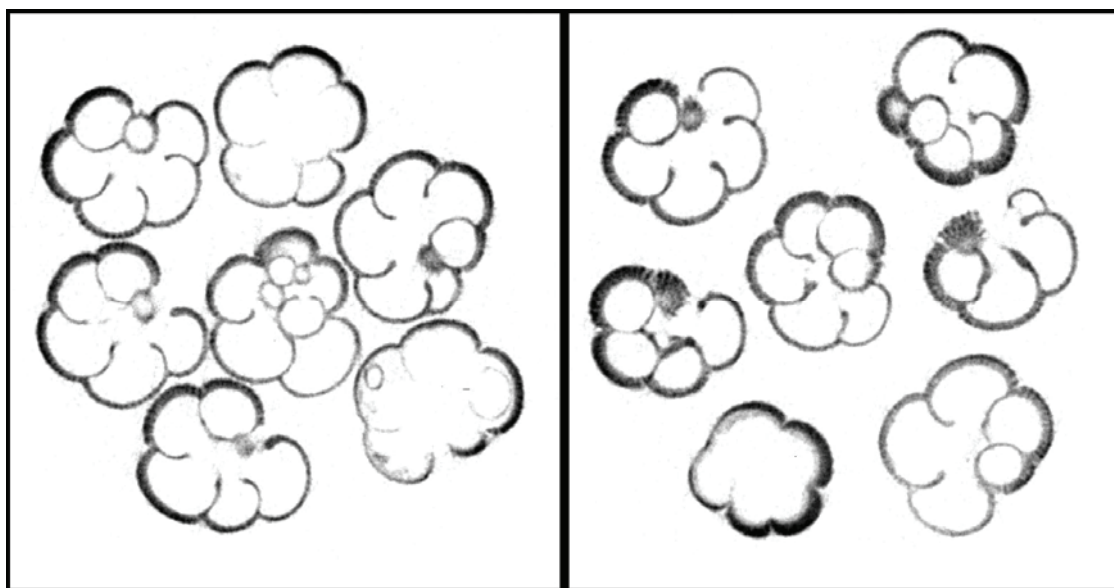
Figure 6.3 CT slice of a typical *N. dutertrei* test from 42 ka (left), where average test mass is 14 µg, and 52 ka (right), where average test mass is 20 µg. Both samples are reasonably well-preserved (XDX ≈1) but the tests from 42 ka formed with thinner walls. Each box is ~1mm wide.

6.3.2 Δ[CO₃²⁻] reconstructed from XDX

Calibrations between XDX and $\Delta[CO_3^{2-}]$ established for core top samples [*Johnstone et al.*, in press (**Chapter 4**)] (constants given in **Table 6. 1**) were used to estimate $\Delta[CO_3^{2-}]$ for core WIND28K (**Figure 6.4**). $\Delta[CO_3^{2-}]$ calculated from *G. sacculifer* and *N. dutertrei* gave similar $\Delta[CO_3^{2-}]$ values throughout the record with some small differences. The highest $\Delta[CO_3^{2-}]$ values calculated from *G. sacculifer* were generally 2 or 3 µmol/kg lower than values derived from *N. dutertrei* (**Figure 6.4**), which is within the precision of the method (error calculated taking into account the error on the slope of the calibration gave an average 1σ error of 7.5 µmol/kg).

The difference in calculated $\Delta[CO_3^{2-}]$ between the two species was more pronounced for the lowest values. In the WIND28K record *N. dutertrei* indicates $\Delta[CO_3^{2-}]$ down to -20 µmol/kg, whereas *G. sacculifer* reaches minimum values of around -12 µmol/kg. These values represent the limits of the calibration [*Johnstone et al.*, in press (**Chapter 4**)]. *G. sacculifer* are less resistant to dissolution than *N. dutertrei* [*Berger*, 1970] and *G. sacculifer* tests are rare in samples from sites where deep water calcite saturation ($\Delta[CO_3^{2-}]$) is below 15 µmol/kg. Where tests are found, they may have been better protected from dissolution in microenvironments and may thus not be representative of the general setting. XDX of the dissolution resistant species *N. dutertrei* is therefore a better recorder of dissolution as this species is present in samples from a wider range of calcite saturation states. Values of $\Delta[CO_3^{2-}]$ which follow refer to that calculated from XDX of *N. dutertrei*. $\Delta[CO_3^{2-}]$ values for MIS 4 and MIS 5.5 are close to the limit of the *N. dutertrei* calibration, and may not capture the full extent of calcite undersaturation over these intervals.

The most recent $\Delta[CO_3^{2-}]$ value (at ~ 6 ka) obtained from WIND28K of -13 μmol/kg is similar to present day values at the site of -11 μmol/kg (calculated using Total Carbon and Alkalinity values from GLODAP [*Key et al.,* 2004]). Reconstructed values of $\Delta[CO_3^{2-}]$ for core WIND28K fluctuates between values of +12 μmol/kg to -20 μmol/kg (**Figure 6.4**). Positive values of calcite saturation occur only during the glacial terminations, the early part of MIS 3 and MIS 6.
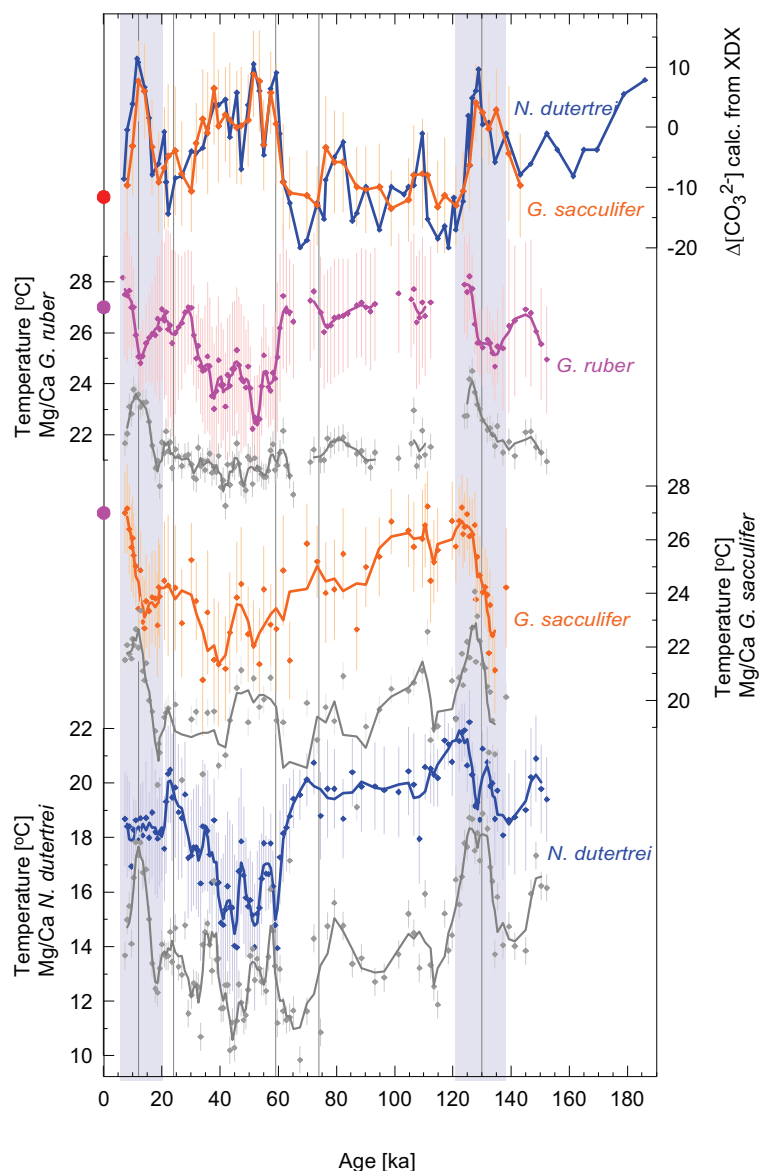
Figure 6.4 Reconstructed $\Delta[CO_3^{2-}]$ and temperature for WIND28K. $\Delta[CO_3^{2-}]$ calculated from XDX for *G. sacculifer* (orange line) and *N. dutertrei* (blue line) give similar values. Vertical bars are estimates of uncertainty based on 1 σ uncertainty of the calibration slopes. Red dot is present day $\Delta[CO_3^{2-}]$ (calculated using World Ocean Atlas 2005 [*Locarnini et al.,* 2006] and GLODAP data [*Key et al.,* 2004]). XDX was interpolated linearly to give values for samples where Mg/Ca was analyzed. Solid lines are 3 point running averages for dissolution-corrected Mg/Ca-derived temperatures for *G. ruber* [white] (pink curve), *G. sacculifer* (orange curve) and *N. dutertrei* (blue curve). Grey lines are temperatures calculated from analyzed Mg/Ca. Pink dot is annual average SST [*Locarnini et al.,* 2006] at WIND28K site.

6.3.3 XDX-corrected temperature record

We used XDX to estimate Mg/Ca ratios before effects of carbonate dissolution and to improve temperature estimates. The effect was to raise reconstructed temperatures throughout most of the record for all three species (**Figure 6.4**). The greatest increase in temperature was for MIS 5 where preservation was very poor. Good preservation during MIS 3 meant that Mg/Ca stayed close to analyzed values. In the new, dissolution-corrected, record warmest temperatures occur in the mid-Holocene and during MIS 5.5. MIS 3 is the coolest stage with temperatures 4 – 5 $^{\circ}$C below present-day annual average (World Ocean Atlas, WOA 2005 [*Locarnini et al.,* 2006]).

Temperatures calculated from the most recent samples, in the mid-Holocene, were also raised significantly, with new values comparable to WOA 2005 annual average (**Figure 6.4**). *G. ruber* inhabits the mixed layer in this area [*Shackleton and Vincent*, 1978] and its calcification temperature is considered to represent SST. Once the dissolution correction has been applied, temperatures calculated from *G. ruber* at 6 ka of 28 $^{\circ}$C are slightly above current annual average SST of 26.5 $^{\circ}$C (WOA 2005). Over the whole record, temperatures derived from *G. ruber* increased from analysed values of 19-24 $^{\circ}$C to 23-28 $^{\circ}$C for XDX-corrected values.

The removal of post-termination drops in temperature in the dissolution-corrected record is confirmed by *G. sacculifer*. Over the whole record temperatures calculated from this species are increased from a range of 14-24 $^{\circ}$C to 20-26 $^{\circ}$C. XDX-corrected temperatures represented by *G. sacculifer* are on average 1 $^{\circ}$C less than those given by *G. ruber*. This reflects the behaviour of the two species, as although *G. sacculifer* also lives in the photic zone, it continues to calcify deeper in the water column [*Duplessy et al.,* 1981, *Rosenthal et al.,* 2000].

Correcting for the poor preservation at the beginning and end of glacial terminations appears to delay deglacial warming in comparison to the original reconstruction. This is true for both deglaciations, but particularly Termination I where initiation of warming shifts from ~ 19 ka to ~ 12 ka in the *G. ruber* and *G. sacculifer* temperature records. This differs from the Indian Ocean Mg/Ca derived SST record of *Saraswat et al.* [2005], a record presumably less affected by dissolution than WIND28K since the core was retrieved from shallower depth. The *Saraswat et al.* [2005] record shows the sub-tropical/tropical Pacific pattern of *Kiefer and Kienast* [2005] with steady warming from 19 ka. However, the apparent temperature trough centred exactly on peak preservation at 12 ka suggests some over-correction of the dissolution-corrected temperature record. In the calibration, study [*Johnstone et al.*, subm. (**Chapter 5**)] Mg/Ca of samples from the Ontong Java Plateau tailed off below -10 µmol/kg. It appears that the calibration overestimates temperatures derived from *G. ruber* from periods where dissolution is very severe, such as 19 to15 ka.

The greater sensitivity to the effect of dissolution on Mg/Ca of *N. dutertrei* compared to the other species considered [*Fehrenbacher et al.,* 2006; *Regenberg et al.,* 2006, *Johnstone et al.,* subm. (**Chapter 5**)], means that the dissolution correction causes the largest temperature adjustment in this species. *N. dutertrei* also has the largest temperature range of the three species, presumably reflecting its wider habitat range [*Hemleben et al.,* 1989]. Temperatures reconstructed from this species increase from a range of 10-19 ^{o}C to 14-22 ^{o}C for XDX-corrected values. Corrected temperatures at the top of the core (7 ka) of 18.5 ^{o}C would represent a calcification depth in the lower part of the thermocline, according to the modern-day temperature profile.

6.3.4 Dissolution corrected test mass

Test mass records for *G. sacculifer* and *N. dutertrei* were reconstructed using XDX according to equations (3) and (6). *G. ruber* test mass was reconstructed using equations (8) and (3). Constants are listed in **Table 6.1**. The correction generally raised the test mass, particularly over MIS 2, 4 and 5 (**Figure 6.5**). The dissolution correction also brought test mass of the most recent samples close to those of core-tops (WIND20B, WIND11B [*Johnstone et al.,* in press (**Chapter 4**)]) from shallow sites with good calcite preservation (XDX < 1) in the western Indian Ocean (**Figure 6.5**). However, drops in test mass of ~4 μg coinciding with preservation maxima during the glacial terminations suggests that this calibration may over-estimate the effect of dissolution on foraminiferal mass, particularly of *G. ruber*, when dissolution is severe, as with the case with temperature above (**Section 6.3.3**).

Good preservation over MIS 3 meant that the correction was small over this interval. Test mass minima, in the record of initial mass, for both *G. sacculifer* and *N. dutertrei* in the XDX-corrected record occur during MIS 3 at ~42 ka (**Figures 6.3, 6.4**).
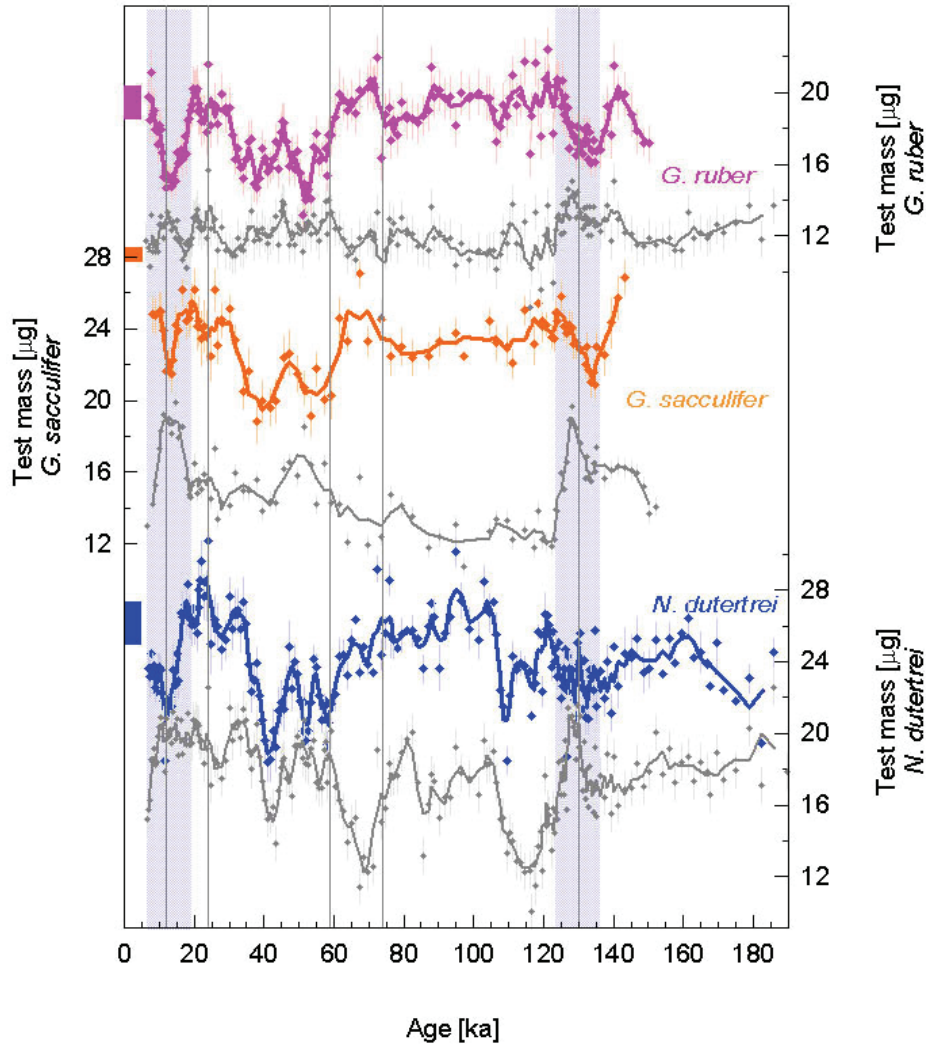
Figure 6.5 Reconstructed test mass for three species of planktic foraminifera from WIND 28K. Solid lines are 3 point running average for *G. ruber* [white] (pink line), *G. sacculifer* (orange) and *N. dutertrei* (blue). Grey lines are measured mass. (Measurement error estimated as ±1 µg.) Coloured bars on the left hand side indicate mass of tests from core-tops (WIND10B and 11B) from shallow sites in the Western Indian Ocean [*Johnstone et al.*, in press (**Chapter 4**)]. Lightest mass of *G. sacculifer* and *N. dutertrei* in the reconstruction occur early in MIS 3 where tests have thin walls.

6.4. Discussion: paleoceanographic implications

6.4.1 Deep ocean processes

$\Delta[CO_3^{2-}]$ reconstructed for WIND28K is consistent with calcite compensation theory [*Broecker and Peng,* 1987] which predicts that change in atmospheric CO_2 content is accompanied by a change in the depth of calcite preservation in the deep ocean. Greater atmospheric CO_2 during an interglacial is associated with the transfer of CO_2 from the deep ocean, via the surface ocean, to the atmosphere. This results in an increase in whole ocean $[CO_3^{2-}]$ leading to a transient deepening of the lysocline.

Carbonate burial removes twice as much alkalinity as dissolved inorganic carbon, and the decrease in deep ocean $[CO_3^{2-}]$ continues until a glacial steady state of high atmospheric and good calcite preservation, particularly in Indian and Pacific Ocean sediments, is reached. Preservation events over glacial terminations have been recorded throughout the Indian and Pacific Oceans [*Berger*, 1977; *Le and Shackleton*, 1992] and the deep south Atlantic [*Hodell et al.,* 2001]. These deglacial preservation peaks are a major feature of the WIND28K record (**Figure 6.4**, **Figure 6.6**).
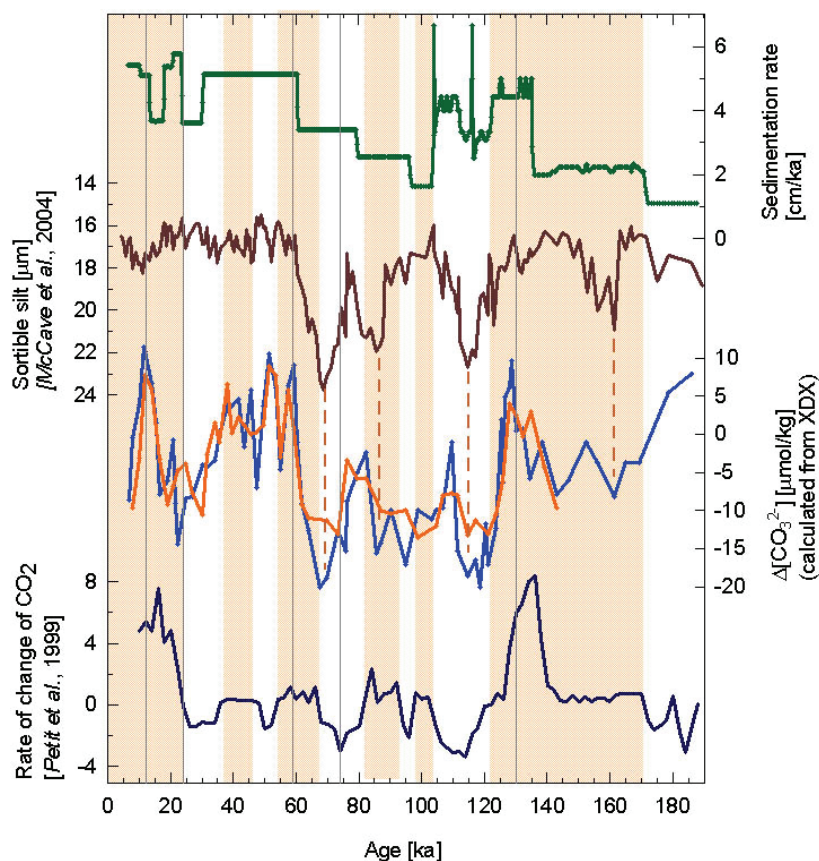
Figure 6.6 The relationship between $\Delta[CO_3^{2-}]$ and CO_2 in WIND 28K. Dark blue line is the rate of change of CO_2 [*Petit et al.,* 1999]. Periods when CO_2 is increasing (pink bars) are generally associated with high values of $\Delta[CO_3^{2-}]$ (calculated from XDX of *N. dutertrei* (blue) and *G. sacculifer* (orange)). Dissolution is enhanced during the four episodes of faster deep water flow (brown dashed lines) through the Amirante Passage, represented by increase in sortible silt size (brown solid line, reversed scale) [*McCave et al.,* 2005].

The opposite occurs during a glacial inception when CO_2 mixed down to the deep ocean acts to dissolve calcite at the seafloor. The dissolution event at the transition from MIS 5.1 to MIS 4 (**Figure 6.4**) is also thought to be a global event [*Crowley*, 1983; *Broecker and Clark*, 2003]. With regard to the timing of the peaks, changes in pCO$_2$ lead peaks in $\Delta[CO_3^{2-}]$ by several thousand years (**Figure 6.6**). This is consistent with phasing of 6 - 20 ka estimated by *Le and Shackleton* [1992].

Change in $\Delta[CO_3^{2-}]$ between the present value (-11 µmol/kg) and Termination I maximum (12 µmol/kg) of ~23 µmol/kg is similar to the change of 25 µmol/kg estimated by *Marchitto et al*. [2005] for the deep Pacific. Termination II peaks at a value 5 µmol/kg lower than the Termination I peak. ($\Delta[CO_3^{2-}]$ values referred to in this section have been calculated from the XDX of *N. dutertrei* as this records $\Delta[CO_3^{2-}]$ over a wider range than *G. sacculifer*.) $\Delta[CO_3^{2-}]$ calculated for MIS 2 is variable, but LGM values of -9 µmol/kg are only slightly higher than those of the present day. It is reasonable to assume that there was little change in $[CO_3^{2-}]$ SATURATION at the WIND28K site during the last glacial. The increase in $[CO_3^{2-}]$ SATURATION due to lower sea-level, and possible decrease in temperature, along with the increase due to higher glacial salinity are likely to result in only a small change in $[CO_3^{2-}]$ SATURATION. Our results indicate little change in glacial $[CO_3^{2-}]$ relative to modern. This is in agreement with estimates by *Anderson and Archer* [2002] and *Marchitto et al*. [2005] for the deep Pacific.

In addition to global changes in calcite preservation, local factors may also impact the record of calcite dissolution at this site. These are (1) change in deep water mass (2) respiration driven dissolution in porewaters and (3) flow speed of deep water through the Amirante Passage.

(1) Transfer of carbon between atmosphere and ocean reservoirs is modified by rearrangement of ocean circulation which redistributes carbon within the ocean Circumpolar Deep Water (CPDW), which forms the deep water at WIND28K, is a mixture of both high $[CO_3^{2-}]$ North Atlantic Deep Water (NADW) and corrosive, low $[CO_3^{2-}]$ Antarctic Bottom Water (AABW). Reduced formation, or shallower circulation, of NADW during cold intervals [*Sarnthein et al*., 1994; *Sigman and Boyle*, 2000] means that glacial CPDW contains more Antarctic Bottom Water and is, therefore, more corrosive than during warmer phases. Increased dissolution in cold intervals has been recorded in sites bathed in CPDW in the Indian Ocean, as well as in deep sites from the Southern Atlantic Cape Basin [*Howard and Prell*, 1994; *Hodell et al.,* 2001]. This may have a small influence on WIND28K calcite preservation.

(2) Another potential confounding factor in estimating $\Delta[CO_3^{2-}]$ of deep water from any proxy based on calcite dissolution, is that acidity produced by the degradation of organic matter means that porewater chemistry is offset from that of the overlying deep water. This is a major cause of carbonate dissolution above the lysocline [*Emerson and Bender*, 1981; *Hales and Emerson*, 1997] and parallel variability of preservation and C_{org} has been recorded in records from shallow sites in the Indian Ocean [*Bassinot et al*., 1994, *Kloecker et al*., 2006]. Although there is likely to have been some variability in productivity at the site due to changing in upwelling intensity, *Jacot des Combes et al.* [1999] find negligible organic carbon content between 38 and 238 ka BP in a core (MD90929) near WIND28K in the Amirante

Passage. We consider the degradation of organic matter to play only a minor role in carbonate dissolution at WIND28K.

(3) Another factor which could leave a local signal on calcite preservation at this site is the position of the core site in the Amirante Passage. At depth the Indian Ocean is divided by a succession of ridges and some of the northern flowing deep water is channelled through the narrow Amirante Passage between Madagascar and the shallow Mascarene Plateau to the East. On glacial to interglacial timescales flow speed through the Amirante Passage varies [*McCave et al.*, 2005]. Periods of ice sheet growth and consequent removal of freshwater from the surface ocean increases the density of surface water. This is subsequently mixed down, temporarily intensifying the vertical density gradient and driving a transiently faster ocean circulation until salinity anomalies were distributed more equally in the global ocean. Periods of global cooling and falling sea-level thus mean faster flow through the Amirante Passage. Times of faster flow are indicated by increases in sortable silt size at transitions from MIS 5.1 to 4; 5.5 to 5.4 and 6.5 to 6.4 [*McCave et al.,* 2005]. These peaks in sortable silt size correspond with episodes of poor preservation (**Figure 6.6**). This suggests that faster current flow through the channel enhances dissolution. One possible mechanism would be that the selective winnowing of the fine-grained fraction from the sediment reduces protection by clays and increase the exposure time of tests to deep water.

6.4.2 Surface ocean temperature records

XDX-corrected SST record from WIND28K bear a strong resemblance to records from other sites which lie within the Asian monsoon system (**Figure 6.7**). Such records bear little similarity to temperature records from tropical sites outwith the monsoon area. Temperatures for the equatorial Indian Ocean [*Bard et al.,* 1997; *Saraswat et al.,* 2005], like those from the Eastern equatorial Pacific [*Lea et al.,* 2000], record a pattern similar to that of high latitude temperatures over the last 150 ka. In these records MIS 2 and MIS 4 temperatures are slightly cooler than those of MIS 3 and warmest temperatures occur during MIS 5.5.

In contrast, sites from the Indian Ocean have coolest temperatures during MIS 3, associated with a period of strong SW monsoon [*Clemens and Prell*, 2003]. SSTs reconstructed from alkenones, and also foraminiferal $\delta^{18}O$, on the Oman margin show a drop of 3 ^{o}C at the beginning of MIS 3 [*Emeis et al.,* 1995]. WIND28K records similar cool temperatures during MIS3 (**Figure 6.7**). Although WIND28K lies in a site of upwelling, upwelling does not explain this cooling. As described by *Emeis et al.* [1995], SST records from upwelling and non-upwelling areas within the monsoon system are very similar to each other (**Figure 6.7**) and reflect a basin-wide change in conditions.
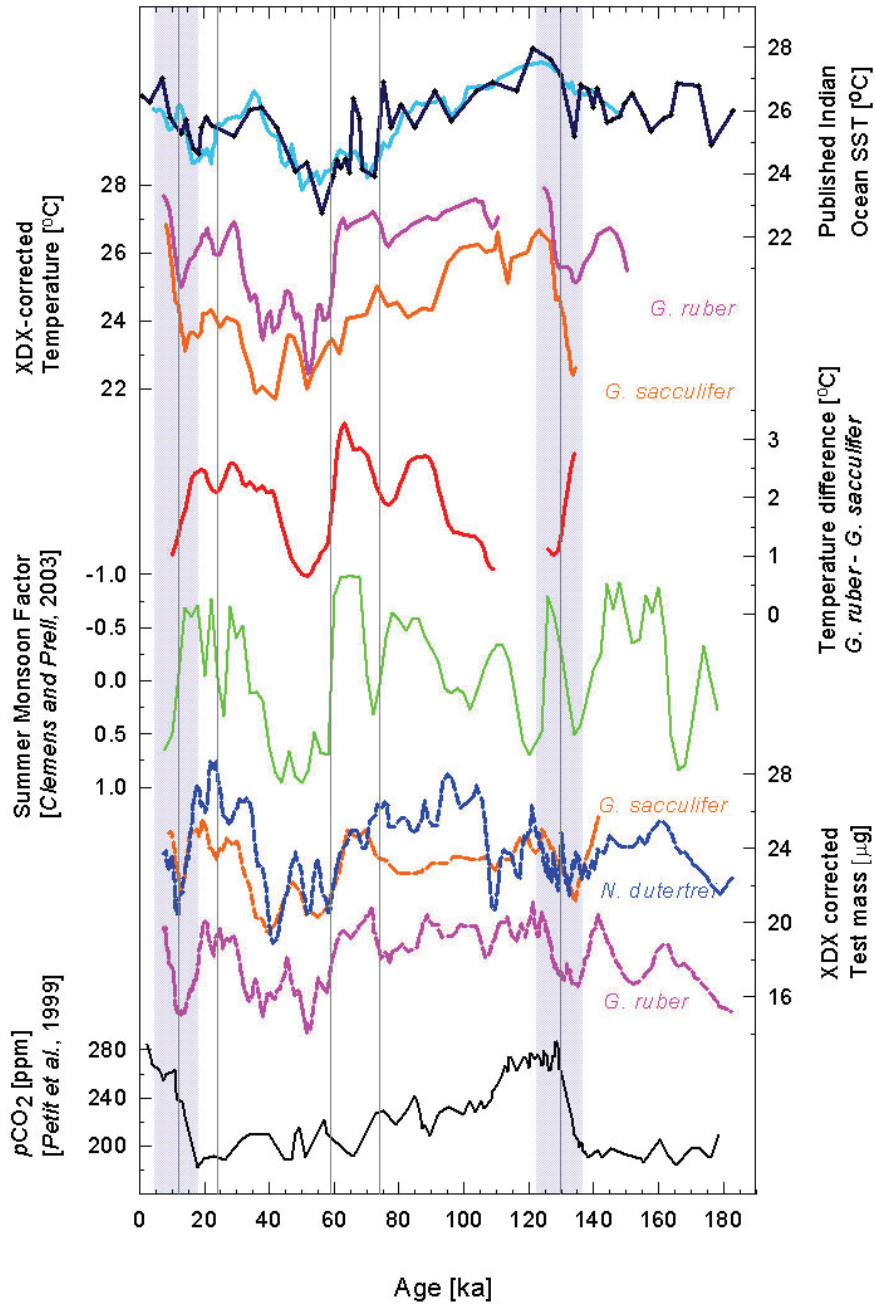
Figure 6.7 Dissolution-corrected SST records for WIND28K (*G. ruber*; pink line; *G. sacculifer*, orange line) are similar to published records from both upwelling (black line with diamonds, ODP site 732 [*Emeis et al.,* 1995]) and non-upwelling (light blue line, Core TY93929/P (13°42'N, 53°15'E) [*Rostek et al.* 1993]) sites in the Indian Ocean. Coolest temperatures in the three records occur during the strong SW monsoon in early MIS 3 (green line). Temperatures calculated from WIND28K *G. ruber* and *G. sacculifer* are more similar during episodes of strong monsoon (red line is *G. ruber* 3 point running average temperature minus *G. sacculifer* 3 point running average temperature). Similarity between this record and monsoon intensity may suggest a less stratified water column at this time. XDX-corrected test mass records of *G. ruber* (pink dashed line), *G. sacculifer* (orange dashed line) and *N. dutertrei* (blue dashed line) show little resemblance to (inverse) of CO_2, which would be the case if $[CO_3^{2-}]$ was the major control on mass. Coincidence of thin-walled *G. sacculifer* and *N. dutertrei* and low SSTs during early MIS 3 suggest that temperature exerts some control on test mass in these species.

Weak monsoon during glacial stages is associated relatively small changes in temperature during these intervals [*Clemens et al.,* 1991; *Naidu and Malmgren,* 2005]. The ~1 ^{o}C difference in SST in the WIND28K record between LGM and mid-Holocene in the XDX-corrected temperatures (**Figure 6.4**) are comparable to other estimates for the area. Temperature estimates based on models and on proxies suggest small changes in temperature for the monsoon zone of the Indian Ocean between LGM and present. Modelled LGM temperatures for the location (LGM simulation following protocol of PMIP [*Braconnot et al.*, 2007; *Ute Merkel*, pers. com.; *Merkel et al.*, 2010] show a similar seasonal pattern to present but are ~1.5^{o}C lower. Temperatures calculated from foraminiferal assemblages show no change in warmest month, coolest month or annual average temperature at the core site during the LGM [*Barrows and Juggins,* 2005].

Monsoon influence in this area may also be reflected in the temperature difference between *G. ruber* and *G. sacculifer* (**Figure 6.7**). When the SW monsoon is strong, such as early MIS 3, there is little difference in temperatures recorded by the two species. During MIS 2 and MIS 4 when monsoon intensity was weak, temperatures recorded by *G. ruber* are up to 2 ^{o}C warmer than those of *G. sacculifer*. The *G. ruber* temperature record, in particular, must be interpreted with caution as XDX was not measured on this species itself; corrections are based on dissolution recorded by *G. sacculifer*. This could result in overcorrection of the temperature record during periods of severe dissolution, as discussed above (3.3). Alternatively, the difference in temperature recorded by the two species could also be explained by changes in stratification. A small temperature difference would indicate a well-stratified water column when the monsoon was weak and upwelling reduced.

A final point about temperature concerns the published temperature record for the past 65 ka [*Kiefer et al.*, 2006]. In the original temperature record (uncorrected for dissolution) it appeared that temperatures recorded by *N. dutertrei* increased in parallel with the Antarctic Warm Events (**Figure 6.8**). This was attributed to Subantarctic Mode Water (SAMW) exchanging heat with the overlying thermocline water during these events. However, the effect of dissolution on Mg/Ca of *N. dutertrei* would amplify preservation changes in the thermocline temperature record. Although a higher sampling resolution may clarify this further, the record of XDX-corrected temperatures does not support warmer thermocline temperatures during Antarctic Warm Events (**Figure 6. 8**).
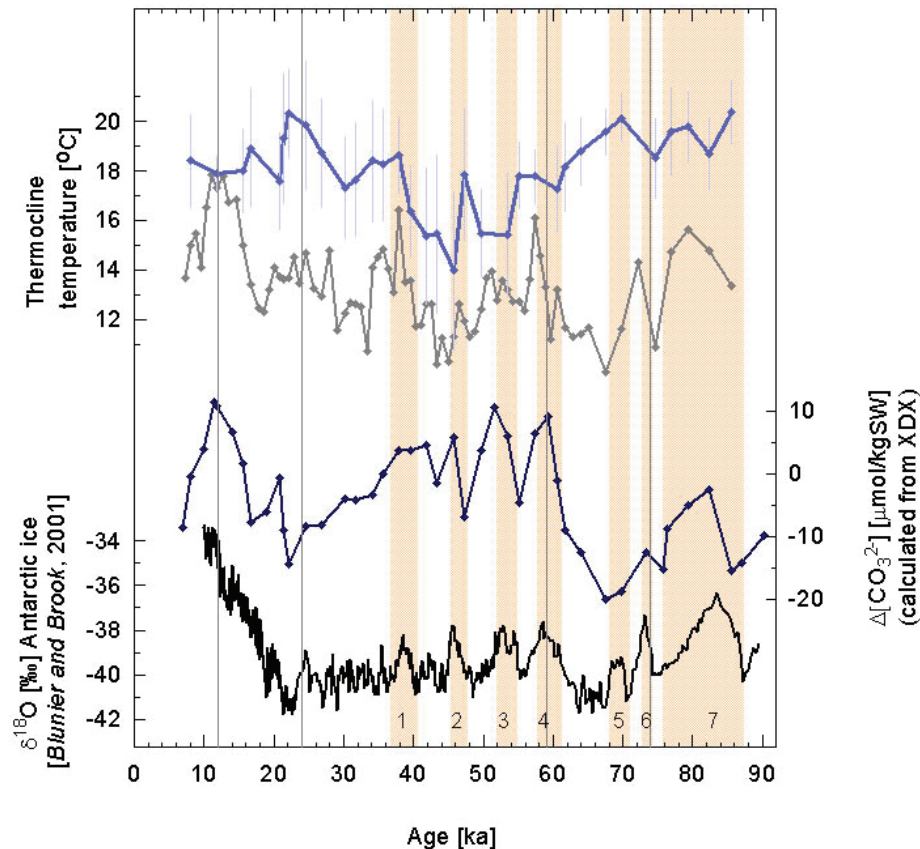
Figure 6.8 90 ka temperature record for core WIND28K derived from Mg/Ca of *N. dutertrei*. Black line is δ18O of *Blunier and Brook* [2001] representing Antarctic Warm Events (vertical pink bars, numbered). Grey line represents temperatures calculated from analyzed Mg/Ca. Apparently warmer temperatures during Antarctic Warm Events [*Kiefer et al.*, 2006] are not seen in the dissolution-corrected temperature record (light blue line) due to better preservation over these intervals (dark blue line is Δ[CO3²⁻] calculated from XDX of *N. dutertrei* for WIND28K).

6.4.3 Factors influencing foraminiferal test mass: evidence of temperature control

Mass of planktic foraminifera tests has been related to sea water conditions during calcification, with a suggested correlation to atmospheric CO_2 [*Barker and Elderfield*, 2002], temperature [*Gonzalez-Mora et al.*, 2008; *Kisakurek et al.*, 2008; *Moy et al.*, 2009] or salinity [*Bassinot and Johnstone*, in prep.]. These parameters control the $[CO_3^{2-}]$ of the water where the foraminifera calcify and it has been proposed that foraminiferal calcification responds to the calcite saturation state of the ambient water [*Spero et al.*, 1997; *Bijma et al.*, 1999].

Temperature has a relatively small control on calcite saturation [*Zeebe and Wolf-Gladrow*, 2001] but it could independently affect test mass by controlling calcification rate of the organism. Temperature controls many biological rates [*Gillooly et al.*, 2002 and references therein] and may act to control growth rate.

The decrease in mass of *G. bulloides* tests in the North Atlantic from the LGM toward the present, as atmospheric CO_2 increased (decreased calcite saturation of surface ocean, inhibiting calcification) and temperatures increased (increases saturation, and possibly growth rate, and therefore mass) argues strongly for CO_2 control on test mass [*Barker and Elderfield*, 2002]. This conclusion was supported by the work of *Gonzalez-Mora et al.* [2008] for *G. ruber* and *G. bulloides*, although these authors suggest that the inverse relationship between CO_2 and mass is modified by the positive relationship between temperature and mass.

Samples from within the monsoon region of the Indian Ocean over MIS 3 offer an opportunity to isolate temperature effect from CO_2 on test mass. During MIS 3 temperature records based on alkenones and foraminifera [*Rostek et al.*, 1993; *Emeis et al.,* 1995] indicate temperatures were ~4 ^{o}C colder at 50 ka compared to 25 ka in the Indian Ocean. Atmospheric CO_2 [*Stauffer et al.,* 1998] changed only a little, a variation of ~20 ppm, over the same interval.

Our dissolution-corrected test mass records suggest that temperature exerts a strong control on this property. During the coldest interval of MIS 3, initial mass of *N. dutertrei* is at a minimum and tests have thin walls (**Figures 6.2, 6.4, 6.6, 6.9**). Initial mass of *G. sacculifer* is also lowest over this interval. *G. ruber* tests are also light, although test mass variation is less clear in this species. This is suggestive of a general change in conditions affecting calcification of both mixed layer and thermocline dwelling species.

6.5 Conclusions

This first application of dissolution proxy XDX to a sediment core shows its value as an indicator of calcite preservation, and as a means to correct dissolution bias in test mass and Mg/Ca derived temperatures.

The pattern of calcite dissolution in Indian Ocean core WIND28K reflects the global reorganisation of carbon on glacial-to-interglacial timescales. Transfer of carbon between the shallow and deep ocean leads to dissolution at glacial inceptions and preservation peaks over terminations. The increase in $\Delta[CO_3^{2-}]$ over Termination I, of ~25 μmol/kg, is similar to that of other estimates of deep ocean calcite saturation.

Local controls on dissolution are superimposed on the global record. Severe dissolution coincides with periods of faster flow through the Amirante Passage at warm to cool transitions, suggesting that faster flow increases exposure time of tests to corrosive deep water.

The dissolution-corrected temperature record of WIND28K is similar to those of other monsoon-dominated sites in the Indian Ocean. LGM SSTs were 1-1.5 ^{o}C cooler than

present. The strong SW monsoon during MIS 3 coincides with a 4 $^{\circ}$C drop in both SST and thermocline temperatures.

The occurrence of foraminifera tests with thin walls and low (initial) mass over the cold interval in MIS 3, when atmospheric CO_2 was low, suggests that temperature exerts a strong control on test mass.

Appendix A

Additional data for core WIND28K [Heather Johnstone and Ed Hathorne] analyzed using Finnegan Element II ICP-MS at MARUM, University of Bremen.

Depth in core [cm]	Li/Ca µmol/mol	B/Ca µmol/mol	Mn/Ca mmol/mol	Sr/Ca mmol/mol	Ba/Ca µmol/mol	U/Ca nmol/mol
0	11.93	72.7	0.048	1.24	4.23	6.58
10	10.63		0.004	1.21	1.77	7.22
20	10.90		0.013	1.22	1.38	7.69
30	11.28	39.8	0.006	1.23	2.34	8.66
40	11.34		0.008	1.23	2.59	8.64
50	11.05	75.8	0.009	1.23	2.81	6.77
60	11.35	67.8	0.007	1.24	1.70	5.04
70	14.52		0.433	1.25		5.11
80	15.55	77.2	0.084	1.26	3.11	5.95
88	15.92	32.5	0.106	1.27	2.92	5.24
100	15.48		0.139	1.27	3.55	97.89
108	15.29	47.3	0.158	1.25	3.21	63.40
120	15.36	79.4	0.143	1.24	2.17	27.42
128	16.62	61.8	0.254	1.23	3.96	30.20
140	13.34		0.245	1.21	2.76	23.19
148	12.07		0.211	1.25	2.48	18.90
160	13.13	50.8	0.376	1.23	4.60	11.81
168	11.20		0.272	1.27	3.75	4.18
180	13.74		0.415	1.23	3.49	9.50
188	12.73		0.310	1.25	3.41	12.57
200	13.21	60.8	0.443	1.26	5.34	11.95
208	12.01	69.3	0.338	1.24	4.03	10.23
220	11.57		0.290	1.23		7.88
230	12.74	70.9	0.487	1.24	5.12	11.31
240	12.05	40.4	0.382	1.23	3.61	8.94
248	11.94		0.313	1.24	3.06	10.16
260	12.65	70.4	0.430	1.25	5.05	17.34
270	12.20	58.2	0.367	1.24	3.17	12.10
280	11.14		0.264	1.26	3.94	7.61
288	8.74		0.168	1.31		2.75
308	10.02		0.147	1.22	1.04	5.58
320	6.31		0.143	1.27		3.93
330	10.71	52.2	0.229	1.22	1.96	6.08
340	10.67	67.5	0.301	1.24	2.78	7.28
348	10.63	65.9	0.256	1.22	2.05	6.39
360	7.17		0.124	1.25	-1.88	3.45
368	10.12	57.3	0.176	1.21	1.48	5.37
380	10.21	71.2	0.235	1.23	2.71	5.77
388	7.23		0.137	1.25	-2.42	2.64
400	10.03	68.5	0.257	1.23	2.01	5.50
408	10.04	80.8	0.203	1.23	1.75	6.08
420	9.46		0.210	1.23		5.99
428	10.71		0.380	1.23		9.06
446	3.93		0.143	1.34		1.49
454	8.93		0.140	1.26		3.04
460	8.42		0.143	1.26		4.12
470	10.89	72.2	0.265	1.24	2.02	5.10
480	11.41		0.271	1.25	5.41	6.03
490	11.60	48.1	0.374	1.26	3.28	5.60
500	11.54	98.5	0.283	1.26	5.39	5.21
510	11.77		0.274	1.25	2.51	4.24
520	12.17		0.300	1.26	3.87	7.46
530	12.79	149.8	0.365	1.24	4.74	29.73
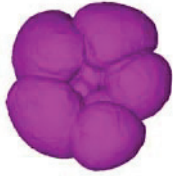
7. Effect of preservation state of planktonic foraminifera tests on the decrease in Mg/Ca due to reductive cleaning and on analytical yield

H.J.H. Johnstone[1], W. Lee[2], T. Kiefer[3], M. Schulz[1] and H. Elderfield[4]

[1] MARUM – Center for Marine Environmental Sciences, University of Bremen, Leobener Straße, 28359 Bremen, Germany

[2] MACSI, Department of Mathematics and Statistics, University of Limerick, Limerick, Ireland

[3] PAGES International Project Office, Zähringerstrasse 25, 3012 Bern, Switzerland

[4] Godwin Laboratory for Palaeoclimate Research, Department of Earth Sciences, University of Cambridge, Cambridge, UK

Abstract

In order to assess the offset in Mg/Ca due to reductive cleaning for samples with a range of preservation states, four species of foraminifera from core-tops spanning a depth transect on the Ontong Java Plateau were prepared for Mg/Ca analysis both with ("Cd cleaning") and without ("Mg cleaning") a reductive cleaning step. Reductive cleaning caused corrosion of foraminiferal calcite, focused on Mg-rich inner calcite, even where tests had already been partially dissolved at the sea-floor. Lower analytical yield after reductive cleaning for *G. ruber*, *G. sacculifer* and *N. dutertrei* confirmed this as the more aggressive method. Decrease in Mg/Ca for "Cd-cleaned" compared to "Mg-cleaned" samples was ~4% for *G. ruber* and ~10% for *N. dutertrei* (averaged from all sites) and ~5 % lower for *G. sacculifer* (from oversaturated sites only). There was no significant correlation between decrease in Mg/Ca due to reductive cleaning and $\Delta[CO_3^{2-}]$. Although *P. obliquiloculata* was physically corroded by reductive cleaning, there was no difference in Mg/Ca between cleaning methods in this species. Effective clay removal potentially contributes to lower Mg/Ca after reductive cleaning. *G. ruber*, *G. sacculifer* and *N. dutertrei* pores retained detrital material after "Mg cleaning". In these species "Cd cleaning" decreased contamination-indicator Al/Ca. There was no significant decrease in Mg/Ca or Al/Ca of the smooth-surfaced species *P. obliquiloculata* after reductive cleaning. Correlation between analytical yield and $\Delta[CO_3^{2-}]$ reached statistical significance ($p < 0.05$) only for "Cd cleaned" *N. dutertrei*. Maxima in analytical yield of *G. ruber* and *G. sacculifer* for a core from the deep Indian Ocean coincided with deglacial preservation peaks. It is suggested that monitoring analytical yield may provide a first estimate of dissolution.

7.1 Introduction

The use of Mg/Ca of foraminiferal calcite to estimate paleo-temperature of seawater has become increasingly common since the development of the proxy in the 1990s [*Nürnberg,* 1995*; Nürnberg et al.,* 1996; *Rosenthal* 1997; *Hastings et al.,* 1998; *Mashiotta et al.,* 1999; *Lea et al.,* 1999; *Elderfield and Ganssen*, 2000]. As the technique becomes established, the importance of standardizing the method becomes greater. In an assessment of reproducibility between laboratories *Rosenthal et al.* [2004] found that the range in Mg/Ca of foraminiferal samples was much greater than that of standard solutions. While it should be reasonably straightforward to reduce analytical discrepancies [*Greaves et al.,* 2008], individual laboratories have developed their own

protocols for cleaning foraminiferal calcite before analysis which may lead to systematic offsets.

Thorough cleaning of tests is necessary to remove contaminants which would otherwise bias trace-metal analysis. Methods in current use derive from that of *Boyle* [1981]. Cleaning involves first breaking open the test chambers, fragments are then rinsed several times with water. This removes fine clays and any other sedimentary material which became trapped inside the test at the sea floor. An oxidative cleaning step (hydrogen peroxide buffered with sodium hydroxide) is necessary to remove organic material. A reductive cleaning step (anhydrous hydrazine-ammonium hydroxide-ammonium citrate solution) removes coatings containing oxides of metals such as Fe, Mn and Cd. Test fragments undergo further rinsing with water followed by a weak acid leach before the sample is finally dissolved for analysis. When Mg/Ca is the main interest, a simplified method which excludes the reductive step is commonly used. This cleaning method is referred to as "Mg cleaning", while the method including a reductive step is known as "Cd cleaning".

Although a study by *Weldeab et al*. [2006] on *G. ruber* found little difference in Mg/Ca between the two cleaning methods in a down-core record, other studies find that the two methods give slightly different results. The interlaboratory comparison study of *Rosenthal et al.* [2004] found Mg/Ca of several species of planktonic foraminifera to be ~15% lower when "Cd cleaning" rather than "Mg cleaning" was used. This is comparable to the 10 to 15% decrease in the Mg/Ca of "Cd cleaned" *G. ruber* measured by *Barker et al*. [2003b].

Calcite containing Mg is more soluble than pure calcite, and dissolution of planktonic foraminifera at the sea floor results in lower Mg/Ca [*Lorens and Willia*, 1977; *Brown & Elderfield*, 1996; *Hastings et al*., 1998; *Rosenthal et al.*, 2000 *Dekens et al.,* 2002,; *Regenberg et al*., 2006]. It has been suggested, therefore, that lower Mg/Ca after "Cd cleaning" is caused by dissolution of test calcite by the reagents used in reductive cleaning [*Barker et al.,* 2003b; *Rosenthal et al*., 2004]. *Yu et al.* [2007] established that the citrate added to buffer the reducing agent (hydrous hydrazine), when applied in isolation of the reducing agent, can dissolve foraminiferal calcite and lower Mg/Ca.

"Mg cleaning" has the advantage that the method requires less time; it also avoids the use of the very toxic reagent, hydrazine. However, there is no doubt that "Cd cleaning" is more effective at removing metal contaminants. *Weldeab et al*. [2006] found that the sample set cleaned by the "Mg cleaning" method gave spurious high Mg/Ca values in the deep part of the core where foraminifera tests were contaminated with coatings containing Mn and Fe. These coatings can also contain Cd and so the reductive step is

necessary before Cd analysis. Although the 10 - 15% difference in Mg/Ca between methods correlates to a significant difference in calculated temperature of 1 - 1.5 $^\circ$C, both methods are in common use. It is, therefore, important to establish what controls the offset, in order that values obtained from different cleaning methods can be compared.

Barker et al. [2003b] raised the question of whether the offset in Mg/Ca between cleaning methods is sensitive to preservation state of tests, and suggested that the magnitude of the offset may be less for foraminifera from dissolved sediments. This would be the case if the decrease in Mg/Ca caused by reductive cleaning was sensitive to Mg concentration.

This would mean that the offset in Mg/Ca between the two methods would be greater for well-preserved, high Mg/Ca, tests than for partially dissolved tests with low initial Mg/Ca. In this scenario, reductive cleaning would give a more reproducible result, insensitive to slight prior dissolution of the test, although less representative of initial Mg/Ca. Alternatively, partial dissolution of the test at the sea floor could allow greater penetration of corrosive reagents during cleaning, meaning that reductive cleaning would cause more dissolution, and associated leaching of Mg, in poorly preserved tests. The primary question of this study is: (1) Does preservation state of a sample control the decrease in Mg/Ca caused by reductive cleaning?

Another issue which arises when considering what happens to samples during cleaning for Mg/Ca analysis, is that of how much of the sample is actually analysed. The severity of cleaning results in a high attrition rate, and analytical yield (the percentage of the sample which actually reaches the instrument) can be a small fraction of the original sample. There is anecdotal evidence that more material is lost from samples which are poorly preserved. Yield may be as much as 80% for well preserved tests with "Mg cleaning" but can fall to less than 10% for poorly preserved tests exposed to the more rigorous "Cd cleaning" (M. Greaves, pers. com.).

The effect of dissolution on Mg/Ca is a major drawback of this proxy. Any direct estimate of dissolution would be a great advantage in the application of the Mg/Ca paleo-thermometer. The second question addressed in this study is: (2) Does analytical yield of a sample indicate the preservation state of foraminifera tests?

7.2 Material and Methods

In order to address the two questions posed in the introduction we compare the effect of the two cleaning methods on the Mg/Ca of four species of planktonic foraminifera from a depth transect on the Ontong Java Plateau. Samples span a range of deep water calcite saturation states ($\Delta[CO_3^{2-}]$) from 13 to -20 µmol/kg. $\Delta[CO_3^{2-}]$ is defined as the difference between $[CO_3^{2-}]_{IN\ SITU}$ (measured $[CO_3^{2-}]$ at the site) and $[CO_3^{2-}]_{SATURATION}$ (calculated $[CO_3^{2-}]$ value at saturation at the site). $\Delta[CO_3^{2-}]$ values in **Table 1** are from *Johnstone et al.*, [in press (**Chapter 4**)]. The calcite saturation horizon is the depth where $\Delta[CO_3^{2-}]$ is equal to zero. This is around 2700 m water depth at the Ontong Java Plateau. The calcite tests of planktonic foraminifera are noticeably dissolved below this depth.

Core	Lat. [° N]	Long. [° W]	Water depth [m]	$\Delta[CO_3^{2-}]$ [µmol/kg]
1BC3	-2.24	-157.00	1616	13.8
1.5BC33	-1.00	-157.85	2015	9.3
2BC13	-0.01	-158.91	2301	4.9
2.5BC37	0.00	-159.48	2445	4.3
3BC16	0.01	-160.45	2959	-2.2
3BC24	0.01	-160.43	2965	-2.3
4BC51	-0.02	-161.02	3411	-5.8
4.5BC53	-0.01	-161.39	3711	-11.8
5BC54	-0.01	-161.77	4025	-14.7
5.5BC58	0.00	-162.22	4341	-22.4
6BC66	0.00	-162.70	4400	-23.0

Calcite saturation ($\Delta[CO_3^{2-}]$) values from *Johnstone et al.*, [in press (**Chapter 4**)].

Table 7.1 Details of cores used in this study.

Samples cleaned using the "Mg cleaning" method had previously been scanned by CT (computed tomography) for another study [*Johnstone et al.*, subm. (**Chapter 5**)]. In this present study, samples from the same sites were prepared using "Cd cleaning" as a comparison between the two cleaning methods. Despite the difference in sample history we consider this to be a true comparison of cleaning methods. CT is a non-destructive technique and neither X-rays passing through the tests, nor the extra sample handling involved, appeared to alter element to Ca ratios presented here.

Four species of planktonic foraminifera were used: *Globigerinoides ruber* (white), *Globigerinoides sacculifer* (with no sac-like final chamber), *Neogloboquadrina dutertrei* and *Pulleniatina obliquiloculata*. The four species are different physically. *G. ruber* and *G. sacculifer* have an open porous texture with surface ridges but little or no outer crust.

N. dutertrei is also porous, but has a thick outer crust. *P. obliquiloculata* has a smooth veneer on top of its calcite crust and no obvious pores [*Hemleben et al.,* 1989].

Each sample ideally consisted of ~30 tests from the 300-355 μm size fraction. Samples were weighed (after CT scanning in the case of the "Mg cleaning" set) before being crushed in order that analytical yield could be calculated. All samples were cleaned and analysed at the Godwin Laboratory, University of Cambridge and were cleaned according to protocols used there. The "Mg cleaning" method is based on *Barker et al.* [2003b]. The method for "Cd cleaning" is based on that of *Boyle* [1981]. There were some slight variations to the published methods, as follows. In both cleaning methods the "coarse silicates removal" step was carried out directly after the deionised water and methanol rinses. The reductive step was carried out before the oxidative step in the "Cd cleaning" method. In order to isolate the effect of reductive cleaning "Mg cleaned" samples received an extra oxidative step in lieu of the reductive step. This ensured that the number of rinses and amount of sample manipulation was the same for the two sets of samples.

After cleaning, samples were analysed, first by ICP-OES (Inductively Coupled Plasma – Optical Emission Spectrometry) to obtain Ca concentrations and also Fe/Ca. Samples were then diluted to a constant Ca concentration and analysed using the ICP-MS (Inductively Coupled Plasma - Mass Spectrometry) method developed for B/Ca analysis [*Yu et al.*, 2005]. All core-top samples were cleaned and analysed over the same two week period. This manuscript deals only with Ca, Mg, Fe, Mn and Al. Other element data (Li, B, Zn, Sr, Cd, Ba, U) exists for these samples exist and will be reported elsewhere [*Yu et al.,* in prep.]. At selected depths, an extra sample was cleaned for SEM (scanning electron microscope) examination to observe the physical effect of cleaning on the tests.

Samples from a core taken from deep (4157 m) in the Indian Ocean WIND 28K (10$^{\text{o}}$ 09.2' S, 51$^{\text{o}}$ 46.2' E) [*McCave*, 2001] were used to further examine the relationship between analytical yield and dissolution.

7.3 Results

7.3.1 Observations from Scanning Electron Microscopy

SEM images show that reductive cleaning was more effective than "Mg cleaning" alone. After "Mg cleaning" pores of *G. ruber* (not shown), *G. sacculifer* (**Figure 7.1a**) and *N. dutertrei* (**Figure 7.2c, 7.2e**) occasionally contained coccoliths or other sediment. Reductively cleaned tests had empty pores. "Cd cleaning" was the more corrosive method and caused slight dissolution of calcite, particularly around the pores and at broken edges of tests (**Figures 7.1b, 7.1d, 7.2d, 7.2f, 7.3b, 7.3f**). Well-preserved tests

from shallow sites of all four species had corrosion and damage to the inner calcite after reductive cleaning (**Figures 7.1d, 7.2d, 7.3b**). The outer surface of well-preserved tests of *G. ruber* (not shown), *G. sacculifer* (**Figure 7.1b**) and to a lesser extent, *N. dutertrei* (**Figure 7.2b**) also showed more corrosion after "Cd cleaning" than after "Mg cleaning" (**Figures 7.1a, 7.2a**). The outer surface of *P. obliquiloculata* appeared undamaged by either cleaning method.

Figure 7.1 SEM images of cleaned *G. sacculifer* tests. Left hand side: tests cleaned using "Mg cleaning" method; right hand side: tests cleaned using "Cd cleaning" method. Samples are from shallow (1616 m), panels (a) to (d); and deep (3400 m), panels (e) and (f), sites on the Ontong Java Plateau. White scale bars are 10 μm long. (a) Test from a shallow site contains coccoliths and detritus trapped in the pores (white arrow) after "Mg cleaning". (b) "Cd cleaned" sample is cleaner, although the test surface appears etched. Side view of broken test wall shows that inner calcite is more damaged by "Cd cleaning" (d) than by "Mg cleaning" (c). (e) "Mg cleaned" test from a deep site (3400 m) shows some dissolution damage to outer surface. (f) "Cd cleaning" causes additional dissolution to the outer surface, even in tests which have already been partially dissolved at the seafloor.

Although tests from deep sites had already undergone dissolution at the sea floor, reductive cleaning caused further corrosion. Again, the inner calcite of all four species was affected. Inner calcite of poorly preserved tests appeared friable and etched after reductive cleaning (**Figure 7.2j, 7.3f**). The outer surface of *G. ruber* (not shown) and *G. sacculifer* (**Figure 7.1f**) from deep sites was more corroded after "Cd cleaning" than after "Mg cleaning" (**Figure 7.1e**). The outer surface of *N. dutertrei* and *P. obliquiloculata* from deep sites did not appear to be further corroded by reductive cleaning (**Figures 7.2g, 7.2h, 7.3d**).
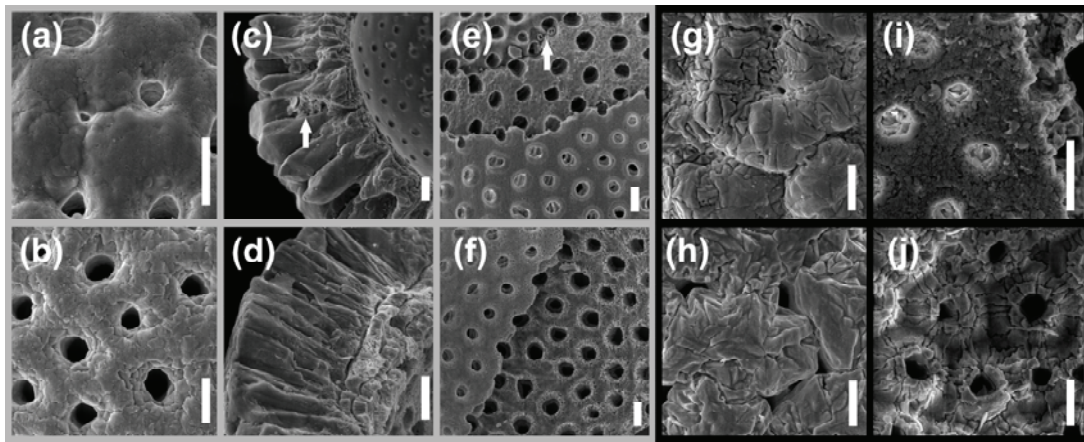
Figure 7.2 SEM images of cleaned *N. dutertrei* tests. Upper row: tests cleaned by "Mg cleaning" method; lower row: tests cleaned using "Cd cleaning" method. Samples are from a shallow (1616 m) site, panels (a) to (f), and a deep (3400 m) site, panels (g) to (j) on the Ontong Java Plateau. White scale bars are 10 μm long. (a) Outer wall of "Mg cleaned" test (a) from shallow site (1616 m) shows less etching than "Cd cleaned" test (b). (c and e) "Cd cleaning" is the more effective cleaning method. "Mg cleaned" samples can retain coccoliths and other detritus (white arrows) in the pores. (d) Side view of wall of "Cd cleaned" test shows that inner calcite is slightly dissolved and separating into layers. The outer calcite is not affected and is still solid. Inner calcite of "Mg cleaned" tests shows damage mainly around the pores (e), whereas "Cd cleaned" tests show more widespread etching of the inner calcite (f). (g, h) The outer surface of tests from a deep site (3400 m) show etching and pitting, due to dissolution at the seafloor, irrespective of cleaning method. Inner calcite, where present, appears porous and dissolved. (i). Inner calcite was often completely separated from the outer crust. (j) shows the inside of an empty outer crust.
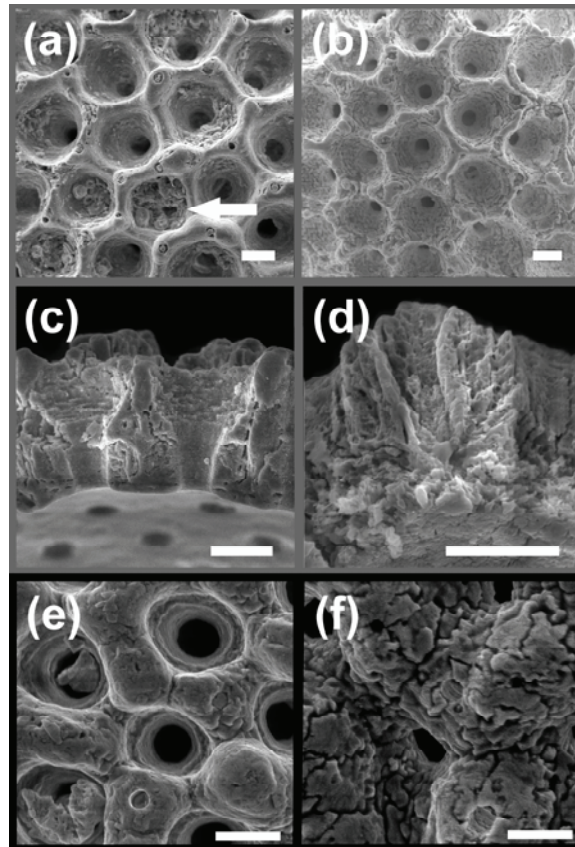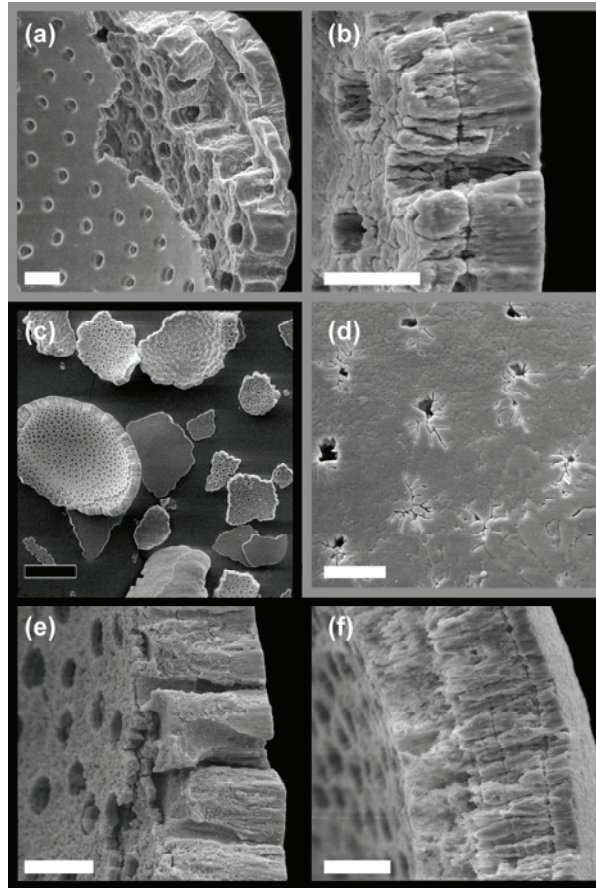
Figure 7.3 SEM images of cleaned *P. obliquiloculata* tests. Left hand side: tests cleaned using "Mg cleaning" method; right hand side: tests cleaned using "Cd cleaning" method. Samples are from a shallow (1616 m) site, panels (a) (b) and (d), and a deep (2965 m) site, panels (c), (e) and (f), on the Ontong Java Plateau. White scale bars are 10 μm long. Black scale bar is 100 μm long. Side view of broken test wall shows that "Cd cleaned" test (b) is more dissolved, particularly the inner calcite, than "Mg cleaned" test (a). The inner and outer calcite of *P. obliquiloculata* (as in *N. dutertrei*, not shown) tends to separate into inner and outer calcite when tests are slightly dissolved (c). *P. obliquiloculata* has a very smooth outer veneer (d). Inner calcite of tests from the deep (2965 m) site is slightly dissolved (e). "Cd cleaned" test (f) is more corroded than "Mg cleaned" test (e).

7.3.2 Effect of reductive cleaning on Mg/Ca and indicators of contamination (Al/Ca, Fe/Ca and Mn/Ca)

Results of analysis are given in **Table 7.2**. The effect of reductive cleaning was evaluated by comparison of pairs of samples where each pair consisted of one "Mg cleaned" and one "Cd cleaned" sample from the same depth. This meant excluding some data (5 out of 35 potential pairs) as one sample was lost during cleaning and in four other cases slightly different sample depths were run for "Mg cleaning" and "Cd cleaning" methods. In a further three cases samples were too small to run on the ICP-MS so there is no Al/Ca data.

Pairwise comparison of sample means was used to assess if average element/Ca of groups of "Cd cleaned" and "Mg cleaned" samples were different from each other. Differences were considered statistically significant when a one sided t-test gave $p < 0.1$. When this was the case, the null hypothesis (reductive cleaning does not result in a lower element/Ca value) was rejected. The difference, or offset, between methods referred to in the text is the element/Ca of the "Cd cleaned" sample subtracted from that of the "Mg cleaned" sample(s).

Mg/Ca of all four species decreased with increasing calcite undersaturation of deep water ($\Delta[CO_3^{2-}]$) (**Figure 7.4**). Sample preservation had no consistent effect on any decrease in Mg/Ca due to reductive cleaning. There was no correlation between the offset in Mg/Ca between cleaning methods and the calcite saturation of deep water ($\Delta[CO_3^{2-}]$). Regressions between Mg/Ca and $\Delta[CO_3^{2-}]$) were also similar for both cleaning methods (**Figure 7.4**). Regressions did not trend toward a common Mg/Ca value.

Pairwise comparison of sample means showed "Cd cleaning" resulted in lower Mg/Ca than "Mg cleaning" for two of the four foraminifera species (**Figure 7.4**). Mean Mg/Ca, for all depths, was 0.17 mmol/mol, or ~10%, lower after "Cd cleaning" than "Mg cleaning" for *N. dutertrei* and 0.18 mmol/mol, ~4%, lower for *G. ruber*. The decrease in mean Mg/Ca due to reductive cleaning did not quite reach statistical significance for *G. sacculifer* (0.10 mmol/mol, or 3%, $\alpha = 0.10$). In this species, there was a significant difference in Mg/Ca between cleaning methods in samples from above the calcite saturation horizon. Mg/Ca was on average 0.21mmol/mol, ~5%, less for "Cd cleaned" rather than "Mg cleaned" samples. There was no difference in the offset between methods in samples from above and below the calcite saturation horizon for any other species. There was no decrease in average Mg/Ca between the two cleaning methods for *P. obliquiloculata*.
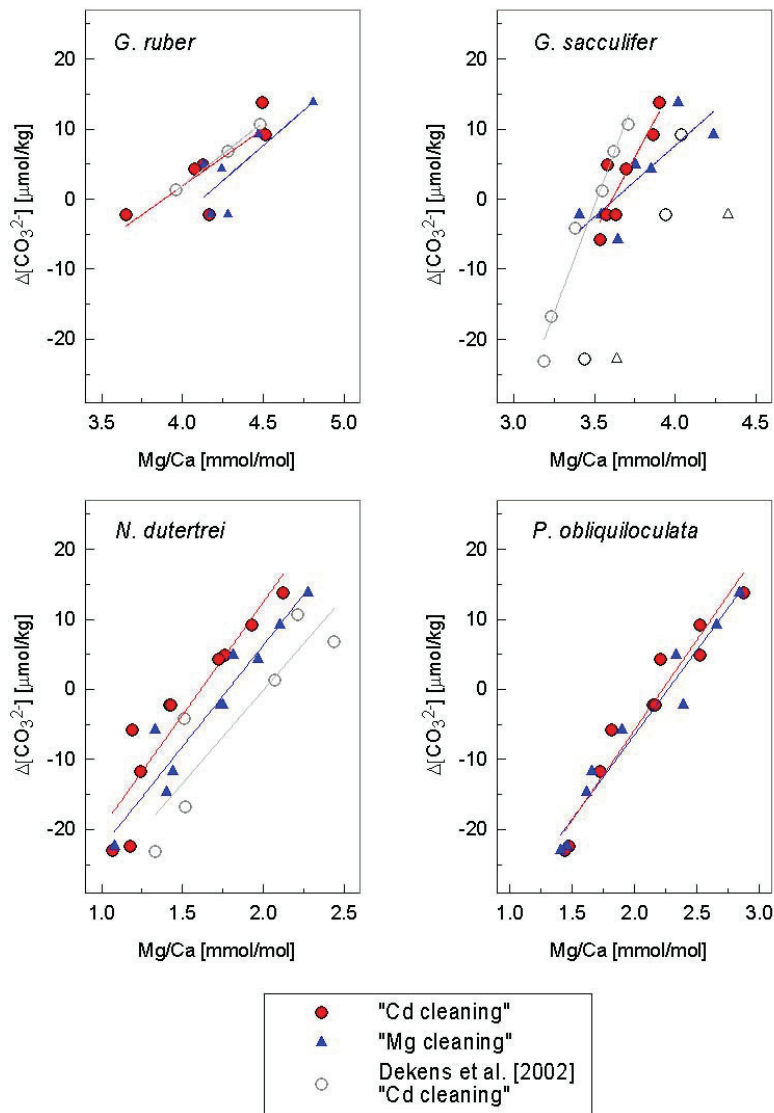
Figure 7.4 Mg/Ca for four species of planktonic foraminifera cleaned by two methods. Regressions between Δ[CO₃²⁻] and Mg/Ca are the same for both cleaning methods for each species. Reductive cleaning decreased mean Mg/Ca of *G. ruber* and *N. dutertrei*. Mean Mg/Ca of *G. sacculifer* and *P. obliquiloculata* is not significantly altered by cleaning method. Regressions between Δ[CO₃²⁻] and Mg/Ca of "Cd cleaned" samples of this study are similar to regressions of *Dekens et al.* [2002].

Core	"Mg-cleaning" method *					"Cd-cleaning" method				
	Yield [%]	Mg/Ca [mmol/mol]	Mn/Ca [µmol//mol]	Al/Ca [µmol/mol]	Fe/Ca [mmol/mol]	Yield [%]	Mg/Ca [mmol/mol]	Mn/Ca [µmol/mol]	Al/Ca [µmol/mol]	Fe/Ca [mmol/mol]
	G. ruber (white), 300-355 µm									
1BC3	38	4.810	4.6	92	0.029	33	4.494	1.2	13	0.012
1.5BC33	34	4.466	3.6	22	0.020	23	4.514	0.5	17	†
2BC13	26	4.133	5.0	26	0.044	24	4.126	0.3	6	†
2.5BC37	32	4.241	7.4	57	0.052	7	4.073	1.2	21	†
3BC16	20	4.175	2.3	22	†	2	• 4.167	•	•	†
3BC24	40	4.282	3.3	19	0.031	10	3.653	0.8	6	†
	G. sacculifer (without sac), 300-355 µm									
1BC3	58	4.020	2.8	27	0.050	42	3.903	-0.3	16	0.012
1.5BC33	51	4.237	2.5	32	0.036	36	3.862	0.2	22	†
2BC13	57	3.756	0.9	6	0.023	29	3.579	-0.3	4	†
2.5BC37	47	3.849	12.3	11	0.012	33	3.697	0.5	17	†
3BC16	25	3.408	2.0	18	†	27	3.576	0.0	16	†
3BC24	52	3.543	3.6	8	0.049	35	3.635	-0.3	4	†
4BC51	35	3.643	1.3	21	0.019	1	• 3.535	•	•	†
	N. dutertrei, 300-355 µm									
1BC3	42	2.280	5.3	80	0.031	25	2.126	1.6	19	0.011
1.5BC33	49	2.104	4.1	25	0.028	48	1.927	1.3	17	0.013
2BC13	50	1.815	4.5	10	0.016	32	1.763	0.6	3	†
2.5BC37	44	1.968	3.4	16	0.015	27	1.725	0.9	7	†
3BC16	35	1.735	1.5	12	†	19	1.419	0.0	1	†
3BC24	38	1.750	1.4	5	†	20	1.424	-0.3	-2	†
4BC51	24	1.330	1.1	36	†	19	1.188	-0.2	1	†
4.5BC53	16	1.441	0.5	14	†	22	1.240	0.0	13	†
5BC54	50	1.400	1.1	19	0.020	not run				
5.5BC58	12	1.082	0.6	18	0.000	15	1.177	0.1	15	†
6BC66	not run					22	1.070	-0.2	4	†
	P. obliquiloculata, 300-355 µm									
1BC3	56	2.843	7.1	39	0.0322	61	2.869	2.6	43	0.0107

Sample	yield	Mg/Ca	Mn/Ca	Al/Ca	Fe/Ca	yield	Mg/Ca	Mn/Ca	Al/Ca	Fe/Ca
1.5BC33	41	2.657	4.2	12	0.0210	54	2.521	2.2	23	0.0135
2BC13	44	2.328	4.4	9	0.0123	22	2.523	2.3	3	0.0089
2.5BC37	sample lost during cleaning					33	2.209	2.1	2	†
3BC16	not run					30	2.144	2.5	5	0.0056
3BC24	33	2.393	12.8	6	0.0085	31	2.161	3.2	6	†
4BC51	11	1.900	2.5	11	†	37	1.818	2.1	18	†
4.5BC53	13	1.653	3.0	36	†	27	1.726	2.0	28	0.0063
5BC54	48	1.617	2.6	12	0.0096	not run				
5.5BC58	3	• 1.458	1.7	•	†	24	1.472	1.7	20	†
6BC66	19	1.404	2.7	32	†	26	1.438	1.8	24	0.0110

* Samples CT scanned before analysis, Mg/Ca data from *Johnstone et al.* [subm. (**Chapter 5**)]

• Sample too small for ICP-MS, Mg/Ca from ICP-OES

† Fe below detection limit of ICP-OES

Table 7.2 Analytical yield and Mg/Ca, Mn/Ca, Al/Ca, Fe/Ca for four species of planktic foraminifera cleaned using "Mg cleaning" and "Cd cleaning" methods.

Efficiency of cleaning was assessed by monitoring Al/Ca, Fe/Ca and Mn/Ca. Al occurs in marine clays and indicates clay contamination. Fe and Mn are also found in clays but are often associated with metal oxide coatings. The highest values of Al/Ca, Fe/Ca and Mn/Ca were found in "Mg cleaned" samples from above the calcite saturation horizon. Samples from deep sites tended to have lower levels of contamination particularly Fe/Ca and Mn/Ca.
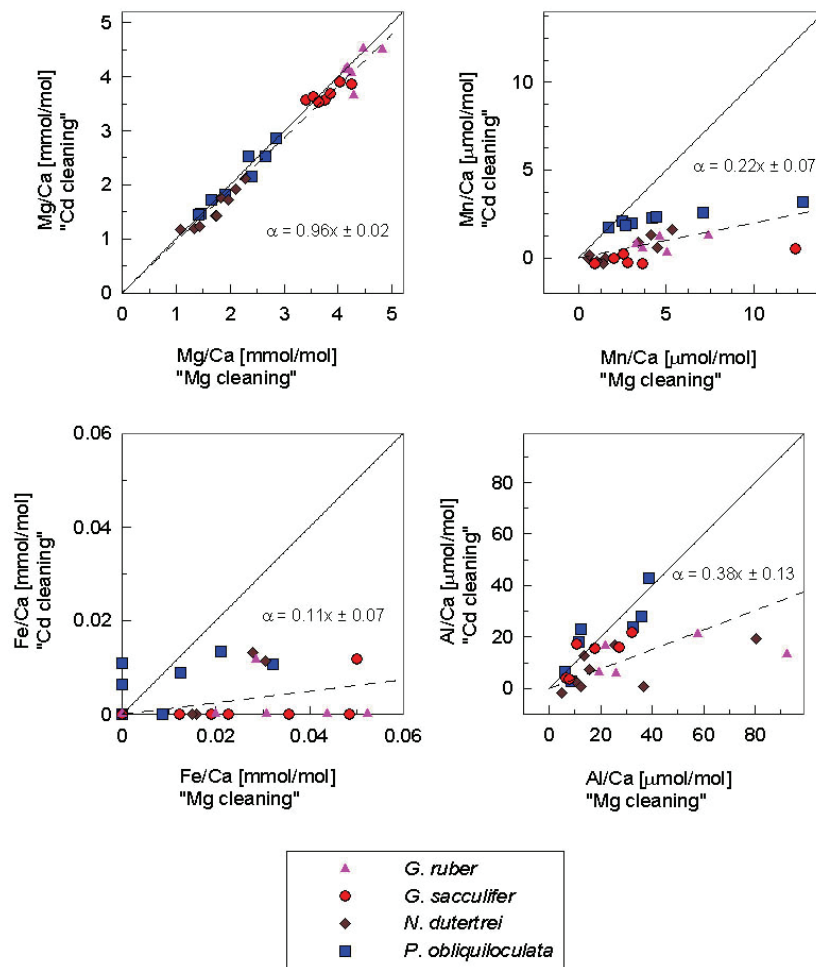
Figure 7.5 Comparison of element/Ca obtained after "Mg cleaning" and "Cd cleaning" for four species of planktic foraminifera. Solid lines are 1:1 lines; dashed line best fit to data forced through the origin. On average Mg/Ca are 4% lower where "Cd cleaning" rather than Mg cleaning was employed. "Cd cleaning" more effectively removes coatings containing Fe and Mn oxides than does "Mg cleaning". (Where analyte does not reach detection limit for Fe/Ca, a value of zero has been plotted.) Cleaning method makes little difference to Al/Ca (representing clay contamination) of *P. obliquiloculata*. "Cd cleaning" appears to more effectively remove clays from *G. ruber*, *G. sacculifer* and *N. dutertrei*.

Metal oxide coatings were more effectively removed by "Cd cleaning" (**Figure 7.5**). Mean Fe/Ca and Mn/Ca were lower after reductive cleaning for all four species. Fe concentrations did not reach the detection limit of the ICP-OES for most of the reductively cleaned samples. Where Fe did not reach the detection limit, a value of zero has been used for Fe/Ca in order to compare samples. Comparison of sample means showed reductive cleaning lowered Fe/Ca by 93% for *G. ruber*; 94% for *G. sacculifer*; 72% for *N. dutertrei*. There was no significant decrease for *P. obliquiloculata*. A negative value was recorded for Mn/Ca when Mn concentration was less than the zero standard on the ICP-MS. This was the case for several of the reductively cleaned samples. In these cases a value of zero was used for the comparison between cleaning methods, but not in the plot (**Figure 7.5**). Reductive cleaning lowered mean Mn/Ca by 83% for *G. ruber*; 97% for *G. sacculifer*; 81% for *N. dutertrei* and 53% for *P. obliquiloculata*.

Mean Al/Ca was lower after reductive cleaning by 71% for *G. ruber*; 23% for *G. sacculifer* and 66% for *N. dutertrei*. This confirmed SEM observations that "Cd cleaning" resulted in cleaner samples, containing less detrital material, in these species. Cleaning method made no difference to Al/Ca of *P. obliquiloculata*.

7.3.4 Relationship between $\Delta[CO_3^{2-}]$ and analytical yield

Analytical yield confirmed that "Cd cleaning" was the more corrosive method and lead to more loss of sample during cleaning. Comparison of sample means showed analytical yield was greater after "Mg cleaning" than after "Cd cleaning" for *G. ruber* ("Mg cleaning" 32%; "Cd cleaning" 16%), *G. sacculifer* (41%; 29%) and *N. dutertrei* (36%; 25%). Yield was not significantly different between methods for *P. obliquiloculata* (30%; 35%).

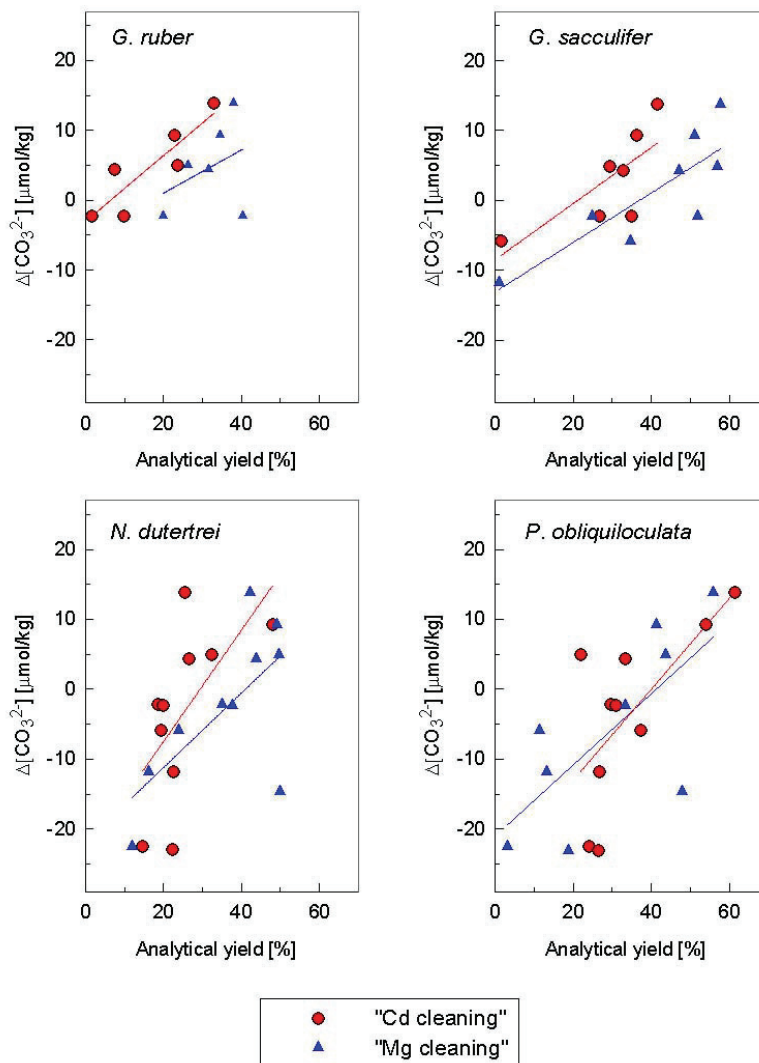**Figure 7.6**. Correlation between analytical yield and $\Delta[CO_3^{2-}]$ reached significance of $p<0.1$ only for "Cd-cleaned" *G. sacculifer*, *N. dutertrei* and *P. obliquiloculata* (**Table 7.3**). For *G. ruber*, *G. sacculifer* and *N. dutertrei* mean analytical yield was greater after "Mg cleaning" than after "Cd-cleaning". Yield was similar for both cleaning methods for *P. obliquiloculata*.

Species	Cleaning protocol	n	r^2	p
G. ruber	"Mg cleaning"	6	0.51	0.919
G. sacculifer	"Mg cleaning"	7	0.49	0.139
N. dutertrei	"Mg cleaning"	10	0.44	0.137
P. obliquiloculata	"Mg cleaning"	9	0.51	0.108
G. ruber	"Cd cleaning"	6	0.78	0.121
G. sacculifer	"Cd cleaning"	7	0.56	0.066
N. dutertrei	"Cd cleaning"	10	0.36	0.036
P. obliquiloculata	"Cd cleaning"	10	0.46	0.096

p calculated using Spearman's rho

Table 7.3 Correlation between analytical yield and $\Delta[CO_3^{2-}]$ (r^2) of deep water for samples from the OJP. Individual correlations are strongest for "Cd cleaned" *G. sacculifer, N. dutertrei* and *P. obliquiloculata*.

A larger fraction of the sample was lost during cleaning of poorly preserved tests. Mean analytical yield for all samples above the calcite saturation horizon was between 2 and 26%, (typically ~15%) greater than for the mean analytical yield of samples from below the calcite saturation horizon. Regressions estimated between analytical yield and $\Delta[CO_3^{2-}]$ all show a positive relationship (**Table 7.3; Figure 7.6**). There are only a small number of datapoints in each set and only for the sample set of reductively cleaned *N. dutertrei* is correlation significant at the 0.05 level. However, $p < 0.15$ for 7 out of the 8 sample sets suggests some correlation between $\Delta[CO_3^{2-}]$ and analytical yield.

7.4 Discussion

7.4.1. Cause of decreased Mg/Ca after reductive cleaning: selective dissolution or better cleaning

The physical corrosion of tests revealed by SEM, and the decrease in analytical yield, of "Cd cleaned" compared to "Mg cleaned" samples demonstrates that reductive cleaning causes dissolution of foraminiferal calcite. There was some evidence that this dissolution preferentially corroded Mg-rich areas of test calcite. Chemical mapping techniques have illustrated that *N. dutertrei* and *P. obliquiloculata* have a low Mg outer crust [*Sadekov et al.*, 2005; *Kunioka et al.*, 2006]. SEM showed that the outer crust calcite of *N. dutertrei* and *P. obliquiloculata* was less corroded by reductive cleaning than the inner parts of the test (**Figures 7.2b, 7.2d, 7.3b, 7.3d**).

The effect on Mg/Ca of dissolution during cleaning is not predicted by dissolution at the seafloor. *N. dutertrei* and *P. obliquiloculata* from the Ontong Java Plateau show a similar sensitivity to the effect of natural dissolution on Mg/Ca (**Figure 7.4**). However, Mg/Ca of *N. dutertrei* was ~10% lower after reductive cleaning, while that of *P. obliquiloculata* was unaffected by cleaning method. It appears that fast dissolution during cleaning does not act in the same way as the complex processes taking place at the sea floor taking place over thousands of years. Tests can be corroded by reductive cleaning without this significantly affecting Mg/Ca.

In contrast to the suggestion of *Barker et al.* [2003b] outlined in the introduction, poorly preserved tests were not less sensitive to the decrease in Mg/Ca caused by reductive cleaning (**Figure 7.4**). This lack of preservation effect brings into question the mechanism which results in lower Mg/Ca after reductive cleaning. If Mg-rich calcite was most susceptible to dissolution during cleaning it is perhaps surprising that the offset in Mg/Ca between the two cleaning methods was insensitive to preservation state of the tests. Well-preserved tests have higher maximum Mg/Ca, hence higher reactivity, than poorly preserved tests where partial solution at the sea floor would mean that the most reactive, Mg-rich, areas have been removed.

Alternatively, lower Mg/Ca after "Cd cleaning" could be result from more effective cleaning. The main motivation for use of reductive cleaning is to remove metal oxides (**Figure 7.5**). Decreased Al/Ca after reductive cleaning in *G. ruber, G. sacculifer* and *N. dutertrei* in this study (**Figure 7.5**) is in agreement with work of *Boyle*, [1981] that "Cd cleaning" also removes sediment from tests more effectively than "Mg cleaning". It is possible that oxides are associated with other contaminants, and the removal of oxides releases coccoliths and other detritus adhering to tests.

"Mg cleaning" does not always clean tests adequately and can leave coccolith plates and detritus in test pores (**Figures 7.1a, 7.2c**). Better removal of contaminants would reduce the Mg contributed by marine clays.

G. sacculifer data would appear to contradict both of the suggested causes of decreased Mg/Ca after reductive cleaning. Corrosion of tests, and lower analytical yield, testify to dissolution during reductive cleaning. Tests are also cleaner after "Cd cleaning" (**Figures 7.1a, 7.1b**); yet mean Mg/Ca was not significantly lower in this species. However, mean Mg/Ca was decreased by reductive cleaning if only samples from above the calcite saturation horizon are considered. If dissolution is the main post-depositional control on Mg/Ca [*Lorens and Willia*, 1977; *Brown & Elderfield*, 1996; *Hastings et al.*, 1998; *Rosenthal et al.*, 2000; *Dekens et al.,* 2002, *Regenburg et al.*, 2006] then correlation between Mg/Ca and $\Delta[CO_3^{2-}]$ can be used as an indicator of reproducibility. "Cd

cleaning" gave stronger correlation between $\Delta[CO_3^{2-}]$ and Mg/Ca in "Cd cleaned"(r^2 = 0.79) than in "Mg cleaned" (r^2 = 0.69) *G. sacculifer*. More evidence that "Cd cleaning" gives a very consistent result was the strong similarity of regressions between $\Delta[CO_3^{2-}]$ and Mg/Ca for the "Cd cleaned" set of this study and the data of *Dekens et al*. [2002] (**Figure 7.4**) which was also cleaned using "Cd cleaning" method. Greater random variation in "Mg cleaned" samples seems more likely to indicate contamination than dissolution effects.

The decrease in Mg/Ca due to reductive cleaning may not be attributable exclusively to either dissolution or better cleaning. It is possible that although "Cd cleaning" does cause slight dissolution of foraminifera tests, which could, in some species, lead to loss of Mg, that at least some of the difference in Mg/Ca is due to the more effective removal of contaminants by "Cd cleaning".

7.4.2 Possible controls on dissolution susceptibility and cleaning efficiency

Susceptibility both to dissolution effect on Mg/Ca and to contamination may be controlled by characteristics of the test. Sensitivity to the reagents used in reductive cleaning may be influenced by intrinsic characteristics of the test calcite such as crystallinity or the arrangement of Mg within the crystal structure. Features of the test could also influence the amount and type of sediment contamination. *Barker et al*. [2003b] demonstrated that *G. bulloides*, with its porous texture and open form, was more prone to clay contamination than other species. In this study, the smooth surface of *P. obliquiloculata* (**Figure 7.3d**) was never seen to be contaminated with sediment, unlike the porous tests of *G. ruber*, *G. sacculifer* (**Figure 7.1**) and *N. dutertrei* (**Figure 7.2**). In contrast to the three species above, Al/Ca of *P. obliquiloculata* was similar for both cleaning methods (**Figure 7.5**) suggesting that there was little clay to be removed. As mentioned above, reductive cleaning did not decrease Mg/Ca in this species.

Other studies have also described distinct offsets in Mg/Ca for different species. *Barker et al*. [2003b] found large offsets (> 15%) for *G. ruber*, *Globorotalia hirsuta* and *Neogloboquadrina pachyderma*, with no offset for *G. sacculifer* or for the benthic species *Uvigerina peregrina*. *Martin and Lea* [2002] discovered that reductive cleaning made no difference to the Mg/Ca of (poorly preserved) *Uvigerina* species, but lead to a 10% decrease in the Mg/Ca of (well preserved) *Cibicidoides wuellerstorfi*. Like *P. obliquiloculata*, foraminifera of the *Uvigerina* genus have a smooth outer surface, although different species are ornamented to different extents. They also have a very small aperture which could mean less likelihood of clay becoming trapped within the test. However, offsets are not consistent between studies. *Yu et al*. [2007] found a 10%

decrease in Mg/Ca with "Cd cleaning" for three species of benthic foraminifera including *Uvigerina* species (also *C. wuellerstorfi* and *Cibicidoides kullenbergi*).

The decrease in Mg/Ca due to reductive cleaning is not, therefore, simply a function of species. Although reductive cleaning may tend to decrease Mg/Ca in some species (particularly those with small deep pores) more than others (the smooth species *P. obliquiloculata* and *Uvigerina*, but also the porous species *G. sacculifer*), there is also significant variation in the offset for one species between studies.

The average offset for *G. ruber* in this study is 4% (**Figures 7.4** and **7.5**). This is less than the 15% found by *Barker et al*. [2003b], or the correction factor of 15% suggested by *Rosenthal et al*. [2004]. *G. ruber* even from the shallowest sites on the Ontong Java Plateau appear slightly dissolved [*Johnstone et al*., in press (**Chapter 4**)]. We therefore cannot completely exclude the possibility that there is, in fact, a preservation effect on the decrease in Mg/Ca due to reductive cleaning in this species. In this case the offset of 10-15% found by other studies would be for well-preserved *G. ruber*, and the smaller offset found in this study would represent slightly dissolved *G. ruber*. However, there was no trend toward a smaller offset with increased calcite undersaturation in the Ontong Java Plateau data.

Alternatively, studies may give different offsets in Mg/Ca between cleaning methods because the offset is controlled by some quantity which can vary either spatially or temporally. If this were the case a universal, or even species specific, factor to correct Mg/Ca between methods would not apply. Both the intrinsic and the extrinsic characteristics which control the effect of reductive cleaning on Mg/Ca could change between locations or through time. Test characteristics such as arrangement of Mg may vary for foraminifera from different areas or for crypto-species. Organic layers within the test can also contain Mg [*Kunioka et al*., 2006]. Although the hydroxide rinse (oxidative cleaning) step should theoretically remove all organic matter, amino acids can survive in foraminifera tests for several million years despite degradation and bacterial activity at the sea floor [*King and Hare*, 1972]. Organic compounds may therefore be very robust, or occur as an integral part of the test calcite. Remnants of organic matter not removed during oxidative cleaning could potentially contribute Mg. If this were the case, the offset between cleaning method may vary with sample age.

The amount and character of sediment contamination can also vary. One reason that the offset between cleaning methods in this study is less than those of previous studies may be that these Pacific samples were not heavily contaminated. In this study "Mg cleaning" gave good results. Fe/Ca was never above the 0.1 mmol/mol value considered suggestive of contamination [*Barker et al*., 2003b]. Samples from other areas or from deeper in the

sediment column may be more heavily contaminated with detritus, or contain clay with a high Mg content. North Atlantic samples, for example, are notoriously difficult to clean as they tend to be highly contaminated both with clay and with silicate grains from ice rafted debris. The amount of Mg contained within ferromanganese coatings, although not a large source of contaminant Mg, also varies with sample history and location. The rigour with which cleaning is carried out may also differ. In this study the "silicate removal step" was carried out for all samples, and in some laboratory protocols this step is omitted. Additionally the "oxidative step" was carried out twice in the "Mg cleaning" method. Less rigorous "Mg cleaning", or more contaminated samples, could result in higher Mg/Ca due to contamination.

7.4.3 Analytical yield as a potential indicator of sample dissolution and bias of Mg/Ca derived temperatures

The decrease in Mg/Ca after "Cd cleaning" compared to "Mg cleaning" leads to calculated temperatures which are ~0.5^{o}C lower for *G. ruber* and *G. sacculifer* and ~1°C lower for *N. dutertrei.* These differences are small relative to the uncertainties on the calibrations used to convert Mg/Ca to temperature [*Barker et al*., 2003b]. While it is important to quantify such differences for future development of the temperature proxy, offsets in Mg/Ca due to cleaning method, and even differences in absolute temperatures between calibrations, are insignificant compared to the effects of sea floor dissolution. For instance, dissolution reduces calculated temperatures for *N. dutertrei* by ~9°C from the shallowest to deepest samples from the Ontong Java Plateau [*Johnstone et al*., subm. (**Chapter 5**)].

This study confirms anecdotal evidence that analytical yield tends to be lower for poorly preserved samples (**Figure 7.6**, **Table 7.3**). Maximum yield was around 60% so a significant part of the original sample was never analysed even in well-preserved samples cleaned by the gentlest ("Mg cleaning") method. Presumably part of the never-analysed fraction is clay, silicates and other contaminants. SEM showed that samples from below the calcite saturation horizon contained less detritus than those from shallower sites. They are also less likely to give high Al/Ca (Al/Ca > 30 μmol/mol) (**Table 7.2**). Most of the loss of material in poorly preserved samples therefore must be from the tests themselves. Samples from deep sites were noticeably more friable than well-preserved tests. They were easy to crush and formed small powdery fragments which remained on the surface of the cleaning solution and could potentially be discarded with the solution. Poorly preserved or small samples were probably treated more carefully than samples where tests appear more robust and this could alter the relationship between yield and dissolution. However, the strong distortion of Mg/Ca by dissolution, and the current lack

of methods to reliably indicate where tests are affected, means that any indication of preservation should be exploited.

In order to test this further, analytical yield of *G. ruber* and *G. sacculifer* was obtained for a core for which a record of calcite dissolution exists [*Johnstone et al.*, subm.(**Chapter 6**)] (**Figure 7.7**). Core WIND28K (51° 46.15' E, 10 ^{o} 09.23' S) [*McCave*, 2001] was retrieved from 4175 m water depth in the Indian Ocean. Analytical yield was obtained from previous analyses of Mg/Ca [*Kiefer et al.,* 2006; *Johnstone et al.*, subm. (**Chapter 6**)]. Currently the site of WIND28K is bathed in corrosive Circumpolar Deep Water and tests are poorly preserved throughout much of the core (**Figure 7.7**). Deglaciations are times of good calcite preservation in the Indian and Pacific Oceans [e.g. *Berger*, 1977] and this is reflected in the low values of dissolution index XDX over these intervals. Another episode of good preservation in WIND28K occurs between 150 and 270 cm.

Figure 7.7 shows that there is some similarity between the record of dissolution and that of analytical yield. Both *G. ruber* ("Mg cleaning" by TK) and *G. sacculifer* ("Mg cleaning" by HJ) show highest analytical yield during or close to the deglacial preservation events. *G. sacculifer* also has high yield values during the episode of good preservation in the middle of the core. This is not so clearly shown in the analytical yield record of *G. ruber,* possibly because the dissolution index was based on *G. sacculifer*. The similarity of the two records, particularly over the glacial terminations, where it is probable that preservation is good for both species, implies that yield is influenced by preservation state.

We suggest it may, therefore, be worth monitoring analytical yield as a first indicator of dissolution bias on Mg/Ca derived temperatures. While there is a great deal of variability between individual data points, a succession of low yields may warn of a dissolved section of core. Correlation between $\Delta[CO_3^{2-}]$ and analytical yield (**Table 7.3**) indicate that reductively cleaned *G. sacculifer* or *N. dutertrei* would be most suitable for this purpose.
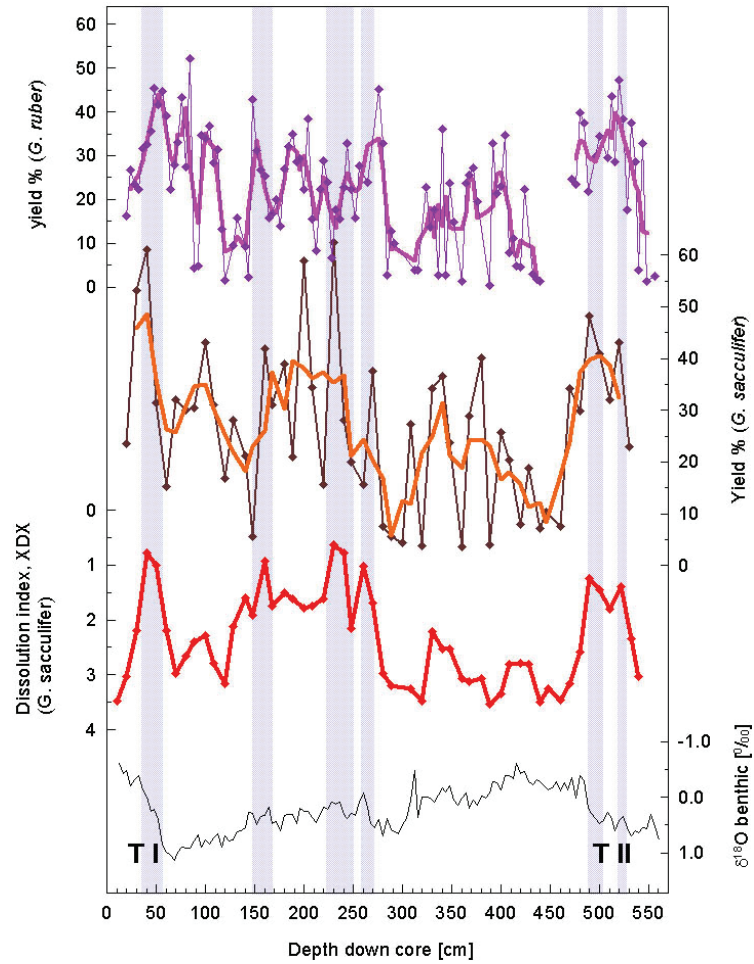
Figure 7.7. Analytical yield for two species of foraminifera from WIND28K, a core from deep (4157 m) in the Indian Ocean [51° 46.15′ E, 10 ° 09.23′ S]. Black line is δ18O of *C. wuellerstorfi* [*Kiefer et al.,* 2006]. Red line is dissolution index XDX [*Johnstone et al.,* subm. (**Chapter 6**)], indicating preservation state of *G. sacculifer* tests. Analytical yield of both *G. ruber* ("Mg cleaning" by TK; purple line, pink line is 3 point running average) and *G. sacculifer* ("Mg cleaning" by HJ; brown line, orange line is 3 point running average) is highest during the periods of enhanced preservation during the deglaciations.

7.5 Conclusions

(1) Preservation state of foraminifera tests does not control the offset in Mg/Ca between "Mg cleaned" and "Cd cleaned" samples. Regressions between $\Delta[CO_3^{2-}]$ and Mg/Ca did not trend towards a common Mg/Ca value. Nor did partially dissolved tests show a greater sensitivity to the effects of "Cd cleaning" than well-preserved ones.

Other findings of this study as to the effect of reductive cleaning are as follows. Reductive cleaning causes slight dissolution of foraminifera tests. Even tests which have already undergone dissolution at the sea floor showed further corrosion after reductive cleaning. "Cd cleaning" generally causes greater sample attrition than "Mg cleaning", resulting in lower analytical yield in *G. ruber, G. sacculifer* and *N. dutertrei* species. Natural dissolution at the sea floor selectively attacks Mg-rich areas of the tests of planktonic foraminifera and lowers Mg/Ca. Reductive cleaning also selectively corrodes Mg-rich areas. Mg/Ca was on average 4% lower for *G. ruber* and 10% lower for *N. dutertrei* after reductive cleaning. However, dissolution of tests during reductive cleaning is not necessarily related to lower Mg/Ca. Despite physical corrosion, focused on Mg-rich areas of the tests, average Mg/Ca of *G. sacculifer* and *P. obliquiloculata* was not significantly lower after reductive cleaning.

Although "Mg cleaning" is an adequate cleaning method if samples are not contaminated with a high Mg phase, reductive cleaning removes contaminants more effectively. SEM showed detritus in pores of *G. ruber*, *G. sacculifer* and *N. dutertrei* after "Mg cleaning". Reductively cleaned tests had clean, empty, pores. Elements indicative of contamination, Al/Ca, Fe/Ca and Mn/Ca, were lower after reductive cleaning in these three species. "Cd cleaning" is therefore recommended for species with large pores such as *G. ruber*, *G. sacculifer* and *N. dutertrei*.

Reductive cleaning may act to lower Mg/Ca both by slight dissolution of test calcite and by removal of clays which contain Mg. Susceptibility both to the effect of dissolution on Mg/Ca and to contamination can be controlled by intrinsic features of the test. Gross morphology affects the likelihood of sediment contamination of tests. Unlike species with large pores, *P. obliquiloculata*, which has a very smooth outer surface, did not have coccolith plates or sediment adhering to tests. Al/Ca was not decreased by reductive cleaning in this species, suggesting there was little clay contamination to be removed. If the decrease in Mg/Ca is controlled by extrinsic factors, such as amount or type of clay contamination, which can change through time, a universal, or species specific, correction factor between methods would not apply.

(2) Analytical yield has some correlation with preservation state of foraminifera tests. We suggest it may be worth monitoring this property during Mg/Ca analysis, as a first indication of dissolution bias on Mg/Ca.
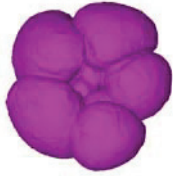
8. Summary and outlook

This Chapter outlines how the objectives (described in **Chapter 2**) were met, summarizes the main findings of the studies presented here and offers perspectives for future work.

8.1 Summary of results

8.1.1 Use of CT to assess dissolution in foraminifera tests, to reconstruct $\Delta[CO_3^{2-}]$ and to correct test mass and Mg/Ca for dissolution

The main focus of this thesis is to present a new way of assessing dissolution in the calcite tests of planktonic foraminifera. The technique of computed tomography reveals the structure of the inner test and thus offers an insight into the progress of dissolution through the test. Examination of the inner test in this way builds on previous studies presenting descriptions of how dissolution affects the outer surface of tests [*Bé et al.*, 1975; *Bonneau*, 1980].

(1) XDX, a $\Delta[CO_3^{2-}]$ proxy based on the appearance of foraminiferal tests in CT scans

(Chapter 4)

CT scans of *G. ruber*, *G. sacculifer*, *N. dutertrei* and *P. obliquiloculata* show that dissolution progresses in a predictable series of stages. These stages of form the basis of dissolution index XDX.

Dissolution stages could be related to $\Delta[CO_3^{2-}]$ of deep water. Above 20 µmol/kg tests were well preserved. Between 20 and 10 µmol/kg the first signs of dissolution were detectable in the inner calcite of the test. This is in agreement with earlier studies showing that tests start to dissolve above the calcite saturation horizon and that inner calcite is first affected [*Lohmann,* 1995; *Brown and Elderfield*, 1996]. Enhanced

vulnerability to dissolution of inner calcite can be explained both by kinetics, which predict surface area controls dissolution susceptibility [*Keir*, 1980], and the fact that inner calcite contains higher levels of trace metals such as Mg^{2+} [*Sadekov et al.*, 2005] which increase solubility.

Around the calcite saturation horizon ($\Delta[CO_3^{2-}]$ = 0 μmol/kg) the walls of the inner test appeared thickened and distorted in CT scans and SEM showed the pores to contain fine grained calcite and coccoliths. This detritus remains even after Mg-cleaning, although it is removed by Cd-cleaning, (**Chapter 7**) which suggests a role for metal oxides in adhering material to the test. Carbonate precipitation within the tests presumably also contributes. Precipitation of calcite within sediments is supported by the benthic chamber results of *Jahnke and Jahnke* [2004]. They found no flux of Ca^{2+} or alkalinity from the sea floor from sites around the calcite saturation horizon, despite mobilisation of calcite in the pore waters, signifying that mobilised calcite re-precipitated within the sediment.

In waters undersaturated with respect to calcite, material of the inner test continued to dissolve. Below -20 μmol/kg only the outer crust of dissolution resistant species remained.

An experiment where 10 volunteers graded a set of samples of various dissolution states found that most people could recognise the stages of dissolution in CT scans. Correlation between XDX and $\Delta[CO_3^{2-}]$ (r^2) above 0.6 for all four species illustrates the potential of the index to estimate $\Delta[CO_3^{2-}]$.

(2) XDX is largely independent of test mass and can be used to correct test mass for dissolution

(Chapter 4)

The strength of dissolution index XDX is that it provides a direct assessment of the dissolution state of a particular sample of foraminifera tests. This overcomes many of the problems associated with other indices of dissolution where environmental factors can bias the dissolution signal. For instance, temperature is a primary control on the foraminiferal assemblage preserved at the seafloor, on to which dissolution effects are superimposed [CLIMAP, 1981]. Dissolution proxies such as test fragmentation, and grain size distribution, are sensitive to physical processes and may be dependant on initial morphology; a shift towards robust species would reduce the likelihood of fragmentation.

Environmental controls on test mass also confound the dissolution signal. The potential of test mass as a proxy for such factors, particularly $[CO_3^{2-}]$ [*Barker and Elderfield*, 2002], or temperature [*Gonzales-Mora et al.*, 2008], emphasises the need for mass-

independent methods of assessing test preservation. In core top samples used here, mass loss from tests was similar between ocean basins and species at 0.33 (±0.18) µg per µmol/kg for *G. ruber* (average of all sites) to 0.55 (±0.14) µg per µmol/kg for *P. obliquiloculata* (average of all sites) (± is half of the 95% Confidence Interval). These values are in agreement with *Broecker and Clarke* [2001] who find a sensitivity of 0.30 (±0.05) µg per µmol/kg. Similar sensitivity of mass to $\Delta[CO_3^{2-}]$ for samples with different initial test mass supports use of $\Delta[CO_3^{2-}]$ proxies to correct dissolution biased test mass. Correlations (r^2) between XDX and mass lost to dissolution above 0.8 for *G. sacculifer*, *N. dutertrei* and *P. obliquiloculata* and 0.32 for *G. ruber* indicate that XDX can be used to estimate initial mass of partially dissolved tests, at least in some species.

(3) Sensitivity of Mg/Ca to dissolution can vary between ocean basins

(Chapter 5)

Use of $\Delta[CO_3^{2-}]$ proxies to correct dissolution bias in Mg/Ca require that the response of Mg/Ca to dissolution is constant. A sensitivity study found Mg/Ca of samples from Atlantic, Pacific and Indian Ocean sites showed similar response of Mg/Ca to dissolution for each species. *G. ruber* was more sensitive than the other species, losing 0.102 (±0.036) mmol per µmol/kg while sensitivity was similar for *G. sacculifer*, at 0.047 (±0.015), *N. dutertrei*, at 0.037 (±0.010) and 0.040 (±0.008) for *P. obliquiloculata* (values are averaged from Ontong Java Plateau, Ceara Rise and Indian Ocean sites). However, Mg/Ca of *N. dutertrei* from the Caribbean appeared more sensitive than *N. dutertrei* from other locations, illustrating that response can vary regionally.

(4) XDX provides an independent estimate of the effects of dissolution on Mg/Ca

(Chapter 5)

The relationship between XDX and ΔMg/Ca was approximately linear with correlation coefficient (r^2) of 0.40 for *G. ruber* and above 0.60 for *G. sacculifer*, *N. dutertrei* and *P. obliquiloculata*. Despite potential variations in the sensitivity of Mg/Ca to dissolution between sites, XDX provides a first estimate of dissolution bias of Mg/Ca.

The use of CT to assess dissolution of foraminiferal tests before Mg/Ca analysis has been applied in one further study [*Steinke et al.*, 2010]. The abstract is given in **Appendix B**. CT scans showed the Miocene samples examined to be extremely well preserved, giving credibility to analytical results.

(5) Reconstructed Δ[CO₃²⁻], dissolution-corrected test mass and dissolution-corrected Mg/Ca-derived temperatures for a sediment core spanning 150 ka from the Indian Ocean

(Chapter 6)

Records of $\Delta[CO_3^{2-}]$, dissolution corrected test mass (using calibrations established in **Chapter 4**) and dissolution corrected Mg/Ca based temperatures (calibrations in **Chapter 5**) applied to core WIND28K illustrate the utility of XDX.

$\Delta[CO_3^{2-}]$ derived from XDX indicated an increase of ~25 µmol/kg during Termination I and ~15 µmol/kg during Termination II in the deep Indian Ocean. Magnitude and timing of the shifts, centred on the deglacial transitions, are similar to those found by *Marchitto et al*. [2005] for the deep Pacific. The site of WIND28K was above the calcite saturation horizon during the latter part of MIS 3, whereas present values of $\Delta[CO_3^{2-}]$ are -11 µmol/kg at the site. This episode of good preservation is not found in the deep Pacific record of *Marchitto et al*. [2005].

The XDX-corrected Mg/Ca-derived temperature record did not show the post-Termination cooling seen in the original SST record [*Kiefer et al.,* 2006]. The dissolution-corrected temperature record is similar to published studies which indicate that MIS 3 was a cold episode in the monsoon dominated Indian Ocean [*Rostek et al*., 1993; *Bard et al*., 1997]. Good preservation during MIS 3 also meant that dissolution-corrected test mass record recorded the lightest tests during MIS 3.

8.1.2 Comparison of two cleaning methods for Mg/Ca analysis

(6) Analytical yield has potential as a proxy for dissolution

(Chapter 7)

Core-top samples from a depth transect on the OJP showed a weak positive correlation between calcite saturation and analytical yield. Correlation was strongest (r^2 above 0.5, p < 0.1) for *G. ruber* and *G. sacculifer* where Cd-cleaning rather than Mg-cleaning was used. This relationship was supported by records from sediment core WIND28K where highest yield was associated with the deglacial preservation events.

(7) Offset in Mg/Ca between Mg-cleaning and Cd-cleaning is species specific and does not depend on preservation state

(Chapter 7)

Comparison of the two commonly used cleaning methods, Mg-cleaning and the more aggressive Cd-cleaning method, found that a universal correction factor to convert Mg/Ca of Cd-cleaned samples to that of Mg-cleaned samples, such as the 15 % suggested by *Rosenthal et al.* [2004], may not be appropriate. Cd-cleaning resulted in lower Mg/Ca than Mg-cleaning for *G. ruber* (where Cd-cleaned samples were on average 4 % lower than Mg-cleaned samples) and *N. dutertrei* (where the decrease was 10 %), but there was no offset in Mg/Ca (averaged for all sample sites) for *G. sacculifer* and *P. obliquiloculata*.

Reductive cleaning is known to physically corrode samples [*Martin and Lea*, 2002] and it has been assumed that reductive cleaning lowers Mg/Ca due to dissolution effects. However, although scanning electron microscopy (SEM) showed reductive cleaning caused more etching and damage to the test surface than oxidative cleaning, the finding of no offset between the two methods in some species brings into question whether the decrease in Mg is really due to dissolution. It was apparent that the Cd-cleaning method resulted in more effective cleaning. SEM showed less sediment adhering to tests after Cd-cleaning. This finding was confirmed by lower levels of contaminant phases, such as clays (Fe and Al) and metal oxide coatings (Mn), in analysed samples. It is therefore possible that some of the decrease in Mg/Ca may be due to better cleaning.

8.2 Outlook

8.2.1 Future development of CT based method to assess dissolution in the tests of foraminifera

It is envisaged that the main potential of XDX is as a proxy for $\Delta[CO_3^{2-}]$. Such proxies are necessary to validate models which aim to reconstruct calcite saturation from theoretical considerations [*Royer et al.*, 2004; *Tyrell and Zeebe*, 2004]. Interesting future applications would be to reconstruct carbon system parameters of time periods when CO_2 was very different from the present day, such as the Miocene, and over large climate switches such as the Eocene - Oligocene transition. Such periods offer opportunities to investigate the workings of the interactions between the carbon and glacial cycles.

One step towards more complete understanding of $\Delta[CO_3^{2-}]$ proxies, is comparison of proxies based on dissolution, such as XDX, to other methods of calculating calcite saturation, for example trace metal methods described in the Introduction.

B/Ca of *Uvigerina* species in core WIND28K has recently been analysed at University of Cambridge. Preliminary results are similar between the two records [*H. Elderfield*, pers. com.]. Similarity between B/Ca and XDX at the WIND28K site is a strong endorsement of both $\Delta[CO_3^{2-}]$ proxies.

Initial results of U/Ca from WIND28K (Appendix A in **Chapter 6**), are less promising. There are similarities in the two records, but also significant differences which highlight the strong diagenetic effects remaining in the U/Ca record when tests are cleaned using only Mg-cleaning [*Barker et al.*, 2003b] rather than the more intensive Cd-cleaning method [*Boyle*, 1981; *Martin et al.*, 2002].

For future application of dissolution index XDX, the method would benefit from being more objective. A potential advantage of digitising images of foraminifera tests is the possibility of developing software algorithms to classify dissolution. One promising parameter is the greyscale colour value of the CT scans. Values become lighter as microporosity develops within the test calcite. However, the relationship between greyscale and preservation state is distorted by the complex processes of dissolution, whereby, rather than a continuous process involving gradual loss of material from the test, interaction with the sediment means that at some stages of test dissolution tests may acquire material.

Progress towards mechanising assessment of CT scans was made by *Jacobi and Kunst* [2006]. Their method relied on measuring the length of the internal walls of the scanned

test. Initial tests of the method gave good results. Correlation (r^2) between $\Delta[CO_3^{2-}]$ and the dissolution assessment of *Jacobi and Kunst* [2006] was 0.87 for *N. dutertrei* from the Ontong Java Plateau. This compares well with r^2 of 0.90 between $\Delta[CO_3^{2-}]$ and XDX for the same sample set. Although the method shows promise, the relationship between internal chamber walls and test thickness may be a feature sensitive to environmental factors. Further work is needed to test this method in different environmental settings. Probably more than one factor will need to be taken into account to reflect that dissolution happens in stages rather than a linear change in one parameter.

As well as potential as a $\Delta[CO_3^{2-}]$ proxy, XDX also has a role to play in assessing the distortion of Mg/Ca based temperature records, for example estimating the bias in such records due to preservation fluctuations during a glacial cycle [*Mix et al.*, 2006]. In order to improve estimates of Mg/Ca derived temperatures, potential temporal and spatial variations in sensitivity of Mg/Ca to dissolution must be constrained.

Another factor which needs to be more fully explored in order to assess the effects of dissolution on Mg/Ca is that of selective removal of specific fractions from a population. *Schiebel* [2002] and *Schiebel et al.* [2007] estimate that a large proportion of foraminiferal calcite (~19 %) dissolves in the 'twilight zone' in the top 1000 m of the ocean. Even in the relatively corrosive Pacific Ocean, water at 1000 m depth is supersaturated with respect to calcite by ~25 μmol/kg. *Schiebel* [2002] and *Schiebel et al.* [2007] attribute dissolution in such oversaturated conditions to low pH microenvironments, in part created by cytoplasm degradation. However, in the studies presented in this thesis, tests from shallow sites (> 25 μmol/kg) appear very well preserved, and no signs of dissolution were detected by CT or SEM examination.

Observations that thin walled species are preferentially lost from assemblages, and that thin walled individuals are first lost within species [*Bé et al.*, 1975; *Berger*, 1970] also support selective removal of particular fractions as a mechanism of dissolution. Such selective removal would shift population distribution and could alter test mass and Mg/Ca while leaving no trace of dissolution in the remaining sample.

A wider view of preservation state of samples may be needed to quantify these effects. Even different sizes of foraminifera tests can exhibit different dissolution histories [*de Villiers*, 2003] due to differential sensitivity. Determination of carbon budgets requires better quantification of calcite dissolution as a whole. Further work would compare dissolution effects on other species such as coccolithophores to foraminiferal dissolution.

8.2.2 Development of analytical yield as a measure of test preservation

Initial results showing correlation between analytical yield and dissolution, both in core-tops and in sediment core WIND28K indicates that there is potential in this method of dissolution assessment. The greater friability of partially dissolved samples probably controls the relationship. Fine powder separates from the larger fragments of test calcite and is lost during the cleaning process. Mechanisation of the Mg/Ca cleaning procedure would offer more consistent analytical yield, and could thus lead to further development of this method of dissolution assessment. Crush strength of the tests may also offer an insight to preservation state of samples.

8.2.3 Test mass as proxy for environmental conditions

An interesting finding from the dissolution-corrected test mass record of WIND28K was that tests mass reached a minimum during MIS 3 when SST was cool. This supports temperature as a control on foraminiferal mass [*Gonzalez-Mora et al*., 2008].

Better understanding of the factors controlling test mass may allow development of this property as a proxy for environmental conditions. Mass may be influenced by several parameters. Surface water $[CO_3^{2-}]$ for instance is thought to play a role [*Barker and Elderfield*, 2002]. Salinity may also be an important control for some species [*Gonzalez-Mora et al*., 2008].

The Indian Ocean during MIS 3 offers a good opportunity to isolate temperature effects on calcification as a large change in temperature is coupled with small changes in CO_2 (hence surface water $[CO_3^{2-}]$) and salinity. A test mass record from a shallow site near WIND28K in the Amirante Passage could verify the apparent link between SST and test mass.

Appendix B

East Asian summer monsoon weakening after 7.5 Ma: Evidence from combined planktonic foraminifera Mg/Ca and δ^{18}O (ODP Site 1146; northern South China Sea)

S. Steinke[1,2]**, J. Groeneveld**[1,3]**, H.J.H. Johnstone**[1]**, R. Rendle-Bühring**[1]

[1] MARUM – Center for Marine Environmental Sciences, University of Bremen, Leobener Straße, 28359 Bremen, Germany

[2] State Key Laboratory of Marine Geology, Tongji University, Shanghai, China

[3] Alfred Wegener Institute for Polar and Marine Research, Bremerhaven, Germany

Abstract

The monsoon system represents one of the basic elements of global atmospheric circulation. Its evolution and variability over long periods of geologic time play a significant role in our understanding of global climate. In this study, we focus on the late Miocene time interval from 10 Ma to 6 Ma, a period of postulated profound ecological and environmental shifts in east and south Asia. The combined approach of measuring planktonic foraminiferal Mg/Ca and stable oxygen isotopes from Ocean Drilling Program (ODP) Site 1146 enabled us to reconstruct temperature independent seawater δ^{18}O (a proxy for sea-surface salinity) variations in order to reconstruct the hydrography in the northern South China Sea (SCS). Located offshore the Pearl (Zhujiang) River, or its predecessor, the location of Site 1146 is considered as providing record most sensitive for detecting potential changes in freshwater input/river-run off as a result of changes in continental humidity/aridity, and hence changes in East Asian monsoon (EAM) climate. Local seawater δ^{18}O reconstructions reveal that the monsoon development during the late Miocene can be regarded as a gradual weakening in East Asian summer monsoon (EASM) intensity with accelerated weakening after 7.5 Ma. We suggest that an accelerated EASM weakening was most likely the driving force for decreasing aridity in east and south Asia at 8-6 Ma. This may have resulted in widespread ecosystem changes in east and south Asia since 8-6 Ma.

REFERENCES

Ahn, J., and E.J. Brook (2008), Atmospheric CO_2 and climate on millennial time scales during the last glacial period, *Science, 322*, 83; doi: 10.1126/science.1160832.

Ambrose, J., and G. Hounsfield (1972) Computerised transverse axial tomography , *British Journal Radiol., 46*, 148-149.

Ambrose, J., and G. Hounsfield (1973), Computerised transverse axial scanning (tomography). Part 2: Clinical applications, *British Journal Radiol., 46,* 1023-1047.

Anand, P., H. Elderfield and M. H. Conte (2003), Calibration of Mg/Ca thermometry in planktonic foraminifera from a sediment trap time series, *Paleoceanography, 18* (2), 1050, doi:10.1029/2002PA000846.

Anderson, D.M., and D. Archer (2002), Glacial-interglacial stability of ocean pH inferred from foraminifer dissolution rates, *Nature, 416*, 70-72.

Anderson, R.F, S. Ali, L.I. Bradtmiller, S.H.H. Nielsen, M.Q. Fleisher, B.E. Anderson and L.H Burckle (2009), Wind-driven upwelling the Southern Ocean and the deglacial rise in atmospheric CO_2, *Science, 323*, 5920, 1443-1448, doi: 10.1126/science.1167441.

Archer, D., (1996), A Data-Driven Model of the Global Calcite Lysocline, *Global Biogeochem. Cycles, 10* (3), 511–526.

Archer, D., A. Winguth, D. Lea and N. Mahowald (2000), What caused the glacial/interglacial pCO_2 cycles? *Rev. Geophys., 38*, 159-189.

Archer, D., and E. Maier-Raimer (1994), Effect of deep-sea sedimentary calcite preservation on atmospheric CO_2 concentration, *Nature, 367*, 260-263.

Archer, D.E., (1991), Equatorial Pacific Calcite Preservation Cycles: Production or Dissolution, *Paleoceanography, 6*, 561-571.

Armstrong, R.A., C. Lee, J.I. Hedges, S. Honjo and S. G. Wakeham (2002), A new, mechanistic model for organic carbon fluxes in the ocean based on the quantitative association of POC with ballast minerals, *Deep Sea Res. II 49,* 219-236, doi:10.1016/S0967-0645(01)00101-1

Arrhenius, G.O.S., (1952), Sediment cores from the East Pacific, *Rep. Swed. Deep-Sea Exped. 1947-1948, 5*, 1-202.

Arrhenius, S., (1896), On the influence of carbonic acid in the air upon the temperature of the ground, *Phil. Mag. (Series 5) 41*, 237-276.

Bard, E., F. Rostek and C. Sonzogni (1997), Interhemispheric synchrony of the last deglaciation inferred from alkenone palaeothermometry, *Nature, 385*, 707-710

Barker, S., and H. Elderfield (2002), Foraminiferal Calcification Response to Glacial Interglacial Changes in Atmospheric CO_2, *Science, 297,* 833-836, doi:10.1126/science.1072815.

Barker, S., J. A. Higgins and H. Elderfield (2003a), The future of the carbon cycle: review, calcification response, ballast and feedback on atmospheric CO_2, *Philos. Trans. R. Soc. Lond. Ser. A-Math. Phys. Eng. Sci., 361*, 1977-1999

Barker, S., M. Greaves and H. Elderfield (2003b), A study of cleaning procedures used for foraminiferal Mg/Ca paleothermometry, *Geochem. Geophy. Geosy., 4* (9), 8407, doi:10.1029/2003GC000559.

Barker, S., T. Kiefer, H., Elderfield (2004), Temporal changes in North Atlantic circulation constrained by planktonic foraminiferal shell weights. *Paleoceanography, 19,* PA3008, doi: 10.1029/2004PA001004.

Barker, S., W. Broecker, E. Clark and I. Hajdas (2007), Radiocarbon age offsets of foraminifera resulting from differential dissolution and fragmentation within the sedimentary bioturbated zone, *Paleoceanography, 22,* PA2205, doi:10.1029/2006PA001354.

Barrows, T., and S. Juggins (2005), Sea-surface temperatures around the Australian margin and Indian Ocean during the Last Glacial Maximum, *Quat. Sci. Rev., 24*, 1017–1047.

Bassinot, F. C., F. Levi, M. Melières, M. Ghelen and L. Labeyrie (2004), Crystallinity of foraminifer shells: a proxy to reconstruct past bottom water $[CO_3^{2-}]$ changes? *Geochem. Geophy. Geosy., 5*, Q08D10, doi: 10.1029/2003GC000668.

Bassinot, F.C., and H.J.H. Johnstone (in prep.), New evidence for the control of *Globigerinoides ruber* calcification by sea surface salinity/ TCO_2: Implications for paleoceanographic reconstructions.

Bassinot, F.C., L. Beaufort, E. Vincent, L.D. Labeyrie, F. Rostek, P.J. Müller, X. Quidelleur and Y. Lancelot (1994), Coarse fraction fluctuations in pelagic carbonate sediments from the tropical Indian Ocean: A 1500-kyr record of carbonate dissolution, *Paleoceanography, 9* (4), 579-600.

Baumann, K.-H., H. Meggers (1996), Paleoceanographical change in the Labrador Sea during the last 3.1 MY: evidence from calcareous plankton records. In: A. Moguilevsky and R. Whatley (Eds.), *Microfossils and Oceanic Environments*. Aberystwyth-Press, Aberystwyth, pp. 131 - 154.

Bé, A. W. H., (1980), Gametogenic calcification in a spinose planktonic foraminifer, *Globigerinoides sacculifer* (Brady), *Mar. Micropaleontol. 5*, 283–310.

Bé, A.W.H., J.W. Morse and S.M. Harrison (1975), Progressive dissolution and ultrastructural breakdown of planktonic foraminifera, *Dissolution of deep-sea carbonates, Special publication No. 13,* Cushman Foundation for Foraminiferal Research.

Bemis, B.E., H.J. Spero, J. Bijma and D.W. Lea (1998), Reevaluation of the oxygen isotopic composition of planktonic foraminifera, *Paleoceanography, 13*, 150-160.

Bender, M.L., R.B. Lorens and F.D. Williams (1975), Sodium, magnesium, and strontium in the tests of planktonic foraminifera. *Micropaleontology, 21,* 448-459.

Bentov, S., and J. Erez (2005), Novel observations on biomineralization processes in foraminifera and implications for Mg/Ca ratio in the shells, *Geology, 33,* 841-844.

Bentov, S., and J. Erez (2006), Impact of biomineralization processes on the Mg content of foraminiferal shells: A biological perspective. *Geochem. Geophy. Geosy., 7,* Q01P08, doi:10.1029/2005GC001015.

Berger, W.H., (1968), Planktonic foraminifera: Selective solution and paleoclimatic interpretation, *Deep Sea Res., 15*, 31-43.

Berger, W.H., (1970), Planktonic foraminifera: Selective solution and the lysocline. *Mar. Geol., 8*, 111-138.

Berger, W.H., (1971), Sedimentation of planktonic foraminifera. *Mar. Geol., 11,* 325-358.

Berger, W.H., (1977), Deep-sea carbonate and the late deglaciation preservation spike in pteropods and foraminifera, *Nature, 269*, 301-304.

Berger, W.H., M.-C. Bonneau, F.L. Parker (1982), Foraminifera on the deep-sea floor: Lysocline and dissolution rate. *Oceanol. Acta, 5*, 249-258.

Berner, R.A., (1977), Stoichiometric models for nutrient regeneration in anoxic sediments. *Limnol. Oceanogr. 22*, 781-786.

Berner, R.A., and J.W. Morse (1974), Dissolution kinetics of calcium carbonate in seawater: IV Theory of calcite dissolution, *American Journal of Science, 274*, 108-134.

Bijma, J., H. J. Spero and D. W. Lea (1999), Reassessing foraminiferal stable isotope geochemistry: Impact of the oceanic carbonate system (experimental results), in *Use of Proxies in Paleoceanography: Examples from the South Atlantic*, G. Fischer and G. Wefer (eds), pp. 489–512, Springer-Verlag, New York, 1999.

Black, E. (2005), The relationship between Indian Ocean sea surface temperature and East African rainfall, *Philos. Trans. R. Soc., Ser. A, 363*, 43–47.

Blunier, T., and E. J. Brook (2001), Timing of millennial-scale climate change in Antarctica and Greenland during the last glacial period, *Science, 291*, 109– 112.

Bonneau, M.-C., F. Mélières and C. Vergnaud-Grazzini (1980), Variations isotopiques (oxygène et carbone) et crystallographiques chez des espèces actuelles de foraminifères planctoniques en fonction de la profondeur de dépôt, *Bull. Soc. Geol. Fr. 22* (5), 791–793.

Bonneau, M-C., (1978), Dissolution expérimentale et naturelle des foraminifères planktoniques. Approche morphologiques, isotopiques et cristallographiques. [Thèse de 3ème cycle , Université de Paris VI, 231 pages. Unpublished thesis].

Boyle, E., (1981), Cadmium, zinc, copper and barium in foraminifera tests, *Geochim. Cosmochim. Acta, 47,* 1815–1819.

Braconnot, P., B. Otto-Bliesner, S. Harrison, S. Joussaume, J.-Y. Peterschmitt, A. Abe-Ouchi, M. Crucifix, E. Driesschaert, Th. Fichefet, C. D. Hewitt, M. Kageyama, A. Kitoh, A. Lainé, O. Marti, U. Merkel, G. Ramstein, P. Valdes, S. L. Weber, Y. Yu, and Y. Zhao (2007), Results of PMIP2 coupled simulations of the Mid-Holocene and Last Glacial Maximum - Part 1: experiments and large-scale features, *Climate of the Past, 3*, 261-277

Brady, H.B., (1877), Supplementary note on the foraminifera of the chalk (?) of the New Britain Group. *Geol. Mag., 2* (4), 534-546.

Broecker, W.S., and Clark, E., (2002), Glacial-to-Holocene Redistribution of Carbonate ion in the Deep Sea, *Science, 294*, 2152-2155

Broecker, W.S., and E. Clark (1999), CaCO$_3$ size distribution, a palaeocarbonate ion proxy? *Paleoceanography, 14*, 596-604.

Broecker, W.S., and E. Clark (2001), An evaluation of Lohmann's foraminifera weight dissolution index, *Paleoceanography, 16* (5) 531-534.

Broecker, W.S., and E. Clark (2002), Carbonate ion concentration in glacial-age deep waters of the Caribbean Sea. *Geochem. Geophys. Geosy., 3*, 10.1029/2001GC000231.

Broecker, W.S., and E. Clark (2003), Pseudo dissolution of marine calcite. *Earth Planet. Sci. Lett., 208*, 291-296.

Broecker, W.S., and E. Maier-Reimer (1992), The influence of air and sea exchange on the carbon isotope distribution in the sea, *Global Biogeochem. Cycles*, *63*, 315-320.

Broecker, W.S., and G.M. Henderson (1998), The sequence of events surrounding Termination II and their implications for the cause of glacial-interglacial CO2 changes, *Paleoceanography, 13*, 352-364.

Broecker, W.S., and T.-H. Peng (1982), *Tracers in the Sea*, Lamont-Doherty Earth Obs., Palisades, N.Y.

Broecker, W.S., and T.-H. Peng (1987), The role of $CaCO_3$ compensation in the glacial to interglacial atmospheric CO_2 change, *Global Biogeochem. Cycles, 1,* 15– 29.

Brown, S., and H. Elderfield (1996), Variations in Mg/Ca and Sr/Ca ratios of planktonic foraminifera caused by postdepositional dissolution – evidence of shallow Mg-dependent dissolution, *Paleoceanography, 11*, 543-551.

Caron, D.A., R.O. Anderson, J.L. Lindsey, J. Faber, W. Walter and E.E. Lin Lim (1990), Effects of gametogenesis on test structure and dissolution of some spinose planktonic foraminifera and implications for test preservation, *Mar. Micropaleontol.*, 16(1-2): 93-116.

Chave, K.E., (1954), Aspects of biochemistry of magnesium: 1. Calcareous marine organisms. *J. Geol., 62,* 266-283.

Cifelli, R., (1982), Textural Observations on Some Living Species of Planktonic Foraminifera, *Smithsonian Contributions to Paleobiology 45*, pp45.

Clemens, S., W. L. Prell, D. Murray, G. Shimmield, and G. Weedon (1991), Forcing mechanisms of the Indian Ocean Monsoon, *Nature, 353*, 720–725

CLIMAP Project Members (1981), Seasonal reconstruction of the Earth's surface at the last glacial maximum, *Geol. Soc. Am. Map Chart Ser. MC-36*, 1-18.

Cormack, A.M., (1963), Representation of a function by its line integrals, with some radiological applications, *J . Appl. Phys.,* 34, 2722.

Cormack, A.M., (1964), Representation of a function by its line integrals, with some radiological applications II, *J. Appl. Phys.,* 35, 2908.

Cormack, A.M., (1973), Reconstruction of Densities from their Projections, with Applications in Radiological Physics, *Phys. Med. Biol., 18*, 2, 195.

Cronblad H.G., and B.A. Malmgren (1981), Climatically controlled variation of Sr and Mg in Quaternary planktic foraminifera. *Nature, 291*, 61-64.

Crowley, T.J., (1983), Depth-dependent carbonate dissolution changes in the eastern North Atlantic during the last 170,000 years, *Mar. Geol., 54*, 25-31.

Curry, W.B., J.-C. Duplessey, L. Labeyrie and N.J. Shackleton (1988),Changes in the distribution of δ13C of deep water ΣCO2 between the last glaciation and the Holocene, *Paleoceanography, 3*, 317–341.

Curry, W.B., R.C. Thunell, S. Honjo (1983), Seasonal changes in the isotopic composition of planktonic foraminifera collected in Panama Basin sediment traps, *Earth Planet. Sci. Lett.*, 64 (1), 33–43.

D'Orbigny, A.D., (1839), Foraminifères; In: R. de la Sagra (ed.) *Histoire physique, politique et naturelle d l'Ile de Cuba, 8*, 1-224.

Darling, K.F., C.M. Wade and A.J. Leigh Brown (1996), Molecular phylogeny of the planktonic foraminifera. *J. Foram. Res., 26*, 324-259.

Darling, K.F., C.M. Wade, D. Kroon and A.J. Leigh Brown (1997), Planktonic foraminiferal molecular evolution and their polyphyletic origins from benthic taxa. *Mar. Micropaleontol., 30*, 251-266.

Darling, K.F., C.M. Wade, D. Kroon, A.J. Leigh Brown and J. Bijma (1999), The diversity and distribution of modern planktonic foraminiferal small subunit ribosomal RNA genotypes and their potential as tracers of present and past ocean circulations. *Paleoceanography, 14*, 3–12.

Darling, K.F., C.M. Wade, I.A. Steward, D. Kroon, R. Dingle and A.J. Leigh Brown (2000), Molecular evidence for genetic mixing of Arctic and Antartic subpolar populations of planktonic foraminifers. *Nature, 405*, 43-47.

Darling, K.F., M. Kucera, C.M. Wade, P. von Langen, D. Pak (2003), Seasonal ocurrence of genetic types of planktonic foraminiferal morphospecies in the Santa Barbara Channel. *Paleoceanography, 18*, 1032. doi:10.1029/2001PA000723.

de Vernal, A., G. Bilodeau, C. Hillaire-Marcel and N. Kassou (1992), Quantitative assessment of carbonate dissolution in marine sediments from foraminifer linings versus shell ratios. *Geology, 20*, 527-530.

de Villiers, S., (2004), Optimum growth conditions as opposed to calcite saturation as a control on the calcification rate and shell-weight of marine foraminifera, *Marine Biology, 144* (1), 45-49.

de Villiers, S., M. Greaves, and H. Elderfield, (2002), An intensity ratio calibration method for the accurate determination of Mg/Ca and Sr/Ca of marine carbonates by ICP-AES, *Geochem. Geophy. Geosy., 3*, doi:10.1029/2001GC000169.

Dekens, P.S., D.W. Lea, D.K. Pak, and H.J. Spero (2002), Core top calibration of Mg/Ca in tropical foraminifera: Refining paleotemperature estimation, *Geochem. Geophy. Geosy., 3* (4), 1022, doi:10.1029/2001GC000200.

Delaney, M.L., A.W.H Bé and E.A. Boyle (1985), Li, Sr, Mg, and Na in foraminiferal calcite shells from laboratory culture, sediment traps, and sediment cores. *Geochim.Cosmochim. Acta, 49,* 1327-1341.

Dittert, N. R., and R. Henrich (2000), Carbonate breakdown in the South Atlantic: evidence from ultrastructure breakdown in *G. bulloides*, *Deep Sea Res. 47*, 603-620.

Donoghue, P.C.J., S. Bengtson, X.-P. Dong, N.J. Gostling, T. Huldtgren, J.A. Cunningham, C. Yin, Z. Yue, F. Peng and M. Stampanoni (2006), Synchrotron X-ray tomographic microscopy of fossil embryos *Nature, 442*, 680-683, doi:10.1038/nature0489

Duckworth, D.L., (1977), Magnesium concentration in the tests of the planktic foraminifer *Globorotalia truncatulinoides*. *J. Foram. Res.,* 7, 304-312.

Dudley, W.C., P. Blackwelder, L. Brand, J.-C. Duplessy (1986), Stable isotopic composition of coccoliths. *Mar. Micropaleontol., 10*, 1-8.

Duplessy, J.-C., J.L. Blanc, A.W.H. Bé (1981), Oxygen-18 enrichment of planktonic foraminifera due to gametogenetic calcification below the euphotic zone, *Science, 213*, 1247-1250.

Duplessy, J.C., L. Labeyrie, A. Juillet-Leclerc, F. Maitre, J. Duprat and M. Sarnthein (1991), Surface salinity reconstruction of the North Atlantic Ocean during the Last Glacial Maximum, *Oceanol. Acta, 14* (4), 311-324.

Eggins, S., P. De Deckker and J. Marshall (2003), Mg/Ca variation in planktonic foraminifera tests: Implications for reconstructing palaeo-seawater temperature and habitat migration, *Earth Planet. Sci. Lett., 212,* 291–306.

Elderfield, H., and G. Ganssen (2000), Reconstruction of temperature and δ18O of surface ocean waters using Mg/Ca of planktonic foraminiferal calcite, *Nature, 405,* 442– 445.

Elderfield, H., C.J. Bertram and J. Erez (1996), A biomineralization model for the incorporation of trace elements into foraminiferal calcium carbonate, *Earth Planet. Sci. Lett. 142,* 409-423.

Elderfield, H., J. Yu, P. Anand, T. Kiefer and B. Nyland (2006), Calibrations for benthic foraminiferal Mg/Ca palaeothermometry and the carbonate ion hypothesis, *Earth Planet. Sci. Lett., 250*, 633– 649, doi:10.1016/j.epsl.2006.07.041.

Emeis K.-C., D.M. Anderson, H. Doose, D. Kroon and D. Schulz-Bull (1995), Sea-surface temperatures and the history of monsoon upwelling in the northwest Arabian Sea during the last 500,000 years, *Quaternary Research, 43*, 355-361.

Emerson, S., and M. Bender (1981), Carbon fluxes at the sediment water interface of the deep-sea: Calcium carbonate preservation, *J. Mar. Res., 39*, 139–162.

EPICA community members (2004), Eight glacial cycles from an Antarctic ice core, *Nature, 429*, 623–627.

Erez, J., (2003), The source of ions for biomineralization in foraminifera and their implications for paleoceanographic proxies, *Reviews in Mineralogy and Geochemistry, 54*, 115-149; doi:10.2113/0540115.

Farrell, J. W., and W. L. Prell (1989), Climatic change and $CaCO_3$ preservation: An 800,000 year bathymetric reconstruction from the central equatorial Pacific Ocean, *Paleoceanography, 4* (4), 447-466.

Farrell, J. W., W.L. Prell (1991), Pacific $CaCO_3$ preservation and $\delta^{18}O$ since 4 Ma: paleoceanic and paleoclimatic implications. *Paleoceanography, 6*, 485–498.

Faul, K.L., A.C. Ravelo M.L. Delaney (2000), Reconstructions of upwelling, productivity and photic zone depth in the eastern equatorial Pacific Ocean using planktonic foraminiferal stable isotopes and abundances, *J. Foram. Res., 30*, 110–125.

Fehrenbacher, J., P. A. Martin and G. Eshel (2006), Glacial deep water carbonate chemistry inferred from foraminiferal Mg/Ca: A case study from the western tropical Atlantic, *Geochem. Geophy. Geosy., 7*, Q09P16, doi:10.1029/2005GC001156.

Feldkamp, L.A., L.C. Davis and J.W. Kress (1984), Practical cone-beam algorithm, *Journal Opt. Soc. Am. (A), 1* (6), 612-619.

Ganssen, G. and M. Sarnthein (1983), Stable-isotopes compositions of foraminifers: The surface and bottom record of coastal upwelling. In: Suess, E. and Thiede, J. (Eds.), *Coastal upwelling: Its Sediment Record (Part A)*. Plenum Press, New York, pp. 99-121.

Garrels, R.M., M.E. Thompson and R. Seiver (1961), Control of carbonate solubility by carbonate complexes, *American Journal of Science, 259*, 24

Gehlen, M., F.C. Bassinot, L. Beck and H. Khodja (2004), Trace element cartography of *Globigerinoides ruber* shells using particle-induced X-ray emission. *Geochem. Geophys. Geosy., 5*, Q12D12, doi:10.1029/2004GC000822.

Ghosh, P., J. Adkins, H. Affek, B. Balta, W. Guo, E. A. Schauble, D. Schrag and J.M. Eiler (2006), ^{13}C - ^{18}O bonds in carbonate minerals: a new kind of paleothermometer, *Geochim. Cosmochim. Acta, 70*, 1439-1456.

Gillooly JF, et al (2002), Effects of size and temperature on developmental time, *Nature, 417,* 70-73

Gonzalez-Mora, B., F.J. Sierro, J.A. Flores (2008), Controls of shell calcification in planktonic foraminifers, *Quat. Sci. Rev., 27*, 956–961.

Gordon, A. L. (2005), Oceanography of the Indonesian seas and their throughflow, *Oceanography, 18*, 14– 26.

Greaves, M., et al. (2008), Interlaboratory comparison study of calibration standards for foraminiferal Mg/Ca thermometry, *Geochem. Geophy. Geosy., 9,* Q08010, doi:10.1029/2008GC001974

Hales, B., and S. Emerson (1997), Calcite dissolution in sediments of the Ceara Rise: In Situ measurements of porewater O_2, pH, and CO_2 (aq). *Geochim. Cosmochim. Acta, 61* (3), 501-514.

Hastings, D. W., A. D. Russell and S. R. Emerson (1998), Foraminiferal magnesium in *Globeriginoides sacculifer* as a paleotemperature proxy, *Paleoceanography, 13,* 161–169.

Hebbeln, D., G. Wefer and W.H. Berger (1990), Pleistocene dissolution fluctuations from apparent depth of deposition in Core ERDC-127P, West-Equatorial Pacific, *Mar. Geol., 92*, 165-176.

Hecht, A.D., E.V. Eslinger and L.B Garmon (1975), Experimental studies on the dissolution of planktonic foraminifera. In: W.V. Sitter, A.W.H. Bé and W.H. Berger (Eds.), *Dissolution of Deep-sea Carbonates*. Cushman Foundation for Foraminiferal Research, 59-69.

Hemleben, C., M. Spindler and O.R. Anderson (1989), *Modern Planktonic Foraminifera,* Springer Verlag, New York, 363 pp.

Henrich, R., (1989), Glacial-interglacial cycles in the Norwegian Sea: Sedimentology, paleoceanography and evolution of late Pliocene to quarternary Northern hemisphere climate. In: O. Eldholm (ed.) *Proceedings of ODP, Sci. Res. 104*, ODP, College Station, TX, 189-232.

Herron-Allen, E., (1915), Contributions to the study of the bionomics and reproductive processes of the foraminifera. *Philos. T. R. Soc. Lon. B, 206*, 227-279, doi: 10.1098/rstb.1915.0005.

Hodell, D.A., C.D. Charles and F.J. Sierro (2001), Late Pleistocene evolution of the ocean's carbonate system, *Earth Planet. Sci. Lett., 192*, 109-124.

Hönisch, B., and N.G. Hemming (2005), Surface ocean pH response to variations in pCO_2 through two full glacial cycles, *Earth Planet. Sci. Lett., 236*, 1-2, 305-314, DOI 10.1016/j.epsl.2005.04.027.

Hounsfield, G.N., (1973), Computerised Transverse Axial Scanning (Tomography). Part 1: Description of System, *British Journal Radiol., 46*, 1016-1022.

Howard, W.R. and W.L Prell (1994), Late Quaternary CaCO3 production and preservation in the Southern Ocean: Implications for oceanic and atmospheric carbon cycling, *Paleoceanography, 9* (3), 453-482.

Imbrie, J., J. D. Hays, D. G. Martinson, A. McIntyre, A. C. Mix, J. J. Morley, N. G. Paces, W. L. Prell, and N. J. Shackleton (1984), The orbital theory of Pleistocene climate: support from a revised chronology of the marine δ18O record. In Berger, A.L., J. Imbrie, J. Hays, G. Kukla, B. Saltzman (eds) *Milankovitch and climate*, Reidel, Dordrecht, pp 269–305.

Izuka, S.K., (1988), Relationship of magnesium and other minor elements in tests of *Cassidulina subglobosa* and *C. oriangulata* to physical oceanic properties. *J. Foram.Res., 18,* 151-157.

Jacobi, J., and O. Kunst, (2006), Löesungsindex der Foraminiferen [unpublished thesis, University of Bremen]

Jacot des Combes, H., Tribovillard, N.P., Caulet, J.P., (1999), Paleoproductivity and paleoceanographic changes in the Amirante Passage area (Equatorial Indian Ocean): a 200 kyr interval of lower pelagic productivity, *Bull. Soc. geol. France, 170* (6) 899-914

Jahnke, R.A., and D.B. Jahnke (2004), Calcium carbonate dissolution in deep sea sediments: Reconciling microelectrode, porewater and benthic flux chamber results, *Geochim. Cosmochim. Acta, 68* (1), 47–59.

Jahnke, R.A., D.B. Craven and J.-F. Gaillard (1994), Influence of organic matter diagenesis on $CaCO_3$, *Geochim. Cosmochim. Acta, 58* (13) 2700-2809.

Johnstone H.J.H, M. Schulz , J. Yu, H. Elderfield (subm.), Calibrating computed tomography based dissolution index XDX to dissolution bias of Mg/Ca in planktic foraminifera

Johnstone H.J.H., M. Schulz, J.Yu, H. Elderfield (in press: *Mar. Micropaleontol.*), Inside story: An X-ray microtomography method for assessing dissolution in foraminifera tests.

Jones, J.I., (1967), Significance of distribution ofplanktonic foraminifera in the Equatorial Atlantic Undercurrent, *Micropaleontology, 13*, 489-501.

Katz, A., (1973), The interaction of magnesium with calcite during crystal growth at 25-90 ºC and one atmosphere, *Geochim. Cosmochim. Acta, 37,* 1563-1586.

Keir, R.S., (1980), The dissolution kinetics of biogenic calcium carbonates in seawater *Geochim. Cosmochim. Acta, 44*, 241-255.

Keir, R.S., (1988), On the late Pleistocene ocean geochemistry and circulation, *Paleoceanography, 3*, 413–44

Key, R. M., A. Kozyr, C. L. Sabine, K. Lee, R. Wanninkhof, J. L. Bullister, R. A. Feely, F. J. Millero, C. Mordy, and T.-H. Peng (2004), A global ocean carbon climatology: Results from Global Data Analysis Project (GLODAP), *Global Biogeochem. Cycles, 18*, GB4031, doi:10.1029/2004GB002247.

Kiefer, T., and M. Kienast (2005), Patterns of deglacial warming in the Pacific Ocean: a review with emphasis on the time intervalof Heinrich event 1, *Quat. Sci. Rev., 24*, 1063–1081.

Kiefer, T., I.N. McCave and H. Elderfield (2006), Antarctic control on tropical Indian Ocean sea surface temperature and hydrography, *Geophys. Res. Lett., 33*, L24612, doi:10.1029/2006GL027097.

King, K. and P. E. Hare (1972), Amino acid composition of the test as a taxonomic character for living and fossil planktonic foraminifera, *Micropaleontology 18* (3), 285-293.

Kisakürek, B., A. Eisenhauer, F. Böhm, D. Garbe-Schönberg and J. Erez (2008), Controls on shell Mg/Ca and Sr/Ca in cultured planktonic foraminiferan, *Globigerinoides ruber* (white), *Earth Planet. Sci. Lett.*, *273,* 260–269.

Kloecker, R., T. S. Ivanochko, G.-J. Brummer, S.J.A. Jung, G. Ganssen, D. Kroon, R. S. Ganeshram, R. Henrich (2007), Variation in production, input and preservation of metastable calcium carbonate off Somalia during the last 90,000 years, *Quat. Sci. Rev., 26*, 2674–2683.

Krinsley, D., (1960), Trace elements in the tests of planktic foraminifera, *Micropaleontology, 63,* 297-300.

Kroon, D., and G. Ganssen (1988), The planktic $\delta^{13}C$ record, upwelling and climate. In: G.-J.A. Brummer and D. Kroon (Eds.), *Planktonic foraminifera as Tracers of Ocean-Climate History*. Free University Press, Amsterdam, pp. 335-346.

Ku, T.-L., and T. Oba (1978), A method of quantitative evaluation of calcite dissolution in deep sea sediments and its application to paleoceanographic reconstruction, *Quat. Res., 10,* 112–129.

Kunioka, D., K. Shirai, N. Takahata, Y. Sano, T. Toyofuku, and Y. Ujiie (2006), Microdistribution of Mg/Ca, Sr/Ca, and Ba/Ca ratios in *Pulleniatina obliquiloculata* test by using a NanoSIMS: Implication for the vital effect mechanism, *Geochem. Geophy. Geosy., 7,* Q12P20, doi:10.1029/2006GC001280.

Kwak, S.-Y., E. DiMasi, Y.-J. Han, J. Aizenberg and I. Kuzmenko (2005), Orientation and Mg Incorporation of Calcite Grown on Functionalized Self-Assembled Monolayers: A Synchrotron X-ray Study, *Crystal Growth & Design, 5* (6) 2139-2145.

Langer, M., (2008), Assessing the Contribution of Foraminiferan Protists to Global Ocean Carbonate Production. *J. Eukaryot. Microbiol., 55*, 163-169.

Le, J., and N.J. Shackleton (1992), Carbonate dissolution fluctuations in the western equatorial pacific during the late Quaternary, *Paleoceanography, 7*, 21-42.

Lea, D.W., D.K. Pak, C.L. Belanger, H.J. Spero, M.A. Hall, N.J. Shackleton (2006), Paleoclimate history of Galapagos surface waters over the last 135,000 years, *Quat. Sci. Rev., 25*.

Lea, D.W., D.K. Pak, H.J. Spero (2000), Climate Impact of Late Quaternary Equatorial Pacific Sea Surface Temperature Variations, *Science, 289*, 1719.

Lea, D.W., T.A. Mashiotta and H.J. Spero (1999), Controls on magnesium and strontium uptake in planktonic foraminifera determined by live culturing, *Geochem. Cosmochim. Acta., 63*, 2369–2379.

LeGrande, A. N., and G. A. Schmidt (2006), Global gridded data set of the oxygen isotopic composition in seawater, *Geophys. Res. Lett., 33,* L12604, doi:10.1029/2006GL026011.

Leuschner, D. C., and F. Sirocko (2000), The low-latitude monsoon climate during Dansgaard-Oeschger cycles and Heinrich Events, *Quat. Sci. Rev., 19,* 243–254.

Locarnini, R. A., A. V. Mishonov, J. I. Antonov, T. P. Boyer, and H. E. Garcia, (2006), *World Ocean Atlas 2005, Volume 1: Temperature. S. Levitus*, Ed. NOAA Atlas NESDIS 61, U.S. Government Printing Office, Washington, D.C., 182 pp.

Lohmann, G.P., (1995), A model for variation in the chemistry of planktonic foraminifera due to secondary calcification and selective dissolution, *Paleoceanography, 10* (3), 445-458, doi:10.1029/95PA00059.

Lorens, R.B., and D.F. Willia (1977), The Early Nonstructural Chemical Diagenesis of Foraminiferal Calcite, *Journal of Sedimentary Research, 47,* DOI: 10.1306/212F73C9-2B24-11D7-8648000102C1865D.

Lüttge, A., and P.G. Conrad (2004), Direct Observation of Microbial Inhibition of Calcite Dissolution, *Applied and Environmental Microbiology, 70,* 3, 1627-1632.

Marchitto, T.M., J. Lynch-Stieglitz and S. R. Hemming (2005), Deep Pacific $CaCO_3$ compensation and glacial–interglacial atmospheric CO_2, *Earth Planet. Sci. Lett., 231,* 317–336.

Marchitto, T.M., W.B. Curry and D.W. Oppo (2000), Zinc concentrations in benthic foraminifera reflect seawater chemis*try, Paleoceanography, 15,* 299–306.

Martin, P.A., and D.W. Lea (2002), A simple evaluation of cleaning procedures on fossil benthic foraminiferal Mg/Ca, *Geochem. Geophy. Geosy., 3* (10), 8401, doi:10.1029/2001GC000280, 2002.

Martin, P.A., D.W. Lea, Y.Rosenthal, N.J. Shackleton, M. Sarnthein and T. Papenfuss (2002), Quaternary deep sea temperature histories derived from benthic foraminiferal Mg/Ca, *Earth Planet. Sci. Lett., 198,* 193-209.

Martin, W.R., and F.L. Sayles (1996), $CaCO_3$ dissolution in sediments of the Ceara Rise, western equatorial Atlantic, *Geochim. Cosmochim. Acta, 60,* 7, 233-263.

Martinson, D. G., N. G. Pisias, J. D. Hays, J. Imbrie, T. C. Moore and N. J. Shackleton (1987), Age dating and the orbital theory of the ice ages: development of a high-resolution 0 to 300 000-year chronostratigraphy. *Quat. Res., 27,* 1–29.

Mashiotta, T.A., D.W. Lea and H.J. Spero (1999), Glacial-interglacial changes in subantarctic sea surface temperature and δ^{18}O-water using foraminiferal Mg, *Earth Planet. Sci. Lett., 170*, 417–432.

McCave, I. N. (2001), *RRS Charles Darwin cruise 129*. Report. Department of Earth Science, University of Cambridge, UK.

McCave, I.N, T. Kiefer, D.R. Thornalley, H. Elderfield (2005), Deep flow in the Madagascar-Marscarene Basin over the last 150,000 years, *Phil. Trans. R. Soc., 363*, 81-99.

McCorkle, D.C., P.A. Martin, D.W. Lea and G.P. Klinkhammer (1995), Evidence of a dissolution effect on benthic foraminiferal shell chemistry: δ^{13}C, Cd/Ca, Ba/Ca, and Sr/Ca results from the Ontong Java Plateau, *Paleocenography, 10*, 699-714.

Mekik, F., and R. Francois (2006), Tracing deep-sea calcite dissolution: agreement between the *Globorotalia menardii* fragmentation index and elemental ratios (Mg/Ca and Mg/Sr) in planktonic foraminifers. *Paleoceanography, 21,* PA4219, doi:10.1029/2006PA001296.

Merkel, U., M. Prange and M. Schulz (2010), ENSO variability and teleconnections during glacial climates, *Quat. Sci. Rev., 29,* 86-100

Metzler, C.V., C.R. Wenkam and W.H. Berger (1982), Dissolution of foraminifera in the eastern equatorial Pacific: an in-situ experiment, *J. Foram. Res., 12*, 362-368.

Milankovich, M., (1930), Mathematische Klimalehre und atsronomische Theorie der Klimaschwankungen. In: W. Köppen and R. Geiger (Eds.) *Handbuch der Klimatologie, 1*, Gebrüder Bornträger, Berlin, pp. 1–176.

Milliman, J.D., P.J. Troy, W.M. Balch, A.K. Adams, Y.-H. Li and F.T. Mackenzie (1999), Biologically mediated dissolution of calcium carbonate above the chemical lysocline? *Deep Sea Res. I, 46*, 1653-1669.

Mix, A., (2006), Running hot and cold in the eastern equatorial Pacific, *Quat. Sci. Rev., 25,* 1147–1149.

Morse, J.W., and R.A. Berner (1972): Dissolution kinetics of calcium carbonate in seawater. II, A kinetic origin for the lysocline, *American Journal of Science, 272*, 840-851

Morse, J.W., and S. He (1972), Influences of T, S and pCO$_2$ on the pseudo-homogeneous precipitation of CaCO$_3$ from seawater : implications for whiting formation, *Marine Chemistry, 41*, 291–298.

Mortlock, R.A., C.D. Charles, P.N. Froelich, M.A. Zibello, J. Salzmann, J.D. Hayes and L.H. Burckle (1991), Evidence for lower productivity in the Antarctic Ocean during the last glaciation, *Nature, 351*, 220-223.

Moy, A.D., W.R. Howard, S.G. Bray and T.W. Trull (2009), Reduced calcification in modern Southern Ocean planktonic foraminifera, *Nature Geoscience, 2*, 276 – 280, doi: 10.1038/ngeo460.

Mucci, A., (1987), Influence of temperature on the composition of magnesian calcite overgrowths precipitated from seawater. *Geochim. Cosmochim. Acta, 51,* 1977-1984.

Mudelsee, M., (2001), The phase relations among atmospheric CO$_2$ content, temperature and global ice volume over the past 420 ka, *Quat. Sci. Rev., 20,* 583-589

Mulitza, S., D. Boltovskoy, B. Donner, H. Meggers, A. Paul, G. Wefer (2003), Temperature: δ^{18}O relationships of planktonic foraminifera collected from surface waters, *Palaeogeography, Palaeoclimatology, Palaeoecology, 202,* 143-152.

Murray, J., (1897), On the distribution of the pelagic Foraminifera at the surface and on the floor of the ocean, *Natl. Sci., 11* (65), 17-27.

Naidu, P. D., and B. A. Malmgren (2005), Seasonal sea surface temperature contrast between the Holocene and last glacial period in the western Arabian Sea (Ocean Drilling Project Site 723A): Modulated by monsoon upwelling, *Paleoceanography, 20*, PA1004, doi:10.1029/2004PA001078

Nathan, S.A., and R.M. Leckie (2009), Early history of the Western Pacific Warm Pool during the middle to late Miocene (~13.2–5.8 Ma): Role of sea-level change and implications for equatorial circulation, *Palaeogeography, Palaeoclimatology, Palaeoecology, 274*, 140–159.

Nouet, J., and F. Bassinot (2007), Dissolution effects on the crystallography and Mg/Ca content of planktonic foraminifera *Globorotalia tumida (Rotaliina)* revealed by X-ray diffractometry, *Geochem. Geophy. Geosy., 8*, Q10007, doi:10.1029/2007GC001647.

Nürnberg, D., (1995), Magnesium in tests of *Neogloboquadrina pachyderma* sinistral from high northern and southern latitudes, *J. Foraminiferal Res., 25*, 350– 368.

Nürnberg, D., J. Bijma and C. Hemleben (1996), Assessing the reliability of Mg in foraminiferal calcite as a proxy for water mass temperatures, *Geochim. Cosmochim. Acta, 60*, 803-814.

Oba, T., (1969), Biostratigraphy and isotopic paleo-temperature of some deep sea cores from the Indian Ocean, *Second Ser. Sci. Rep., 41*, 129– 195, Tohoku Univ., Sendai, Japan.

Oldenborgh, G.J. van, S.S. Drijfhout, A. van Ulden, R. Haarsma, A. Sterl, C. Severijns, W. Hazeleger and H. Dijkstra (2009), Western Europe is warming much faster than expected, *Climate of the Past, 5,* 1, 1-12.

Parker, F.L., (1962), Planktonic foraminiferal species in Pacific sediments, *Micropaleontology,8* (2), 219-254.

Parker, F.L., and W.H. Berger (1971), Faunal solution patterns of planktonic foraminifera in surface sediments of the South Pacific. *Deep-Sea Res., 8,* 73-107.

Parker, W.K., and T.R. Jones (1865), On some foraminifera from the North Atlantic and Arctic Oceans, including Davis Straits, Baffin's Bay. *Phil. Trans., 155*, 325-441.

Passow, U., and C.L. de la Rocha (2006), Accumulation of mineral ballast on organic aggregates, *Global Biogeochem. Cycles, 20*, GB1013, doi:10.1029/2005GB002579.

Peacock, S., E. Lane and J.M. Restrepo (2006), A possible sequence of events for the generalized glacial-interglacial cycle, *Global Biogeochem. Cycles, 20*, GB2010, doi:1029/2005GB002448.

Pearson, P.N., P.W. Ditchfield, J. Singano, K.G. Harcourt-Brown, C.J. Nicholas, R.K. Olsson, N.J. Shackleton and M.A. Hall (2001), Warm tropical sea surface temperatures in the Late Cretaceous and Eocene epochs, *Nature, 413*, 481-487, doi:10.1038/35097000

Pelletier, G., E. Lewis and D. Wallace (2005), *A calculator for the CO_2 system in seawater for Microsoft Excel/VBA*, Washington State Department of Ecology, Olympia, WA, Brookhaven National Laboratory, Upton, NY.

Peterson, L.C., and W.L. Prell (1985), Carbonate dissolution in recent sediments of the Eastern Equatorial Indian Ocean: Preservation patterns and carbonate loss above the lysocline, *Mar. Geol., 64*, 259-290.

Peterson, M.N.A., (1966), Calcite: rates of dissolution in a vertical profile in the central Pacific, *Science, 153*, 3756, 1542-1544.

Petit, J. R., J. Jouzel, D. Raynaud, N. I. Barkov, J.-M. Barnola, I. Basile, M. Bender, J. Chappellaz, M. Davis, G. Delaygue, M. Delmotte, V. M. Kotlyakov, M. Legrand, V. Y. Lipenkov, C. Lorius, L. Pépin, C. Ritz, E. Saltzman and M. Stievenard (1999), Climate and atmospheric history of the past 420,000 years from the Vostok ice core, Antarctica, *Nature, 399*, 429-436, doi:10.1038/20859.

Pilson, M.E.Q., (1998), *An introduction to the chemistry of the sea*, Prentice Hall, New Jersey, 431pp.

Prahl, F.G., A.C. Mix, M.A. Sparrow (2006), Alkenone paleothermometry: biological lessons from marine sediment records off western South America. *Geochim. Cosmochim. Acta,* 70, 101–117.

Puechmaille, C., (1985), Teneurs en strontium et magnésium dans les tests de foraminifères planctoniques - Premiers indices de l'altération post-mortem. *Bull. Inst. Geol. Bassin d'Aquitaine,* 38, 81-94.

Radon, J., (1917), "Über die Bestimmung von Funktionen durch Ihre Integralwerte längs gewisser Mannigfaltigkeiten", *Berichte über die Verhandlungen der Sächsische Akademie der Wissenschaften (Reports on the proceedings of the Saxony Academy of Science), 69,* 262-277. *Translation:* Radon, J.; Parks, P.C. (translator) (1986), "On the determination of functions from their integral values along certain manifolds", *IEEE Transactions on Medical Imaging, 5,* 170-176, doi:10.1109/TMI.1986.4307775.

Raitzsch, M., E.C. Hathorne, H. Kuhnert, J. Groeneveld and T. Bickert (in prep.), B/Ca and U/Ca in benthic foraminifers: New proxies for the seawater carbonate system.

Raitzsch, M., H. Kuhnert, J. Groeneveld and T. Bickert (2008), Benthic foraminifer Mg/Ca anomalies in South Atlantic core top sediments and their implications for paleothermometry, *Geochem. Geophy. Geosy., 9* (5), Q0510, doi:10.1029/2007GC001788.

Rasaband, W.S., *ImageJ,* U. S. National Institutes of Health, Bethesda, Maryland, USA, http://rsb.info.nih.gov/ij/, 1997-2007.

Ravelo, A. C., and R. G. Fairbanks (1992), Oxygen isotopic composition of multiple species of planktonic foraminifera: Recorders of the modern photic zone temperature gradient, *Paleoceanography, 7* (6), 815–831.

Rayner, N. A.; Parker, D. E.; Horton, E. B.; Folland, C. K.; Alexander, L. V.; Rowell, D. P.; Kent, E. C.; Kaplan, A. (2003) Global analyses of sea surface temperature, sea ice, and night marine air temperature since the late nineteenth century *J. Geophys. Res., 108* (D14), 4407, doi:10.1029/2002JD002670

Regenberg, M., D. Nürnberg, S. Steph, J. Groeneveld, D. Garbe-Schönberg, R. Tiedemann and W.-C. Dullo (2006), Assessing the effect of dissolution on planktonic foraminiferal Mg/Ca ratios: Evidence from Caribbean core tops, *Geochem. Geophy. Geosy., 7, Q07P15, doi:10.1029/2005GC001019.*

Rosenthal, Y., and E.A. Boyle (1993), Factors controlling the fluoride content of planktonic foraminifera: An evaluation of its paleoceanographic applicability. *Geochim. Cosmochim. Acta, 57,* 335-346.

Rosenthal, Y., and G.P. Lohmann (2002), Accurate estimation of sea surface temperatures using dissolution corrected calibrations for Mg/Ca paleothermometry, *Paleoceanography, 17* (3), 1044, doi:10.1029/2001PA000749.

Rosenthal, Y., E.A. Boyle and N. Slowey (1997), Environmental controls on the incorporation of Mg, Sr, F and Cd into benthic foraminifera shells from Little Bahama Bank: Prospects for thermocline paleoceanography, *Geochim. Cosmochim. Acta, 61,* 3633– 3643.

Rosenthal, Y., et al. (2004), Interlaboratory comparison study of Mg/Ca and Sr/Ca measurements in planktonic foraminifera for paleoceanographic research, *Geochem. Geophy. Geosy., 5,* Q04D09, doi:10.1029/2003GC000650.

Rosenthal, Y., G.P. Lohmann, K.C. Lohmann and R.M. Sherrell (2000), Incorporation and preservation of Mg in *Globigerinoides sacculifer*: Implications for reconstructing the temperature and ^{18}O /^{16}O of seawater, *Paleoceanography, 15* (1), 135.

Rostek, F., G. Ruhland, F.C. Bassinot, P.J. Mueller, L.D. Labeyrie, Y. Lancelot and E. Bard (1993), Reconstructing sea surface temperature and salinity using $\delta^{18}O$ and alkenone records, *Nature, 364*, 319-321.

Royer, D.L., R.A. Bemer, I.P. Montanez, N.J. Tabor and D.J. Beerling (2004), CO_2 as a primary driver of Phanerozoic climate, *GSA Today, 14,* 4–10.

Ruddiman, W.F., and B.C. Heezen (1967), Differential solution of planktonic Foraminifera, *Deep Sea Res., 14* (6), 801-808.

Russell, A.D., B. Hoenisch, H.J. Spero and D.W. Lea (2004), Effects of seawater carbonate ion concentration and temperature on shell U, Mg, and Sr in cultured planktonic foraminifera, *Geochim. Cosmochim. Acta, 68*, 21, 4347–4361.

Sadekov, A.Y., S.M. Eggins, P. De Deckker (2005), Characterization of Mg/Ca distributions in planktonic foraminifera species by electron microprobe mapping. *Geochem. Geophys. Geosy., 6*, Q12P06, doi:10.1029/2005GC000973.

Sanyal, A., N.G. Hemming, G.N. Hanson and W.S. Broecker (1995), Evidence for a higher pH in the glacial ocean from boron isotopes in foraminifera, *Nature, 373*, 234 – 236, doi:10.1038/373234a0.

Saraswat, R., R. Nigam, S. Weldeab, A. Mackensen, and P. D. Naidu (2005), A first look at past sea surface temperatures in the equatorial Indian Ocean from Mg/Ca in foraminifera, *Geophys. Res. Lett., 32,* L24605, doi:10.1029/2005GL024093.

Sarnthein, M., K. Winn, S. J. A. Jung, J.-C. Duplessy, L. Labeyrie, H. Erlenkeuser, and G. Ganssen (1994), Changes in East Atlantic deepwater circulation over the last 30,000 years: Eight time slice reconstructions, *Paleoceanography, 9* (2), 209–267.

Sasov, A., and D. Van Dyck (1998), Desktop X-ray microscopy and microtomography, *J. Microsc., 191*, 151-158.

Savin, S.M., and R. G. Douglas (1973), Stable isotope and magnesium geochemistry of recent planktonic foraminifera from the South Pacific, *Geol. Soc. Am. Bull., 84* (7), 2327–2342.

Schiebel, R., (2002), Planktic foraminiferal sedimentation and the marine calcite budget, *Global Biogeochem. Cycles, 16* (4), 1065, doi:10.1029/2001GB001459.

Schiebel, R., S. Barker, R. Lendt, H. Thomas and J. Bollmann (2007), Planktic foraminiferal dissolution in the twilight zone. *Deep-Sea Res. II, 54,* (5-7), 676-686, doi:10.1016/j.dsr2.2007.01.009

Schlitzer, R., (2007), Ocean Data View, http://odv.awi.de.

Schmucker, B., (2000), Recent planktic foraminifera in the Caribbean Sea: Distribution, ecology and taphonomy [Unpublished thesis, ETH Zürich, Zurich, Switzerland].

Schott, F. A., M. Dengler, and R. Schoenefeldt (2002), The shallow overturning circulation of the Indian Ocean, *Prog. Oceanogr., 53,* 57– 103.

Schott, F. A., S.-P. Xie, and J. P. McCreary Jr. (2009), Indian Ocean circulation and climate variability, *Rev. Geophys., 47*, RG1002, doi:10.1029/2007RG000245.

Schott, W., (1935), Die Foraminiferen in dem aequatorialen Teil des Atlantischen Ozeans, Deut. Atlant. Expedition "Meteor" 1925-1927, *Wiss. Erdch., 3* (3B), 43 – 143.

Sexton, P.F., and P.A. Wilson (2009), Preservation of benthic foraminifera and reliability of deep-sea temperature records: Importance of sedimentation rates, lithology and the need to examine test wall structure, *Paleoceanography, 24*, PA2208, doi:10.1029/2008PA001650.

Shackleton, N. J., and E. Vincent (1978), Oxygen and carbon isotope studies in recent foraminifera from the Southwest Indian Ocean, *Mar. Micropaleontol., 3*, 1 –13.

Shackleton, N., (1974), Attainment of isotope equilibrium between ocean water and the benthic foraminifera Genus *Uvigerina*: isotope changes in the ocean during the last glacial, *Les méthodes quantitative d'étude des variations du climat au cours du Pleistocene,* Colloques Internationaux de Centre National de la Recherche Scientifique CNRS, Paris: 203-210.

Shackleton, N.J., (1977), ^{13}C in *Uvigerina*: Tropical rainforest history and the equatorial Pacific carbonate dissolution cycles. In: N. Anderson and A. Malahof (Eds.), *Fate of Fossil Fuel CO_2 in the Oceans,* Plenum, New York, pp. 401-427.

Shackleton, N.J., and E. Vincent (1978), Oxygen and carbon isotope studies in recent foraminifera from the southwest Indian Ocean. *Mar. Micropalentol., 19*, 275-285.

Sigman, D.M., and E.A. Boyle (2000), Glacial/interglacial variations in atmospheric carbon dioxide, *Nature, 407,* 859–869.

Sigman, D.M., D. C. McCorkle and W. R. Martin (1998), The Calcite Lysocline as a Constraint on Glacial/Interglacial Low-Latitude Production Changes, *Global Biogeochem. Cycles, 12* (3), 409–427.

Sigman, D.M., M.P. Hain and G.H. Haug (2010), The polar ocean and glacial cycles in atmospheric CO_2 concentration, *Nature, 466,* doi:10.1038/Nature09149

Skinner, L.C., S. Fallon, C. Waelbroeck, E. Michel and S. Barker (2010), Ventilation of the Deep Southern Ocean and Deglacial CO_2 Rise, *Science, 328*, 1147, doi:10.1126/science.1183627

Slutz, R.J., S. J. Lubker, J. D. Hiscox, S. D. Woodruff, R. L. Jenne, D. H. Joseph, P. M. Steuer, J. D. Elms (1985), *Comprehensive Ocean-Atmosphere Data Set: Release 1*, 268 pp.

Sowers, T., and M. Bender (1995), Climate records covering the last deglaciation, *Science, 269*, 5221, 210-214, doi: 10.1126/science.269.5221.210.

Speijer, R.P., D. Van Loo, B. Masschaele, J. Vlassenbroeck, V. Cnudde and P. Jacobs (2008), Quantifying foraminiferal growth with high-resolution X-ray computed tomography: New opportunities in foraminiferal ontogeny, phylogeny, and paleoceanographic applications, *Geosphere, 4* (4), 760–763; doi: 10.1130/GES00176.1

Spero, H.J., J. Bijma, D.W. Lea and B.E. Bemis (1997), Effect of seawater carbonate concentration on foraminiferal carbon and oxygen isotopes, *Nature, 390* (4), 497.

Srinivisan, M.S., and J.P. Kennett (1976), Evolution and Phenotypic Variation in the Late Cenozoic *Neogloboquadrina dutertrei* Plexus, In: Y. Takayanagi and T. Saito (eds.) *Progress in Micropaleontology, special publication*, New York: Micropaleontology Press, American Museum of Natural History, pp329-355.

Stauffer, B., T. Blunier, A. Daellenbach, A. Indermuehle, J. Schwander, T. F. Stocker, J. Tschumi, J. Chappellaz, D. Raynaud, C. U. Hammer and H. B. Clausen (1998), Atmospheric CO_2 concentration and millennial-scale climate change during the last glacial period, *Nature, 392.*

Steinke, S., J. Groeneveld, H. Johnstone, R. Rendle-Bühring (2010), East Asian summer monsoon weakening after 7.5 Ma: Evidence from combined planktonic foraminifera Mg/Ca

and $\delta^{18}O$ (ODP Site 1146; northern SCS), *Palaeogeography, Palaeoclimatology, Palaeoecology, 289*, 33-43.

Stoll, H.M., J. Ruiz Encinar, J. Ignacio Garcia Alonso, Y. Rosenthal, I. Probert and C. Klaas (2001), A first look at paleotemperature prospects from Mg in coccolith carbonate: Cleaning techniques and culture measurements, *Geochem. Geophys. Geosys., 2*, 2000GC000144.

Stott, L., A. Timmermann and R. Thunell (2007), Southern hemisphere and deep-sea warming led deglacial atmospheric CO_2 rise and tropical warming, *Science, 318*, 435, DOI: 10.1126/science.1143791

Sundquist, E. T., and W.S. Broecker (eds.) (1985), *The Carbon Cycle and Atmospheric CO2: Natural Variations Archean to Present.* Geophysical Monograph Ser., (32) 627 pp, AGU, Washington D.C.

Thunell, R.C., (1976), Optimum indices of calcium carbonate dissolution in deep-sea sediments, *Geology, 4*, 525-527.

Thunell, R.C., R.S. Keir, S. Honjo (1981), Calcite Dissolution—an in situ study in the Panama Basin, *Science, 212*, 659–661.

Tripati, A.K., C.D. Roberts, R.A. Eagle (2009), Coupling of CO_2 and Ice Sheet Stability Over Major Climate Transitions of the Last 20 Million Years, *Science, 326*, 1394–1397.

Troy, P.J., Y.-H. Li and F.T. Mackenzie (1997), Changes in surface morphology of calcite exposed to the oceanic water column. *Aquatic Geochemistry, 3*, 1–20.

Tyndall, J., (1861), On the absorption and radiation of heat by gases and vapors and on the physical connexion of radiation, absorption and conduction, *Phil. Mag. (Series 4), 22*, 169-194, 273-285.

Tyrrell, T., and R. E. Zeebe (2004), History of carbonate ion concentration over the last 100 million years, *Geochim. Cosmochim. Acta, 68*, 3521–3530.

Urey, H. C., (1947), The thermodynamic properties of isotopic substances, *J. Chem. Soc., 1947*, 562-581.

Van Dyck, D., and A. Sasov (1998), Desktop microtomograph: gateway to the 3D world, *Microsc. Analysis (European edn), 3*, 21-3.

Waelbroeck, C., L. Labeyrie, E. Michel, J.C. Duplessy, J.F. McManus,K. Lambeck, E. Balbon and M. Labracherie (2002), Sea-level and deep water temperature changes derived from benthic foraminifera isotopic records, *Quat. Sci. Rev., 21*, 295–305.

Walter, L.M., and J.W. Morse (1985), The dissolution kinetics of shallow marine carbonates in seawater: A laboratory study, *Geochim. Cosmochim. Acta, 49*, 1503-1514.

Webb, S., (1988), *The Physics of Medical Imaging*, Taylor & Francis, pp 633.

Weldeab, S., R. R. Schneider and M. Kölling (2006), Comparison of foraminiferal cleaning procedures for Mg/Ca paleothermometry on core material deposited under varying terrigenous-input and bottom water conditions, *Geochem. Geophy. Geosy., 7*, Q04P12, doi:10.1029/2005GC000990.

Wilke, I., and F.J.C Peeters, Depth integrated growth of planktic foraminiferal shells part 2. Model fits to field observations, in Wilke, I., (2006) *Ecological preferences and calcification processes on the incorporation of stable oxygen and carbon isotopes in planktic foraminiferal calcite shells*, [Unpublished Thesis, Univ. of Bremen, Bremen, Germany].

Wilke, I., H. Meggers, T. Bickert (2009), Depth habitats and seasonal distributions of recent planktic foraminifers in the Canary Islands region (29 °N) based on oxygen isotopes, *Deep-Sea Res. I, 56,* 89-106.

Wu, G., and W. H. Berger (1989), Planktonic foraminifera: Differential dissolution and the Quaternary stable isotope record in the west equatorial Pacific, *Paleoceanography, 4*, 181–198.

Wu, G., and W.H. Berger (1991), Pleistocene $\delta^{18}O$ records from Ontong-Java Plateau: effects of winnowing and dissolution, *Mar. Geol., 96*, 193-209.

Yu, J., (in prep). Dissolution effects in planktic foraminifera from the Ontong Java Plateau

Yu, J., and H. Elderfield (2007), Benthic foraminiferal B/Ca ratios reflect deep water carbonate saturation state, *Earth Planet. Sci. Lett., 258,* 73–86

Yu, J., H. Elderfield, M. Greaves and J. Day (2007), Preferential dissolution of benthic foraminiferal calcite during laboratory reductive cleaning, *Geochem. Geophy. Geosy., 8*, Q06016, doi:10.1029/2006GC001571.

Yu, J., H. Elderfield, Z. Jin and L. Booth (2008), A strong temperature effect on U/Ca in planktonic foraminiferal carbonates, *Geochim. Cosmochim. Acta, 72,* 4988–5000.

Yu, J., J. Day, M. Greaves and H. Elderfield (2005), Determination of multiple element/calcium ratios in foraminiferal calcite by quadrupole ICP-MS, *Geochem. Geophy. Geosy., 6,* Q08P01, doi:10.1029/2005GC000964.

Zeebe, R.E., and D.A. Wolf-Gladrow (2001), CO_2 In: *Seawater: Equilibrium, Kinetics, Isotopes,* Elsevier Sciences, B.V., Amsterdam, The Netherlands, 346 pp.